



UNIVERSITAT DE
BARCELONA

Heterogeneity of carcinoma-associated fibroblasts and REV-ERB-induced phenotype molding in pancreatic ductal adenocarcinoma

Nerea Albert Colomer

ADVERTIMENT. La consulta d'aquesta tesi queda condicionada a l'acceptació de les següents condicions d'ús: La difusió d'aquesta tesi per mitjà del servei TDX (www.tdx.cat) i a través del Dipòsit Digital de la UB (diposit.ub.edu) ha estat autoritzada pels titulars dels drets de propietat intel·lectual únicament per a usos privats emmarcats en activitats d'investigació i docència. No s'autoritza la seva reproducció amb finalitats de lucre ni la seva difusió i posada a disposició des d'un lloc aliè al servei TDX ni al Dipòsit Digital de la UB. No s'autoritza la presentació del seu contingut en una finestra o marc aliè a TDX o al Dipòsit Digital de la UB (framing). Aquesta reserva de drets afecta tant al resum de presentació de la tesi com als seus continguts. En la utilització o cita de parts de la tesi és obligat indicar el nom de la persona autora.

ADVERTENCIA. La consulta de esta tesis queda condicionada a la aceptación de las siguientes condiciones de uso: La difusión de esta tesis por medio del servicio TDR (www.tdx.cat) y a través del Repositorio Digital de la UB (diposit.ub.edu) ha sido autorizada por los titulares de los derechos de propiedad intelectual únicamente para usos privados enmarcados en actividades de investigación y docencia. No se autoriza su reproducción con finalidades de lucro ni su difusión y puesta a disposición desde un sitio ajeno al servicio TDR o al Repositorio Digital de la UB. No se autoriza la presentación de su contenido en una ventana o marco ajeno a TDR o al Repositorio Digital de la UB (framing). Esta reserva de derechos afecta tanto al resumen de presentación de la tesis como a sus contenidos. En la utilización o cita de partes de la tesis es obligado indicar el nombre de la persona autora.

WARNING. On having consulted this thesis you're accepting the following use conditions: Spreading this thesis by the TDX (www.tdx.cat) service and by the UB Digital Repository (diposit.ub.edu) has been authorized by the titular of the intellectual property rights only for private uses placed in investigation and teaching activities. Reproduction with lucrative aims is not authorized nor its spreading and availability from a site foreign to the TDX service or to the UB Digital Repository. Introducing its content in a window or frame foreign to the TDX service or to the UB Digital Repository is not authorized (framing). Those rights affect to the presentation summary of the thesis as well as to its contents. In the using or citation of parts of the thesis it's obliged to indicate the name of the author.

UNIVERSITAT DE BARCELONA
FACULTAT DE FARMÀCIA I CIÈNCIES DE L'ALIMENTACIÓ
PROGRAMA DE DOCTORAT EN BIOMEDICINA

**HETEROGENEITY OF CARCINOMA-ASSOCIATED
FIBROBLASTS AND REV-ERB-INDUCED
PHENOTYPE MOLDING IN PANCREATIC
DUCTAL ADENOCARCINOMA**

NEREA ALBERT COLOMER

2020



UNIVERSITAT DE BARCELONA

FACULTAT DE FARMÀCIA I CIÈNCIES DE L'ALIMENTACIÓ

PROGRAMA DE DOCTORAT EN BIOMEDICINA

**HETEROGENEITY OF CARCINOMA-ASSOCIATED
FIBROBLASTS AND REV-ERB-INDUCED PHENOTYPE
MOLDING IN PANCREATIC DUCTAL
ADENOCARCINOMA**

NEREA ALBERT COLOMER
2020

Memòria presentada per Nerea Albert Colomer per optar al grau de Doctor/a
per la Universitat de Barcelona

Dr. David Garcia Molleví

Director

Dr. Francesc Viñals Canals

Tutor

Nerea Albert Colomer

Autora

TABLE OF CONTENTS

ABBREVIATIONS	11
SUMMARY	19
RESUMEN	23
INTRODUCTION	29
1. PANCREAS	31
2. CANCER	32
3. PANCREATIC CANCER	32
3.1 TYPES OF PANCREATIC CANCER	33
4. PANCREATIC DUCTAL ADENOCARCINOMA (PDAC)	34
4.1 EPIDEMIOLOGY AND RISK FACTORS	34
4.2 DIAGNOSIS AND PROGNOSIS	34
4.3 PDAC STAGES	36
4.3.1 Resectable	36
4.3.2 Borderline resectable	36
4.3.3 Locally advanced	36
4.3.4 Metastatic	36
4.4 TREATMENT	37
4.4.1 Neoadjuvant treatment.....	37
4.4.2 Adjuvant treatment.....	38
4.4.3 Palliative therapy.....	39
4.4.4 Chemotherapeutic agents.....	39
4.5 HISTOLOGICAL FEATURES	40
4.6 BIOLOGICAL TUMOR SUBTYPES	43
4.6.1 Molecular classification	43
4.6.2 Metabolic classification	45

5.	TUMOR MICROENVIRONMENT	46
5.1	TUMOR STROMA COMPOSITION	47
5.1.1	Immune cells	47
5.1.2	Endothelial cells	49
5.1.3	Extracellular matrix (ECM)	49
6.	CARCINOMA-ASSOCIATED FIBROBLASTS (CAFS)	50
6.1	FROM FIBROBLAST TO CAFs	50
6.2	CAFs FUNCTIONS	51
6.3	HETEROGENEITY OF CAFs	53
6.3.1	Activated vs Normal stroma	53
6.3.2	Myofibroblast CAF (myCAF) vs Inflammatory CAF (iCAF)	53
6.3.3	myCAF, iCAF and antigen-presenting CAF (apCAF)	54
6.3.4	A – D subtypes	55
6.3.5	In other cancer types and diseases	56
6.4	CAFs, METABOLISM, AND CANCER	58
6.4.1	Cancer metabolism	58
6.4.2	PDAC metabolism	60
6.4.3	Metabolic crosstalk within PDAC microenvironment	61
7.	CANCER TREATMENT STRATEGIES TARGETING THE TUMOR STROMA	64
7.1	SELECTIVE STROMA DEPLETION	66
7.2	EXTRACELLULAR MATRIX (ECM) DEGRADATION	67
7.3	BLOCKING THE TUMOR-STROMA CROSSTALK	69
7.4	STROMAL REPROGRAMING	72
8.	REV-ERB NUCLEAR RECEPTORS	75
8.1	REV-ERB AS DRUG TARGETS	78
8.1.1	Inflammation	78
8.1.2	Myogenic disorders	79

8.1.3	Metabolic disorders.....	79
8.1.4	Cancer.....	82
PREMISES, HYPOTHESIS, AND OBJECTIVES.....		85
MATERIALS AND METHODS.....		89
1.	CELL CULTURE	91
1.1	CELL LINES AND CULTURE CONDITIONS.....	91
1.1.1	Primary CAFs isolation.....	91
1.1.2	Culture of CAFs.....	92
1.1.3	Culture of tumoral cells.....	92
1.1.4	Co-culture of tumoral cells and CAFs	94
1.2	MYCOPLASMA TEST.....	94
1.3	CELL COUNTING.....	95
1.4	CELL CRYOPRESERVATION AND THAWING	95
1.5	CONDITIONED MEDIA HARVESTING.....	96
1.5.1	From pancreatic CAFs.....	96
2.	MOLECULAR ANALYSIS.....	96
2.1	CYTOMETRY ASSAYS.....	96
2.1.1	Fluorescence-activated cell sorting (FACS).....	96
2.1.2	Fluorescence flow cytometry (FFC)	98
2.2	RNA ANALYSIS.....	98
2.2.1	RNA isolation and quantification.....	98
2.2.2	cDNA obtention from RNA	99
2.2.3	Real-Time quantitative PCR.....	99
2.2.4	RNA sequencing of cultured CAFs and tumoral cells.....	101
2.3	PROTEIN ANALYSIS.....	101
2.3.1	Western Blot (WB).....	101
2.3.2	Immunocytofluorescence (ICF)	104

3.	<i>IN SILICO</i> ANALYSES.....	106
3.1	TRANSCRIPTOMIC ANALYSES: DEG.....	106
3.2	FUNCTIONAL ANALYSES OF GENE EXPRESSION.....	107
3.3	PROGNOSTIC ASSESMENT OF GENE SIGNATURES USING ssGSEA	108
3.4	METABOLIC RECONSTRUCTION FROM TRANSCRIPTOMIC DATA	109
3.4.1	Signaling pathways	109
3.4.2	Metabolic modules metabolites.....	109
4.	CELL-BASED ASSAYS	110
4.1	MIGRATION ASSAYS	110
4.1.1	Wound closing assay.....	110
4.1.2	Directional migration assay	110
4.2	COLONY FORMATION ASSAYS.....	111
4.3	PROLIFERATION ASSAYS	111
4.4	LIPID DROPLETS STAINING	112
4.5	INTRINSIC MODULATION OF CAFs	112
5.	DRUGS	113
5.1	PHARMACOLOGIC MODULATORS OF REV-ERB	113
5.1.1	SR9009	113
5.1.2	SR8278	114
6.	HISTOLOGICAL STUDIES.....	114
6.1	HEMATOXILIN & EOSIN (H&E) STAINING	114
6.2	IMMUNOHISTOCHEMISTRY (IHC).....	115
6.3	DOUBLE IMMUNOHISTOFLUORESCENCE (D-IHF)	115
7.	STATISTICAL ANALYSIS	117
	RESULTS	119
1.	STROMAL TRANSCRIPTOMIC AND METABOLOMIC PROFILING FROM AN <i>IN VITRO</i> APPROACH OF PDAC: <i>IN SILICO</i> DATA.....	121

1.1	PRINCIPAL COMPONENT ANALYSIS (PCA) CLASSIFIED CAFs ACCORDING TO CULTURE CONDITIONS	123
1.2	<i>IN VITRO</i> TOP 100 GENES DIFFERENTIAL EXPRESSED GENES BETWEEN MONO-CULTURED AND CO-CULTURED CAFs	124
1.3	GENE SET ENRICHMENT ANALYSIS (GSEA) REVEALED DIFFERENT TRANSCRIPTOMIC PHENOTYPES BETWEEN MONO- AND CO-CULTURED CAFs..	126
1.4	GSEA REVEALED DIFFERENT METABOLOMIC PROFILE BETWEEN MONO- AND CO-CULTURED CAFs	130
1.4.1	Metabolic reconstruction analysis confirmed the relevance of lipids signaling pathways and metabolism in the co-cultured CAFs	132
1.5	ssGSEA CLUSTERED PATIENTS TO PARTICULAR <i>IN VITRO</i> CAFs GENE SIGNATURES.....	136
2.	PROGNOSTIC VALUE OF CAF SIGNATURES.....	137
2.1	MONO-CULTURED CAFs CORRELATED WITH BETTER SURVIVAL PROBABILITY IN THE TWO-CLASSES SIGNATURES	137
2.1.1	Cholesterol and TNF were the hallmarks with prognostic value in the two-classes signatures.....	138
2.2	THREE-CLASSES TRANSCRIPTOMIC SIGNATURES SHOWED DIFFERENCES IN THE SURVIVAL PROBABILITY FOR TWO INDEPENDENT PATIENTS' DATASETS	140
2.3	MYOFIBROBLAST-LIKE PHENOTYPE CORRELATED WITH A BETTER PROGNOSIS	145
3.	IDENTIFICATION OF SPECIFIC BIOMARKERS WITHIN THE DIFFERENT PHENOTYPES IN <i>IN VITRO</i> CULTURES.....	146
3.1	CAF _s FROM PDAC SHOWED HETEROGENEITY AT TRANSCRIPTIONAL LEVEL.....	146
3.1.1	Identification of different phenotypes in CAFs isolated from primary human PDAC.....	146

Table of contents

3.1.2	The correlation plot of “classical” CAFs markers in the Moffitt series classify patients in three clusters with a different prognostic association.....	148
3.2	CAF_s FROM PDAC SHOWED HETEROGENEITY AT FUNCTIONAL LEVEL	150
3.2.1	CAF C (ecmCAF) had the highest proliferation rate	150
3.2.2	CAF B (lipoCAF) had a higher content of intracellular lipids	151
3.3	CULTURE CONDITIONS MODIFY CAF_s PHENOTYPE	151
3.3.1	Transcriptional background of CAFs (CAF A, CAF B or CAF C) mediate their phenotype in the direct co-culture (DCC) with tumor cells.....	152
3.3.2	The mixture of CAFs (mixCAF _s) modify the expression pattern of the CAF _s subtypes	154
3.3.3	Myofibroblast markers and fibroblast-activation markers expression in the mixture of 3 CAF _s correlated with the mixture of 5 CAF _s	158
4.	CAF_s SUBTYPES IN HUMAN PDAC SAMPLES	161
5.	CELL-BASED FUNCTIONAL ASSAYS	166
5.1	MIA PaCA-2 CELLS MIGRATION CAPACITY IS MODULATED BY CAF _s ’ CONDITIONED MEDIUM.....	166
5.2	COLONY FORMATION AND PROLIFERATION CAPACITY OF TUMOR CELLS ARE MEDIATED BY CAF _s ’ CONDITIONED MEDIUM.....	168
6.	REV-ERB-INDUCED PHENOTYPE MOLDING	170
6.1	REV-ERB TREATMENT MODIFY CAF _s SUBTYPES (CAF A, CAF B, AND CAF C) PHENOTYPES. THE RESPONSE OF EACH CAF _s SUBTYPES IS MEDIATED BY THE GENETIC BACKGROUND	170
6.2	MIXCAF _s ACQUIRED A DEDIFFERENTIATED STATE AFTER SR9009 TREATMENT.....	173
6.2.1	The treatment with REV-ERB agonist SR9009 increased lipid droplets (LD) content in the mixCAF _s	173

6.2.2 Treatment with SR9009 decreased the expression of REV-ERB downstream target genes in mixCAFs 174

6.2.3 Pre-treatment of mixCAFs with SR9009 diminished the expression of activated-fibroblast markers and maintain the expression of PSC under co-culture conditions..... 176

DISCUSSION 181

1. CAFS’ HETEROGENEITY IN PDAC..... 183

2. REPROGRAMMING CAFS TOWARDS A LESS SUPPORTIVE SUBPOPULATION..... 189

CONCLUSIONS..... 195

REFERENCES 199

ANNEXES..... 219

LIST OF FIGURES

Figure 1. Pancreas anatomy with its corresponding glands and functions..... 31

Figure 2. Histology of normal pancreatic tissue..... 41

Figure 3. Schematic progression of human PDAC..... 42

Figure 4. Schematic development of tumor microenvironment, from normal stroma to highly fibrotic tumoral stroma 47

Figure 5. Summary of CAFs’ functions and the mechanisms by which they are orchestrated..... 52

Figure 6. Cellular metabolism of glucose and its connection with fatty acids and cholesterol synthesis..... 59

Figure 7. Mechanisms of CAFs heterogeneity..... 63

Figure 8. Mechanism of stroma-mediated chemoresistance 65

Table of contents

Figure 9. Schematic representation of REV-ERB α circadian expression patterns and regulatory effects in different tissues.	78
Figure 10. Schematic representation of the experimental design	113
Figure 11. Schematic representation of the in vitro approximation and cell sorting conditions.....	122
Figure 12. Principal component analysis (PCA) for the most 500 differentially expressed genes as PC1 and PC2 variables	124
Figure 13. Heatmap of the top 100 differential expressed genes (DEG).....	124
Figure 14. Protein staining by ICF to validate RNA-seq DEG	125
Figure 15. Protein staining by IHC to validate the RNA-seq DEG over different human PDAC tissue samples	126
Figure 16. Transcriptomic phenotypes between mono- and co-cultured CAFs (A) and Moffitt correlation (B)	128
Figure 17. Lung cancer (GSE66616) correlation	129
Figure 18. GSEA showing a correlation between mono- and co-cultured CAFs of differentially expressed processes that define our phenotypes	131
Figure 19. Data of the metabolic reconstruction analysis performed with Metabolizer and Metabolica	135
Figure 20. Heatmap of ssGSEA of CAFs signatures	136
Figure 21. Prognostic association of two-classes transcriptomic signatures of CAFs in the Moffitt series.....	137
Figure 22. Prognostic association of cholesterol homeostasis (A) and TNF signaling via NF κ B (B) hallmarks.....	139
Figure 23. Heatmap of ssGSEA of CAFs' signatures	141
Figure 24. Three-classes transcriptomic signatures (A, B), survival probability (C, D), and enrichment plots of enriched GSEA processes in each cluster (E, F, G)	143
Figure 25. Survival probability of the three-classes signature (right panel) and enrichment plots (EP) of myofibroblast markers and cholesterol pathway (left panel) in the Moffitt patient's dataset	145

Figure 26. CAFs subtypes characterization by protein and gene expression. 147

Figure 27. Correlation plot of CAFs’ markers in the Moffitt series 149

Figure 28. Heatmap of CAFs’ classical markers (A) and survival probability (B) . 150

Figure 29. Proliferation rate of CAFs subtypes..... 151

Figure 30. Nile red staining in the 3 CAFs subtypes 151

Figure 31. Gene expression profile of CAFs subtypes mono-cultured and co-cultured with tumor cells..... 153

Figure 32. Schematic representation of the experimental design..... 155

Figure 33. Gene expression profile of CAFs subtypes isolated from a mixCAF’s mono-cultured and co-cultured with tumor cells..... 158

Figure 34. Gene expression profile of mono-culture of mixCAF’s and co-culture of mixCAF’s with tumor cells..... 161

Figure 35. α SMA and FAP protein expression detected by immunohistochemistry (IHC) (A and B) and double immunohistofluorescence (D-IHF) (C) in human PDAC tissue samples..... 162

Figure 36. Histological study of 4 human PDAC tissue samples by H&E staining and α SMA and FAP protein expression detected by immunohistochemistry. 163

Figure 37. H&E staining and IHC protein detection in 2 myofibroblast low human PDAC. 166

Figure 38. Migration capacity of MIA PaCa-2 cells..... 167

Figure 39. Clonogenic (A) and proliferation (B) capacity of tumor cells (HPAC and MIA PaCa-2) mediated by CAFs subtypes (CAF A, CAF B, CAF C) conditioned media (CM) 169

Figure 40. Relative gene expression (mean \pm SD) of CAFs subtypes (CAF A, CAF B, and CAF C) treated with REV-ERB agonist (SR9009) and antagonist (SR8278) compared with the control (DMSO)..... 172

Figure 41. Nile red staining in a mono-culture of mixCAF’s treated with REV-ERB agonist (SR9009), REV-ERB antagonist (SR8278), and DMSO (control) 174

Table of contents

Figure 42. Gene expression levels (mean \pm SD) of a mixture of our CAFs subtypes (mixCAFs: CAF A + CAF B + CAF C) in mono-culture treated with REV-ERB agonist (SR9009) and antagonist (SR8278) and compared with the control	176
Figure 43. Gene expression levels (mean \pm SD) of a mixture of our CAFs subtypes (mixCAFs: CAF A + CAF B + CAF C) treated with REV-ERB agonist (SR9009) and co-cultured with HPAC cells	177
Figure 44. Protein expression detected by immunofluorescence (ICF) of a mixture of our CAF subtypes (mixCAFs: CAF A + CAF B + CAF C) treated with REV-ERB drugs (SR9009 and SR8278)	178

LIST OF TABLES

Table 1. Tumoral cell lines classification and main mutations in PDAC.....	93
Table 2. Primers used to detect mycoplasma contamination.	95
Table 3. List of genes and the sequences of the corresponding primers used in RT-qPCR assays.	100
Table 4. Sequences of QARS primers used as housekeeping gene	100
Table 5. List of secondary antibodies used in WB	104
Table 6. List of primary antibodies used for protein detection in different applications and their dilutions	106
Table 7. List of primary antibodies used for protein detection by IHC or D-IHF and their specific conditions	116
Table 8. List of secondary antibodies used in ICF or D-IHF.....	117
Table 9. Summary of the highest up- or downregulated signaling pathways in the co-cultured mixCAFs analyzed with HiPathia	133

ABBREVIATIONS

LIST OF ABBREVIATIONS

%	Percentage
ADEX	Aberrantly differentiated endocrine exocrine
AECC	Asociación española contra el cancer
anti-CTLA 4	anti-cytotoxic T-lymphocyte-associated protein 4
anti-PDL 1	anti-programmed cell death 1 ligand 1
APC	Allophycocyanin
apCAF	Antigen presenting CAF
APS	Ammonium persulfate
AR	Androgen receptor
ATCC	American type culture collection
ATRA	all-trans retinoic acid
BAC	Bacterial artificial chromosome
BCA	Bicinchoninic acid
BSA	Bovine serum albumin
CA 19-9	Carbohydrate antigen 19-9
CAFs	Carcinoma-associated fibroblasts
CCR	Colorectal cancer
cDNA	complementary DNA
CFSE	Carboxyfluorescein succinimidyl ester
CM	Conditioned medium
CTL	CD8+ cytotoxic lymphocytes
CYP	Cytochrome P450
DAB	Diaminobenzidine
DAPI	4',6-diamidino-2-phenylindole
DBD	DNA binding domain
DCC	Direct co-culture

Abbreviations

DEG	Differentially expressed genes
DEPC	Diethyl pyrocarbonate
dH₂O	Distilled water
DMSO	Dimethyl sulfoxide
DNA	Deoxyribonucleic acid
DTR	Diphtheria receptor
ECIS	European cancer information system
ECM	Extracellular matrix
ecmCAFs	Extracellular matrix CAFs
EDTA	Ethylenediaminetetraacetic acid
EMT	Epithelial mesenchimal transition
EP	Enrichment plot
ER	Estrogen receptor
ESMO	European society for medical oncology
FA	Fatty acid
FACS	Fluorescence activated cell sorting
FBS	Fetal bovine serum
FC	Fold Change
FDR	False discovery rate
FFC	Fluorescence flow cytometry
FGF	Fibroblast growth factor
FXR	Farnesoid X receptor
GAGs	Glycosaminoglycans
gDNA	Genomic DNA
GO	Gene ontology
GSEA	Gene set enrichment analysis
HA	Hyaluronic acid
HF	Halofunginone

HGF	Hepatocyte growth factor
HKG	Housekeeping gene
HSC	Hepatic stellate cells
iCAF	Inflammatory CAF
ICC	Indirect co-culture
ICF	Immunocytofluorescence
IDIBELL	Institut d'investigació biomèdica de Bellvitge
IFP	Interstitial fluid pressure
IgG	Immunoglobulin G
IgM	Immunoglobulin M
IHC	Immunohistochemistry
IHF	Immunohistofluorescence
INE	Instituto nacional de estadística
IPMN	Intraductal papillary-mucinous neoplasm
ITS	Insulin, Transferrin, Selenium
KDa	Kilodalton
KEGG	Kyoto Encyclopedia of Genes and Genomes
LD	Lipid droplets
lipoCAFs	Lipogenic CAFs
LSC	Liver stellate cells
mAb	Monoclonal antibody
MCN	Mucinous cystic neoplasm
mg	Milligram
MgCl₂	Magnesium chloride
MHC	Major histocompatibility complex
mL	Milliliter
mM	Millimolar
MMP	Matrix metalloproteinase

Abbreviations

MRI	Magnetic resonance imaging
MSC	Mesenchymal stem cells
myoCAFs	Myofibroblast CAFs
NaCl	Sodium chloride
NEAA	Non-essential amino acids
ng	Nanograms
nm	Nanometers
NMF	Non matrix factorization
°C	Centigrade grade
ON	Overnight
OS	Overall survival
OXPHOS	Oxidative phosphorylation
PanIN	Pancreatic intraepithelial neoplasia
PBS	Phosphate-buffered saline
PBS-T	PBS, 0.1% Triton X-100
PCR	Polymerase chain reaction
PDAC	Pancreatic ductal adenocarcinoma
PDVF	Polyvinylidene fluoride
PEGPH20	PEGylated human recombinant PH20 hyaluronidase
PI	Propidium iodide
PMSF	Phenylmethanesulphonyl fluoride
PNETs	Pancreatic neuroendocrine tumors
PPARs	Peroxisome proliferator-activated receptors
ProCURE	Programa contra la resistència terapèutica del càncer
PSC	Pancreatic stellate cells
RARβ	Retinoid acid receptor
REDECAN	Red española de registros de càncer
RNA	Ribonucleic acid

RNA-seq	Ribonucleic acid sequencing
ROR	Retinoid orphan receptor
ROS	Reactive oxygen species
rpm	Revolution per minute
RT	Room temperature
RT-qPCR	Real-Time quantitative PCR
RXR	Retinoid X receptor
SD	Standard deviation
SDS	Sodium dodecyl sulfate
SEM	Standard error mean
Shh	Sonic Hedgehog
Smo	Smoothened
ssGSEA	Single sample gene set enrichment analysis
TAMs	Tumor-associated macrophages
TBS-T	Tris-buffered saline, 0.1% Tween 20
TCA	Tricarboxylic acid cycle
TCGA - PAAD	The cancer genome atlas program – Pancreatic
TG	Triglycerides
Th	CD4+ lymphocytes T helper
TILs	Tumor-infiltrating lymphocytes
TME	Tumor microenvironment
Tris-HCl	Tris-hydrochloride
US	Ultrasound
UV	Ultraviolet
V	Volts
VDR	Vitamin D receptor
VEGF	Vascular endothelial growth factor
WB	Western blot

Abbreviations

WHO	World health organization
µg	Microgram
µL	Microliter
µM	Micromolar

Amino acids

F	S	Y	K
Phe, phenylalanine	Ser, serine	Tyr, tyrosine	Lys, lysine
L	P	H	D
Leu, leucine	Pro, proline	His, histidine	Asp, aspartic acid
I	T	Q	E
Ile, isoleucine	Thr, threonine	Gln, glutamine	Glu, glutamic acid
M	A	N	C
Met, methionine	Ala, alanine	Asn, asparagine	Cys, cysteine
W	R	G	V
Trp tryptophan	Arg, arginine	Gly, glycine	Val, valine

Nucleotides

A, Adenine **T**, Thymine **G**, Guanine **C**, Cytosine **U**, Uracil

SUMMARY

Tumor-stroma crosstalk is essential for PDAC formation. Therefore, the stroma, and specifically the carcinoma-associated fibroblasts (CAFs), are the target of therapeutic alternatives to treat highly desmoplastic tumors such as PDAC.

Lately, many CAFs-targeted therapies have been published. However, some of these strategies have not been completely satisfactory and, some of them have been counterproductive. These differences may be a consequence of the presence of CAFs subpopulations with inter- and intratumor heterogeneity. Therefore, the identification of specific biomarkers and pathways is necessary to improve PDAC treatment by targeting specific CAFs subpopulations.

The aims of this thesis are to identify specific biomarkers of CAFs subpopulations to describe specific signatures to each one. And, with this information, to develop strategies to reprogram pro-tumoral CAFs towards a less supportive subpopulation.

In order to develop these objectives, firstly we isolated CAFs from human PDAC samples. These CAFs were used to perform *in vitro* cultures without or with pancreatic tumor cells. The transcriptional analysis of these cultures revealed the presence of two different CAFs signatures: the mono-culture and the co-culture. The first one obtained from the culture of CAFs without tumor cells and the second one from the culture of CAFs with tumor cells. Specifically, mono-cultured CAFs show a myofibroblast-like phenotype, while de co-cultured CAFs present an enrichment in inflammatory processes, proliferation and lipid biosynthesis. In addition, these signatures correlated with others described in different patients' datasets. Afterwards, we used independent PDAC patients' datasets to study the prognostic value of our signatures. Our signatures, their signaling pathways or even specific markers of such processes were associated with a prognostic value. In particular, patients with high expression of the mono-cultured CAFs signature, their corresponding pathways or, biomarkers, correlated with a better prognosis. However, patients with high expression of co-cultured CAFs signature were associated with a worse prognosis.

Secondly, we performed a transcriptomic characterization of all CAFs isolated from human PDAC tumor samples and we defined 3 CAFs subpopulations with different expression patterns and functional features: the myoCAFs, the lipoCAFs, and the ecmCAFs. This result confirmed the presence of CAFs heterogeneity in PDAC.

Summary

We also used our different CAFs subtypes to evaluate the effects of the tumor-stroma crosstalk by some functional assays. The results suggested that paracrine communication between CAFs and tumor cells, was not able to induce functional changes in tumor cells. However, the transcriptional analysis of CAFs co-cultured with tumor cells, in which there is contact between different cell types, confirmed that the presence of tumor cells induced the expression of activated-fibroblast genes in CAFs.

Finally, we evaluated the CAFs' subtypes biomarkers spatial distribution on human PDAC tissue samples. This validation confirmed the coexistence of different subpopulation of CAFs in the same tumor. And, at the same time, it confirmed the existence 2 main type of PDAC tumors, ones characterized by a high myofibroblast content ($\alpha\text{SMA}^{\uparrow}/\text{FAP}^{\downarrow}$) and, others with a low myofibroblast content ($\alpha\text{SMA}^{\downarrow}/\text{FAP}^{\uparrow}$). We could also correlate the distribution of these biomarkers with the tumor histology. Poorly differentiated tumors, without well-defined glandular structure, usually showed a low expression of myofibroblast markers.

In this and other previous works haven been described that CAFs undergo transcriptomic and metabolomic modifications in response to tumor signals. Many of these changes are modulated by nuclear receptors and transcription factors. Therefore, in this thesis CAFs were treated with REV-ERB drugs. The REV-ERB is a nuclear receptor that acts as a repressor of many processes up- or down-regulated in our CAFs signatures. The intention of this treatment was to modulate CAFs towards a less tumor-supportive state. Specifically, the treatment of CAFs with SR9009, a REV-ERB agonist, caused a dedifferentiation state in CAFs. The dedifferentiation state was characterized by an increased capacity to store intracellular lipids, a reduced lipid metabolism and a reduced expression of the classic fibroblast-activation biomarkers. These events have been described as a properly of pancreatic stellate cells (PSCs), a cell type considered CAFs' precursors.

Thus, this study offers new therapeutic opportunities for PDAC and other highly desmoplastic tumors treatment through modulation of CAFs toward less activated stages.

RESUMEN

La comunicación tumor-estroma es esencial para la formación del adenocarcinoma ductal de páncreas (PDAC). Por ello, el estroma y, más concretamente los fibroblastos asociados al carcinoma (CAFs), son el objetivo terapéutico para tratar tumores altamente desmoplásicos como el PDAC.

En los últimos años se han descrito varias estrategias terapéuticas basadas en CAFs. Algunas con resultados satisfactorios mientras que otras no han demostrado ser satisfactorias o incluso han resultado ser contraproducentes para frenar el desarrollo tumoral. Estas diferencias en cuanto a resultado terapéutico pueden ser debidas a la heterogeneidad intra- e inter-tumoral determinada por la existencia de varias subpoblaciones de CAFs. Por ello, la identificación de marcadores específicos y vías de señalización en CAFs podría mejorar el tratamiento de PDAC permitiendo actuar sobre subpoblaciones específicas de CAFs.

Los objetivos de esta tesis son la identificación de marcadores específicos de las subpoblaciones de CAFs para definir firmas de cada uno. Y, con esta información, diseñar estrategias para reprogramar los CAFs pro-tumorales hacia una subpoblación de CAFs de menor soporte tumoral.

Para el desarrollo de estos objetivos, primero se aislaron CAFs de tumores de PDAC humanos. Estos CAFs se utilizaron para hacer cultivos in vitro, con o sin células tumorales. El análisis transcripcional de estos cultivos reveló la existencia de dos firmas: mono-cultivo y co-cultivo obtenidas del cultivo de los CAFs solos y del cultivo de CAFs con células tumorales, respectivamente. Concretamente, los CAFs en mono-cultivo presentan un fenotipo similar a los miofibroblastos, mientras que los CAFs co-cultivados con células tumorales presentan un enriquecimiento en procesos inflamatorios, proliferación y síntesis de lípidos. Posteriormente se utilizaron bases de datos de pacientes de PDAC para estudiar el valor pronóstico de estas firmas. Tanto las firmas como sus vías de señalización o incluso marcadores específicos de dichos procesos se asociaron a un valor pronóstico. Concretamente los pacientes con mayor expresión de la firma de mono-cultivo, de sus respectivas vías o marcadores se correlacionaron con un mejor pronóstico. Mientras que los pacientes con mayor expresión de la firma, procesos específicos o marcadores concretos de CAFs co-cultivados se asoció a un peor pronóstico.

En segundo lugar, hicimos una caracterización transcripcional de los CAFs aislados de tumores humanos de PDAC y definimos 3 subpoblaciones de CAFs con diferentes perfiles de expresión y características funcionales: los myoCAFs, los

lipoCAFs y los ecmCAFs. Resultado que confirmó la existencia de heterogeneidad en los CAFs de PDAC.

Con los diferentes tipos de CAFs también realizamos una serie de ensayos funcionales con la intención de evaluar el efecto de la comunicación entre el tumor y el estroma. La comunicación paracrina, en la que no hay contacto entre los diferentes tipos celulares, no fue capaz de inducir cambios funcionales. Mientras que, el análisis transcripcional de los CAFs co-cultivados con células tumorales, donde existe contacto directo entre tumor-estroma, confirmó que la presencia de células tumorales induce la expresión de genes de activación en los CAFs.

Finalmente, evaluamos la distribución espacial de nuestros marcadores de los diferentes subtipos de CAFs sobre muestras de PDAC humanas. Esta validación confirmó la coexistencia de las distintas subpoblaciones en un mismo tumor, así como también la existencia de tumores con alto contenido en miofibroblastos ($\alpha\text{SMA}^{\uparrow}/\text{FAP}^{\downarrow}$) o de tumores con bajo contenido en miofibroblastos ($\alpha\text{SMA}^{\downarrow}/\text{FAP}^{\uparrow}$). La distribución de estos marcadores en muestras humanas se relacionó con la histología tumoral. Aquellos tumores poco diferenciados, sin estructura glandular definida, suelen ser tumores con baja expresión de marcadores de miofibroblastos.

En este y otros trabajos se ha descrito que los CAFs, como respuesta a señales tumorales, sufren modificaciones a nivel transcripcional y metabólico. Muchos de estos cambios son modulados por receptores nucleares y factores de transcripción. Por ello, en este trabajo tratamos los CAFs con fármacos moduladores de REV-ERB, un receptor nuclear que actúa como represor de genes o factores de transcripción involucrados en muchos de los procesos que se encuentran infra o sobre expresados en las diferentes firmas de CAFs. La intención de este tratamiento era conseguir modular los CAFs hacia un estado menos diferenciado que no promoviese el desarrollo tumoral. El tratamiento de CAFs con el SR9009, un fármaco agonista del REV-ERB, provoca una desdiferenciación de los CAFs hacia un estado menos activado. Esta desdiferenciación se caracteriza por una mayor capacidad de las células para almacenar lípidos intracelulares, poseer un metabolismo lipídico reducido y una menor expresión de genes característicos de fibroblastos activados. Fenómenos propios de las células estrelladas del páncreas (PSCs), un tipo celular que se ha descrito como precursor de CAFs.

De modo que este estudio ofrece nuevas oportunidades terapéuticas para el tratamiento de PDAC y otros tumores altamente desmoplásicos a través de la modulación de CAFs hacia estadios menos activados.

INTRODUCTION

1. PANCREAS

The pancreas is an elongated and tapered organ that belongs to the gastrointestinal system and is located in the upper abdomen behind the stomach.

Anatomically, the pancreas is divided into 3 parts (Figure 1):

The **head** is the widest part of the organ, located on the right side of it and lying in the curve of the duodenum. The tapered left side is called the **body**, which extends slightly upward and ends in the **tail**, near the spleen (Longnecker, 2014; www.hopkinsmedicine.org).

Functionally, the pancreas is divided into 2 types of glands:

The exocrine gland produces and secretes digestive enzymes into the duodenum. The exocrine components include acinar and duct cells with associated connective tissue, vessels, and nerves. The secreted enzymes help carbohydrates, fats, proteins, and acids to be decomposed. More than 95% of the pancreatic tissue is exocrine pancreas (Longnecker, 2014; www.hopkinsmedicine.org).

The **endocrine** gland, which consists of the islets of Langerhans, produces and secretes hormones into the bloodstream. The main secreted hormones are insulin and glucagon, which regulate the levels of glucose in the blood, and somatostatin, which prevents the release of insulin and glucagon. Islets comprise the 1-2% of the pancreatic mass (Longnecker, 2014; www.hopkinsmedicine.org).

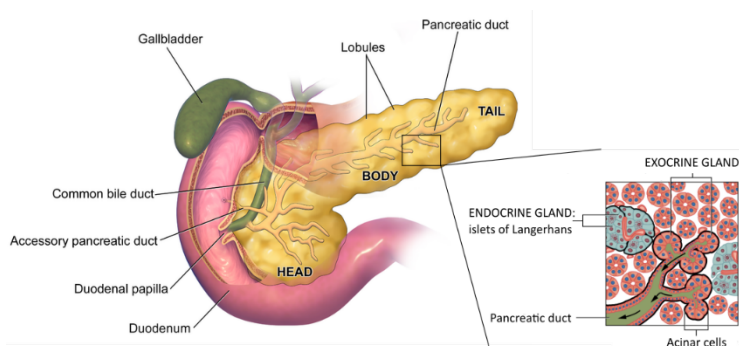


Figure 1. Pancreas anatomy with its corresponding glands and functions. Yellow organ corresponds to the pancreas with its different parts (head, body and tail). The image on the right side is a schematic draw of the functional structures of the pancreas. Image modified and

Introduction

adapted from Johns Hopkins Medicine and Anatomy & Physiology from OpenStax (www.hopkinsmedicine.org; www.openstax.org).

2. CANCER

In a healthy body, human cells grow and divide to form new cells, in order to replace old or damaged cells. When this orderly process breaks down, cancer develops, and abnormal, old, or damaged cells are able to survive even in those conditions that would normally lead them to cell death. These malignant cells can divide indefinitely, giving rise to a tumor and eventually spreading to surrounding tissues. Tumors can be solid tumors, i.e. masses of tissues, or no-solid tumors, as cancer of the blood (www.aecc.es; www.cancer.gov; www.nih.gov).

At a biological level, cancer is a genetic disease caused by changes in the genes that control cell functions as growth and division. These genetic changes can be inherited, or they can be brought about as the consequences of DNA damages caused by certain environmental exposures (www.aecc.es; www.cancer.gov; www.nih.gov).

According to data from the World Health Organization (WHO; www.who.int), cancer is the second leading cause of death in **the world**, accounting for an estimated 9.6 million deaths in 2018. It means that 1 in 6 worldwide deaths is due to cancer. Globally, lung, prostate, colorectal, stomach, and liver cancer are the most common types of cancer in men; while breast, colorectal, lung, cervical, and thyroid cancer are the most common among women. In **Europe**, 3 million new cancer cases were diagnosed in 2018 with a total of 1.5 million cancer deaths, based on data from the European Cancer Information System (ECIS; www.ecis.jrc.ec.europa.eu). The *Asociación Española Contra el Cancer* (AECC; www.aecc.es) estimated that around 270.000 new cancer cases were diagnosed in **Spain** in 2019. Cancer types with higher mortality rates are lung, colorectal, pancreas, and breast, with a survival rate at 5 years post-diagnosis of 415.000 patients from the total of cases.

3. PANCREATIC CANCER

Globally, only 2.1% of cancer cases are due to pancreatic cancer. Nevertheless, it has an increasing incidence, since around 233.000 new pancreatic cancer cases are diagnosed every year. In fact, it has been postulated that pancreatic cancer would

be the second leading cause of cancer-related death in 2030. In the case of Spain, pancreatic cancer is an infrequent type of tumor, with an annual incidence of around 8.169 cases. The latest report from *Red Española de Registros de Cáncer* (REDECAN) and *Instituto Nacional de Estadística* (INE) estimated a mortality of 6.868 patients in 2017 (www.aecc.es).

3.1 TYPES OF PANCREATIC CANCER

Pancreatic cancer types can be divided into two larger categories:

Endocrine pancreatic cancer. These are also called pancreatic neuroendocrine tumors (PNETs) or islet cell tumors, and they develop from cells in the endocrine gland of the pancreas. PNETs are rare, accounting for less than 5% of all pancreatic cancer cases (www.hopkinsmedicine.org; www.nih.gov).

Exocrine pancreatic cancer. Disturbances in exocrine cells, which correspond to the exocrine gland and ducts of the pancreas, are the cause of exocrine pancreatic cancer. The different types of exocrine pancreatic cancers accounted for more than 95 percent of all cancers of the pancreas (www.hopkinsmedicine.org; www.nih.gov). They include the following:

- Acinar adenocarcinoma is a very rare form of pancreatic cancer that affects acini, the cells responsible for enzyme production.
- Squamous cell carcinoma appears in the pancreatic ducts and is made by squamous cells, a cell type that is not typically seen in the pancreas.
- Adenosquamous carcinoma is a more aggressive tumor with characteristics of both ductal adenocarcinoma and squamous cell carcinoma.
- Colloid carcinoma consists of malignant cells floating in a gelatinous substance called mucin.
- Intraductal papillary-mucinous neoplasm (IPMN) is a tumor that grows within the ducts of the pancreas.
- Ductal adenocarcinoma (PDAC) occurs in the lining of the ducts in the pancreas. Most of the diagnoses of pancreatic malignancies are for ductal adenocarcinoma.

4. PANCREATIC DUCTAL ADENOCARCINOMA (PDAC)

4.1 EPIDEMIOLOGY AND RISK FACTORS

As more than 90% of pancreatic cancer cases correspond to pancreatic ductal adenocarcinoma (PDAC), epidemiological data of pancreatic cancer are the same for PDAC.

PDAC presents in general at a median age of 70 years. Pancreatic cancer has a complex multistep etiology, where acquired and germline genetic variants are implicated in the failure to repair DNA damage. The most commonly mutated genes are *KRAS*, *CDKN2A*, *TP53*, and *SMAD4/DPC4* (H. Bekkali and Oppong, 2017).

Tobacco smoking is one of the biggest risk factors for pancreatic cancer which, together with alcohol consumption and obesity, constitute the modifiable risk factors of PDAC (H. Bekkali and Oppong, 2017; Rawla et al., 2019). The non-modifiable risk factors include gender, since slightly more men than women are diagnosed; age, due to the fact that the risk of cancer increases with age; and ethnicity, because the risk of pancreatic cancer is considerably higher in black people. Chronic pancreatitis, diabetes mellitus, and *Helicobacter pylori* infections also increase the probability to develop PDAC. Regarding genetic predisposition, it is estimated that up to 10% of PDAC have an inherited basis (H. Bekkali and Oppong, 2017; Rawla et al., 2019).

4.2 DIAGNOSIS AND PROGNOSIS

Early PDAC is usually asymptomatic, and there are still no effective screening strategies. The initial presentations manifest with a range of non-specific symptoms, which further delays the diagnosis. Consequently, 80% of patients are diagnosed with advanced and non-resectable illness (Szymańska, 2018).

It is suspected of pancreatic cancer when patients report a series of non-specific **symptoms** such as jaundice, dark urine, lightening stools, anorexia, malaise, nausea, fatigue or weakness, and mid-epigastric or back pain. Weight loss occurs in 60% of patients as a result of cancer-associated anorexia and/or fat malabsorption due to pancreatic duct obstruction by the tumor (Szymańska, 2018).

No reliable and specific blood **biomarker** has been identified for diagnosis neither PDAC prognosis. The carbohydrate antigen 19-9 (CA 19-9) is the most well-known and useful biomarker for PDAC (Guillén-Ponce et al., 2017; H. Bekkali and Oppong, 2017).

CA 19-9 levels are often increased in the serum of PDAC patients. Its levels normally correlate with the tumor stage, so it is a helpful prognostic biomarker. Therefore, elevated CA 19-9 levels are considered to be an unfavorable prognostic factor (Guillén-Ponce et al., 2017; H. Bekkali and Oppong, 2017; Szymańska, 2018).

Nevertheless, this antigen has low positive predictive value and as it is also expressed in other pancreatic and hepatobiliary diseases, CA 19-9 is not recommended as a screening marker. However, circulating tumor cells, cell-free circulating tumor DNA and exomes can be detected in body fluids and could potentially be used together with CA 19-9 as early diagnostic tools for PDAC (Guillén-Ponce et al., 2017; H. Bekkali and Oppong, 2017; Szymańska, 2018).

Screening is aimed to detect small solid pancreatic tumor irregularities, less than 1 cm, in the pancreatic duct, and pancreatic lesions such as intraductal papillary mucinous neoplasms (IPMNs), pancreatic intraepithelial neoplasias (PanINs), or mucinous cystic neoplasms (MCNs), which usually appear as precursors of PDAC (Guillén-Ponce et al., 2017).

Abdominal ultrasound imaging is often the first procedure performed on patients with ventral pain or jaundice. The ultrasound imaging (US) is an accessible, non-invasive, and low-priced technique that can detect dilation of the ducts or the presence of a pancreatic mass. However, the US imaging shows low accuracy and the sensitivity for detecting PDAC is around 50 to 70% (Guillén-Ponce et al., 2017).

Computed tomography scan or failing that, magnetic resonance imaging (MRI), should be included in the examination of a pancreatic mass. Nonetheless, population screening is not currently feasible because of the low incidence of PDAC and the lack of simple, harmless, inexpensive, sensitive, and non-invasive tests. Until now, screening has predominantly been performed on high-risk individuals with genetic predisposition (H. Bekkali and Oppong, 2017).

Histological confirmation is difficult in small lesions associated with pancreatitis. Biopsy interpretation and histological verification of PDAC are done in cases of

borderline resectable tumors susceptible to chemotherapy (Guillén-Ponce et al., 2017).

4.3 PDAC STAGES

Stratification and classification of pancreatic cancer are usually done at the time of diagnosis. Commonly, PDAC is classified into 4 main categories based on if it can be removed surgically or not and depending on where it is located (www.cancer.gov; www.nih.gov):

4.3.1 Resectable

PDAC can be removed by surgical intervention. Surgery can be done right after diagnosis, or sometimes, an additional treatment (neoadjuvant chemotherapy) is required before surgery. Approximately 10 to 15% of patients are diagnosed at this stage.

4.3.2 Borderline resectable

Tumors at this stage cannot be removed surgically at diagnosis time. However, after neoadjuvant chemotherapy and/or radiation, the tumor becomes smaller and resectable.

4.3.3 Locally advanced

The tumor is mainly located in the pancreatic area but has also grown into or close to arteries, veins, or nearby organs. For that reason, this tumor type cannot be surgically removed. Approximately 35 to 40% of patients are diagnosed at this stage.

4.3.4 Metastatic

The tumor has spread beyond the pancreas and to other organs (liver, lungs, or distant parts of the abdomen). Approximately 45 to 55% of patients are diagnosed at this stage.

As well as this main classification system, doctors also assign the stage of cancer to better design treatment strategies. The two main ways of staging cancers are the TNM system and number system (www.cancer.gov; www.nih.gov).

In TNM stages classification, PDAC tumor is included in one or another group depending on whether it is a primary tumor (T), whether there are lymph nodes with cancer cells (N) and whether cancer has metastasized to other parts of the body (M).

The numeric system classification considers the location and the tumor size:

- Stage 0 or Carcinoma in situ; abnormal cells are found in the pancreas.
- Stage I; localized tumor of 2 – 4 cm of size.
- Stage II; localized tumor of 4 – 6 cm of size.
- Stage III; any tumor size but spread to lymph nodes.
- Stage IV; any tumor size and spread to other parts of the body.
- Recurrent PDAC; a pancreatic tumor that comes back after treatment, in the pancreas or other parts of the body.

4.4 TREATMENT

Usually, the strategy of PDAC treatment is determined by the disease stage at the diagnosis. However, some factors such as patients' overall health can also influence the approach. Most of the available treatments are palliative, i.e. they try to dismiss disease-related symptoms and prolongate survival. Currently, existing therapeutic options are surgery, radiation, chemotherapy, immunotherapy, and the use of targeted drugs (Adamska et al., 2017).

Surgery remains the only chance for curing PDAC, but surgery alone is not enough, and most patients relapse after surgery without additional therapy. Besides, it is only possible when the tumor is well-localized on the pancreas and health status of patients is good, which is an uncommon situation because PDAC diagnosis usually occurs at advanced stages, the tumor is non-resectable and patients present compromised health (Adamska et al., 2017; Tesfaye and Philip, 2019).

4.4.1 Neoadjuvant treatment

Perioperative therapy before surgical treatment is recommended so as to increase resection rates by downsizing the tumor and decreasing surgical complexity. Neoadjuvant therapy is also used to improve the status of patients that suffer from

weight loss or biliary obstruction, and to increase the possibility of including more patients into surgical treatment. Finally, this presurgical therapy is also done to treat the locally invasive disease before resection and micro-metastatic disease at the time of diagnosis. However, neoadjuvant treatment toxicity and systemic effect must be considered, because they can affect the perioperative morbidity and even mortality, especially when the most aggressive chemotherapy protocols are used. Despite these counterproductive effects, neoadjuvant treatment has a benefit/risk positive ratio since it improves survival (Karakas et al., 2018; Maeda et al., 2019; Raufi et al., 2019; Seufferlein and Ettrich, 2019; Tesfaye and Philip, 2019).

Recent randomized controlled trials support the use of neoadjuvant therapy for surgical patients at diagnosis. However, considering the variety of neoadjuvant regimens and different definitions of resectability status, data from each study should be interpreted with caution (Karakas et al., 2018; Maeda et al., 2019; Raufi et al., 2019; Seufferlein and Ettrich, 2019; Tesfaye and Philip, 2019).

4.4.2 Adjuvant treatment

Systemic chemotherapy after resection is accepted as standard-of-care. According to the European Society for Medical Oncology (ESMO) guidelines committee, postoperative adjuvant therapy has been evaluated in two major randomized trials (www.esmo.org).

The first is ESPAC-4, where patients were randomized to receive either gemcitabine alone (monotherapy) or a combination of gemcitabine/capecitabine for 6 months, starting within 12 weeks of surgery (Karakas et al., 2018; Tesfaye and Philip, 2019; www.esmo.org).

The second trial is PRODIGE 24/CCTG PA.6, in which post-resection patients were randomly assigned to receive a modified regimen of FOLFIRINOX (mFOLFIRINOX): 5-fluorouracil (5-FU)/irinotecan/oxaliplatin or, gemcitabine alone (control group) for 6 months, starting at 3-12 weeks after surgery (Karakas et al., 2018; Tesfaye and Philip, 2019; www.esmo.org).

Considering the results from these trials, the standard-of-care for patients after the resection of their pancreatic tumor should be the combined postoperative chemotherapy, instead of gemcitabine monotherapy. Although there is no direct comparison between gemcitabine/capecitabine and mFOLFIRINOX, it seems that

the triplet chemotherapy would be the best treatment for fit patients. In weaker patients, gemcitabine/capecitabine could be the option of choice, and gemcitabine alone should be given to really frail patients (www.esmo.org).

4.4.3 Palliative therapy

Palliative therapy is used to relieve many symptoms of pancreatic cancer patients, from pain or nausea and vomiting to gastric obstructions, among others. In the case of patients with unresectable disease, palliative management of gastric or bowel obstruction and obstructive jaundice remains challenging. Doctors have different modalities, including surgery or endoscopy, to relieve symptoms durably and to improve the patients' quality of life (Adham and Perinel, 2019).

4.4.4 Chemotherapeutic agents

Many therapeutic agents can be used to treat PDAC. In this thesis, we have described in detail those that are considered first-line chemotherapeutic agents, gemcitabine and nab-paclitaxel.

Gemcitabine

Gemcitabine is an antineoplastic anti-metabolite. Gemcitabine is a purine/pyrimidine analog structurally similar to cytarabine that is metabolized intracellularly to two active metabolites, the gemcitabine diphosphate (dFdCDP) and the gemcitabine triphosphate (dFdCTP). The cytotoxic effects of gemcitabine are exerted through incorporation of dFdCTP into DNA with the assistance of dFdCDP, causing DNA synthesis inhibition and induction of apoptosis. It is cell-cycle phase specific (S and G1/S-phases). Gemcitabine blocks an enzyme which converts the cytosine nucleotide into the deoxy derivative. In addition, DNA synthesis is further inhibited because Gemcitabine blocks the incorporation of the thymidine nucleotide into the DNA strand. Gemcitabine is a radiation-sensitizing agent (www.pubchem.ncbi.nlm.nih.gov; www.bccancer.bc.ca/drug-database-site).

Gemcitabine monotherapy was the standard of care for first-line palliative chemotherapy in patients with advanced PDAC until 2011. Gemcitabine is now indicated as first-line therapy for locally advanced (non-resectable stage II or III) or metastatic (stage IV) adenocarcinoma of the pancreas. It is also indicated as

Introduction

second-line therapy for patients who have previously been treated with fluorouracil (www.pubchem.ncbi.nlm.nih.gov).

Nab-paclitaxel (Abraxane®)

Nanoparticle albumin-bound paclitaxel (Nab-paclitaxel) is an anti-microtubule agent that promotes the assembly and stabilization of microtubules, thus inhibiting normal dynamic reorganization of the microtubule network. Paclitaxel induces abnormal bunches of microtubules during the cell cycle and multiple asters of microtubules during mitosis. Nab-paclitaxel is cell cycle phase-nonspecific (www.pubchem.ncbi.nlm.nih.gov).

Paclitaxel is an antineoplastic agent which acts by inhibitor of cellular mitosis. The formulation as nanoparticle protein-bound facilitates the transport of active molecule (paclitaxel) across the endothelial cell through a protein (albumin)-receptor mediated pathway (www.pubchem.ncbi.nlm.nih.gov; www.bccancer.bc.ca/drug-database-site).

Abraxane® is administrated in combination with gemcitabine. Gemcitabine/Nab-paclitaxel combination improve overall survival (OS) compared to gemcitabine alone in advanced PDAC. So, it has been approved as first-line treatment of adult patients with metastatic adenocarcinoma of the pancreas as palliative chemotherapy. Other combination regimens have been included in PDAC treatment besides gemcitabine/Nab-paclitaxel. Among them, FOLFIRINOX, a combination of 5-fluorouracil (5-FU)/folinic acid/irinotecan/oxaliplatin that shows superior efficacy than gemcitabine alone but it has more adverse side-effects so, it is reserved for patients with good performance status. (Chandana et al., 2019).

4.5 HISTOLOGICAL FEATURES

The **normal pancreas** is divided into lobules surrounded by a stroma of loose connective tissue. The lobules are composed of grape-like clusters of exocrine cells, acinar cells, called acini (Figure 2). Secretions from acini flow through ducts and finally into the duodenum through the main pancreatic duct. Embedded within the pancreatic exocrine tissue are the Islets of Langerhans, the endocrine component of the pancreas (Distler et al., 2014; Hruban and Fukushima, 2007; Ottenhof et al., 2009; www.hopkinsmedicine.org).

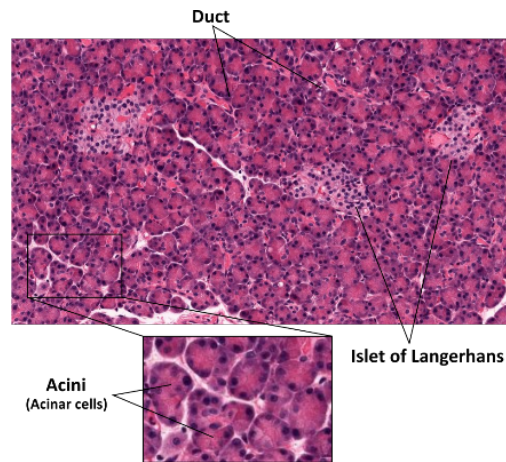


Figure 2. Histology of normal pancreatic tissue. The exocrine pancreas with ducts and acini (grouped acinar cells) is shown, and also the endocrine pancreas with Islets of Langerhans. Image modified and adapted from Johns Hopkins medicine (www.hopkinsmedicine.org)

PDAC starts with genetic changes (mutations) leading to abnormal cell growth. Several microscopic tissue alterations have been recognized as precursor lesions of pancreatic cancer, including PanINs, IPMNs, and MCNs. These cellular changes are caused by either gene mutations or epigenetic changes, and worsened by changes in the stroma. Over time, these events lead to uncontrolled growth and invasive spread (Distler et al., 2014; Hruban and Fukushima, 2007; Ottenhof et al., 2009; www.hopkinsmedicine.org).

PanINs, also called hyperplasia or metaplasia, arise in the pancreatic ducts (Distler et al., 2014). They are smaller than 5 mm, and PanINs are classified into three grades, based on the degree of architectural or cytonuclear abnormalities (Figure 3):

PanIN-1 lesions are composed by columnar epithelial cells with basally located and round nuclei, and abundant supranuclear mucin. PanIN-1 lesions can be flat (PanIN-1A) or with papillary or basally pseudostratified architecture (PanIN-1B) (Hruban and Fukushima, 2007; www.hopkinsmedicine.org). **PanIN-2** lesions may be flat or papillary and are more complex than PanIN-1 lesions. Cytologically, they are characterized by nuclear alterations as loss of nuclear polarity, nuclear crowding, pleomorphism, nuclear hyperchromatism, and nuclear pseudostratification (Distler et al., 2014; Hruban and Fukushima, 2007; Ottenhof et al.,

Introduction

2009; www.hopkinsmedicine.org). **PanIN-3** lesions, also known as high-grade PanINs, can be papillary or micropapillary and they show the greatest degree of dysplasia. These lesions are characterized by loss of nuclear polarity and a basement membrane-oriented cytoplasm. Other nuclear abnormalities like macro nucleoli are also frequent (Distler et al., 2014; Hruban and Fukushima, 2007; Ottenhof et al., 2009; www.hopkinsmedicine.org).

IPMNs and MCNs are mucinous neoplasm larger lesions than PanINs. IPMNs lesions occur in the main pancreatic duct while MCNs are characterized by the presence of spindle-shaped stromal cells (ovarian stroma) and the absence of connection to the pancreatic duct system (Distler et al., 2014; Hruban and Fukushima, 2007; Ottenhof et al., 2009).

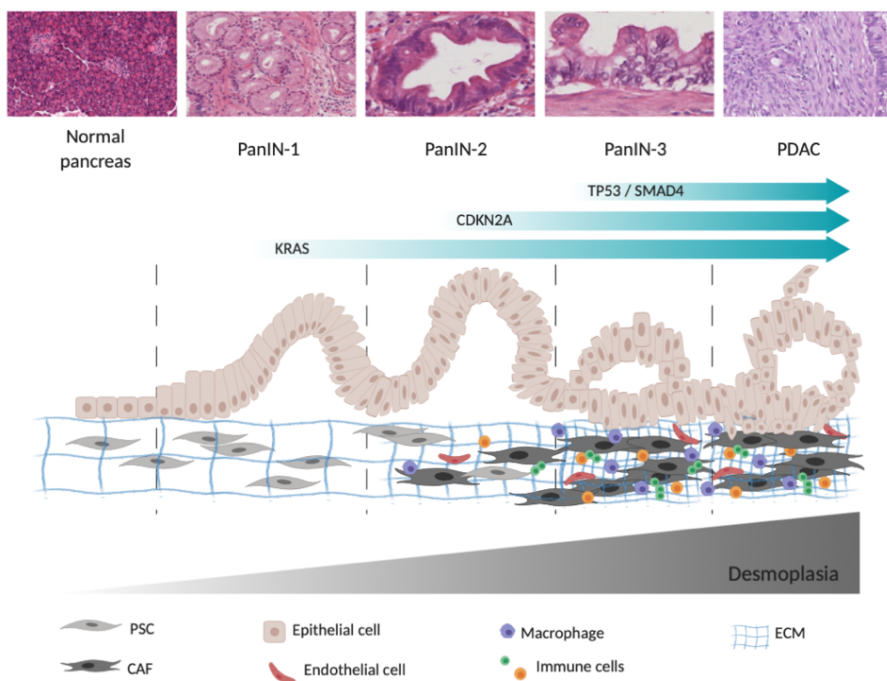


Figure 3. Schematic progression of human PDAC. From normal tissue to PDAC including the most common mutations in tumoral cells and the development of tumor stroma. *KRAS* activating mutations occur at the PanIN-1 stage, followed by the loss of the functional tumor suppressor gene *CDKN2A* at PanIN-2 and the inactivating mutations in *TP53/SMAD4* genes at late PanIN-3 stages. During carcinogenesis, PSCs become CAFs that start to produce a dense ECM and increase the desmoplastic reaction. PSC: pancreatic stellate cell; CAF: carcinoma-associated

fibroblast; ECM: extracellular matrix. Image adapted and modified from Hezel et al. (Hezel et al., 2006).

4.6 BIOLOGICAL TUMOR SUBTYPES

From the last years, tumoral cells in PDAC have been classified depending on their molecular or metabolic features. To describe the different classification methods, we have only considered the cells that have been used in this thesis.

4.6.1 Molecular classification

There are many studies based on a molecular classification. They consider the main mutations (genotype) and/or *in vitro* and *in vivo* behavior of those cells.

In 2011, Collisson *et al.* analyzed the transcriptional profiles of primary PDAC from different studies along with human and mouse PDAC cell lines. With all data, they defined 2 main PDAC subtypes: **classical** and **quasimesenchymal (QM)**. The classical subtype showed a high expression of adhesion-associated and epithelial genes, while the QM had higher expression of mesenchyme-associated genes. The prognostic association exhibited better prognosis for patients with the classical pattern than individuals with QM transcriptional subtype (Collisson et al., 2011).

A few years later, in 2015, Moffitt *et al.* identified tumor and stroma subtypes from a set of 106 primary and metastatic human PDAC samples. They performed virtual microdissection to classify the tumor and the stroma and associated subtypes with prognosis and biological relevance (Moffitt et al., 2015). Stromal classification will be explained later on (point 6.3.1).

Moffitt tumor subtypes were classified into two groups: **classical** and **basal-like**; and tumors with basal-like subtype were associated with a worse prognosis. When they compared their subtypes with the previously described ones by Collisson (Collisson et al., 2011), they found that their classical subtype overlapped with the classical one from Collisson, while Collison's QM subtypes had a mix of genes from basal-like and stroma subtypes in the Moffitt classification (Moffitt et al., 2015). Moreover, the transcriptional analysis revealed a different location of *KRAS* codon mutations between classical and basal-like subtypes; loss of *SMAD4* that is related with tumor growth, in the basal-like subtype, the ones associated with worse prognosis; and *GATA6* overexpression in the classical subtype, a gene that promotes epithelial cell differentiation (Moffitt et al., 2015).

Introduction

In 2016, Bailey *et al.* analyzed the expression pattern of 382 PDAC tumors where 92% of tumors presented *KRAS* mutations, 78% disruption of G1/S checkpoint machinery (*TP53* and *CDKN2A*) and 47% alterations on TGF- β signaling (SMADs, TGFBRs, and ACVRs). Other mutations were founded in less than 30% of the tumors. Taking differential expression of transcription factors and downstream targets of lineage and differentiation processes into account, they resolved four stable classes: **squamous**, **pancreatic progenitor**, **immunogenic**, and **aberrantly differentiated endocrine exocrine (ADEX)** (Bailey *et al.*, 2016). Squamous subtype was associated with worse prognosis possibly by the implication of altered transcriptional activity (*TP53* and *KDM6A*), inflammation, metabolism, ECM, TGF β , and WNT among others. The pancreatic progenitor class was defined by the alteration in *PDX1*, *MX1*, *HNFS*, *FOXAS*, and *HES1* transcription factors, and metabolic alterations. ADEX subtype was identified by the upregulation of the transcription factors involved in exocrine function together with altered genes associated with endocrine differentiation. Finally, the immunogenic class was associated with a significant immune infiltrate and it also shared some components with the pancreatic progenitor subtype (Bailey *et al.*, 2016; Torres and Grippo, 2018). Once again, they compared their subtypes with previous classifications (Collisson *et al.*, 2011; Moffitt *et al.*, 2015) and, three of the subclasses defined by Bailey directly overlap with the Collisson subtypes. QM and classical subtypes from Collisson were renamed as squamous and pancreatic progenitor, respectively. In addition, approximately 50% of squamous subtype tumors correlated with the basal subtype of Moffitt (Bailey *et al.*, 2016).

Recently, in 2019, Yu *et al.* performed a correlation analysis between cell lines and primary tumors across 22 different tumor types. In PDAC, they found a group of cell lines with low correlation with the primary tumors because this group showed a neuroendocrine component. Next, they included the tumor classification described by Moffitt *et al.* to predict PDAC cell lines subtypes. Thus, 15 cell lines were fitted in the basal-like subtypes, 10 cell lines in the classical, and 16 could not be included in any subtypes (Yu *et al.*, 2019).

These results suggest that some cell lines are less appropriate to be used as a model of PDAC tumors than others, and different authors classify PDAC cells differently.

4.6.2 Metabolic classification

Carbohydrates, amino acids, and fatty acids are nutrients that supply energetic and biosynthetic demands to PDAC cells. Common genetic mutations generated during PDAC development drive to abnormal metabolic signaling that, in turn, promotes PDAC development (Li et al., 2019). Constitutive activation of *KRAS* enhances glycolysis and promotes the proliferation of cancer cells (Li et al., 2019; Yao et al., 2020). *P53* mutation also supports glycolysis to avoid apoptosis and autophagy (Li et al., 2019; Yao et al., 2020). To sustain uncontrolled cell proliferation, lipid synthesis is required so lipogenic enzymes, such as FASN (fatty acid synthase) or HMGCR (3-hydroxy-3-methylglutaryl CoA reductase) are frequently overexpressed in PDAC (Li et al., 2019).

These premises support the necessity to classify PDAC focusing on the metabolic features. Some studies based on the metabolic classification are described below.

Daemen *et al.* reported that PDAC cells could be divided into 2 subtypes according to the metabolic profile, **glycolytic** and **lipogenic**. They also defined a **slow proliferative** subtype that had not a specific metabolic profile (Daemen et al., 2015). Therefore, 27% of all cell lines were classified in the glycolytic subtype because they exhibited high levels of glycolytic and serine pathways and their corresponding genes, together with low levels of redox metabolites. In contrast, 39% of total cells were enriched for lipid metabolites and genes involved in lipogenesis and cholesterol synthesis, as well as elevated levels of mitochondrial metabolites. They associated their metabolic subtypes with the molecular classifications from PDAC tumor samples and the results showed that, in general, cell lines within the glycolytic subtype were associated with the QM subtype, whereas most lipogenic cell lines were associated with the classical subtype. Despite the high correlation between glycolytic metabolic subtype and QM molecular subtype mentioned by Daemen *et al.*, quasimesenchymal PANC-1 cells classify as lipogenic instead of glycolytic (Daemen et al., 2015).

In 2020, Karasinska *et al.* developed another classification considering genomic, transcriptomic, and clinical data from 325 PDAC samples (Karasinska et al., 2020). They selected gene sets of glycolysis and cholesterol biosynthesis for the analysis and identified four subgroups: **quiescent**, **glycolytic**, **cholesterogenic**, and **mixed**, considering the expression levels of those gene sets. The glycolytic subtype was characterized by *KRAS* and *MYC* mutations that lead to increased expression of

Introduction

glycolytic genes, while the cholesterogenic subtype showed high expression of sterol synthesis pathway genes such as *SREBF2* (sterol synthesis transcriptional activator). Quiescent cells did not show a high expression of any gene sets and mixed subtypes expressed genes from both gene sets (Karasinska et al., 2020). Finally, they studied the overlap of their metabolic subtypes (Karasinska et al., 2020) with previously established molecular subtypes from Moffit (Moffitt et al., 2015). The glycolytic subtype correlated with the basal-like and the cholesterogenic with the classical (Karasinska et al., 2020).

Pancreatic progenitor subtype described by Bailey *et al.* could be linked with metabolic classification, so gene programs regulating fatty acid oxidation, steroid hormone biosynthesis, drug metabolism, and glycosylation of mucins defined the pancreatic progenitor PDAC tumors (Bailey et al., 2016).

5. TUMOR MICROENVIRONMENT

As we mentioned before, PDAC is histologically characterized by the presence of high content of tumor stroma. All components of the tumor, excluding the tumoral cells, are known as tumor microenvironment (TME) or tumor stroma. These components are the result of the body response towards cancer cells, including the immune system reaction (Kalluri, 2016). Both terms, TME and tumor stroma, can be used interchangeably and when the tumor stroma is highly fibrotic and comprises up to 80% of the tumor mass, it is referred as desmoplasia or desmoplastic reaction (Erkan et al., 2012).

In healthy tissue, pancreatic stellate cells (PSC) or quiescent fibroblasts are spindle-shaped cells that are embedded within a lax fibrillar ECM (Figure 4). In pancreatitis, PanINs, MCNs and IPMNs, those quiescent fibroblasts are accumulated in the pancreas. However, it is during carcinogenesis when PSC are activated and become carcinoma-associated fibroblasts (CAFs) (Whittle and Hingorani, 2019). CAFs are cells with a stellate-shaped morphology, and producers of dense ECM (Figure 4).

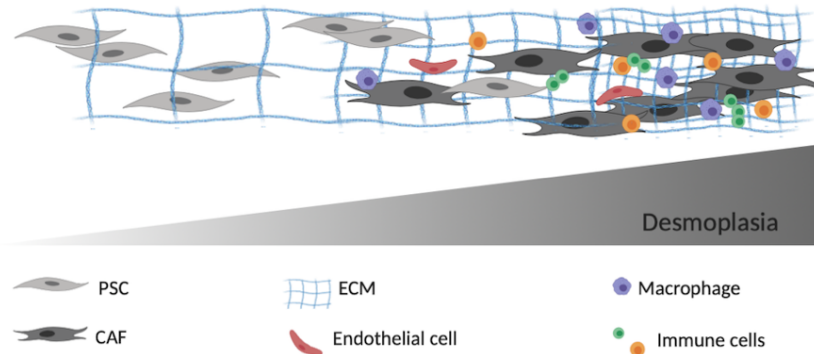


Figure 4. Schematic development of tumor microenvironment, from normal stroma to highly fibrotic tumoral stroma. During carcinogenesis, PSCs are activated and become CAFs that produce a dense and highly fibrotic ECM. CAFs recruit distinct cell types such as immune cells, or endothelial cells to promote angiogenesis.

For tumor formation, tumor cells need to establish a crosstalk with ECM, endothelial and immune cells, as well as carcinoma-associated fibroblasts. These mutual interactions between stroma and tumor cells result in the production of soluble growth factors, chemokines, proteolytic enzymes, and cytokines that support tumorigenesis, angiogenesis, chemoresistance, and metastatic spread of tumoral cells (Erkan et al., 2012).

5.1 TUMOR STROMA COMPOSITION

Immune cells, endothelial cells forming capillaries, ECM, and CAFs constitute the tumor stroma. Although CAFs and immune cells constitute much of the cellular mass in PDAC, ECM proteins secreted by CAFs are also important in the tumor (Kalluri, 2016; Whittle and Hingorani, 2019). All stroma components have been described below excepting CAFs, which deserve special mention (point 6) as being the main subject of study of this thesis.

5.1.1 Immune cells

Immune infiltrate in the TME is composed mainly of lymphocytes (B and T cells), natural killer cells, monocytes/macrophages, eosinophils, mast cells, dendritic cells, and immature myeloid cells (Werb and Pengfei, 2015). These immune cells could have a dual function in cancer since they could act as anti- or pro-

Introduction

tumorigenic factors. The principal function of the immune system in a tumor is to recognize and to eliminate the tumor cells. However, chemokines, cytokines, and soluble growth factors secreted by CAFs can modulate the immune system towards a pro-tumorigenic response (Li et al., 2007).

Monocytes migrate to the tissue following chemoattractant signals, extravasate from the blood vessels, and undergo differentiation into macrophages. Once in the tumor, macrophages differentiate into tumor-associated macrophages (TAMs). TAMs are preferentially retained in necrotic areas where they upregulate hypoxia signaling. Macrophages also release several factors (VEGF, vascular endothelial growth factor; HGF, hepatocyte growth factor; MMP2, matrix metalloproteinase-2; and interleukins) that influence endothelial cell behavior (Li et al., 2007; Veenstra et al., 2018).

Neutrophils, mast cells, and eosinophils are stimulators of angiogenesis, while myeloid suppressor cells induce immune suppression through MMP9 and VEGF production (Li et al., 2007; Veenstra et al., 2018).

Lymphocytes are the white blood cells of the immune system that mediate adaptative immune response by activating antigen-specific effector cells and by recruiting cells of the innate immune system (Veenstra et al., 2018). When lymphocytes infiltrate the tumor are named tumor-infiltrating lymphocytes (TILs) (Veenstra et al., 2018). Different subsets of TILs are present in the TME. T cells are classically divided into either CD8⁺ cytotoxic lymphocytes (CTL) or CD4⁺ T helper (Th). In turn, Th cells are divided into Th1 cells (interferon- γ and tumor necrosis factor- α expression) and Th2 cells (interleukin expression) (Knutson and Disis, 2005). Th1 cells are implicated in the tissue-specific destruction and their activation directly kills tumor cells via release of cytokines that activate death receptors on tumor cells' surface (Knutson and Disis, 2005). Th2-mediated immunity has traditionally related to tumor growth, both by promoting angiogenesis and by inhibiting cell-mediated immunity (Ellyard et al., 2007). Th1 and cytotoxic T cell functionality are generally impaired, whereas the functions of Th2 and Treg cells are enhanced because Treg lymphocytes help tumor cells to evade the immune system (Li et al., 2007; Veenstra et al., 2018).

5.1.2 Endothelial cells

The endothelial cells form the internal layer of blood vessels, acting as a selective permeability barrier between the vessel walls and the blood flow. Endothelial cells, together with pericytes (i.e. specialized mesenchymal cells that recover the blood vessels endothelium), are responsible for angiogenesis. That is the formation, regulation, and maintenance of blood vessels (Hida et al., 2018). Angiogenesis is intimately linked to metastasis, as the delivery of nutrients and oxygen through blood vessels is required for invasive tumor growth and spread to other parts of the body (Hida et al., 2018; Li et al., 2007).

Moreover, tumor endothelium is a regulator of T-cell trafficking. The tumor-associated endothelium can act as an immune barrier to T-cells, inhibiting the effectiveness of immune therapies (Buckanovich et al., 2008).

5.1.3 Extracellular matrix (ECM)

The ECM is composed by glycosaminoglycans (GAGs), hyaluronic acid, growth factors, chemokines, cytokines, antibodies, metabolites and fibrotic proteins such as collagen (type I, type III or type V, among others), fibronectin, and laminin (Kalluri, 2016; Whittle and Hingorani, 2019).

ECM proteins and GAGs contribute to high interstitial pressures that collapse blood vessels and isolate tumor cells from anti-tumorigenic immune cells and chemotherapy (Whittle and Hingorani, 2019). These matrix proteins and GAGs are differentially expressed by distinct CAF populations (Kalluri, 2016; Whittle and Hingorani, 2019). Besides, ECM components are involved in many functional processes such as control of gene expression, cell proliferation, migration, and differentiation, or cell to cell communication, and also structural processes. ECM is also implicated in the maintenance of tissue architecture and integrity through the regulation of rigidity, porosity, spatial arrangement, and orientation (Lu et al., 2012). Normal ECM guarantees a correct homeostasis and harmonic microenvironment. However, when quiescent fibroblasts become activated, they regulate ECM turnover through the expression of ECM-degrading proteases (MMPs), which facilitates the motility and further invasion of cancer cells (Kalluri, 2016).

6. CARCINOMA-ASSOCIATED FIBROBLASTS (CAFs)

6.1 FROM FIBROBLASTS TO CAFs

In normal tissue, fibroblasts are a cell type with spindle-shaped morphology, originated during embryonic development. Most of them come from the primitive mesenchyme, but a small subset are derived from the neural crest (Kalluri, 2016; Sahai et al., 2020). Fibroblasts are non-epithelial, neither immune cells, but their embryonic origin is shared with other mesenchymal lineages, such as adipocytes, chondrocytes, and osteoclasts (Sahai et al., 2020).

Fibroblasts are the cells of the body that can support severe stress thanks to intrinsic survival programs and cellular plasticity (Kalluri, 2016). In normal development and physiology, quiescent fibroblasts are the principal producers of fibrillar ECM, in which they are embedded (Kalluri, 2016).

Phenotypically, they cannot be identified by the presence of specific markers (Kalluri, 2016; Nurmik et al., 2020; Sahai et al., 2020). Although they can be defined by the lack of epithelial, endothelial, or leukocytes markers, this may not be sufficient to exclude other mesenchymal lineages such as pericytes or adipocytes (Sahai et al., 2020). It has been described that CAFs could arise from mesenchymal stem cells (MSC), endothelial cells, liver stellate cells (LSC), PSC, adipocytes, or even resting tissue fibroblasts (Kalluri, 2016).

In response to tissue injury, quiescent or normal fibroblasts become activated. Activated fibroblasts acquire a stellate shape and gain the expression of activation markers such as fibroblast-specific protein 1 (FSP-1 or S100A4), vimentin, smooth muscle actin-alpha (α SMA), fibroblast-activation protein (FAP), PDGF receptor $-\alpha$ and $-\beta$ (PDGFR α , PDGFR β), and desmin (Kalluri, 2016). When activated fibroblasts are associated with tumorigenesis, they are known as carcinoma-associated fibroblasts, hereinafter referred to as CAFs. Despite CAFs acquire the expression of activated fibroblast markers, none of these are specific for fibroblasts, and CAFs may not express all of these markers at the same time, introducing the heterogeneity of this cell type.

CAFs come from local fibroblasts that suffer some kind of dysfunction, which results in proliferation. This phenomenon can be tumor suppressive at initial stages

of tumorigenesis (Kalluri, 2016) but switch towards pro-tumorigenic as the disease progress (Sahai et al., 2020).

Despite there is not a consensus about the origin of CAFs, most authors hold the idea that CAFs result from the activation of resting-tissue fibroblasts (Sahai et al., 2020). During the process in which fibroblasts become CAFs, fibroblasts suffer some phenotypical changes. Epigenetic alterations and changes in non-coding RNA generate the early CAFs phenotypes; the latter phenotypes, which require crosstalk with tumoral cells, are characterized by the up-regulation of pro-tumorigenic and desmoplastic genes (Gascard and Tlsty, 2016).

Many processes can promote CAFs activation. Activating signals include TGF β family ligands and some lipidic mediators that promote the activity of SMAD and SRF (serum response factor) transcription factors, respectively (Sahai et al., 2020). Inflammatory modulators (IL-1, IL-6), JAK-STAT signaling pathway and physical changes in the ECM can also promote CAFs activation (Kalluri, 2016; Sahai et al., 2020).

6.2 CAFs FUNCTIONS

Once CAFs are present in the tumor stroma, they start to act as activated fibroblasts themselves but crosstalk with tumor cells and other cells within the TME may also command CAFs functions (Sahai et al., 2020).

Many scientific reports describe the functions developed by CAFs (Figure 5) and the consequences within a tumor (Kalluri, 2016; Sahai et al., 2020):

CAF s deposit ECM proteins leading to a desmoplastic TME.

They increase tumor stiffness by the action of matrix-crosslinking enzymes. As a consequence, tumor cells activate survival and proliferation pathways that, at the same time, cause mechanical stress. This stress collapses blood vessels, leading to hypoxia and tumor aggressiveness.

CAF s promote tumor motility and invasion via ECM remodeling with MMPs. They also induce metastasis of tumor cells through signals produced by proteins such as periostin and tenascin (Malanchi et al., 2011).

CAF s action supports the immune system evasion by immunomodulatory signaling and by changes in ECM that increase leukocytes infiltration.

Introduction

They undergo metabolic adaptations to provide nutrients for the tumor and other cells of the TME. For example, CAFs suffer an increase in the Warburg effect, catabolic activity, or autophagy.

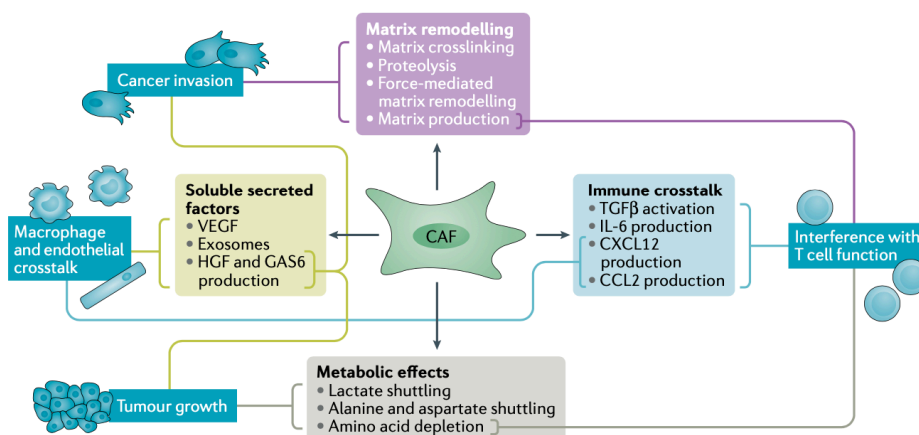


Figure 5. Summary of CAFs' functions and the mechanisms by which they are orchestrated.

Dark blue text boxes indicate the biological functions in which CAFs are involved. Light blue, green, purple, and grey text boxes indicate the processes and mechanisms leading to the control of function. CCL2: chemokine ligand 2; CXCL12: chemokine ligand 12; IL-6, interleukin-6; GAS6: growth arrest-specific protein 6; HGF: hepatocyte growth factor; TGF β : transforming growth factor- β ; VEGF: vascular endothelial growth factor. Image from Sahai *et al.* (Sahai *et al.*, 2020).

Other authors are focused on signaling functions that promote angiogenesis and inflammation (Gascard and Tlsty, 2016; Nurmik *et al.*, 2020). They also refer to drug resistance mediated by CAFs, because they can alter cell sensitivity to apoptosis, secrete proteins that control cell survival, and create physical barriers.

Finally, some research works describe clinical functions so CAFs can be used as prognostic and predictive factors (Berdiel-Acer *et al.*, 2014; Nurmik *et al.*, 2020).

As we mentioned previously, despite the existence of activated fibroblast markers, none of these markers are specific for fibroblasts. Besides, CAFs may not express all of these markers at the same time, introducing heterogeneity in this cell population. CAFs heterogeneity may be due to different marker expression, to different functions, or to the origin of precursor fibroblasts (Kalluri, 2016).

Due to the functional and pathological relevance of the TME in many solid tumors and the presence of CAFs heterogeneity, during the last years, many studies have

focused on the molecular and metabolic classifications of CAFs, the main component of the TME.

6.3 HETEROGENEITY OF CAFs

6.3.1 Activated vs Normal stroma

One of the previous studies based on the stroma characterization was developed by Moffitt *et al.* (Moffitt *et al.*, 2015). They performed virtual microdissection from a set of 106 PDAC human samples to classify the tumor and the stroma and associated subtypes with prognostic.

Primary tumor samples, metastases, and cell lines were clustered into 3 groups by using genes from stromal factors: activated, normal, or absent/low stromal genes. To eliminate samples with absent/low stroma they used a tumor deconvolution strategy and these samples were not included for subsequent analysis. Normal stroma showed high expression of pancreatic stellate cells markers, *ACTA2*, *VIM*, and *DES*. In contrast, activated stroma was characterized by the expression of genes associated with macrophages and tumor promotion (*SPARC*, *WNT* family, and *MMPs*) and *FAP α* . Patients included in the activated stroma cluster had a worse prognosis, which was possibly associated with the presence of *FAP*.

As they also perform a tumor subtypes classification (point 4.6.1), they conducted the survival analysis from all possible combinations of tumor and stroma subtypes. Their two tumor subtypes were found in both stroma subtypes, and patients with basal-like tumor subtype plus activated stromal had the highest hazard ratio.

They described different subtypes across PDAC patients (intertumoral heterogeneity) that may explain the different effects of stroma observed in preclinical models and should be taken into account in stroma-targeted therapies.

6.3.2 Myofibroblast CAF (myCAF) vs Inflammatory CAF (iCAF)

In 2017, D. Tuveson's lab defined the intratumoral heterogeneity. They characterized CAFs from *in vitro* cultures and from mouse and human PDAC tissues, considering the transcriptomic profile and the location within a tumor, regarding tumoral cells (Öhlund *et al.*, 2017).

Introduction

First, they investigated the spatial distribution of α SMA and FAP, considered as myofibroblast and PSC markers, respectively. Here they noticed that most fibroblasts expressed FAP and levels of α SMA, whereas a subpopulation of FAP-positive showed α SMA high expression. These FAP⁺/ α SMA^{high} cells were located surrounding cancer cell clusters, and they were defined as myofibroblast CAF (myCAF).

Afterwards, they studied the presence of CAFs subtypes in co-cultures and confirmed them on PDAC tissues. From those studies, they identified distinct subsets of CAFs. One with α SMA^{high}/IL-6^{low} expression and located proximal to the tumor cells (myCAF), and the other being α SMA^{low}/IL-6^{high}, distantly distributed throughout the tumor and stimulated by paracrine signaling from the tumor compartment. The second ones were named inflammatory CAF (iCAF), according to their properties as cytokine producers.

Transcriptomic profiles of both subtypes revealed differences at gene expression and up or downregulated pathways. myCAF had overexpressed genes (*ACTA2* and *TGF β*) and pathways (smooth muscle contraction and ECM remodeling), periglandular location, and formation linked to juxtacrine interactions with cancer cells. Whereas, iCAF were located far from tumor cells and showed a more secretory profile with overexpression of cytokines (IL-6, IL-11) and chemokines (CXCL1, CXCL2) that stimulate the JAK/STAT pathway in cancer cells (paracrine modulation).

These data confirm the presence of intratumoral heterogeneity of the stroma in PDAC and provides an opportunity to develop therapeutic targets aimed at specific CAFs populations.

6.3.3 myCAF, iCAF and antigen-presenting CAF (apCAF)

In a later study of D. Tuveson's lab, they performed an RNA-seq analysis from human and mouse PDAC tissues (Elyada et al., 2019).

Data obtained from human PDAC confirmed previous results of the group and, besides, they identified a third PDAC CAF subpopulation named antigen-presenting CAF (apCAF). ApCAF were characterized by the expression of major histocompatibility complex (MHC) class II family genes and CD74, for that apCAF

were considered as immunomodulatory fibroblasts that may contribute to immune suppression in the PDAC microenvironment.

In the analysis of the fibroblast-enriched fraction isolated from mice tumors, they distinguished two main clusters of CAFs and an additional small cluster. CAFs of this small cluster were defined as lipofibroblasts, a lineage with lipid droplets (LD) content and with expression of lipid metabolism genes. The analysis of the two main clusters confirmed human results, and they found concordance between human and mouse myCAF, iCAF, and apCAF at gene expression levels and up-regulated pathways.

They also demonstrated that CAFs are a dynamic and interconvertible cell type. In particular, apCAF can revert into myCAF under suitable conditions, meaning that apCAF may require environmental signals to be maintained as a subpopulation.

6.3.4 A – D subtypes

In 2019, Neuzillet *et al.* defined four subtypes of human PDAC CAF (A – D) based on transcriptomic analysis and prognostic association. Therefore, they put forward a classification system (pCAFassigner), taking different expression profiles and functions into account (Neuzillet *et al.*, 2019).

Different selection criteria were used to identify markers for each pCAF subtypes. Periostin (POSTN), myosin 11 (MYH11), and podoplanin (PDPN) were selected as related markers for subtypes A, B, and C, respectively. In the case of subtype D, no marker accomplished the selection criteria. Besides, PDGFR α was highlighted as a potential pan-marker of CAF.

Subtype A CAFs, with POSTN as a characteristic biomarker and low expression of α SMA, were present at the invasive front in human PDAC samples and in the metastatic niche preparation at distant sites. They also looked for an association between pCAFassigner samples and previous tumor and stroma classifications. In subtype A samples, QM tumor cells from Collisson and Moffitt activated stroma signature were more frequent (Collisson *et al.*, 2011; Moffitt *et al.*, 2015). These samples were related to aggressiveness and shorter overall survival (OS).

Subtype B CAFs expressed MYH11 as a pCAFassigner biomarker but also had higher expression of α SMA, revealing myogenic properties that correlate with fibroblasts cluster 2 of Lambrechts' classification (Lambrechts *et al.*, 2018a).

Introduction

PDPN, the specific biomarker of subtype C, was an indicator of an immunogenic tumor and, as a result, samples with subtype C showed prolonged survival.

Finally, samples with a predominant content of subtype D CAFs had the poorest prognosis.

6.3.5 In other cancer types and diseases

CAFs heterogeneity was also studied in other cancer types with highly desmoplastic stroma.

For example, Lambrechts *et al.* described seven clusters of fibroblasts in the normal and the tumor-associated microenvironment of the lung. Fibroblast types express a different combination of collagens, and as different collagens have different roles in the ECM, this suggests functional specialization of CAFs. α SMA, a myofibroblast marker, was higher in cluster 2 that also displayed higher expression of other genes involved in myogenesis (Lambrechts *et al.*, 2018a).

In an ovarian cancer study, CAFs isolated from primary tumors distinguished two main subpopulations: FAP^{high} (FH) and FAP^{low} (FL). Upregulated genes in the FH subset were *TGF β* , *COL11A1*, *SULF1* and inflammatory cytokines, and altered pathways were those related to tumor proliferation, invasion, and therapy resistance. In contrast, in FL subpopulation the upregulated genes were associated with glucose and lipid metabolism and muscle contraction. Moreover, looking at the prognostic association they found that TCGA (The Cancer Genome Atlas program) patients classified within FH or FL subtypes showed differences in illness progression: FH patients showed shorter OS (Hussain *et al.*, 2020).

Another group studied 344 samples of urothelial bladder cancer (UBC) patients and identified 4 CAFs markers (α SMA, FAP, CD90, and PDGFR α/β) with a prognostic association. Samples with FAP expression had the worst prognosis (Mezheyeuski *et al.*, 2020).

Fibroblast classification is also important in non-cancerous diseases as idiopathic pulmonary fibrosis (IPF), a chronic lung disease where fibroblasts play an important role. Specifically, the main feature of IPF is the accumulation of activated myofibroblasts with the corresponding deposit of ECM proteins, generating a fibrotic niche that compromises lung functions (El Agha *et al.*, 2017; Xie *et al.*, 2018). Fibroblast heterogeneity is also recognized in mouse and human

lungs. Various studies based on IPF classify fibroblasts subsets to better understand the roles of fibroblasts in fibrotic diseases.

In 2017, El Agha *et al.* demonstrated a lipogenic to myogenic switch in fibroblasts during fibrosis formation and the reverse process during fibrosis resolution. Gene expression of IPF samples showed elevated fibrotic markers (*ACTA2* and *COL1A1*) and downregulation of lipofibroblast markers (*ADRP*, *CEPBA*, and *PPAR*) compared with healthy donors. They reported that lipofibroblasts serve as a source of activated myofibroblasts in lung fibrosis, where TGF signaling mediates the differentiation of lipofibroblast to activated myofibroblast, whereas *PPAR* γ signaling mediates the opposite event through the activation of lipogenesis, cholesterol metabolism, and adipocyte differentiation pathways. These results evidence the plasticity of fibroblasts, as well as the lack of knowledge regarding their heterogeneity in IPF, apart from the existence of lipo and myogenic populations (El Agha *et al.*, 2017).

Trying to fill this gap, one year later, Xie *et al.* performed a more exhaustive analysis where they classified fibroblasts from normal and fibrotic mouse lungs using single-cell deconvolution methodology. Studying mesenchymal cells, the major contributor in the fibrotic process of IPF, they distinguished between six clusters in normal lungs and seven subtypes in fibrotic lungs. These clusters were: myofibroblast, identified by the expression of classical myofibroblasts markers; *Col13a1* matrix fibroblasts and *Col14a1* matrix fibroblast, both with high expression of genes associated with ECM and cell adhesion; lipofibroblasts, a subset of fibroblast containing lipid synthesis and transport specific gene signature; mesenchymal progenitors, with enrichment in proliferative gene signature; and the mesothelial cells lineage, a source of desmin/CD34 fibroblasts and smooth muscle cells. Finally, an extra *Pdgfrb* high cluster was identified in the fibrotic lung, which differentiates from the myofibroblast cluster by the expression of *Postn* and *Col8a1*, despite it also expressed *Acta2* (Xie *et al.*, 2018).

6.4 CAFs, METABOLISM, AND CANCER

6.4.1 Cancer metabolism

Cancer cell metabolism is defined as the capacity to obtain nutrients from a poor environment and the use of these nutrients to maintain cell viability and to produce energy (Pavlova and Thompson, 2016).

Two principal nutrients that support survival and biosynthesis in mammalian cells are glucose and glutamine. In normal cells or quiescent tumor cells, glucose is degraded by glycolysis, whose final product is degraded again by Krebs cycle (TCA cycle, tricarboxylic acid cycle) followed by oxidative phosphorylation (OXPHOS), providing cells with the amount of ATP they need to grow (Pavlova and Thompson, 2016). However, proliferating cells modify their carbon metabolism towards aerobic glycolysis (the Warburg effect) in which cells consume glucose and produce lactate to obtain energy (ATP), even in the presence of oxygen (Buckley et al., 2017; Menendez and Lupu, 2007; Pavlova and Thompson, 2016). Glutamine provides not only carbon, but also the nitrogen that cells need for the biosynthesis of nucleotides, non-essential amino acids (NEAA), and polyamines (Pavlova and Thompson, 2016).

Fatty acids (FAs) and cholesterol are essential lipidic constituents of biological membranes and lipid rafts. Besides, they can be substrates for energy metabolism or precursors for steroid hormones, respectively (Kuzu et al., 2016; Menendez and Lupu, 2007; Pavlova and Thompson, 2016). In normal cells, FA come from two different sources, the diet (exogenous FA) or the *de novo* synthesis (endogenous), catalyzed by FASN (Menendez and Lupu, 2007). Acetyl-CoA, (acetyl coenzyme A) produced during normal glucose metabolism, together with malonyl-CoA, become FASN substrates for the synthesis of FA (Jones and Infante, 2015; Menendez and Lupu, 2007). In turn, acetyl-CoA is the metabolic link between FA and cholesterol synthesis processes, because it is an essential intermediate in both of them. (Carroll et al., 2018). This metabolic pathway is schematically described in Figure 6.

FASN concentration is very low in non-cancerous cells and highly dependent on nutritional conditions (Menendez and Lupu, 2007). However, overexpression of FASN has been detected in multiple tumor types, including pancreas, colorectal, ovarian, breast, and prostate cancer (Jones and Infante, 2015). Altered expression

levels and mutations of genes involved in the cholesterol homeostasis pathways have also been identified in cancer cells (Kuzu et al., 2016).

Despite proliferating cells obtain energy from aerobic glycolysis, tumor cells possess functional mitochondria and maintain the capacity to conduct OXPHOS. Low levels of ROS (reactive oxygen species) generated during mitochondria respiration contribute to retain the tumorigenic status and also serve as a signal for CAFs to produce metabolites that feed tumoral cells (Pavlova and Thompson, 2016; Pereira et al., 2019).

Tumorigenesis is associated with high lipid production and *de novo* synthesis of cholesterol. Increased consumption of glucose by the tumor correlates with poor prognosis (Pavlova and Thompson, 2016) and high levels of FASN in patient tumor tissues are present at later stages of disease and associate also with poor prognosis (Buckley et al., 2017; Jones and Infante, 2015).

A lipogenic phenotype and glycolytic metabolism constitute a malignant phenotype, allowing metabolism targeting to battle cancer (Menendez and Lupu, 2007).

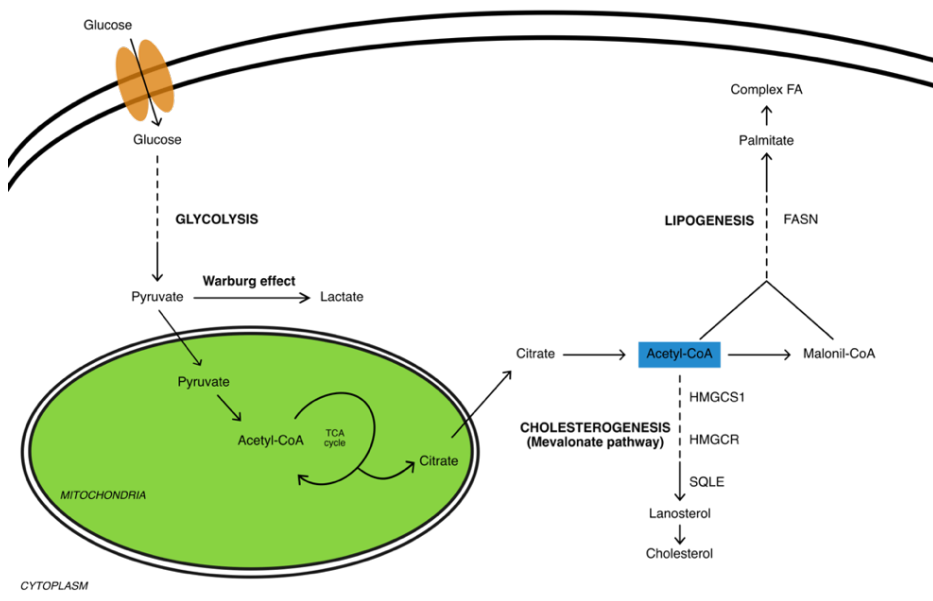


Figure 6. Cellular metabolism of glucose and its connection with fatty acids and cholesterol synthesis. In normal cells, most of the glucose is degraded to pyruvate by glycolysis. This pyruvate goes into the mitochondria and is transformed to citrate as a result of the TCA cycle,

Introduction

and citrate is then exported to the cytoplasm and metabolized to acetyl-CoA, which is a common substrate of cholesterologenesis and lipogenesis (blue box). In cancer cells, most of the glucose is converted to lactate (Warburg effect), but some can also be converted in pyruvate, which follows the same steps as in normal cells. Discontinuous arrows: many steps are involved in the process; acetyl-CoA: acetyl-coenzyme A; TCA cycle: tricarboxylic acid cycle; HMGCS1: 3-Hydroxy-3-Methylglutaryl-CoA Synthase 1; HMGCR: 3-hydroxy-3-methylglutaril-CoA reductase; SQLE: squalene monooxygenase; FASN: fatty acid synthase; Complex FA: complex fatty acid.

6.4.2 PDAC metabolism

In light of the link between metabolic alterations and cancer development described above, the metabolic changes involved in PDAC development will be commented on in the present chapter.

As in many other cancer types, pancreatic cancer cells have to activate multiple mechanisms to obtain enough fuel and grow. In addition to genetic and epigenetic alterations, the development of PDAC involves reprogramming of glucose, amino acids and lipid metabolisms (Qin et al., 2020; Swierczynski et al., 2014). Autophagy is another cellular process by which cells get energy and metabolic substrates, i.e. through the recycling of intracellular components. Moreover, autophagy controls ROS production and maintains OXPHOS, promoting PDAC progression (Qin et al., 2020).

As a result of increased glycolysis, most of the generated pyruvate is metabolized to lactate, and some is used in the TCA cycle to produce citrate and further in FA biosynthesis (Figure 6) (Swierczynski et al., 2014). Consequently, many enzymes of *de novo* fatty acid and cholesterol synthesis pathways are upregulated in pancreatic cancer cells, including FASN and HMGCR among others (Guillaumond et al., 2015; Qin et al., 2020).

Cholesterol is *de novo* synthesized from cytoplasmic acetyl-CoA by the mevalonate pathway and HMGCR is the rate-limiting enzyme in the pathway (Figure 6) (Sunami et al., 2018; Swierczynski et al., 2014). Apart from *de novo* synthesis, pancreatic cancer cells can obtain cholesterol by endocytosis of low-density lipoproteins (LDL) through the LDL receptor. HMGCR and LDL receptors are both targets of sterol regulatory element-binding protein 2 (SREBP-2), and both are overexpressed in PDAC (Guillaumond et al., 2015; Sunami et al., 2018).

High tumor-hypoxia present in PDAC alters cancer cell metabolism by stimulating a cell signaling network that results in the activation of the SREBP-1c transcription factor, which binds to FASN promoter and induces FASN and other lipogenic genes (Sunami et al., 2018; Swierczynski et al., 2014). Prognostic association of metabolic-related molecules revealed that patients with overexpression of FASN, both in tumor and in serum, have a poor prognosis and lower response to gemcitabine treatment (Sunami et al., 2018; Swierczynski et al., 2014). High expression of SREBP-1 is associated with shorter OS (Sunami et al., 2018).

Other metabolic molecules such as caveolins, which are components of the lipid rafts, or cyclooxygenase 2 (COX-2), an enzyme of lipid metabolism, play important roles in PDAC development. Overexpression of CAV-1 and COX-2 is associated with poor PDAC differentiation status and greater invasiveness and angiogenesis, respectively (Swierczynski et al., 2014).

FASN, HMGCR, or other lipogenic enzymes could be viable candidates for pharmacological treatment in PDAC. Preclinical studies of pharmacologic inhibition of FASN and different mevalonate pathway enzymes decreased tumor growth (Guillaumond et al., 2015; Swierczynski et al., 2014). However, in the case of *in vitro* inhibition, pancreatic tumor cells with glycolytic phenotype seemed to be sensitive to an inhibitor of glycolysis, whereas most of the cells with lipogenic phenotype were not affected by FASN inhibitor. These piece of evidence supports the necessity to refine the signature and identify subsets (Buckley et al., 2017).

6.4.3 Metabolic crosstalk within PDAC microenvironment

Metabolic changes on cancer cells and microenvironment modulation by them assist tumor growth, and most tumorigenic contexts are associated with the depletion of nutrients from the TME (Li et al., 2019; Pavlova and Thompson, 2016; Sunami et al., 2018). Tumor cells promote metabolic changes to themselves and also modulate stromal cells, which can send signals to cancer cells and vice versa (Pavlova and Thompson, 2016; Sunami et al., 2018). Understanding the molecular crosstalk between tumor and the surrounding stroma is essential to improve metabolic targeting strategies (Beloribi-Djefafia et al., 2016; Sunami et al., 2018).

Aberrantly activated oncogenes and/or loss of tumor suppressors maintain cancer cells in a state through which they can obtain nutrients from the TME to promote tumor proliferation (Pavlova and Thompson, 2016).

Introduction

PDAC cells can uptake collagen fragments from the TME to produce free amino acids that serve as a substrate for the TCA cycle (Li et al., 2019). Pancreatic tumor cells also induce autophagy in PSC and CAFs which, in response, secrete alanine to feed tumor cells, in order to provide substrates for the TCA cycle and fatty acid biosynthesis (Li et al., 2019; Qin et al., 2020; Sahai et al., 2020).

Lipids can be tumor-stroma crosstalk mediators. Therefore, FAs induce metabolic reprogramming of CAFs and inflammation in the stroma which, at the same time, induce tumor malignancy (Auciello et al., 2019; Beloribi-Djefaflija et al., 2016; Hata et al., 2017; Qin et al., 2020).

In response to tumor signals, CAFs undergo a metabolic modification (Auciello et al., 2019; Li et al., 2019; Qin et al., 2020; Santi et al., 2015; Sunami et al., 2018). CAFs secrete glycolysis metabolites such as pyruvate and lactate (Qin et al., 2020). This extracellular lactate, structural proteins or glycolytic enzymes excess is used by surrounding cancer cells (reverse Warburg effect) in OXPHOS (Li et al., 2019; Qin et al., 2020; Santi et al., 2015; Sunami et al., 2018). The metabolic change is also characterized by the downregulation of genes involved in lipid storages, which causes abundant secretion of lipids that promote PDAC proliferation and migration pathways (Auciello et al., 2019). In the metabolic ambit, CAFs also have a dual activity. On one hand, they suppress tumor growth by creating a nutrient-poor environment. On the other, CAFs support tumor growth by secreting factors that assist PDAC cells (Auciello et al., 2019).

The permanent demand for nutrients and lack of supply in growing tumors favor the appearance of hypoxic areas (Pavlova and Thompson, 2016). Hypoxic microenvironment activates specific molecular programs to supplement the missing fatty acids (Sunami et al., 2018), but tumor cells can also import them from the surrounding environment. Stromal activation of FASN may compensate for the hypoxia status in the malignant phenotype promoting carcinoma *in situ* (Menendez and Lupu, 2007; Pavlova and Thompson, 2016).

Adipocytes, the main components of adipose tissue, can also be in the tumor stroma. Adipocytes exchange FA with bone marrow-derived prostate cancer cells (Beloribi-Djefaflija et al., 2016; Qin et al., 2020). In PDAC, they promote cancer cell proliferation through glutamine transfer (Meyer et al., 2016).

Immune cells that are present in the TME, specifically TAMs, also promote cancer progression by increasing glucose metabolism (Li et al., 2019; Qin et al., 2020). In PDAC, TAMs communicate with cancer cells via paracrine signaling and induce aerobic glycolysis on them (Qin et al., 2020). In ovarian cancer, Goossens *et al.* confirmed the metabolic crosstalk between tumor cells and TAMs. They demonstrated that cancer cells induce cholesterol efflux and depletion of lipid rafts from macrophages. In particular, ovarian cancer cells produce hyaluronic acid and Th2 cytokines (IL-4) that induce cholesterol depletion from TAMs and promote tumor development, while Th1-mediated signaling (IFN γ) assists pro-inflammatory and immunostimulatory states on TAMs. TAMs suffer a dynamic reprogramming during tumor development with the upregulation of cholesterol efflux pathways in established tumors (Goossens et al., 2019).

Considering the link between metabolism and cancer development, the tumor-stroma interactions, and the molecular heterogeneity (point 6.3) of CAFs reported in solid tumors, further studies to perform metabolic profiling of CAFs are needed. Despite there is not specific metabolic classification in cancer, some studies (El Agha et al., 2017; Xie et al., 2018) consider the presence of metabolic subtypes of fibroblasts in other pathologies (point 6.3.5). In

Figure 7, we have summarized the main mechanism involved in molecular and metabolic CAFs heterogeneity reported in solid tumors, which has to be considered to precise profiling of CAFs. Such profiles should take the identity and functions, both temporally and spatially, into account, so as to better design and develop stroma-targeted treatments (Pereira et al., 2019).

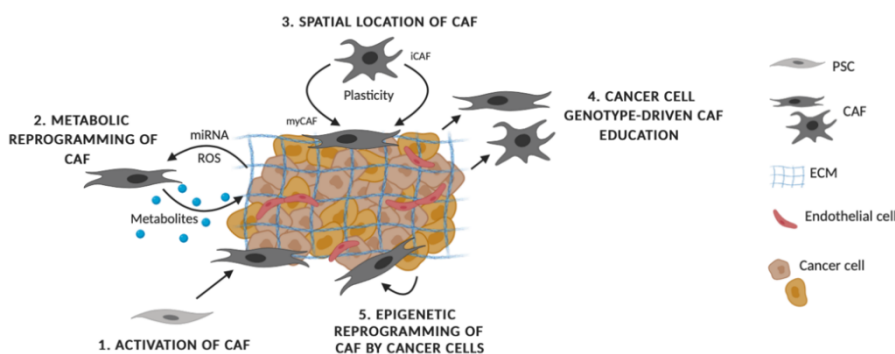


Figure 7. Mechanisms of CAFs heterogeneity. (1) CAFs commonly come from PSCs but can originate from different cell types and, therefore, exhibit a range of activation states that can

Introduction

be further stimulated to alter cancer development. (2) Metabolic crosstalk between CAFs and tumor cells induces the production of energy-rich metabolites by CAFs to feed the tumor cells. (3) Different localization of CAFs within the TME with respect to tumor cells leads to differences in the signals that CAFs receive, resulting in distinct CAFs subpopulations. (4) The molecular heterogeneity of cancer cells drives differences in CAFs subpopulations via paracrine signaling. (5) Cancer cells secrete factors that can reprogram the epigenome of CAFs. PSC: pancreatic stellate cells; ECM: extracellular matrix; iCAF: inflammatory CAFs; myCAF: myofibroblastic CAFs; ROS: reactive oxygen species. Image adapted from Pereira *et al.* (Pereira *et al.*, 2019).

In light of all these data, targeting or modulating metabolic tumor-stroma crosstalk may emerge as novel strategies to fight against cancer. (Goossens *et al.*, 2019; Sherman *et al.*, 2014; Sunami *et al.*, 2018).

7. CANCER TREATMENT STRATEGIES TARGETING THE TUMOR STROMA

Cancer therapies usually target tumor cells while skipping the effect over the tumor microenvironment. However, tumor stroma responds to therapies by inducing therapeutic resistance (Valkenburg *et al.*, 2018). The mechanisms by which the tumor stroma compartment can induce resistance to therapy are many (Figure 8) and depend on the activation status of such stroma (Valkenburg *et al.*, 2018).

After any type of anticancer therapy administration, the tumor stroma can limit the access of therapeutic agents to the corresponding target due to fibrosis, high interstitial pressure, or as a result of drug metabolism by stromal enzymes, such as cytochrome P450 (CYP) (Figure 8a). After radio or chemotherapy cycles, fibroblasts increase integrin expression and secretion of soluble factors that may induce chemoresistance in cancer cells (Figure 8b). In the case of therapies targeting specific pathways, the organism usually responds by activating other supplementary pathways resulting in adaptation, resistance to therapy or illness recurrence. Thus, tumor stroma assists cancer cells in all these processes (Figure 8c). Hormone dependent cancers, such as prostate or breast cancer, usually respond to androgen or estrogen therapies, respectively. The loss of androgen receptor (AR) in the stroma of prostate cancer correlates with cancer progression (Figure 8d). However, concerning breast cancer, CAFs reduce the expression of estrogen receptor (ER) on cancer cells, which correlates with resistance to hormone antagonists (Figure 8d). Immune therapies that target cancer cells may be blocked by the organization and composition of the ECM, which plays a role in

regulating the infiltration of immune cells through the stroma (Figure 8e) (Valkenburg *et al.*, 2018).

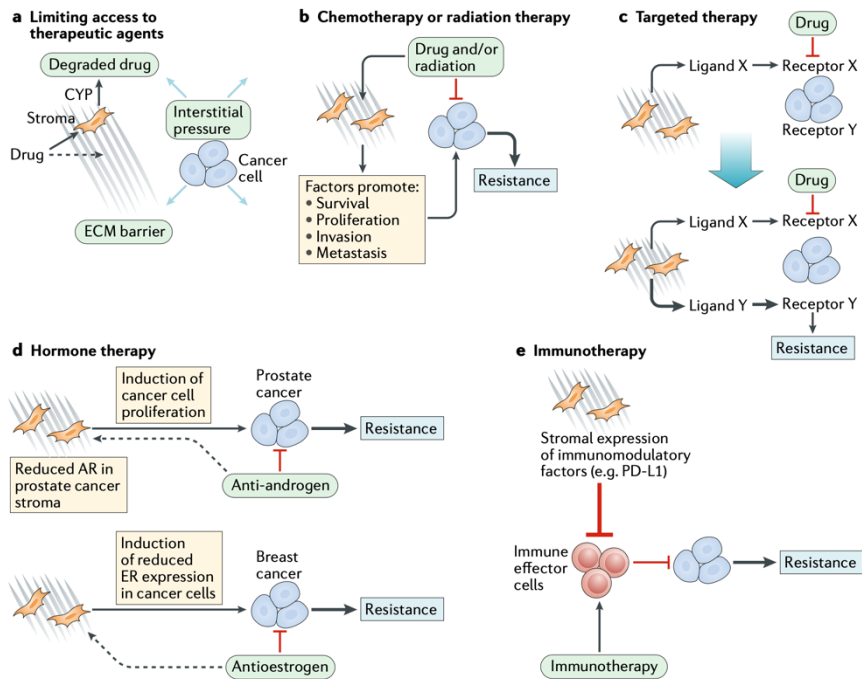


Figure 8. Mechanism of stroma-mediated chemoresistance. After therapy, the stroma promotes resistance to treatment and disease recurrence by different mechanisms. (a) Limited access to therapeutic agents via creating an ECM barrier and/or increasing the interstitial pressure (IP) that blocks drug diffusion and promoting drug metabolism by stromal cytochrome P450. (b) Radiated CAFs secrete growth factors, cytokines, and chemokines that activate specific pathways on cancer cells that promote therapy resistance. (c) Targeted inhibition of specific pathway results in the stromal activation of supplementary pathways. (d) In hormone-dependent cancers such as prostate or breast cancer, changes in hormone receptors expression mediate resistance. In prostate cancer, decreased AR expression in the stroma leads to resistance, while in breast cancer, the stroma causes a decrease in ER expression in cancer cells, leading to resistance to antihormonal therapies. (e) CAF, MSC, and ECM suppress the activation of the immune response. ECM: extracellular matrix; CAF: carcinoma-associated fibroblasts; AR: androgen receptor; ER: estrogen receptor; MSC: mesenchymal stem cells. Image obtained from Valkenburg *et al.* (Valkenburg *et al.*, 2018).

Novel anticancer therapies should target both tumor cells and the microenvironment. To improve the results of cancer treatments, specific cell types

and/or targetable molecules in the stroma should be identified, as well as performing a proper patient stratification into treatment subgroups, considering clinically relevant molecules of stromal origin, which would predict the effectiveness of specific therapies (Valkenburg et al., 2018).

Stroma-targeted therapies can be directed towards PSCs, inhibiting their activation, or towards CAFs, modulating their activity, or blocking the crosstalk with the tumor. The stromal immune response can also be targeted just like the non-cellular component of the stroma, the ECM (Chen, 2012).

7.1 SELECTIVE STROMA DEPLETION

Previous pieces of evidence that PDAC patients and mice do not respond to immunotherapies such as anti-cytotoxic T-lymphocyte-associated protein 4 (anti-CTLA-4) and anti-programmed cell death 1 ligand 1 (anti-PDL-1), together with the fact that stromal cells expressing FAP mediate immunosuppression in a murine mouse model, lead Feig *et al.* to develop a modified KPC mouse model. They inserted in the KPC line a bacterial artificial chromosome (BAC) transgene containing a modified *Fap* gene that drives the expression of the human diphtheria receptor (DTR). Diphtheria toxin administration to transgenic mice (KPCD) eliminated more than 50% of the tumoral FAP content, and tumor growth slowed down. When they combined FAP depletion with immunological therapy (anti-CTLA-4 or anti-PDL-1) the tumor growth was diminished even more. FAP immunosuppression signaling is linked to CXCL12 (chemokine ligand 12), and therefore, its receptor CXCR4 (chemokine ligand-receptor 4). To check this connection, they administered AMD3100, a CXCR4 inhibitor, to mice. AMD3100/anti-PDL-1 combination increased AMD3100 antitumor activity while there were no differences in the AMD3100/anti-CTL-4 combination. In conclusion, FAP stromal cell depletion or the inhibition of the CXCL12-CXCR4 axis uncovers the antitumor activity of anti-CTLA-4 and anti-PDL-1. Nonetheless, anti-CTLA-4 was effective when combined with FAP depletion (Feig et al., 2013).

Following the strategy of FAP depletion, Lo *et al.* designed a plan of selective elimination by using an immunotherapy strategy mediated by CAR T cells targeting FAP⁺ stromal cells. They not only studied the effects of FAP stromal depletion *per se* over tumor development, but also the improvement of drug delivery on weakly immunogenic but highly desmoplastic solid tumors. The tumor infiltrated FAP-CAR

T cells depleted FAP positive stromal cells, and reduced collagen and hyaluronic acid of the stroma, so desmoplasia was disrupted and tumor growth diminished. The combination therapy with FAP-CAR T cells and gemcitabine showed an additive anti-tumor activity in PDAC (Lo et al., 2015).

From preliminary data for a binary classification based on FAP and α SMA expression, in 2014, Özdemir *et al.* studied the effect of α SMA⁺ myofibroblast depletion in tumor development and mice survival. The initial strategy for selective elimination of fibroblast used PKT mice, which developed spontaneous PDAC. PKT mice were then crossed with α SMA-tk transgenic mice (PKT; α SMA-tk). Upon systemic ganciclovir (GCV) administration, cells that expressed *Acta2* were selectively depleted. This selective elimination resulted in more invasive, undifferentiated, and necrotic tumors and a significant reduction in survival. Researchers also checked the same effect over other mice models, and they observed a reduction in survival in all of them. These findings correlate with low α SMA content in patients' samples that also showed worse survival. Besides the effect on survival, they also checked the consequences of myofibroblast depletion on collagen and ECM organization; angiogenesis, hypoxia, and epithelial-to-mesenchymal transition (EMT); gemcitabine efficacy; and tumor immunity. Myofibroblast-depleted tumors revealed a modified ECM without changes in hyaluronic acid content, but decreased vimentin, and the cellular composition of the stroma revealed a reduction in FSP-1 mesenchymal cells, while FAP⁺ cells remained unchanged. α SMA-depleted tumors were more hypoxic, acquired the EMT program but vessel permeability and perfusion were not altered, and gemcitabine efficacy was not improved in terms of overall survival. Tumor immunity gene signature was downregulated, but increased CTLA-4 expression. Hence, treatment with anti-CTLA-4 antibodies rescued the phenotype of myofibroblast-depleted tumors and attenuated PDAC progression (Özdemir et al., 2014).

7.2 EXTRACELLULAR MATRIX (ECM) DEGRADATION

The ECM is one of the major components of the tumor stroma and is involved in tumor development and chemoresistance. Different research works have been developed through targeting different components within the complex ECM by different strategies.

Introduction

PDAC is one of the cancer types with the highest ECM content, which is composed by high hyaluronic acid (HA) levels. The same features were reproduced in tumors of KPC mice, the transgenic mouse model used by D. Tuveson's group and Hingorani's Lab (Jacobetz et al., 2013; Provenzano et al., 2012). In their works, both groups enzymatically depleted HA content by PEGylated human recombinant PH20 hyaluronidase (PEGPH20). HA depletion was linked to decompression of intratumoral vessels (decrease the interstitial fluid pressure, IP) and, as expected, mice receiving gemcitabine after PEGPH20 showed increased concentrations of the active metabolite of gemcitabine, without changes in pharmacokinetic properties. The comparison between monotherapy or the combination of PEGPH20/gemcitabine demonstrated a higher reduction of tumor growth in the combination compared to gemcitabine alone, and PEGPH20 monotherapy did not modify tumor growth. Finally, they evaluated possible toxic effects of all agents in monotherapy or in combination, and there were no effects regarding the lethality of KPC mice. However, the extended PEGPH20/gemcitabine improved overall survival above gemcitabine alone (Jacobetz et al., 2013; Provenzano et al., 2012).

The study developed by Provenzano *et al.* provided extra data of collagen content and distribution, that both decreased after combined therapy (PEGPH20/gemcitabine), possibly as a consequence of collagen-secreting cells elimination. They also evaluated the effects in liver metastasis and responses were similar, so the combination regimen effectively treated the primary tumor and the metastatic sites (Provenzano et al., 2012).

These previous promising results led PEGPH20 to clinical trials. Phase-II trials demonstrated a benefit in HA-high PDA patients (Hingorani et al., 2018). However, phase-III trial with the multitherapeutic PEGPH20 regimen failed (Tempero et al., 2020).

Later, P. Provenzano collaborated in another study of ECM targeting. In this case, it consisted of a stroma reengineering strategy to normalize TME with an antifibrotic agent, the halofuginone (HF). HF is a potent antifibrotic agent that blocks the TGF β signaling via inhibition of SMAD2 and SMAD3 phosphorylation. As a result, it decreases PSC activation, reduces fibrosis, disrupts physical barriers, reestablishes blood vessels function and IP, facilitating drug delivery, and promotes infiltration of immune cells. KPC tumors (*in vivo* mouse models) also use the TGF β signaling pathway to promote fibrosis and dense ECM deposition. As a

consequence, the use of HF against KPC tumors caused inhibition of α SMA and fibrosis-related genes expression, disrupting transport barriers without an increase in vessel density, which improved drug distribution. Particularly, HF increases the susceptibility of tumor cells to gemcitabine and promotes the distribution of immune therapies and antitumor immune cells populations. The same antifibrotic effects were seen *in vitro*, in mice and human cells. HF also inhibited the proliferation of pancreatic carcinoma cells at higher concentrations, so it showed a dual-action, targeting the stroma and also primary tumor cells (Elahi-Gedwillo et al., 2019).

Due to the fact that immunotherapy can also be blocked by the TME, some works used stroma degradation strategies to facilitate the delivery of immunological agents. For example, oncolytic virus delivery is also limited by the stromal barrier that blocks viral penetration and spread. The elimination of FAP⁺ stromal population with a FAP-targeting Bispecific T-cell Engager (FBiTE) improves oncolytic adenoviral (OAd) spread and therapeutic activity using the OAd-FBiTE construction (De Sostoa et al., 2019).

These studies support the hypothesis that improvement of pharmaco-delivery through depletion of specific stromal components may improve the therapeutic response (Elahi-Gedwillo et al., 2019; Hingorani et al., 2018; Jacobetz et al., 2013; Provenzano et al., 2012). However, not all stroma-targeting approaches have demonstrated clinical benefit to date. One phase Ib/II trial (IPI-926/gemcitabine) was stopped early because of adverse effects, while a separate trial (IPI-926/FOLFIRINOX) suggested therapeutic benefit in preclinical models (Elahi-Gedwillo et al., 2019; Mpekris et al., 2017; Zhao et al., 2018).

7.3 BLOCKING THE TUMOR-STROMA CROSSTALK

In tumor tissues, cancer cells and TME form a network where the crosstalk between cancer cells and CAFs contributes to CAFs activation, cancer growth, and progression and evasion from cancer therapies. Many research works are focused on blocking this communication between tumor and stroma as a possible cancer therapy.

Sonic Hedgehog (SHh) is one of the most studied pathways in the field of blocking the tumor-stroma crosstalk as an anticancer therapy. Mechanistically, SHh promotes stromal desmoplastic reaction, mediated by the paracrine signal induced

Introduction

by tumoral cells. The union Hh ligands-Hh receptor represses the transmembrane protein Smoothed (Smo), causing the activation of Gli family transcription factors. SHh signal is increased in human and mouse pancreatic tumors, while Gli activity is restricted to the stromal compartment (Lee et al., 2014; Mpekris et al., 2017; Olive et al., 2009; Rhim et al., 2014; Zhao et al., 2018). SHh inhibitors act by blocking this paracrine signal. Different inhibitors have been tested in various studies; IPI-926 (Olive et al., 2009), Vismodegib (Mpekris et al., 2017) and Cyclopamine (CPA) formulated with a polymeric micelle (M-CPA) (Zhao et al., 2018). These are Smo inhibitors used in PDAC mouse models. In general, all of them demonstrated reduction of myofibroblast (α SMA) proliferation, lower levels of ECM components (hyaluronan and collagen), higher blood vessel perfusion leading to a better chemotherapy diffusion and, consequently, tumor volume reduction and better overall survival (Mpekris et al., 2017; Olive et al., 2009; Zhao et al., 2018). The main difference among these studies lies in the fact that in the CPA one, all formulations tested showed moderate reduction of α SMA population, but M-CPA/PTX (paclitaxel) combination dramatically reduced the expression of FAP, HA and lysyl oxidase, a stromal stiffness mediator, significantly extending animal survival. These results agree with previous clinical studies, where high α SMA expression in PDAC correlated with high collagen deposition and longer survival, while FAP upregulation predicted shorter survival (Zhao et al., 2018).

Despite these promising data, SHh inhibitors produced disappointing results in other studies, where stroma ablation created invasive tumor phenotypes and reduced animal survival. Lee *et al.* investigated the effect of genetic and pharmacologic inhibition of SHh pathway in PDAC formation and survival. They generated 3 different mice models with SHh ablation, and they found that genetic elimination or pharmacologic inhibition of SHh signal induced acceleration of PDAC and its precursor lesions formation, and increased proliferation of epithelial cells (Lee et al., 2014). Rhim *et al.* performed a deeper study to further understand the opposite results to those obtained by themselves (Olive et al., 2009) a few years before. Briefly, in this case, they concluded that short-term exposure to SHh inhibitor had a beneficial effect on drug delivery, while chronic exposure was translated into negative effects, mediated by less differentiated and more aggressive tumors (Rhim et al., 2014). These data prove beyond reasonable doubt that some components of the stroma can block tumor growth.

The investigations commented on above were also translated into clinical trials on PDAC patients, where SHh inhibitors did not provide them with any survival benefits over the standard therapies (Catenacci et al., 2015; De Jesus-Acosta et al., 2014; Ko et al., 2016).

Galectin-1 (Gal-1), a family of beta-galactoside-binding proteins implicated in modulating cell-cell and cell-matrix interactions, is highly overexpressed in PDAC stroma and regulates different processes during tumor progression (Orozco et al., 2018). To evaluate the potential of targeting Gal-1 to treat PDAC, Orozco *et al.* designed a combination of a genetically engineered mouse model and a human-based experimental system in which Gal-1 was silenced. A *Kras*-driven mouse model and a co-injection model of epithelial cells and hPSC (human PSC) showed, both, that Gal-1 ablation impeded PDAC tumor progression by blocking the paracrine tumor-stroma signaling, and generated tumors with less activated stroma by blocking the autocrine loop. In more detail, the absence of Gal-1 impaired PDAC initiation, progression, and liver metastasis; diminished stroma activation (less α SMA⁺ CAF) and tumor vascularization; and enhanced immune cells recruitment. These results offer a new therapeutic strategy by targeting Gal-1 alone or in combination with other therapeutic modalities (Orozco et al., 2018).

Focal adhesion kinases (FAK), a family of protein tyrosine kinases, modulate the activity of both epithelial cells and stromal cells. FAK signaling induces cytokine secretion and promotes fibrotic and immunosuppressive TME, which protects tumors from the immune response. Therefore, FAK expression is upregulated in PDAC tissue and mediates the crosstalk with the stroma. Consequently, pharmacologic inhibition of FAK (VS-4718) reduced fibrosis by decreasing collagen deposition and the number of FAP⁺ and α SMA⁺ fibroblasts, and also impaired disease progression in a PDAC mouse model. In turn, the genetic ablation of FAK also altered cell proliferation, fibrosis deposition, and immune cell infiltration. The combined therapy of VS-4718 plus gemcitabine or immunotherapeutic agents (anti-PDL-1 or anti-CTLA-4) improved the efficacy of gemcitabine plus anti-PDL-1, but did not modify the effectiveness of anti-CTLA-4 (Jiang et al., 2016).

The last example that we consider worth mentioning was developed by our research group in colorectal cancer (CRC). With it, we demonstrated the significance of TGF β signaling to tumor development and chemoresistance, and the benefit of targeting the crosstalk. We concluded that the combination of TAK1

Introduction

(TGF β -activated Kinase 1 protein)/TGFBR1 inhibitors decreased ECM deposition and, as a result, tumor cells became more sensitive to chemotherapy and reduced their metastatic potential and CAFs recruitment. TAK1/ TGFBR1 inhibitors blocked the IL-1 β and TGF β 1-mediated conversion of resident fibroblasts into CAFs by inhibiting the secretion of pro-tumorigenic and proinflammatory soluble factors. Instead of inhibiting the conversion to CAFs, the combination also altered the expression pattern of CAFs that presented low levels of FAP and IL7R but maintained the myofibroblast profile. In the *in vivo* model, the combination of TAK1/TGFBR1 inhibitors decreased the metastatic spreading of tumor cells and the recruitment of resident fibroblasts in the TME (Díaz-Maroto et al., 2019).

These data offer new opportunities in cancer therapy. However, the complex network in the tumor-stroma communication and the presence of some discouraging results, together with the still little knowledge on this challenging subject, reveal the necessity of performing further studies that provide insight into all these matters.

7.4 STROMAL REPROGRAMING

The interplay between cancer cells and CAFs is associated with cell metabolic changes that contribute to CAFs activation, cancer growth and progression, and evasion from cancer therapies (Avagliano et al., 2018). To reprogram or return CAFs to non-activated states is a potential cancer therapy.

As we previously mentioned (point 6.4.3), CAFs suffer a metabolic reprogramming towards a more glycolytic phenotype, in order to generate higher levels of metabolic substrates to feed adjacent cancer cells. This metabolic symbiosis helps cancer cells to acquire drug-resistant phenotypes (Avagliano et al., 2018).

PDGF and TGF β protein cytokines produced by tumoral cells induce CAFs to undergo a metabolic change from OXPHOS to aerobic glycolysis. Zhang *et al.* identified TCA cycle enzyme isocitrate dehydrogenase 3 α (IDH3 α) downregulation as a critical marker for this metabolic switch. The reduction in the expression of IDH3 α decreases levels of α -ketoglutarate (α -KG), resulting in HIF-1 α protein accumulation, which, in turn, promotes glycolysis. Researchers modulated the expression of IDH3 α in CAFs to further investigate its effect in tumor progression. They generated fibroblasts from CRC or melanoma with IDH3 α knockdown or

overexpression. The results showed that tumors containing CAF with IDH3 α knockdown grew faster and were bigger than those with overexpression of IDH3 α . Therefore, overexpression of IDH3 α prevents the transformation of fibroblasts into CAFs (Zhang et al., 2015).

In the field of metabolic adaptation in cancer, Nardi *et al.* postulated that prostate CAFs acquired a tumor-promoting phenotype by reprogramming lipid metabolism and amplifying microtubule-organizing centers (MTOCs) through signaling mediated by pigment epithelium-derived factor (PEDF). PEDF is a glycoprotein with anti-inflammatory, anti-angiogenic, and anti-tumorigenic functions, which also acts as a Wnt/ β -catenin inhibitor. Adipose triglyceride lipase (ATGL) and PEDF that are involved in lipid metabolism, are both highly expressed in normal fibroblasts, but their levels are strongly reduced in prostate CAFs. In contrast, CAFs showed amplification of MTOCs levels. Normalization of MTOCs levels after PEDF treatment or by blocking lipogenesis in CAFs highlights as a reprogramming mechanism of CAFs biology (Nardi et al., 2018).

Metabolic targeting can also modulate fibroblast morphology and histological features. For example, Yanase *et al.* described that HMG-CoA reductase inhibitor (simvastatin) modified hepatic myofibroblast-like stellate cells morphology, the attachment to surrounding ECM and the contraction capacity by a mechanism involving protein geranylgeranylation (Yanase et al., 2004).

Instead of targeting CAFs, the main component of the stroma, there are studies of reprogramming immune cells of the stroma, especially TAMs. Goossens *et al.* demonstrated that ovarian cancer cells induce cholesterol efflux and depletion of lipid rafts from macrophages' cell membranes. Ovarian cancer cells produce hyaluronic acid and Th2 cytokines (IL-4) that induce cholesterol depletion from TAMs and promote tumor development. At the same time, tumor cells inhibit Th1-mediated signaling (IFN γ) which assists pro-inflammatory and immunostimulatory states on TAMs. Cholesterol efflux in TAMs is regulated by membrane cholesterol transporters (ABCA1 and ABCG1). They demonstrated that targeting cholesterol efflux by genetic deletion of ABC transporters reverted TAMs to an immune-suppressive population and so avoided tumor progression (Goossens et al., 2019).

On the other hand, stromal reprogramming can be mediated by targeting nuclear receptors (NRs). NRs are a family of proteins with the ability to recognize and bind to specific DNA motifs across the genome, and to regulate gene expression (Cheng

Introduction

et al., 2019). NRs are involved in tumor supporting processes such as tumor proliferation, angiogenesis, immune response suppression, chemoresistance, and metastasis (Chan et al., 2018; Cheng et al., 2019). Due to their implication in malignant processes and given that they are easily druggable with molecules that mimic their natural ligands, NRs are ideal therapeutic targets (Chan et al., 2018; Cheng et al., 2019). Targeting NRs in tumor cells is well studied, but considering the pro-tumorigenic function of TME and NR features, understanding the roles of NRs in TME is of great interest (Cheng et al., 2019). Therefore, some works targeting NR on CAFs, the dominant cell type within the stroma, will be summarized on below.

AR (androgen receptor) and ER (estrogen receptor) are steroid nuclear receptors with a specific role in hormone-dependent cancers. Loss of AR in CAFs aggravate the EMT and metastatic capacity of prostate cancer cells (Cheng et al., 2019; Valkenburg et al., 2018), while AR blockade in the tumor cells has the opposite effects. Hence, the ideal anti-androgenic ligand should decrease tumor AR but enhance AR stromal activity (Cheng et al., 2019). ER showed unlike effects depending on the tumor type. For example, ER overexpression in prostate and endometrial CAFs promote tumor cell proliferation, while the reverse effect was seen in cervical cancer (Cheng et al., 2019). In breast cancer, CAFs reduced the expression of ER in cancer cells, which resulted in resistance to hormone antagonists (Valkenburg et al., 2018).

In addition to steroid hormone NRs, non-steroid hormone NRs have also been studied. VDR (vitamin D receptor), PPAR γ (peroxisome proliferator-activated receptor- γ), RXR (retinoid X receptor) and FXR (farnesoid X receptor) overexpression in CAFs have anti-tumor properties, while PPAR subunits β/δ and RAR β (retinoic acid receptor) have pro-tumor effects (Cheng et al., 2019).

Pancreatic and hepatic stellate cells induce inflammation, fibrosis, and tumor proliferation by activating and turning into CAFs (Cheng et al., 2019; Sherman et al., 2014). Sherman *et al.* demonstrated that this activation process is mediated by VDR induction. Moreover, treatment with the vitamin D analog calcipotriol maintained the quiescent state of PSCs by diminishing α SMA levels and reducing inflammation and fibrosis. These observations mean that VDR activation drives the reversion of PSCs to a more quiescent, less tumor-supportive state. In addition, combined therapy with gemcitabine to target tumor cells, plus the addition of the

VDR ligand to avoid PSCs activation, enhanced survival in animal models (Sherman et al., 2014). Despite the initial promising results from preclinical studies, clinical trials with VDR therapy failed to lead to a positive outcome (Cheng et al., 2019).

Coactivation of PPAR γ and RXR in CAFs of breast cancer and melanoma modify the activation and supportive properties of CAFs by silencing the pro-inflammatory response and metastatic phenotype (Cheng et al., 2019). However, PPAR β/δ activation in CAFs showed pro-tumor effects (Cheng et al., 2019), but PPAR β/δ knockdown in CAFs and tumor cells abrogated chemoresistance of squamous cell carcinoma tumor cells (Chan et al., 2018).

FXR is a NR responsible for the regulation of gene expression of lipid, cholesterol, and bile acids metabolism. In liver and CRC, loss of function of FXR is associated with carcinogenesis. In breast cancer, tumor cells that are exposed to conditioned medium from CAFs treated with FXR agonists showed less capacity to proliferate and invade (Cheng et al., 2019).

RAR β activation promotes tumor growth. Different authors reported that genetic or pharmacologic blocking of RAR β reduced the chemoresistance of tumoral cells (Chan et al., 2018; Cheng et al., 2019). However, other studies showed that RAR β activation by ATRA, an active metabolite of vitamin A, restored the mechanical quiescence of PSCs, creating an unfavorable microenvironment for tumor invasion. Nonetheless, they were not able to demonstrate *in vivo* effects, where tumoral cells and CAFs could both have been affected (Chronopoulos et al., 2016).

8. REV-ERB NUCLEAR RECEPTORS

In mammals, the circadian rhythm is an essential regulatory component for many aspects of behavior and physiology. Disruption of circadian rhythms leads to an increased incidence in many diseases (Bugge et al., 2012; Yin et al., 2010). At cellular levels, circadian rhythms also control the transcription of many genes, including some nuclear receptors (NRs) such as REV-ERB (Ramakrishnan and Muscat, 2006; Yin et al., 2010). REV-ERB, in turn, manages the expression of metabolic genes. Variations in the expression of metabolic genes lead to metabolic disorders, such as diabetes or obesity, and increase the risk of other pathologies like cancer (Bugge et al., 2012).

Introduction

REV-ERB subgroup, REV-ERB α (NR1D1) and REV-ERB β (NR1D2), are a family of NRs that are highly expressed in skeletal muscle, adipose tissue, brain, liver, and kidney (Marciano et al., 2014; Ramakrishnan and Muscat, 2006). REV-ERB α was firstly described by Mitchel E. Lazar in the '80s. A few years later, the second member, REV-ERB β was identified (Ramakrishnan and Muscat, 2006; Wang et al., 2020; Yin et al., 2010).

NRs recruit co-regulator complexes towards specific genomic regions, DNA binding domains (DBD), where they modify the transcription of target genes. Specifically, REV-ERBs recruit the Nuclear Corepressor 1 (NCoR) that interacts with class I histone deacetylase 3 (HDAC3), forming a complex (NCoR/HDAC3) to repress the transcription of target genes (Bugge et al., 2012; Everett and Lazar, 2014; Yin et al., 2010). REV-ERB α and β are potent transcriptional repressors because they lack the C-terminal helix required for co-activator recruitment and the consequent transcriptional activation (Everett and Lazar, 2014; Ramakrishnan and Muscat, 2006; Yin et al., 2010).

Despite being usually known as orphan nuclear receptors, the metabolite heme is the endogenous ligand for REV-ERBs (Everett and Lazar, 2014). Heme promotes de recruitment of NCoR/HDAC3 corepressor complex, binds to REV-ERBs in a specific and reversible manner, and it finally stabilizes the union between REV-ERBs and NCoR (Yin et al., 2010). Heme levels control its synthesis, which is regulated by REV-ERBs. REV-ERB α -induced repression reduces ALAS1, the rate-limiting enzyme in the heme synthesis pathway, and therefore heme biosynthesis; while low levels of heme promote transcriptional activation of ALAS1 and heme synthesis by decreasing REV-ERBs repression (Yin et al., 2010). Functionally, heme group is involved in mitochondrial respiration and redox balance, so REV-ERB α and β may therefore act as sensors of the metabolic state of the cells. (Yin et al., 2010)

REV-ERBs and RORs (retinoid related orphan nuclear receptors) bind to the same DBD, known as RORE motif (Bugge et al., 2012; Everett and Lazar, 2014; Yin et al., 2010). However, they have opposite functions, REV-ERBs are transcriptional silencers and repress the activation mediated by RORs (Bugge et al., 2012; Everett and Lazar, 2014; Ramakrishnan and Muscat, 2006). RORs and REV-ERBs are considered core clock machinery because they are major regulators of the cyclic expression of BMAL1 and CLOCK, a feedback loop in the circadian cycle (Marciano et al., 2014; Solt et al., 2011). REV-ERBs transcription is activated by the

BMAL1/CLOCK heterodimer and repressed by the CRY/PER, resulting in circadian oscillations of REV-ERBs (Solt et al., 2011). In turn, REV-ERBs suppress *BMAL1* and *CLOCK* transcription, genes that drive the expression of REV-ERBs and RORs, which repress or activate downstream target genes involved in immune response, metabolic homeostasis, cancer or nervous system (Chatterjee et al., 2019; Wang et al., 2020).

REV-ERB α and REV-ERB β share physiological ligand, mechanism of action, and cooperate in the regulation of the circadian clock and metabolic functions (Bugge et al., 2012; Everett and Lazar, 2014). However, most studies demonstrate that REV-ERB α has principal regulator effects (Bugge et al., 2012; Everett and Lazar, 2014; Kojetin and Burris, 2014; Wang et al., 2020), although REV-ERB β may regulate metabolic processes when REV-ERB α is absent. This is the reason why circadian rhythms or metabolic disorders could need to modify the activity of both REV-ERBs (α and β) (Bugge et al., 2012).

REV-ERB α acts in a tissue-specific manner (Figure 9) to regulate circadian rhythms as well as metabolic processes including lipid and glucose metabolism, inflammation, and behavioral functions by repressing target gene activities. Furthermore, REV-ERB α expression is circadian in all tissues (Everett and Lazar, 2014).

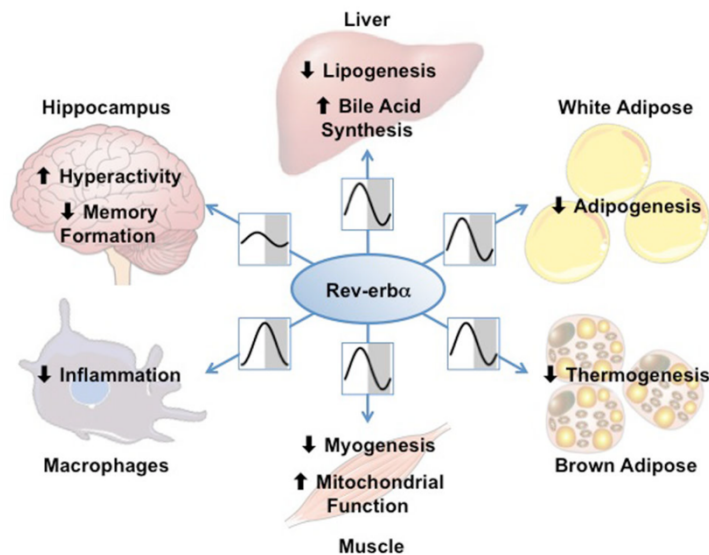


Figure 9. Schematic representation of REV-ERB α circadian expression patterns and regulatory effects in different tissues. In the liver, REV-ERB α maintains the lipid and cholesterol homeostasis; it regulates adipose tissue differentiation, in brown adipose tissue REV-ERB α is involved in thermogenic regulation to maintain body temperature rhythms, and in white adipose tissue it regulates adipogenesis; in skeletal muscle cells, REV-ERB α expression suppresses myoblast differentiation; REV-ERB α represses the inflammatory function by repression of macrophages gene expression; and in the brain, REV-ERB α alters memory and behavior. Image from Everett and Lazar (Everett and Lazar, 2014).

In the field of REV-ERBs modulation, the effects of REV-ERB in lipid/cholesterol homeostasis and myogenesis/adipogenesis are of special interest to us. On one hand, the metabolic homeostasis falls under our scope because of the link between metabolic alterations and cancer (point 6.4 on this section). On the other hand, the myogenesis/adipogenesis ratio is also of relevance for this thesis due to the presence of different CAFs types within the tumor microenvironment, considering their myogenic or adipogenic profiles (point 6.3 in this section).

8.1 REV-ERB AS DRUG TARGETS

REV-ERBs suppress transcription of target genes involved in immune response, metabolic homeostasis, cancer, or nervous system (Chatterjee et al., 2019; Wang et al., 2020). These are some reasons why REV-ERBs could be used as therapeutic targets in different pathologies. Therefore, some studies based on REV-ERBs modulation as therapeutic strategies will be highlighted and summarized below.

8.1.1 Inflammation

Inflammatory processes are controlled by circadian rhythms, since many inflammatory diseases show daily rhythmicity in the severity of symptoms. Such rhythmicity may be associated with circadian REV-ERB α , a negative regulator of inflammatory factors. REV-ERB α activation promotes anti-inflammatory responses of macrophages, blocks the NF- κ B signaling in human and mouse cells and downregulates the expression of inflammation-related genes (*IL-6*, *IL-1 β* , and *CCL2*) (Wang et al., 2020).

Inflammation promotes human pulmonary fibrosis, a pathology characterized by the presence of fibrotic nuclei in the lung tissue, which is mainly composed of activated myofibroblasts. Cunningham *et al.* proposed targeting REV-ERB α as a

therapeutic approach, since blocking REV-ERB α activation reduced fibrosis by inhibiting myofibroblast differentiation and collagen secretion in pulmonary fibrotic tissues (Cunningham et al., 2020).

8.1.2 Myogenic disorders

Fibrosis and myogenesis have a different outcome depending on the tissue type. For example, myogenic processes are needed for proper skeletal muscle functions (Chatterjee et al., 2019; Wang et al., 2020; Welch et al., 2017; Woldt et al., 2013). Studies of REV-ERBs modulation in skeletal muscle pathologies demonstrated that REV-ERBs antagonism (SR8278) reduced fibrosis and increased myogenesis, that is, stimulated muscle regeneration in muscular dystrophy (Welch et al., 2017).

As part of the core clock, REV-ERBs repress *BMAL1*, and *BMAL1* promotes myogenic differentiation in skeletal muscle. Therefore, REV-ERBs ablation or pharmacological inhibition (SR8278) promoted myogenesis, while REV-ERBs agonist (SR9011) treatment attenuated this effect (Chatterjee et al., 2019).

Woldt et al. also analyzed REV-ERBs modulation on skeletal muscle, but they did it considering mitochondrial number and function. Mitochondria are crucial in the maintenance of skeletal myofiber homeostasis and muscle energy production. In this case, activation of REV-ERBs increased mitochondrial number and their oxidative capacity, which resulted in skeletal muscle tissue being more functional (Woldt et al., 2013).

Authors from these studies concluded that REV-ERBs activation may be a useful treatment for skeletal muscle diseases through different mechanisms and pathways.

8.1.3 Metabolic disorders

Many metabolic genes show circadian oscillations. REV-ERB α is essential in the circadian regulation of lipid and cholesterol homeostasis, and bile acid synthesis by influencing rhythmic SREBPs (sterol-regulatory element-binding protein) activity and CYP7A1 (cholesterol 7 α -hydroxylase) expression, respectively (Le Martelot et al., 2009).

Human cells express two SREBPs genes, *SREBP-1* and *SREBP-2*. Besides, mammalian *SREBP-1* encodes two major proteins identified as SREBP-1a, which

Introduction

regulates all SREBP-responsive genes in cholesterol and fatty acid biosynthetic pathways; and SREBP-1c, which controls the expression of genes involved in the fatty acid synthesis and adipocyte differentiation. SREBP-2 controls the expression of genes involved in cholesterol homeostasis. High sterols activate the expression of the *SREBP-1* gene but do not exert this effect on the *SREBP-2* gene (www.themedicalbiochemistrypage.org; Ye and DeBose-Boyd, 2011). Transcriptional control of lipid homeostasis is mediated by the union of SREBP to the proteic complex SCAP-INSIG (insulin-induced protein). When the cells have enough sterol content, SREBP/SCAP are retained in the endoplasmic reticulum through the SCAP-INSIG interaction and INSIG proteins activate *HMGCR* degradation (www.themedicalbiochemistrypage.org; Ye and DeBose-Boyd, 2011).

Several authors have used genetic or pharmacologic targeting of REV-ERBs to regulate metabolic disorders.

In the event of glucose metabolism, REV-ERB α activation reduced cellular and plasma glucose levels. In pancreatic tissue, REV-ERB α can regulate insulin secretion in β -cells or glucagon in α -cells depending on glucose levels (Everett and Lazar, 2014; Kojetin et al., 2011).

REV-ERB α modulates lipid and bile acid metabolism by affecting the transcription of the SREBP pathway and *CYP7A1*, the rate-limiting enzyme of bile acid synthesis, in mice models (Le Martelot et al., 2009; Marciano et al., 2014). More specifically, REV-ERB α represses *INSIG* expression and promotes the accumulation of SREBP in the nucleus in a circadian manner, which induces transcription of *HMGCR* and therefore cholesterol synthesis (Le Martelot et al., 2009). Elevated oxysterols indirectly control rhythmic *CYP7A1* transcription, a gene also regulated by REV-ERB α (Le Martelot et al., 2009; Marciano et al., 2014). However, after pharmacological treatment with REV-ERBs agonists, the expression of SREBP-1c and its target gene *FASN* were decreased, as well as the expressions of *HMGCR* and *SREBP-2*, with the corresponding reduction in cholesterol and triglycerides synthesis in liver and white adipose tissue of treated mice (Kojetin and Burris, 2014; Solt et al., 2011).

According to these data, REV-ERBs may have a dual role considering the final transcriptional result. Whether REV-ERB acts on *INSIG*, it promotes nuclear SREBP accumulation and therefore it activates the transcription of target genes. Whereas,

if REV-ERB acts directly on target genes, it represses their transcription (Chatterjee et al., 2019; Le Martelot et al., 2009; Marciano et al., 2014; Ramakrishnan et al., 2009; Sitaula et al., 2017). Also, REV-ERBs regulate lipid metabolism and cholesterol homeostasis at other levels, since REV-ERB α controls the transcriptional regulation of lipoproteins (LPL) that are responsible for cholesterol trafficking (Marciano et al., 2014). However, REV-ERBs expression could also be controlled by other molecules. For instance, HDAC3, whose genomic recruitment promotes the expression of REV-ERB itself (Feng et al., 2011).

Data from Sitaula and colleagues were in accordance with the repressor activity of REV-ERBs, since a mice model with metabolic syndrome treated with REV-ERB agonist (SR9009) showed reduced expression of *Hmgcr* and better plasma lipid profile. Similar effects were seen when they treated HepG2 cells. REV-ERB also regulates the expression of *Srebp-2*, which itself is a transcriptional regulator of cholesterol synthetic genes. Therefore, it has a double repressive function, against *SREBP* or target genes (Sitaula et al., 2017).

Intriguingly, despite REV-ERBs have always been known as transcriptional repressors, some groups have reported conflicting results. For example, Ramakrishnan *et al.* discovered a novel function of REV-ERB β in which REV-ERB β acts as a transcriptional activator, for it activates the *Srebp-1c* promoter in skeletal muscle mouse cells, by using the N-terminus domain (Ramakrishnan et al., 2009).

Lipid homeostasis is closely related to adipogenesis, both processes being regulated by REV-ERB α expression. During adipogenesis, REV-ERB α is highly induced, which is a fact that correlates with the elevated expression of adipogenic markers (PPAR γ and CEBP α), as well as an increased lipid accumulation (Kojetin and Burris, 2014; Kumar et al., 2010). REV-ERB α levels are regulated during adipogenesis. Its expression is increased in the initial stages but then they are degraded at late stages of adipogenesis, when natural ligand (heme) levels are abundant (Kojetin and Burris, 2014; Kumar et al., 2010). In particular, high heme levels mean high *ALAS1* expression, and when such expression is blocked, adipogenesis is reduced (Kumar et al., 2010). Kumar et al. studied the ability of SR6452, a REV-ERB agonist, to induce adipocyte differentiation in 3T3-L1 cells. Their results showed increased levels of adipogenic markers and cellular processes, such as lipid accumulation, bringing out the ability of REV-ERBs to modulate adipogenesis. Recently, adipogenesis has been associated with

Introduction

metabolic disorders, so they proposed that REV-ERBs agonists may be a possible therapeutic strategy to fight against obesity and type 2 diabetes. Due to the fact that PPAR γ is also involved in adipogenesis, the researchers compared the ability of PPAR γ agonist (rosiglitazone) and REV-ERB agonist (SR6452) to induce adipogenesis, and the results suggested that the combination of both drugs may offer a clinical advantage in the treatment of type 2 diabetes (Kumar et al., 2010).

8.1.4 Cancer

The circadian clock controls the rhythmicity of cell proliferation, metabolism, inflammation, and DNA damage response. Alteration of the circadian rhythms makes individuals susceptible to tumor development (Altman et al., 2015; De Mei et al., 2015; Sulli et al., 2018; Wagner et al., 2019; Wang et al., 2015).

Pharmacological or genetic modulation of the tumor-intrinsic clock by REV-ERBs cause alterations in cell metabolism and promote cytotoxicity on malignant cells (De Mei et al., 2015; Wagner et al., 2019), diminish the proliferation of breast cancer cells (Wang et al., 2015) and induce apoptosis on tumor cells (Sulli et al., 2018).

REV-ERBs subtypes α and β , are both transcriptional repressors (Everett and Lazar, 2014; Ramakrishnan and Muscat, 2006). Opposite to normal tissue, in cancer cells, the expression of subtype REV-ERB β is higher in many different tissue types (De Mei et al., 2015; Wang et al., 2015), being this the reason why performed works on the field are differently focused on one, the other or both.

Pharmacological induction of REV-ERBs with synthetic agonists decreased tumor growth, activated apoptosis, downregulated the expression of autophagy and *de novo* lipogenesis genes and, finally, improved animal survival in a brain tumor mice model (Sulli et al., 2018). In addition, REV-ERBs agonist (SR9009) showed similar chemotherapeutic activity and less toxicity than temozolomide, the standard treatment in glioblastoma (Sulli et al., 2018). Same REV-ERBs agonist altered metabolism by a reduction in ROS species and an increased lipid droplet content, which translated into lower levels of free FA available to mitochondrial β -oxidation. As a result, SR9009 promoted cytotoxicity in glioma and hepatic malignant cells (Wagner et al., 2019). The last example of pharmacological REV-ERBs induction was performed on breast cancer cells, where Want *et al.* studied the effect of this modulation over the cell cycle by blocking Cyclin A gene (*CCNA2*)

transcription. It is a target gene of REV-ERBs, whose repression stopped the cell cycle (Wang et al., 2015).

By contrast, blocking REV-ERBs also demonstrated promising results (Altman et al., 2015; De Mei et al., 2015). De Mei *et al.* evaluated the effect of a dual inhibition, REV-ERB β plus autophagy, to induce cytotoxicity in cancer cells. Their observations showed that genetic or pharmacologic inhibition of REV-ERB β increased the cytotoxicity of chloroquine, an autophagy inhibitor. They designed a drug with the ability to inhibit REV-ERB β and autophagy, and it showed higher cytotoxic effect than chloroquine (De Mei et al., 2015). REV-ERBs inhibition may also affect the circadian clock and hence, tumor development.

MYC is a transcription factor with the same DBD than *BMAL1*, and its expression induces REV-ERBs which, in turn, represses *BMAL1* expression and alters the circadian clock in human cancer cells. The axis *MYC*/REV-ERBs/*BMAL1* modulates cancer development because *BMAL1* is a tumor suppressor gene. As Altman and colleagues reported, therefore, knockdown of REV-ERBs rescues *BMAL1* expression and activity in tumor cells. Epidemiologic data from neuroblastoma patients with high expression of *MYC* and REV-ERBs is associated with poor prognosis (Altman et al., 2015).

Most of these works about REV-ERBs modulation have been conducted in tumoral cells, omitting the effect on the TME, and demonstrated that pharmacological modulation of the clock machinery may be an effective therapy against cancer (Altman et al., 2015; De Mei et al., 2015; Sulli et al., 2018; Wagner et al., 2019). However, as we mentioned previously (point 7.4), targeting CAFs by altering nuclear receptors expression and downstream pathways may be also a promising therapy to treat chemoresistant tumors (Chan et al., 2017).

**PREMISES,
HYPOTHESIS AND
OBJECTIVES**

Tumor-stroma crosstalk is essential for PDAC formation. Overall, the mutual interactions between stroma and tumor cells support tumorigenesis, angiogenesis, chemoresistance, and metastatic dissemination of tumor cells. Therefore, the stroma, and specifically the CAFs, are the target of therapeutic alternatives to treat highly desmoplastic tumors such as PDAC.

Different CAFs-targeted therapies have been previously reported, for instance, the blockage of the tumor-stroma crosstalk, a complete CAFs depletion, the degradation of ECM proteins secreted by CAFs, or reprogramming the stroma. However, some of these strategies have not been entirely satisfactory, furthermore, some of them have proven to be counterproductive. These differences may be the consequence of the stroma sometimes may act as a non-tumor-supportive compartment. And, as CAFs are the major cellular component within the stroma, these differences may be due to the presence of CAFs subpopulations with inter- and intratumor heterogeneity.

In response to tumor signals, CAFs undergo transcriptomic and metabolomic modifications, some of them managed by nuclear receptors and transcription factors. Consequently, the identification of specific biomarkers and pathways in CAFs would be valuable to improve PDAC treatment by targeting specific CAFs subpopulations, those conferring and enhancing malignant properties of tumor cells.

We hypothesized that a selective reprogramming of specific CAFs subpopulations may be a promising strategy to treat PDAC patients.

The objectives set out to demonstrate this hypothesis were:

- 1. Identify specific biomarkers of CAFs subpopulations, pro-tumoral, or quiescent (less supportive), to describe specific signatures to each one.**
- 2. Design strategies to reprogram pro-tumoral CAFs towards a less supportive subpopulation.**

MATERIALS AND METHODS

1. CELL CULTURE

1.1 CELL LINES AND CULTURE CONDITIONS

In this work we used four different tumoral cell lines of pancreatic ductal adenocarcinoma, and five primary CAFs lines.

1.1.1 Primary CAFs isolation

Primary CAFs lines (CAF A – CAF E) were derived from PDAC tumor samples of patients. Tumor samples were handled in sterile conditions under a laminar airflow cabinet.

The tumor sample was chopped with a sterile scalpel in a petri dish with PBS 1X (phosphate-buffered saline, Gibco™). The small pieces of tissue were transferred to a gentleMACS™ C tube (Miltenyi Biotec) containing 2mL of collagenase type IV (1mg/mL) and 2mL of dispase (1U/mL), both from STEMCELL™ Technologies. Then, the C tube was placed in the gentleMACS™ dissociator where three different pre-defined programs were run, followed by an incubation of 1h at 37°C in the rotator to dissociate the sample in very small pieces of tumor. When incubations end, the suspension was centrifuged at 350g for 5min. Then, tumor pieces were re-suspended with 5mL of ACK Lysing buffer (ThermoFisher scientific) and incubated for 10min to lyse the red blood cells. The suspension was centrifuged again at 350g for 5min and we discarded the supernatant. Immediately, the cell pellet was re-suspended in 300µL of buffer A (PBS 1X, 1% BSA) per 5×10^7 of total cells and transferred to an Eppendorf tube.

Once at this point, the following steps were performed to separate the cell types of interest, CAFs or tumoral cells, present in the sample. The strategy used to separate the cell types was based on the expression of CD326. CD326, also known as epithelial cell adhesion molecule (EpcAM) or epithelial-specific antigen (ESA) is expressed on cells of epithelial origin, epithelium-derived tumor cells, circulating tumor cells, and cancer stem cells. First, we added 100µL of CD326 (EpcAM) MicroBeads per 5×10^7 total cells, mixed well with the rotator and incubate for 30 minutes in the refrigerator (2–8°C). Secondly, we washed the suspension with buffer B (PBS 1X, 0.1% BSA, 0.6% sodium citrate), placed the tubes into the magnet rack and waited for 2-5min. After that time, EpcAM positive cells were attracted by the magnet and EpcAM negative cells (CAFs, endothelial cells and immune cells)

remained on the supernatant. We collected the supernatant in a 15mL tube and repeated this final step once more. Finally, the suspension on 15mL tube was centrifuged at 700g for 5min, aspirated the supernatant completely and resuspended in culture medium and, seeded in a petri dish plate. As the EpCAM negative fraction was not pure in CAFs, we performed a selective trypsinization by which we were isolating mesenchymal cells by passaging. Finally, the purity of the culture was checked by western blot using CD31 to discard endothelial source and, vimentin, α SMA and FAP to confirm CAFs population.

1.1.2 Culture of CAFs

The five primary fibroblasts cell lines, named as CAF A, CAF B, CAF C, CAF D, and CAF E, were isolated in our laboratory (point **¡Error! No se encuentra el origen de la referencia.**) from PDAC biopsy of patients from *Hospital Universitari de Bellvitge*.

The culture medium used for CAFs was DMEM-GlutaMAX™-I (Ref. 31966-021, Gibco™) supplemented with 10% heat-induced activated FBS (Gibco™), 1% penicillin/streptomycin (Gibco™), 1M HEPES (Sigma-Aldrich), 1% NEAA (non-essential amino acids, Gibco™), 1% ITS (insulin-transferrin-selenium, Gibco™) and recombinant human FGF-basic (fibroblast growth factor, 154 a.a.) (PeproTech®). Confluent cells (90-100%) were split 1:2 or 1:3 once a week until passage number 15. All CAFs were maintained at 37°C and 5% CO₂ atmosphere.

1.1.3 Culture of tumoral cells

As tumoral cell lines, we used HPAC, BxPc3, MIA PaCa-2 and PANC-1 pancreatic cancer cells, all of them from the ATCC (American Type Culture Collection).

As we mentioned in point 4.6 of the previous section, PDAC tumors and consequently, tumoral cells could be classified by different criteria. In **Table 1** we classify the cells used in this work at molecular and metabolic levels, and we summarized the main mutations on them.

CELL LINE	MOLECULAR SUBTYPE	METABOLIC SUBTYPE	GENOTYPE			
			<i>KRAS</i>	<i>TP53</i>	<i>CDKN2A/p16^{INK4A}</i>	<i>SMAD4/DPC4</i>
HPAC	Classical	Lipogenic	12Asp	WT	112 amber STOP	WT
BxPc3			WT	220Cys	WT	HD
PANC-1	Basal – like / QM		12Asp	273Hys 273Cys	HD	WT
MIA PaCa-2		Glycolytic	12Cys	248Trp	HD	WT

Table 1. Tumoral cell lines classification and main mutations in PDAC. WT: wild type; HD: homozygous deletion. Modified and adapted from Deer et al. (Deer et al., 2010).

Briefly, classical cells are characterized by the expression of CEA (carcinoembryonic antigen protein), adhesion-associated genes and common epithelial genes. While QM cells show migration and invasion abilities in cell cultures and the expression of KRT7 (Keratin type II cytoskeletal 7) and mesenchymal-like genes characterized its expression profile. Considering the expression of GATA binding protein 6 (GATA6) which is implicated in PDAC development, GATA6 is highly expressed in classical cells compared with QM (Bailey et al., 2016; Collisson et al., 2011; Deer et al., 2010; Gradiz et al., 2016; Moffitt et al., 2015; Yao et al., 2020).

Despite excysting discrepancies on the classification of cells between different authors (Deer et al., 2010; Moffitt et al., 2015; Yu et al., 2019), we have considered MIA PaCa-2 cells and BxPc3 as QM and classical respectively, taking into account the morphology and culture features.

Cells were maintained with DMEM-GlutaMAX™-I (Ref. 31966-021, Gibco™), supplemented with 10% heat-induced activated FBS (fetal bovine serum, Gibco™), 1% penicillin/streptomycin (Gibco™) and 1M HEPES (Sigma-Aldrich) at 37°C and 5% CO₂ atmosphere. Sub-confluent cells (70-80%) were split 1:10 (PANC-1 and BxPc3) or 1:20 (MIA PaCa-2 and HPAC) twice a week until passage number 30-40.

1.1.4 Co-culture of tumoral cells and CAFs

Direct co-culture (DCC)

In order to evaluate the effect of paracrine communication as well, as the effect of cell-cell contact between different cell types, both cell types were grown in the same culture dish.

First, we seeded tumoral cells at a very low confluence and waited until colony formation, normally 48h. Secondly, we added CAFs to the cell culture (1:5, tumoral:CAF proportion). Finally, 24h after CAFs were seeded, we replaced culture medium by DMEM-GlutaMAX™-I with 2% FBS instead of 10% and this cell culture was incubated for 72h more.

Indirect co-culture (ICC)

The purpose of indirect co-culture was to assess the effect of soluble factors of the culture media in cell-cell communication between different cell types. To perform ICC special inserts (Transwell®) are needed.

Transwell® Permeable Supports (Corning®) are some inserts with a polycarbonate permeable membrane that are placed in the well and allow for growth cells in both, top part (membrane) and bottom (well). Transwell® systems are available for different plate formats and with different membrane pore sizes ranging from 0.4 to 8µm. With 0.4µm pore size only soluble factors can pass through the membrane while with 8µm pore size, both soluble factors and cells seeded in the membrane (upper compartment) can go through that membrane.

We chose one pore size or another depending on the final purpose of the experiment. The number of seeded cells and specific culture conditions will be explained in the corresponding experiments.

1.2 MYCOPLASMA TEST

All cell lines were routinely tested for mycoplasma contamination by RT-qPCR. To perform the test, we seeded the cells in over-confluence in culture media without antibiotics. 48h later the media were collected and diluted 1/100 to perform the analysis.

4µL of sample were loaded onto each well of the plate mixed with 5.15µL of LightCycler® 480 SYBR Green I Master (Roche), 0.35µL of each primer and ddH₂O to a final volume of 10µL. The primers described in Table 2 were used and RT-qPCR conditions were 40 cycles and annealing temperature of 55°C.

PRIMER	SEQUENCE
Forward	5'- GGC GAA TGG GTG AGT AAC ACG -3'
Reverse	5'- CGG ATA ACG CTT GCG ACT ATG -3'

Table 2. Primers used to detect mycoplasma contamination.

1.3 CELL COUNTING

Cell counting was done manually using the trypan blue solution (Sigma-Aldrich) to determine the viability of the cells by staining-exclusion test. The staining-exclusion test is based on the concept that viable cells do not absorb trypan blue.

Firstly, adherent cells were washed with PBS 1X (Gibco™) and detached by incubating them for 5min at 37°C with pre-warmed 0.25% trypsin-EDTA (ethylenediaminetetraacetic acid), phenol red (Gibco™). Secondly, trypsin was inactivated adding fresh complete culture medium. The cell suspension was then centrifuged for 5min at 1000rpm and re-suspended again in fresh complete medium. Finally, to proceed with cell counting, 20 to 50µL of cell suspension were diluted 1:1 with trypan blue solution and 10µL of the mix was loaded on the loading groove in the Neubauer chamber. The number of cells from four squares/cell type were counted and cell concentration was calculated according to the following formula:

$$\text{Concentration} \left(\frac{\text{cells}}{\text{mL}} \right) = \frac{\text{viable cells per quadrant}}{\text{number of quadrants}} \times \frac{10^4}{\text{dilution factor}}$$

1.4 CELL CRYOPRESERVATION AND THAWING

After trypsinization and centrifugation processes, cells were re-suspended in cold freezing medium (FBS with 10% DMSO (dimethyl sulfoxide, Sigma-Aldrich)) in a 1/3 dilution of a p100 plate of tumoral cells or 1/2 dilution of a p100 plate of CAFs. The cell suspension was distributed in cryotubes (1mL/tube) and cryotubes were placed in a Mr. Frosty™ freezing container (ThermoFisher scientific) filled with

Materials and methods

100% isopropyl alcohol. For freezing, Mr. Frosty™ was stored at -80°C at least 24h. Lastly, for long term storage cryotubes were stored in a liquid nitrogen tank.

For cell thawing, cryotubes were warmed in the water bath at 37°C and were diluted in a pre-warmed culture medium. Then, the cell suspension was centrifuged at 1000rpm for 5min and the cell pellet was re-suspended in fresh complete medium. Finally, they were grown into a p100 plate.

1.5 CONDITIONED MEDIA HARVESTING

Conditioned medium (CM) is medium harvested from cultured cells under specific culture conditions. It contains metabolites, growth factors, and extracellular matrix proteins secreted into the medium by the cultured cells.

1.5.1 From pancreatic CAFs

To collect CM from CAFs, cells were seeded in normal conditions of culture medium and growth requirements until reaching 70-80% of confluence. Then, CAFs were washed once with PBS 1X and incubated with fresh DMEM-GlutaMAX™-I, without FBS for 48h. After 48h, the media were recovered, filtered in 22µm filter (Millex® - GS) and finally, stored at -20°C until use.

2. MOLECULAR ANALYSIS

2.1 CYTOMETRY ASSAYS

2.1.1 Fluorescence-activated cell sorting (FACS)

FACS was the tool used to separate the different cell types present in a DCC. This technic allowed us to work with separated cells for further purposes. For example, culture again after separation, RNA and protein isolation from separated cells or cell tracing. Concretely, we compared variations in the expression levels of CAFs seeded in DCC with tumoral cells regarding CAFs in mono-culture.

The staining used to discriminate the different populations were Cell Trace™ CFSE (Carboxyfluorescein succinimidyl ester) from Invitrogen™ (Cat.no. C34554) and APC (allophycocyanin) anti-human CD90 (Thy1) antibody (CD90-APC) from BioLegend® (Cat.no. 328113), both for staining CAFs.

Tumoral cells were seeded at a very low confluence to allow colony formation, 1.2×10^5 cells in a p100 plate. 48h later, CAFs previously stained with Cell Trace™ were seeded on the same plate where tumoral cells were growing in a proportion 1:5 (tumoral:CAF) getting a DCC. Cell Trace™ staining was performed following the manufacturer's instructions at $2 \mu\text{M}$ concentration.

After 24h of DCC, the culture medium was replaced by fresh medium supplemented with 2% FBS and incubated for 3 days more.

On cell sorting day, seeded cells were trypsinized, centrifuged and resuspended in the appropriate volume of human FcR blocking reagent (Milteny Biotech, 130-059-901). FcR blocking reagent acts blocking Fc receptor of human cells to increase the specificity of the antibody and thereby improves the purity of target cells. Human FcR blocking was used following manufacturer's instructions. Then, cells were stained with CD90-APC antibody. For that, the cell suspension was incubated with $2 \mu\text{L}$ of CD90-APC per million cells in $100 \mu\text{L}$ FACS buffer for 30 minutes, on ice and darkness. After incubation, cells were washed three times with FACS buffer to remove antibody excess and resuspended in a final volume of $500 \mu\text{L}$. Finally, $2 \mu\text{L}$ of 1mg/mL propidium iodide (PI) was used to discard between live and dead cells. PI is a membrane impermeant dye, its staining method is based on a dye exclusion test which lies in the concept that viable cells do not absorb PI.

Beckman Coulter's MoFlo XDP was used to perform the cell sorting. First, we got PI negative viable cells and then, with CFSE – CD90 double staining we separated 2 populations of cells. On one hand CAFs as a double positive population and the other the tumoral cells as a double negative population. Obtained cell pellets were processed as described in point 2.2.1 or 2.3.1 on this section depending on the final purpose.

Staining and washes were performed using FACS buffer: PBS supplemented with 5% FBS and 1:1000 DNase I (RNase – free) from BioLabs. FACS buffer was moreover supplemented with 0.1% DEPC (diethyl pyrocarbonate) when the final purpose of the cell pellet was RNA sequencing analysis.

In case that we used a mixture of different CAFs to perform the DCC and when the goal of the experiment was separate each CAF type, we stained the CAFs with Cell Trace™ of distinct colors (CFSE, Violet (Cat.no. C34571) or Far Red (Cat.no. C34572)).

2.1.2 Fluorescence flow cytometry (FFC)

FCC is a technique used to detect and measure physical and chemical characteristics of a cell population. FFC was performed on a Gallios cytometer (Beckman Coulter) and data were processed with Kalluza Analysis version 2.1 software (Beckman Coulter). PI was used to discard between live and dead. Staining and washes were performed using FFC buffer: PBS supplemented with 5% FBS.

We used FFC to process different experiments. The specific conditions and biological markers used are described in detail in each experiment.

2.2 RNA ANALYSIS

2.2.1 RNA isolation and quantification

From cell pellet after cell sorting

Cell pellets from cell sorting were frozen at -80°C until RNA extraction.

RNA was isolated using the RNeasy® Micro Kit (Qiagen) following the manufacturer's instructions. Obtained RNA was quantified in the Qubit™ fluorometer (ThermoFisher scientific). To avoid genomic DNA (gDNA) contamination, an additional DNase treatment was performed by using the DNase I (RNase-free) from BioLabs, according to manufacturer's instructions.

Finally, RNA samples were sent to CNAG (Centro Nacional de Análisis Genómico, Barcelona – Spain) to perform the RNA sequencing.

If RNA samples were used to analyzed transcriptomic differences by RT-qPCR, samples were quantified in the spectrophotometer NanoDrop TM1000 (ThermoFisher scientific) and stored at -80°C until use.

From cells in a petri dish

Culture plates with adherent cells were washed with sterile PBS 1X and frozen at -80°C until RNA extraction.

RNA was extracted using the RNeasy® Mini Kit (Qiagen) following manufacturer's instructions. Cells were scrapped with the corresponding volume of Buffer RLT to

detached them from the plate. In the case of CAFs, after cell detachment samples were homogenized with needle and syringe to improve RNA content. Obtained RNA was quantified in the spectrophotometer NanoDrop TM1000 (ThermoFisher scientific) and stored at -80°C until use.

2.2.2 cDNA obtention from RNA

First-strand cDNA (complementary DNA) was obtained with SuperScript™ IV VIL0™ Master Mix (Invitrogen™) reaction following the manufacturer's instructions. Briefly, a mix composed of 100-500ng from each sample of RNA template, 4µL of SuperScript™ IV VIL0™ Master Mix and nuclease-free water until reach 20µL was placed into a microcentrifuge tube.

Then, this mix was placed in the thermocycler and the reverse transcription reaction took place with the following conditions: 10min at 25°C, 10min at 50°C, 5min at 85°C and ∞ at 4°C. Obtained cDNA was stored at -20°C until use.

2.2.3 Real-Time quantitative PCR

RNA expression levels were detected by Real-Time quantitative PCR (RT-qPCR) using PowerUp™ SYBR® Green Master Mix (Applied Biosystems). 1µL of cDNA obtained from different cells were loaded onto 384-well plate mixed with 5µL of PowerUp™ SYBR® Green Master Mix (Applied Biosystems), 0.2µL of the probe of interest (Table 3) and ddH₂O to a final volume of 10µL. The plate was read at the LightCycler® 480 Instrument II (Roche). Results were visualized and analyzed using LightCycler® 480 Software 1.5 (Roche).

GENE	FORWARD (5' → 3')	REVERSE (5' → 3')
<i>ACTA2</i>	CATCACCAACTGGGACGACA	CAATGAGCTTCGTGTTGCC
<i>CCL2</i>	GAAAGTCTCTGCCGCCCTT	GGGGCATTGATTGCATCTGG
<i>CEPBA</i>	TGGACAAGAACAGCAACGAG	TCACTGGTCAACTCCAGCAC
<i>COL11A1</i>	TGGAATGAGGGGAGAAGATG	GTCCTGGATTCCCTTGTGA
<i>COL1A1</i>	AGCCAGCAGATCGAGAACAT	TCTTGTCTTGGGGTTCTTG
<i>COL1A2</i>	CTGCAAGAACAGCATTGCAT	GGCGTGATGGCTTATTTGTT

Materials and methods

GENE	FORWARD (5' → 3')	REVERSE (5' → 3')
<i>FAP</i>	TACCCAAAGGCTGGAGCTAA	ACAGGACCGAAACATTCTGG
<i>FASN</i>	CAGAGCAGCCATGGAGGAG	TAGAGCCCCGCCTTCCAG
<i>HMGCR</i>	TGATTGACCTTTCCAGAGCAAG	CTAAAATTGCCATTCCACGAGC
<i>IL1B</i>	GGAGAATGACCTGAGCACCT	GGAGGTGGAGAGCTTTCAGT
<i>IL6</i>	CATCCTCGACGGCATCTCAG	GCCTCTTTGCTGCTTTCACA
<i>MYH11</i>	CGCCAAGAGACTCGTCTGG	TCTTTCCAACCGTGACCTTC
<i>PDPN</i>	AACCAGCGAAGACCGTATAA	CGAATGCCTGTTACTACTGTTGA
<i>POSTN</i>	CTCATAGTCGTATCAGGGGTCG	ACACAGTCGTTTTCTGTCCAC
<i>PPARG</i>	AGCCTGCGAAAGCCTTTTGGTG	GGCTTACATTAGCAAACCTGG
<i>S100-A4</i>	GATGAGCAACTTGGACAGCAA	CTGGGCTGCTTATCTGGGAAG
<i>SQLE</i>	TGACAATTCTCATCTGAGGTCCA	CAGGGATACCCTTTAGCAGTTTT
<i>SRF</i>	CAAGCCGGGTAAGAAGACCC	CATAGGCCTTCTTCATGATGCC

Table 3. List of genes and the sequences of the corresponding primers used in RT-qPCR assays.

The differences between genes were measured using the $\Delta\text{-}\Delta\text{Ct}$ method. The number of cycles needed for detection of the fluorescent signal (Ct) for each gene was normalized against the value of *QARS* (Table 4), used as housekeeping gene.

PRIMER	SEQUENCE
Forward	5'- ATCCTACTGAGGTGCCTGGT - 3'
Reverse	5'- ACCACGTGTAGTGATGCCAG - 3'

Table 4. Sequences of *QARS* primers used as housekeeping gene.

Finally, RNA expression was calculated using the obtained ΔCt following this formula:

$$2^{-\Delta\text{Ct}} = 2^{-(\text{Ct gene A} - \text{Ct housekeeping gene})}$$

2.2.4 RNA sequencing of cultured CAFs and tumoral cells

Stranded mRNA sequencing (RNA-seq; 50M PE reads, Illumina® HiSeq 3000 system) was performed in order to detect differentially expressed genes (DEG) between experimental groups. Analyzed samples consisted of RNA coming from the pellet of co-cultured and mono-cultured mixCAF.

To obtain the co-cultured mixCAF sample, a DCC of mixCAF with each one of the tumoral cells (MIA PaCa-2, PANC-1, HPAC, and BxPC3) were seeded. The same mixCAF was used to get the mono-culture sample and it was used as control for the transcriptomic analysis. We refer as mixCAF when we seed a mixture of five different CAFs: CAF A + CAF B + CAF C + CAF D + CAF E, at equitable proportions on the same plate.

Culture conditions were performed as described in sections **¡Error! No se encuentra el origen de la referencia.** and 1.1.4. Cell sorting method is detailed in 2.1.1. and the obtained cell pellets processed as described in section 2.2.1.

Poly-A pull-down was used to enrich for mRNAs from total RNA samples (0.2-1µg per sample, RIN>8) and proceeded to library preparation using Illumina TruSeq RNA Prep Kit. Libraries were then sequenced using Illumina® HiSeq3000 at the CNAG (Barcelona – Spain).

We multiplexed samples in each lane, which yielded targeted number of 2× pair-end 75bp reads for each sample, as a fraction of 50 million reads per lane.

2.3 PROTEIN ANALYSIS

2.3.1 Western Blot (WB)

Tumor cell lines or CAFs were seeded in different culture dishes accordingly to their proliferation rate to reach a final confluence of 70-80%. 24h later, the corresponding treatment, CM or drug, was added. On control samples, regular DMEM-GlutaMAX™-I was used. After 24, 48 or 72 hours of treatment exposure all supernatants were removed and plates were washed once with PBS 1X and stored at -20°C.

Protein lysate from cell culture

For western blotting of cellular lysates, CAFs or tumoral cells were scrapped with protein lysis buffer (dH₂O, 25mM HEPES pH 7.5, 0.3M NaCl, 1.5mM MgCl₂, 0.2M EDTA, 1% Triton X-100, 0.1% SDS, 0.5% sodium deoxycholate) supplemented with complete EDTA-free Protease Inhibitor Cocktail Tablets (Roche), orthovanadate, PMSF, β -glycerol, aprotinin and leupeptin. Lysates were cleared by centrifugation at 12.000rpm for 20min. Protein lysates were stored at -80°C until use.

Quantification of protein extract

Protein concentration was determined using colorimetric Pierce™ BCA Protein Assay Kit (ThermoFisher scientific) using a 96-round well plate.

To perform a standard curve, decreased volumes of a standard of bovine serum albumin (BSA, 0.4 μ g/ μ L) ranging from 0 to 6.4 μ g/ μ L were loaded in duplicate. To quantify samples, 2 μ L of samples of interest were loaded in triplicate. Then, BCA Working Reagent (50:1, Reagent A:B) was loaded onto wells to a final volume of 200 μ L.

The plate was incubated at 37°C for 30min and then the absorbance was measured at 560nm wavelength by spectrophotometry (Victor™ X5, PerkinElmer) using the PerkinElmer 2030 Workstation software. Finally, protein concentration was calculated by extrapolation in the BSA standard curve.

Once quantified, each lysate was boiled in sample buffer (2x Laemmli sample buffer from Bio-Rad Laboratories + 5% β -mercaptoethanol) at a final concentration of 1:1 for 5min at 95°C to denature the proteins. Ready to use lysates were stored at -20°C until use.

Electrophoresis, blotting, and detection

Ready to use protein lysates were loaded onto sodium dodecyl sulfate-polyacrylamide (SDS-PAGE) electrophoresis gels. These gels were composed of two fractions: the stacking (up) and the resolving (down).

Gels were prepared with a mixture of dH₂O, 30% acrylamide-bis (Bio-Rad), Tris-HCl with 0.4% SDS, ammonium persulfate (APS) and TEMED (ApliChem). The volumes of each reagent depend on the acrylamide content of the gel. The stacking fraction was always prepared with Tris-HCl 1.5mM, pH 8.8 and at 4% acrylamide content.

While the resolving fraction was made with Tris-HCl 0.5mM, pH 6.8 and the acrylamide concentration could range from 8 to 15% depending on the molecular weight of proteins of interest, this fraction separated the proteins by their molecular size.

Usually, 30µg of protein were loaded into the wells and a molecular weight marker (BenchMark™ pre-stained protein ladder, ThermoFisher scientific) was used. The gel was placed into the running buffer (25mM Tris, 192mM glycine, 0.1% SDS) and the separation of proteins was carried out at a constant voltage of 120V for 90min at room temperature (RT).

For the blotting process, wet transfer was carried out. Proteins were transferred to 0.45µm pore-size polyvinylidene fluoride (PVDF) membranes (Immobilon-P, Merck Millipore). The membranes were previously quickly activated in pure methanol and washed with dH₂O. The acrylamide gel together with the PVDF membrane, filter papers (Whatman® paper) and pads were assembled in a “transfer sandwich” as follows: pad – filter paper – acrylamide gel – PVDF membrane – filter paper – pad. Finally, this “transfer sandwich” was placed into the transfer tank full of transfer buffer (25mM Tris, 192mM glycine, 20% Methanol) and an 80V constant voltage was applied for 120min at 4°C. In case of proteins smaller than 20KDa of molecular weight, transfer conditions were 40V of constant voltage for 30min at 4°C.

Once the transfer process finished and before primary antibody incubation, membranes must be blocked to prevent unspecific primary antibody unions. Membrane blocking was made in 5% nonfat milk in TBS-T (0.1% Tween in TBS 1X) for 1h at room temperature. After blocking, membranes were washed once with TBS-T, and incubated overnight (ON) at 4°C with the corresponding dilution of primary antibodies in 1% nonfat milk in TBS-T listed on Table 6.

The following day, after washing the membranes three times with TBS-T for 10min, a secondary antibody incubation was performed using ECL horseradish peroxidase-linked secondary mouse/rabbit antibody (5) diluted in 1% nonfat milk in TBS-T for 1h at RT.

SECONDARY ANTIBODY	REFERENCE	MANUFACTURER	DILUTION
Mouse	sc-516102	Santa Cruz Biotechnologies	1:2000
Rabbit	sc-2357	Santa Cruz Biotechnologies	1:2000

Table 5. List of secondary antibodies used in WB.

Finally, after washing the membranes three times with TBS-T for 10min, blots of proteins were detected by ECL homemade chemiluminescent substrate (solution A: 1M Tris pH 8.5, 250mM luminol, 90mM coumaric acid; solution B: 1M Tris pH 8.5, hydrogen peroxidase) at 1:1 proportion with the ChemiDoc™ Touch imaging system (Bio-Rad Laboratories). All measurements were performed without saturation and were normalized to β -actin (Sigma-Aldrich, A5441, mouse mAb) loading control. Band densitometric analyses were performed with Image Lab 6.0 software (Bio-Rad Laboratories).

2.3.2 Immunocytofluorescence (ICF)

To detect protein levels in co-cultured cells, cells were seeded over 12mm diameter glass coverslips previously sterilized under ultraviolet radiation (UV) for a minimum of 30min. Then, they were placed onto 24-well plates and 4000 tumoral cells were seeded over them. After 48h, 30000 CAFs were seeded with the tumoral cells to get the direct co-culture. The next day, the medium was replaced by fresh medium supplemented with 2% FBS containing the different treatments. 48h later, the coverslips were washed with PBS 1X and then fixed with cold 4% paraformaldehyde (PFA) shaking for 10min at RT.

After fixation, cells were washed thrice with PBS 1X and then permeabilized for 15min with PBS-T (PBS with 0.1% Triton X-100). Later, blocking was performed using 5% BSA (bovine serum albumin) in PBS and shaking for 15min at RT.

Then, cells were incubated with primary antibodies (Table 6) for 1h at RT diluted in 1% blocking solution. After incubation, coverslips were washed three times with PBS followed by a second incubation with Alexa Fluor secondary antibodies (Table 8) diluted 1:200 also in 1% blocking solution for 1h at RT.

Finally, coverslips were mounted with one drop of VECTASHIELD® Mounting Medium with DAPI (4',6-diamidino-2-phenylindole). With this mounting medium

cell nuclei were counterstained with DAPI. Coverslips were permanently sealed around the perimeter with nail polish. Sealed slides were stored at -20°C protected from light until reviewed in a Fluorescence DM6000 microscope. Afterward, photos were analyzed using Image J software.

PROTEIN SYMBOL	ANTIBODY REFERENCE	HOST	APPLICATION	DILUTION
ACTB	A5441	M	WB	1:1000
CALD1	HPA008066	R	WB	1:250
			ICF	1:100
CNN1	sc-58707	M	WB	1:200
DESM	HPA018803	R	ICF	1:100
FAP α	sc-100582	M	WB	1:100
	sc-65398		ICF	1:100
FASN	CS #3180	R	ICF	1:25
FIBRONECTIN	ab2416	R	WB	1:1000
FSP-1	HPA007973	R	WB	1:250
			ICF	1:50
IL6	ab6672	R	WB	1:500
KCNN4	HPA053841	R	ICF	1:100
L2GL2	HPA022913	R	ICF	1:200
MYH11	HPA015310	R	WB	1:250
PDGFRA	CS #3174	R	WB	1:1000
POSTN	ab219057	R	WB	1:1000
PDPN	HPA007534	R	WB	1:250

PROTEIN SYMBOL	ANTIBODY REFERENCE	HOST	APPLICATION	DILUTION
RARB	NBP1-81776	R	ICF	1:100
SQLE	LS-C497943	R	ICF	1:100
VIME	ab45939	R	WB	1:1000
			ICF	1:500
	M0725	M	ICF	1.100
α SMA	A2547	M	WB	1:1000
	M0851		ICF	1:100

Table 6. List of primary antibodies used for protein detection in different applications and their dilutions. R: rabbit; M: mouse. Protein extended name described in ANNEX 1.

3. IN SILICO ANALYSES

3.1 TRANSCRIPTOMIC ANALYSES: DEG

As we mentioned previously, RNA-seq was performed to detect mRNA expression differences between groups. Analyzed samples consisted of four mono-cultured mixCAF and four mixCAF co-cultured with tumoral cells, described in 2.2.4 in this section. Samples were sequenced at *Centro Nacional de Análisis Genómico* (CNAG-CRG, Barcelona – Spain). RNA-seq reads were aligned to GRCh38.

Genes expressed in fewer than two libraries were filtered out before differential expression testing. The principle component analysis was calculated using the `prcomp` function available in R and plotted using a customized R script. Expression, normalization and differential expression testing were performed using DESeq2, in case for comparison with two experimental groups (mono-cultured cells vs co-cultured cells, either CAFs or tumor cell lines). DESeq2 methodology estimate variance-mean dependence in RNA-seq count data and test for differential expression based on a model using the negative binomial distribution.

For the analyses comparing three experimental groups, DEG were determined using eBayes (empirical Bayes; (Phipson et al., 2016)), a methodology that compute moderated T-statistics, moderated F-statistics, and log-odds of

differential expression by empirical Bayes moderation of the standard errors towards a common value.

First, a matrix for all coding genes (19865) was generated. Then, dummy variables were assigned to identify the reference group. A dummy variable is a numerical variable used in regression analysis to represent the subgroups in the study. In our case, the subgroups were mono-culture, co-culture with classical or co-culture with quasisenchymal cell lines. Each dummy variable was compared with the reference group.

Finally, multiple testing across genes and contrasts were applied using `decideTests`. These functions implement multiple testing procedures for determining whether each statistic in a matrix of t-statistics should be considered significantly different from zero.

3.2 FUNCTIONAL ANALYSES OF GENE EXPRESSION

In order to explore the biological meaning of the gene expression of our experimental groups we used Gene Set Enrichment Analysis (GSEA) (Subramanian et al., 2005). GSEA is a computational method that determines whether an *a priori* defined set of genes shows statistically significant, concordant differences between two biological states. Such *a priori* defined gene sets are compiled in the Molecular Signature Database (MSigDB). In addition, GSEA determines whether genes that constitute a predefined gene set tend to be represented at the top or bottom of our ordered list of genes, correlating with our experimental phenotypes. Also, one of the virtues of GSEA is that several small changes in expression of a set of genes, which in a coordinated way, have biological significance, are taken into account.

The expression profiles of our *in vitro* experimental conditions were subjected to a pre-ranked GSEA, using the T-statistics to rank the genes. When the matrix expression from patients of the Moffitt series cohort (Moffitt et al., 2015) or the TCGA PAAD cohort were considered, we used GSEA with default settings.

In our analyses, the collection of gene sets that have been matter of study were:

- H: hallmark gene sets; coherently expressed signatures derived by aggregating many MSigDB gene sets to represent well-defined biological states or processes.

Materials and methods

- C2: curated gene sets, CP: canonical pathways; these gene sets are canonical representations of a biological process compiled by domain experts.
- C3: regulatory target gene sets, TFT: transcription factor target genes; all transcription factor target prediction gene sets.
- C5: gene ontology (GO) gene sets, BP: GO biological process; gene sets derived from the GO biological process ontology.

The results of the functional enrichment analyses of our samples were also compared with the signatures from the normal and activated stroma described in Moffitt *et al.* (Moffitt *et al.*, 2015) and with data from GSE66616, corresponding to lung CAF mono-cultured or co-cultured with Calu-1 cells (Rudisch *et al.*, 2015).

3.3 PROGNOSTIC ASSESMENT OF GENE SIGNATURES USING ssGSEA

Single sample GSEA (ssGSEA), an extension of GSEA, calculates a gene set enrichment score (ES) for each sample (Barbie *et al.*, 2009). After ssGSEA, a hierarchical cluster analysis using Euclidean distance and complete linkage was computed in order to group patients according to a particular gene signature. The output heatmap and dendrogram were developed using MORPHEUS (<https://software.broadinstitute.org/morpheus/>). Survival analyses were carried out using GraphPad Prism v6 software and Cox proportional-hazards regression model.

The cohorts used in this thesis were:

- Moffitt series; a cohort of 108 primary PDAC tumors enriched in stroma tissue from a complete cohort of 145 patients. Low stroma samples (25%) were excluded from the analyses using a non-matrix factorization (NMF) methodology of tumor deconvolution described in (Moffitt *et al.*, 2015).
- TCGA – PAAD series; a cohort of 123 primary PDAC tumors enriched in stroma tissue from a complete cohort of 168 patients. Low stroma samples were excluded from the analyses using MCP-counter (Becht *et al.*, 2016). Furthermore, we excluded from the analyses the 25% of samples with lower fibroblasts amount.

3.4 METABOLIC RECONSTRUCTION FROM TRANSCRIPTOMIC DATA

In order to evaluate the effects of differential gene expression levels in signaling and metabolism, we performed a metabolic reconstruction analysis. The analyses were carried out at *Fundación Progreso y Salud* (FPS, Sevilla – Spain) by the clinical bioinformatics area.

3.4.1 Signaling pathways

The interpretation of the consequences of the combined changes of gene expression levels in the context of signaling pathways was performed using the Hipathia (High throughput pathway interpretation and analysis) web tool (<http://hipathia.babelomics.org>) (Hidalgo et al., 2017).

Gene expression data after TMM normalization were used to analyze pathways activation status. Hipathia considers the expression of the genes in a pathway and the relation between them to obtain a value for the activation status of the pathway to each sample. The comparison of these data between groups showed up- or down-regulated pathways regarding the control group, mixCAF mono-culture. Results were also related to Gene Ontology (GO) functions. p-values were obtained by the comparison of mixCAF mono-culture vs mixCAF co-culture with FDR adjustment.

3.4.2 Metabolic modules metabolites

Two different analyses were performed for metabolism (Çubuk et al., 2019). First, we used Metabolizer, a web tool for analysis of modular architecture of metabolic pathways using transcriptomic data. Metabolizer calculates impact of modules on production of metabolites (<http://metabolizer.babelomics.org>). Metabolizer uses KEGG (Kyoto Encyclopedia of Genes and Genomes) Module activities and transcriptomic data. For the analyses, the t-test was applied for statistical assessment and p-values were adjusted by the Benjamini-Hochberg method. Log-fold changes were calculated as log (median of mixCAF co-culture/ mixCAF mono-culture). The second type of analysis was an in-silico prediction of differentially altered metabolite production using the Metabolica tool. Significant results using adjusted or non-adjusted p-values were $p < 0.05$ or $p < 0.01$, respectively.

4. CELL-BASED ASSAYS

4.1 MIGRATION ASSAYS

4.1.1 Wound closing assay

We performed a wound-healing assay to evaluate the migration capacity of the tumoral cells with conditioned medium from different CAFs. The assay was done using 2-well silicone inserts from Ibdⁱ® (Cat.no. 80209) with a defined cell-free gap in the middle. Inserts were placed in 24-well plates at least 2h before cell seeding. Then, 40000 MIA PaCa-2 cells were seeded in each well of the silicone insert at a final volume of 70µL, and 500µL of culture medium were added surrounding the inserts. 24h later, when cells were well attached and confluent in a monolayer of cells, the inserts were removed. After that, cells were washed with PBS 1X to remove the floating cells and finally, 500µL of conditioned medium from different CAFs supplemented with 2% of FBS were added.

For each condition, two photographs/well were taken at 14, 24 and 40h using a DMi1 microscope (Leica Microsystems). Migration capacity was quantified as the percentage of the closed area using Image J software.

4.1.2 Directional migration assay

Directional migration was the other method used to evaluate the migration capacity of cells. This method is based in an ICC using Transwell® Permeable Supports (Corning®) with 8µm pore size. Migratory cells were seeded in the top part, over the transwell membrane, and migration inducer was plated at the bottom part, in the well. To quantify the migration capacity, cells that went through the membrane were counterstained with hematoxylin and we counted the number of cells in the lower part of the membrane. 24-well plates were used to perform the assays.

75000 MIA PaCa-2 cells were seeded in the transwell membrane in a final volume of 100µL and 30000 CAFs at the well. 24h later, migratory cells were put in touch with the migration inducer so the transwells were placed on the corresponding well with CAFs. The culture medium was replaced by media supplemented at 2% of FBS and plates were incubated for 40h at 37°C in humid conditions with 5% CO₂. DMEM-GlutaMAX™-I supplemented at 2% of FBS was used as a control medium.

After that time, membranes were wiped with a cotton swab to remove non-migratory cells from the upper part of the membrane and fixed for 5min with methanol. Then, membranes were washed twice with PBX 1X followed by hematoxylin staining for 2min. Hematoxylin excess was removed by washing with dH₂O. Finally, the membrane was removed from the Transwell® insert using a blade and mounted with a drop of dH₂O on a slide.

For each condition, three Transwell® were used and they were visualized under the Nikon Eclipse 80i microscope. To analyze migration, ten images/membranes were taken with Nikon DS-Ri1 digital camera using NIS-Elements BR 3.2 software and the migratory cells were manually counted using Image J software and represented as the total number of migratory cells/field for each condition.

4.2 COLONY FORMATION ASSAYS

Colony formation assay is an *in vitro* cell survival assay based on the ability of a single cell to grow into a colony, considering a colony a group of more than 50 cells. For that purpose, cells were dissociated into a single-cell suspension and then seeded onto 12-well plates at a density of 100 HPAC/well or 50 MIA PaCa-2/well. The day after seeding, the medium was replaced by CAF CM with or without gemcitabine treatment. Cells were cultured for up to 10-12 days. At the end of the experiment, cells were washed twice with PBS 1X, fixed with cold methanol and stained with 0.1% crystal violet (1mg/mL). Three wells were used for each condition and colonies were counted manually using Image J software.

4.3 PROLIFERATION ASSAYS

Proliferation capacity of adherent cell cultures were evaluated with crystal violet staining. The principle of the assay is based on the fact that viable cells remained attached on the plate and stained with crystal violet.

Cells were harvested onto 96-well plates at a density of 4000 cells/well by six times. Once cells were adhered in the plate, they were washed twice with PBS 1X and fixed with 100µL of methanol per well for 10-15min. Fixation was performed at different time points.

To complete the staining, cells were covered with 100µL of 0.1% crystal violet (1mg/mL) for 15 more minutes. Colorant excess was washout with tap water.

Materials and methods

Finally, crystal violet dye was solubilized with 50 μ L of 10% methanol – 5% acetic acid solution incubating at RT and shaking for 30min. The absorbance was measured at 590nm in the PowerWave™ XS microplate reader with KCjunior software (BioTek Instruments, Inc.).

Cell proliferation was evaluated comparing the absorbance values of different time points.

4.4 LIPID DROPLETS STAINING

Lipid droplets are cytoplasmatic organelles involved in the storage and regulation of triglycerides (TG) and cholesterol esters. Nile red (Sigma-Aldrich laboratories, ref. 19123) is a lipophilic fluorescent dye with a fluorescence color range from golden yellow to deep red used for the staining of intracellular neutral lipids (triglycerides) and polar membrane lipids (phospholipids).

Cells were seeded over 12mm diameter glass coverslips previously sterilized under ultraviolet radiation (UV) for a minimum of 30min. Then, they were placed onto 24-well plates and 25000 CAFs were seeded over them. The next day, the medium was replaced by fresh medium supplemented with 2% FBS containing the different treatments. 24 to 48h later, the coverslips were washed with PBS 1X and then fixed with cold 10% formaldehyde for 30min at RT. Meanwhile, 1:1000 working solution of Nile red in 150mM NaCl was prepared. After 30min of fixation, cells were covered with 1mL of Nile re and incubated 10min at RT protected from light. Afterwards, cells were washed thrice with PBS 1X.

Finally, coverslips were mounted with one drop of VECTASHIELD® Mounting Medium with DAPI and lipid droplets were reviewed in a Fluorescence Nikon Eclipse 80i microscope. Images were taken with a Nikon DS-Ri1 digital camera using NIS-Elements BR 3.2 software and photographs were analyzed using Image J software.

4.5 INTRINSIC MODULATION OF CAFs

In order to evaluate if there were changes on the expression patterns between CAF subtypes when they were seeded as a mixture of CAFs, we harvested the culture of mixCAF where each CAF subtype was stained with a Cell Trace™ of a different color. The Cell Trace colors used were CFSE (Cat.no. C34554), Violet (Cat.no.

C34571), Far Red (Cat.no. C34572), all from Invitrogen™. The staining procedure was performed following the manufacturer's instructions at 2 μ M final concentration.

After 24h, the culture medium was replaced by fresh medium supplemented with 2% of FBS and incubated for 3 days more.

On cell sorting day, CAFs types were separated by color following the procedure described in 2.1.1 from this section avoiding the steps related to antibody staining. Obtained cell pellets were processed as described in point 2.2.1.

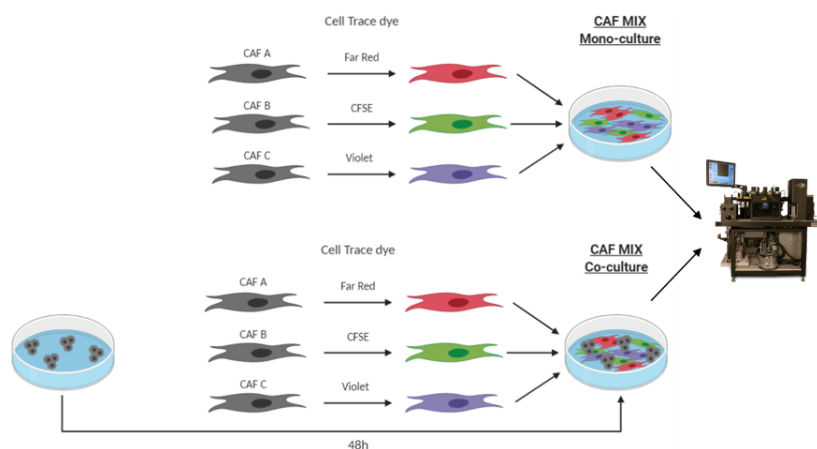


Figure 10. Schematic representation of the experimental design.

5. DRUGS

5.1 PHARMACOLOGIC MODULATORS OF REV-ERB

5.1.1 SR9009

SR9009, also known as stenabolic, is a dual REV-ERB agonist (α and β) that exhibits a specific, direct and reversible binding. Although it is considered a compound with NRs specific union, SR9009 may have some agonist activity at the liver X receptor (LXR) (Kojetin and Burris, 2014).

SR9009 derived from GSK4112, the first synthetic REV-ERB ligand, with structural modifications to improve pharmacodynamics and pharmacokinetics properties

(Kojetin and Burris, 2014). It potently increases REV-ERB-dependent repressor activity (www.selleckchem.com).

SR9009 was purchased from Selleckchem (Catalog No. S8692). Specific treatment conditions are described in the corresponding experimental procedure and/or figure legend. The control condition was treated at the same concentration of DMSO.

5.1.2 SR8278

SR8278 is a REV-ERB α synthetic antagonist that blocks the activity of endogenous ligand (heme). *In vitro* treatments with SR8278 resulted in increased expression of REV-ERB α target genes with higher potency than other synthetic agonists. However, SR8278 exhibits poor pharmacokinetic properties (Kojetin et al., 2011).

SR8278 was obtained from Sigma-Aldrich laboratories (Ref. S9576). Specific treatment conditions are described in the corresponding experimental procedure and/or figure legend. The control condition was treated at the same concentration of DMSO.

6. HISTOLOGICAL STUDIES

6.1 HEMATOXILIN & EOSIN (H&E) STAINING

H&E stain is a tissue staining procedure to visualize the anatomy of tissues at microscopic level. Paraffin-embedded blocks were cut into 3 μ m-thick sections using a microtome (Thermo Fisher scientific) and set down on poly-L-lysine pretreated slides. Tissue sections were deparaffinized by submitting them to submersions in a battery of xylene (4x10min), absolute ethanol (3x5min), 96% ethanol (3x5min), 70% ethanol (1x5min), and 50% ethanol (1x5min). Lastly, sections were rehydrated by submerging them in dH₂O.

After deparaffination and rehydration processes slides were stained with H&E. For that, they were submerged for 10min in hematoxylin 0.1% (Merck) in 96% ethanol and rinsed in tap water to eliminate the excess. Next, they were submerged in 1% HCl until the tissue color turned to red and then in ammonia water solution (200mL of dH₂O with 1mL of 30% ammonia) until the color shifted to blue. Sections were finally counterstained in eosin (2.5g of eosin in 1L of 50% ethanol) for 10min, dehydrated and mounted using DPX (Merck).

Tissues were visualized using the Nikon Eclipse 80i microscope and images were taken with a Nikon DS-Ri1 digital camera using NIS-Elements BR 3.2 software.

6.2 IMMUNOHISTOCHEMISTRY (IHC)

To evaluate protein expression in human tissues, paraffin-embedded tissue blocks were cut and sections were deparaffinized and rehydrated following the protocol described in the 6.1 section of this chapter.

The next step was antigen retrieval, it was done by submerging the tissue slides in the corresponding buffer (Table 7) depending on the antibody, for 5min in a pressure cooker. Then, samples were cooled within the same buffer for 20-30min and washed with dH₂O for 5min.

Endogenous peroxidase activity was blocked by incubation on dH₂O with 40% methanol and 6% H₂O₂ for 15min. Slides were washed with dH₂O for 5min and cell membranes were permeabilized by immersion in TBS-T for 10min.

Afterward, to reduce non-specific antibody binding tissue sections were blocked with goat serum diluted 1:5 in TBS-T for 1h at RT, followed by incubation ON at 4°C in a humid chamber with primary antibodies diluted in blocking solution (Table 7).

Following day, slides were washed thrice with TBS-T for 10min, then incubated with secondary anti-mouse or anti-rabbit Envision⁺-System-HRP (Dako) antibodies for 1h at RT in a humid chamber. After that, samples were washed again and antigen-antibody unions were developed by adding 2 drops/tissue of DAB⁺ EnVision™ Kit (Dako), a chromogenic substrate. Samples were incubated from 1 to 5min, depending on the antibody, until a brown precipitate appeared. DAB reaction was stopped by rinsing the slides with tap water. Finally, sections were counterstained with hematoxylin, dehydrated, mounted and analyzed as H&E-stained slides (6.1).

6.3 DOUBLE IMMUNOHISTOFLUORESCENCE (D-IHF)

D-IHF allowed us to visualize the expression of two different proteins in the same tissue sample by a fluorescence method. The first steps were the same as for IHC. The main differences consist in the fact that slides were incubated with a mix of two primary antibodies (Table 7) diluted in a special IHF solution (1% BSA, 1% goat/horse serum, 0.3% Triton X-100, 0.01% sodium azide in PBS 1X). This solution

Materials and methods

was used to reduce the fluorescent background of paraffin. In D-IHF the secondary antibodies used were goat anti-mouse Alexa Fluor® 488 plus goat anti-rabbit Alexa Fluor® 546 as described in Table 8. Some slides were incubated solely with the blocking solution, which served as a specificity control for secondary antibodies.

After washing the samples thrice with TBS-T, an extra step was added to prevent paraffin autofluorescence, it consisted of incubation with 0.1% Sudan black (Sigma) in 70% ethanol for 30min at RT and darkness. After incubation, samples were washed again thrice with TBS-T and finally, tissue sections were mounted with VECTASHIELD® Mounting Medium with DAPI so cell nuclei were counterstained with DAPI. Slides were stored at -20°C until visualization under Fluorescence DM6000 microscope.

PROTEIN SYMBOL	ANTIBODY REFERENCE	HOST	RETRIEVAL BUFFER	DILUTION
CALD1	HPA008066	R	Sodium Citrate pH6	1:200
CING	HPA027657	R	Sodium Citrate pH6	1:100
FAP α	ab227703	R	EDTA pH8	1:100
FSP-1	HPA007973	R	Sodium Citrate pH6	1:1000
KCNN4	HPA053841	R	Sodium Citrate pH6	1:200
L2GL2	HPA022913	R	Sodium Citrate pH6	1:200
MYOSIN 11	HPA015310	R	Sodium Citrate pH6	1:200
PDPN	HPA007534	R	Sodium Citrate pH6	1:1000
POSTN	ab219057	R	Sodium Citrate pH6	1:150
RARB	NBP1-81776	R	Sodium Citrate pH6	1:250
α SMA	M0851	M	Sodium Citrate pH6	1:400

Table 7. List of primary antibodies used for protein detection by IHC or D-IHF and their specific conditions. R: rabbit; M: mouse. Protein extended name described in ANNEX 1.

SECONDARY ANTIBODY	FLUOROCROME	REFERENCE	MANUFACTURER	DILUTION
Mouse	Alexa Fluor 488	A11001	Invitrogen	1:200
Rabbit	Alexa Fluor 546	A11010	Invitrogen	1:200

Table 8. List of secondary antibodies used in ICF or D-IHF.

7. STATISTICAL ANALYSIS

Experiments were carried out at least 3 independent times with at the minimum 3 technical replicates.

Data were statistically analyzed with GraphPad Prism v8 software to determine if there were significant differences between samples. Results were presented as mean \pm SD.

Data were analyzed using the most appropriate statistical test for each experiment and specific analysis are described in the figure legends. In general terms, non-parametric statistics, U Mann Whitney for unpaired samples and Wilcoxon's test for paired samples were applied for *in vitro* experiments. For experiments involving more than two experimental groups, the Kruskal-Wallis test was used, subsequently applying the Dunn test for multiple comparisons. More details are described in the figure legends.

RESULTS

1. STROMAL TRANSCRIPTOMIC AND METABOLOMIC PROFILING FROM AN *IN VITRO* APPROACH OF PDAC: *IN SILICO* DATA

Previous studies confirmed the presence of CAFs heterogeneity in different tumor types, including PDAC, but no specific biomarkers, pathways neither their contribution to the tumorigenic process have been described yet.

To develop the objective 1 of this thesis, we performed an *in vitro* approach to mimic the real situation in a PDAC human tumor (Figure 11A). As we mentioned previously, PDAC is characterized by a dense desmoplastic stroma and this stroma could be divided topographically, into proximal and distal stroma.

The main feature in the proximal stroma is the crosstalk between CAFs and tumor cells. CAFs and tumor cells can communicate by juxtacrine signaling (cell-to-cell contact) to perform an intercellular exchange. And, they can also communicate by paracrine signaling in which cells transfer signals from one to other through soluble factors.

In the distal stroma, the crosstalk between CAFs and tumor cells is almost absent due to the low vascularization of the desmoplastic stroma and the high interstitial fluid pressure, which prevents the diffusion of soluble factors and hamper the paracrine communication.

In our approximation, we seeded CAFs and tumor cells in a direct co-culture system (DCC; CAFs and tumor cells are in contact in the culture dish) to mimic the proximal stroma, and CAFs in a mono-culture to mimic the distal stroma. The main limitation is the lack of a 3D structure, i.e. the organization of the tumor cells as glands. Each tumor cell type (HPAC, BxPc3, MIA PaCa-2, and PANC-1) was seeded with a mixture of CAFs (mixCAF: CAF A + CAF B + CAF C + CAF D + CAF E; each one coming from a different patient) under DCC conditions (1.1.4 from the previous section) and the same mixCAF as mono-culture (Figure 11B). After 3 days, tumor cells and mixCAF were separated by FACS (Figure 11C) (2.1.1 from the previous section). The obtained pellets were processed to perform the RNA-seq analysis.

Results

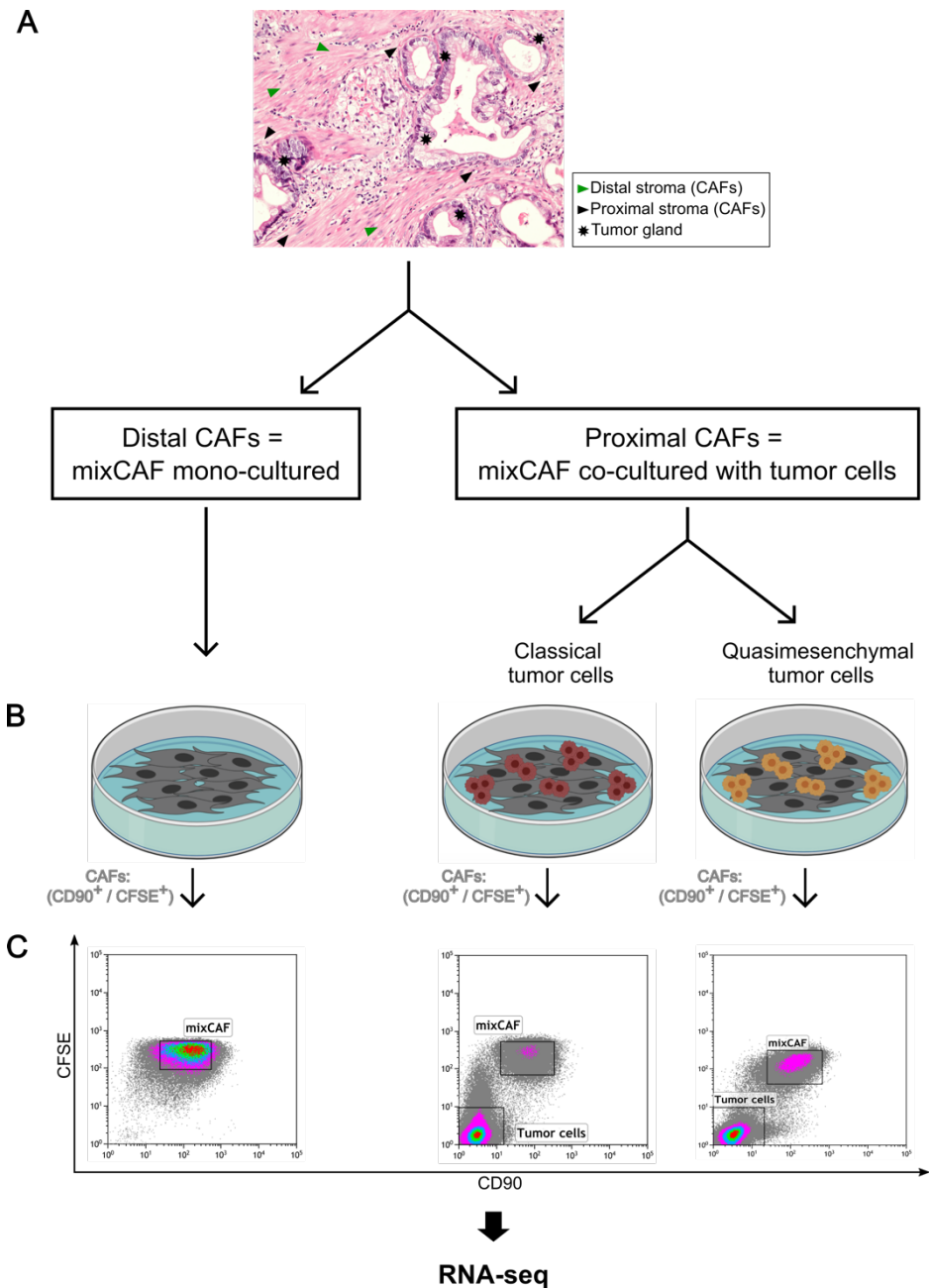
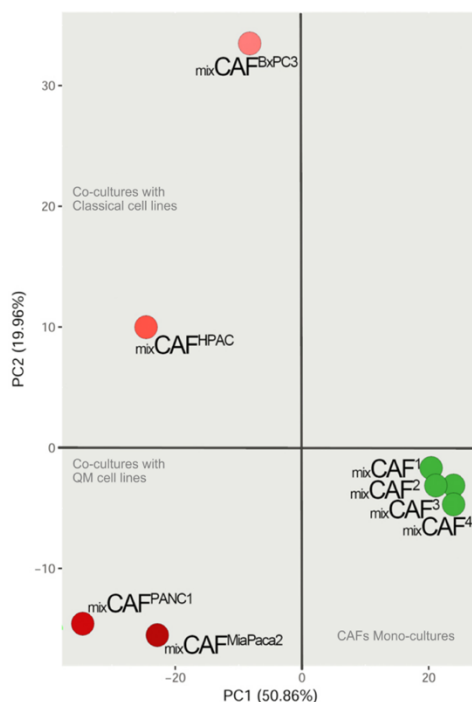


Figure 11. Schematic representation of the *in vitro* approximation and cell sorting conditions. (A) H&E staining of a human PDAC tissue sample. Green arrowheads: distal CAFs located far from the tumor glands; black arrowhead: proximal CAFs located close to tumor gland; asterisks: tumor gland. (B) *In vitro* approach, from left to right: mono-culture of CFSE-labeled mixCAFs; same

CFSE-labeled mixCAFs seeded with tumor cells (DCC) to mimic the proximal situation. (C) Example of cell sorting procedure where CFSE-labeled mixCAFs were also stained with CD90-APC and isolated by FACS. Double positive (CD90⁺/CFSE⁺) population defined mixCAFs and the double negative population defined tumor cells.

1.1 PRINCIPAL COMPONENT ANALYSIS (PCA) CLASSIFIED CAFs ACCORDING TO CULTURE CONDITIONS

To identify patterns in our data, we performed a PCA using the most 500 differentially expressed genes between our conditions as PC1 and PC2 variables (Figure 12). The analysis divided the samples in mono-cultures (right – green dots) and co-cultures (left – red dark and red light dots). Samples of mono-cultured mixCAFs clustered together showing a high degree of homogeneity. Around 50% of variability in PC1 divided our samples in mono-culture and co-culture, the distribution in the co-cultured samples was defined by about 20% of variability in PC2. Samples of the co-cultures were divided depending on the type of tumor cell included in the culture, co-cultures with QM tumor cells also displayed high correlation while co-cultures with the classical showed the highest differences.



Results

Figure 12. Principal component analysis (PCA) for the most 500 differentially expressed genes as PC1 and PC2 variables. The analysis of gene expression data between mono-culture and co-culture conditions by PCA showed a high correlation in the mono-cultured samples (green dots) and in the co-cultured samples (red dots), with a specific distribution of the co-cultured samples depending on the type of tumor cells (classical: up; or QM: down). PC1 and PC2 represent 50.86% and 19.96% of variability, respectively.

1.2 *IN VITRO* TOP 100 GENES DIFFERENTIAL EXPRESSED GENES BETWEEN MONO-CULTURED AND CO-CULTURED CAFs

A total of 2494 protein-coding genes were differentially expressed between mono- and co-cultured CAFs, the analysis of differential expressed genes (DEG) was performed by using a FC (fold change) > 2. Specifically, 762 genes were up-regulated in the mono-cultured CAFs and 1732 genes appeared up-regulated in the co-cultured CAFs.

We represented a list of 100 genes as the best differentially expressed between mono-cultured (mixCAF) and co-cultured CAFs, independently of the tumor cell type (Figure 13). Fifteen genes were upregulated in the mono-culture and eighty-five were upregulated in the co-cultured CAFs.

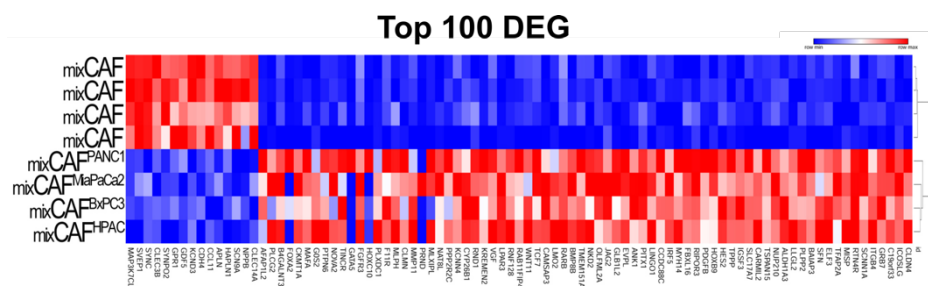


Figure 13. Heatmap of the top 100 differential expressed genes (DEG). Hierarchical clustering heatmap of up- and downregulated gene expression, red and blue respectively. Rows: samples; columns: genes.

As an internal validation, we checked the protein expression of some of these differentially expressed genes.

On one hand, we performed immunocytofluorescence (ICF) staining over *in vitro* cultures to evaluate if the differences observed at transcriptomic level were reproduced at protein level. *KCNN4*, *LLGL2*, and *RARB* were some of the genes that appeared overexpressed in the co-cultured CAFs and their protein expression

(*KCNN4*, *L2GL2*, and *RARB*) were also higher in the co-culture condition (Figure 14A). In turn, *CALD1* and *ACTA2* appeared as overexpressed genes in mono-cultured CAFs. At protein level, CALDESMON was expressed in both conditions but, the intensity of fluorescence was higher for the mono-culture. α SMA was highly downregulated in the co-cultured CAFs (Figure 14B). Finally, we also checked the protein expression of VIMENTIN, a cytoskeletal protein which gene expression levels were not modified between mono- and co-cultured CAFs (Figure 14C – left and right, respectively).

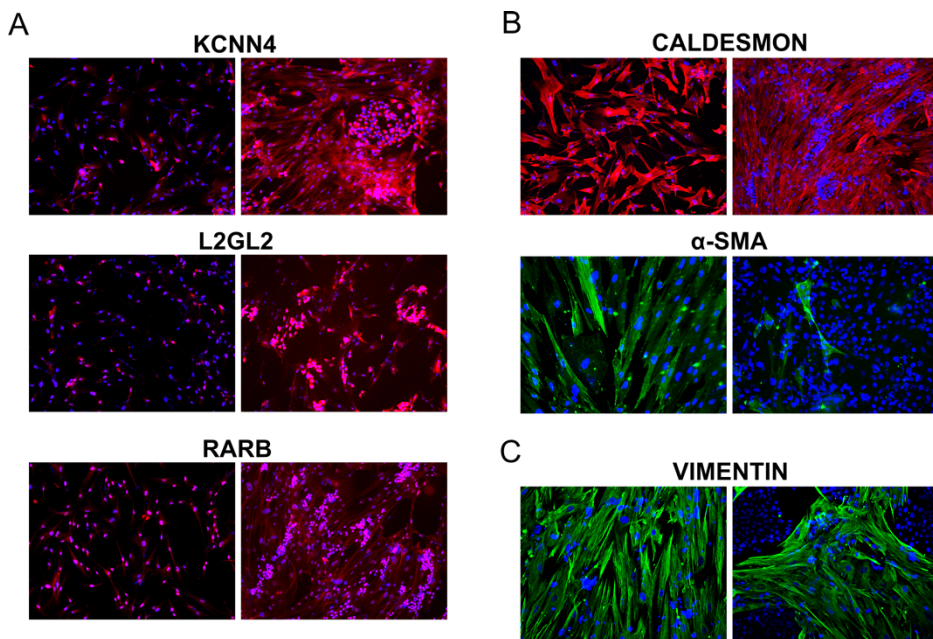


Figure 14. Protein staining by ICF to validate RNA-seq DEG. (A) Protein staining of some genes overexpressed in co-cultured CAFs. (B) Protein staining of some genes overexpressed in mono-cultured CAFs. (C) Protein staining of VIMENTIN which gene expression did not differ between mono and co-culture of CAFs. In all panels, left image: mono-culture of CAFs; right image: direct co-culture of CAFs with tumor cells; green and red: corresponding protein staining; blue: DAPI staining for nucleic acids. The extended names of protein symbols are described in the ANNEX 1. Microscope objective: 20X

We also performed immunohistochemistry (IHC) staining over human PDAC tissue samples to demonstrate that these gene and protein expression observed *in vitro* were also observed in tissue samples. And, therefore, they were not a consequence of the *in vitro* condition.

Results

We validated the protein expression of some genes identified as up-regulated in the *in vitro* co-culture in PDAC surgical specimens. All the proteins were detected close to tumor cells, and in areas of reactive and poorly organized stroma. Some markers such as RARB and L2GL2, were also identified in the tumor cells (Figure 15).

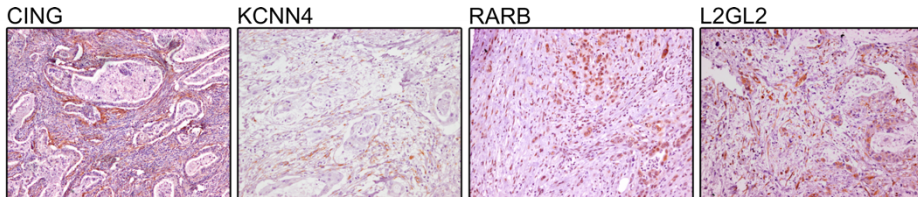


Figure 15. Protein staining by IHC to validate the RNA-seq DEG over different human PDAC tissue samples. Protein name as protein symbol, the extended names are described in the ANNEX 1. Microscope objective: 10X.

1.3 GENE SET ENRICHMENT ANALYSIS (GSEA) REVEALED DIFFERENT TRANSCRIPTOMIC PHENOTYPES BETWEEN MONO- AND CO-CULTURED CAFs

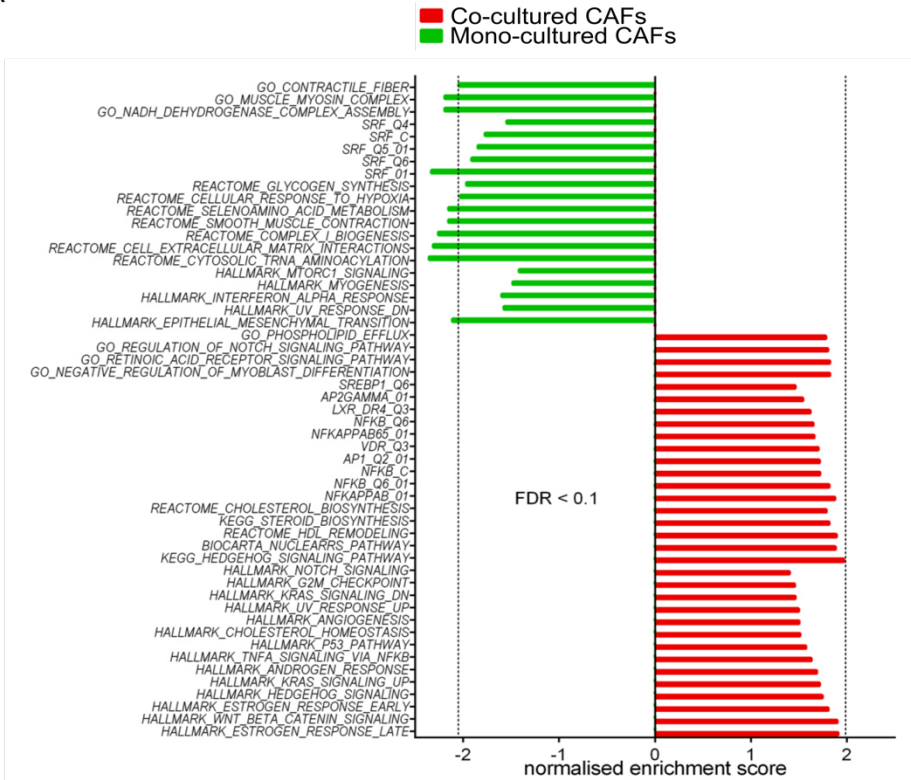
The expression profiles of our *in vitro* experimental conditions were subjected to a pre-ranked GSEA. We focused on the analysis of a collection of gene sets associated with hallmarks, canonical pathways, transcription factors target genes, and gene ontology biological processes (Figure 16). We also compared our phenotypes with other previously reported in the literature, the GSE66616 (Rudisch et al., 2015) and the Moffitt *et al.* signatures (Moffitt et al., 2015).

According to the up-regulated gene sets, the mono-cultured mixCAFs (Figure 16A – green) showed an enrichment in processes involved in myogenesis and muscle contraction displaying an overrepresentation of targets of the SRF (serum response factor). Therefore, mono-cultured mixCAFs described a phenotype similar to a myofibroblast. In turn, co-cultured mixCAFs (Figure 16A – red) showed an enrichment in inflammation, proliferation, and lipid biosynthesis processes among the highest overexpressed.

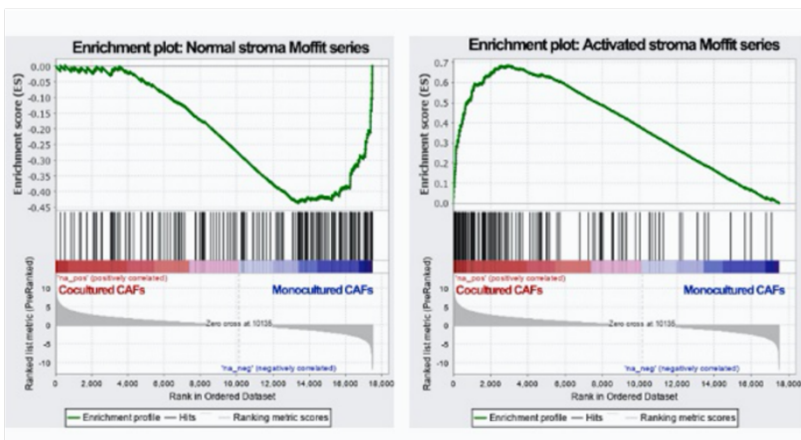
The results of the functional enrichment analyses of our samples were compared with the signatures described by Moffitt *et al.* (Moffitt et al., 2015). This comparison demonstrated that up-regulated processes in mono-cultured CAFs

correlated with normal/quiescent stroma in the Moffitt dataset (Figure 16B – left panel) while overexpressed pathways in co-cultured CAFs correlated with Moffitt activated stroma (Figure 16B – right panel).

A



B



Results

Figure 16. Transcriptomic phenotypes between mono- and co-cultured CAFs (A) and Moffitt correlation (B). (A) GSEA in the Moffitt cohort. Green bars: up-regulated gene sets in mono-cultured mixCAF; red bars: up-regulated gene sets in co-cultured mixCAF. (B) Correlation with stroma signatures in the Moffitt dataset. Mono-cultured CAFs correlated with normal stroma (blue phenotype), and CAFs co-cultured with tumor cells correlated with Moffitt activated stroma (red phenotype).

In order to verify that the correlation is not a matter of the organ, the results of the functional enrichment analyses were also compared with data from a lung cancer dataset (Rudisch et al., 2015). The GSE66616 cohort is composed of mono-cultured lung CAFs, and the same lung CAFs co-cultured with the metastatic lung cancer cells Calu-1. The comparison revealed a correlation between lung and PDAC mono-cultured CAFs and between lung and PDAC co-cultured CAFs (Figure 17).

As we have seen in the comparison with the Moffitt series, the overexpressed processes in mono-cultured CAFs defined a myofibroblast phenotype, whereas in the co-cultured CAFs processes such as inflammation, proliferation, and lipid biosynthesis stood out.

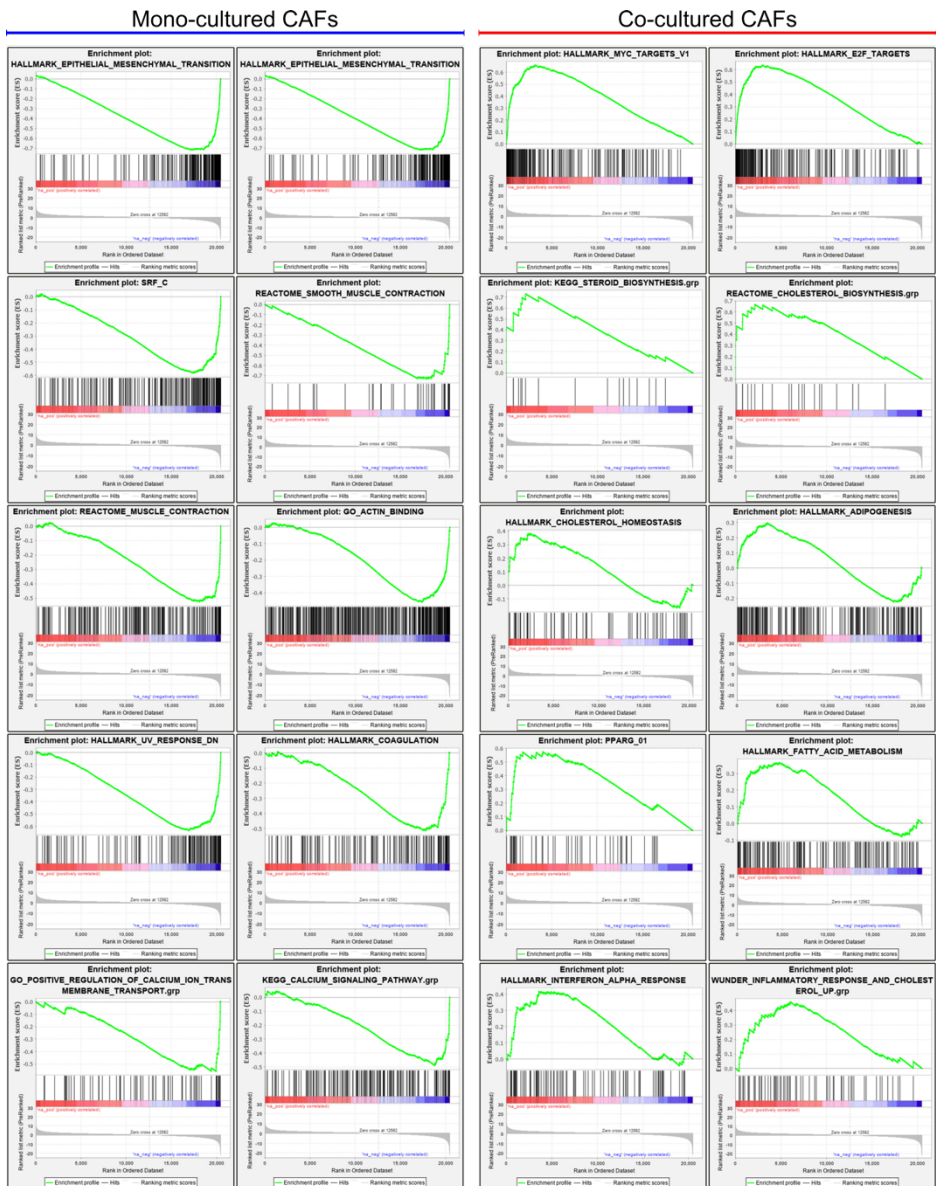


Figure 17. Lung cancer (GSE6616) correlation. PDAC mono-cultured CAFs correlated with lung CAFs mono-cultured (left panel) while PDAC co-cultured CAFs with pancreatic tumor cells correlated with lung CAFs co-cultured with lung cancer cells (Calu-1) (right panel).

1.4 GSEA REVEALED DIFFERENT METABOLOMIC PROFILE BETWEEN MONO- AND CO-CULTURED CAFs

As we mentioned previously, our mono-cultured and co-cultured CAFs correlated with normal/quiescent stroma and activated stroma described in the Moffitt patients' dataset, respectively.

We performed a GSEA to check the correlation of the specific processes that define our phenotypes with gene sets of metabolic and myogenic processes. The processes with high correlation with our mono-cultured CAFs, were associated with the production of muscular tissue (Figure 18 – blue). The production of muscular tissue included the hallmark of myogenesis, GO of muscle filament sliding, muscle alpha actin binding, myosin filament and muscle myosin complex, and signaling regulation of the actin cytoskeleton by Rho GTPases.

The co-cultured PDAC CAFs showed overexpression in the processes related with the metabolism of lipids. According to the enrichment plots (EP), the highest correlations with our co-cultured CAFs were found in the biosynthesis and transport of steroids, the adipogenesis, and the metabolism of phospholipids (Figure 18 – red). Specifically, all the genes and transporters of mevalonate pathways, that were included in the steroid biosynthesis EP, appeared overexpressed in our co-cultured CAFs compared with the mono-cultured PDAC CAFs.

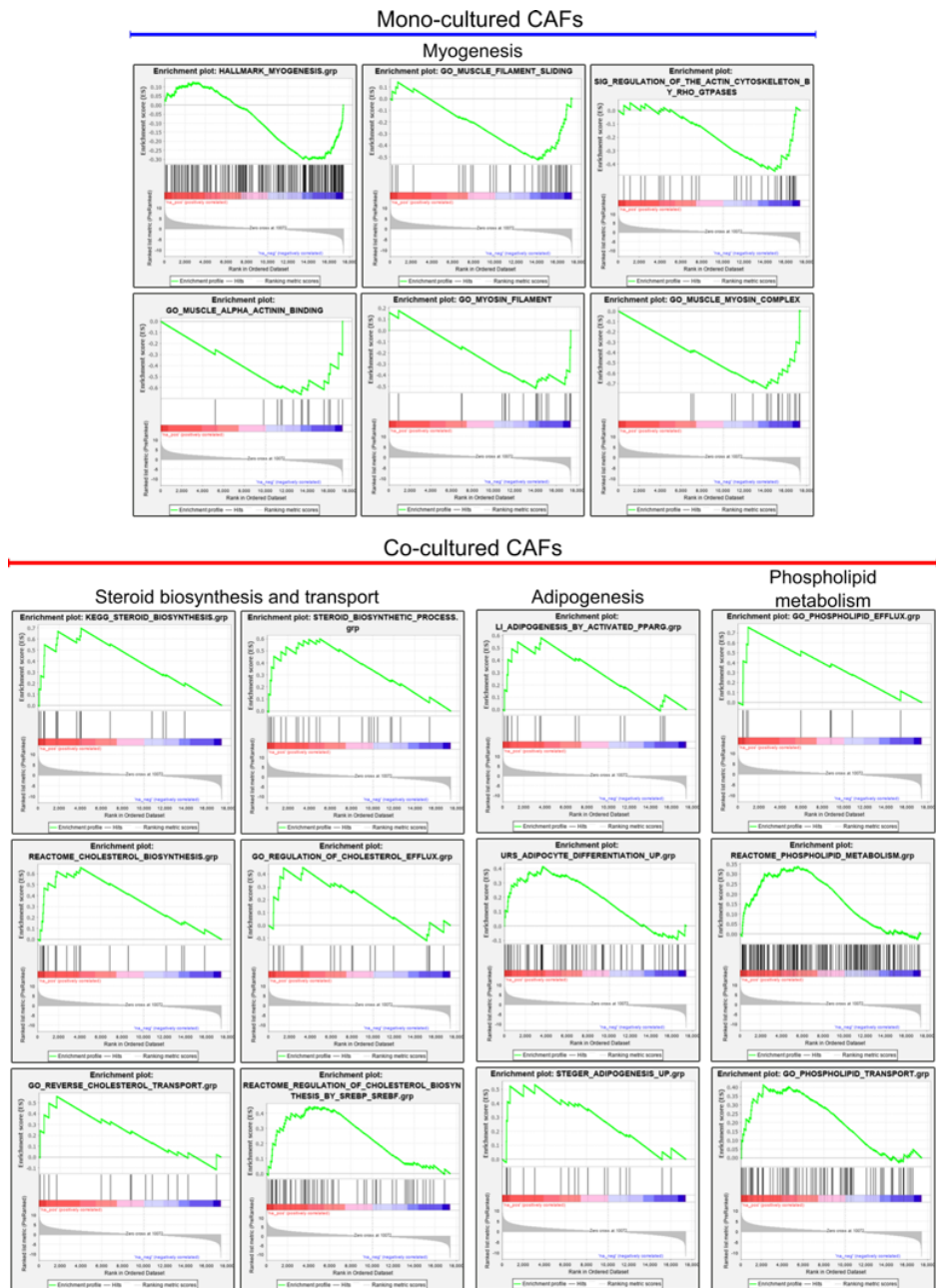


Figure 18. GSEA showing a correlation between mono- and co-cultured CAFs of differentially expressed processes that define our phenotypes. Enrichment plots (EP) of mono-cultured CAFs (blue) showed the highest correlation with hallmark of myogenesis, GO of muscle filament sliding, muscle alpha actin binding, myosin filament and muscle myosin complex, and signaling regulation of the actin cytoskeleton by Rho GTPases. EP of co-cultured CAFs (red) showed the

Results

highest correlation with KEGG steroid biosynthesis, steroid biosynthetic processes, reactome of the cholesterol biosynthesis and its regulation by SREBP and SREBF, GO of the regulation of cholesterol efflux and reverse cholesterol transport, synthesis and differentiation of adipocytes and efflux, metabolism and transport of phospholipids.

1.4.1 Metabolic reconstruction analysis confirmed the relevance of lipids signaling pathways and metabolism in the co-cultured CAFs

As lipid metabolism-related pathways and processes were overexpressed in our co-cultured CAFs compared with the mono-cultured, we wanted to evaluate the effects of these differential gene expression levels in signaling and metabolism. For that, we asked for the collaboration of Dr. Dopazo's bioinformatics group that performed a metabolic reconstruction analysis.

In summary, they used our RNA-seq data to report us information about genes, pathways, and metabolites vulnerable to be modified and the possible consequences.

First, they studied and interpreted the consequences of the combined changes of gene expression levels in the context of signaling pathways using the Hipathia web tool (<http://hipathia.babelomics.org>) (Hidalgo et al., 2017). Gene expression data after normalization were used to analyze pathways activation status. The comparison of these data between groups showed up- or downregulated pathways regarding the control group (mixCAF's mono-culture).

The results were also related to Gene Ontology (GO) functions and revealed that the highest upregulated pathways were involved in cholesterol efflux and lipids metabolism. While the most downregulated pathways included energetic processes related to calcium transport (Table 9). These results confirmed and complemented the ones obtained by GSEA. Thus, an enrichment in lipid metabolic processes in co-cultured CAFs, specifically, transport and efflux. And, the upregulation of ion Calcium transport and ATPase activity confirmed myogenesis and muscle contraction processes in the mono-cultured CAFs, since, both biological processes are needed for the muscle contraction and synthesis.

CATEGORY 1	CATEGORY 2	GO FUNCTION	T	FC	P.VALUE	FDR P.VALUE	CO-CULTURED CAFs
Lipids	cholesterol	positive regulation of cholesterol efflux	8.234	0.020	0.0001	0.018	UP
Lipids	lipid	lipid metabolic process	8.004	0.035	0.0001	0.018	UP
Lipids	lipid	long-chain fatty acid metabolic process	7.972	0.026	0.0001	0.018	UP
Lipids	lipid	membrane raft localization	7.599	0.020	0.0002	0.018	UP
Energetics	calcium	negative regulation of calcium ion transmembrane transporter activity	-9.480	-0.048	0.0000	0.011	DOWN
Energetics	calcium	negative regulation of calcium ion binding	-9.480	-0.048	0.0000	0.011	DOWN
Energetics	calcium	regulation of calcium-transporting ATPase activity	-9.480	-0.048	0.0000	0.011	DOWN
Energetics	calcium	negative regulation of calcium-transporting ATPase activity	-9.480	-0.048	0.0000	0.011	DOWN
Energetics	calcium	negative regulation of calcium ion transport	-9.480	-0.048	0.0000	0.011	DOWN

Table 9. Summary of the highest up- or downregulated signaling pathways in the co-cultured mixCAFs analyzed with HiPathia. Category 1 and 2: standard and specific biological processes, respectively; p.values were obtained by the comparison of mixCAFs mono-culture vs mixCAFs co-culture with FDR adjustment. Complete table in the ANNEX 2

Then, we explored the prediction of KEGG modules involvement and particular metabolite production on each CAFs' phenotypes. For this purpose we used

Results

Metabolizer (Çubuk et al., 2019) and Metabolica tools. FA and TG biosynthesis were the KEGG modules overexpressed in the co-cultures (Figure 19A – red cluster) while, nucleotide biosynthesis, urea cycle, and methionine degradation were the overexpressed KEGG modules in the mono-cultured CAFs (Figure 19A – black cluster).

The second type of analysis was an *in silico* prediction of differentially altered metabolite production using the Metabolica tool. As shown in Figure 19B, among the overexpressed metabolites in the co-cultured CAFs we found those involved in steroids and fatty acids biosynthesis. While, metabolites involved in folate biosynthesis and, pentose and glucuronate metabolism, were overexpressed in the mono-cultured CAFs.

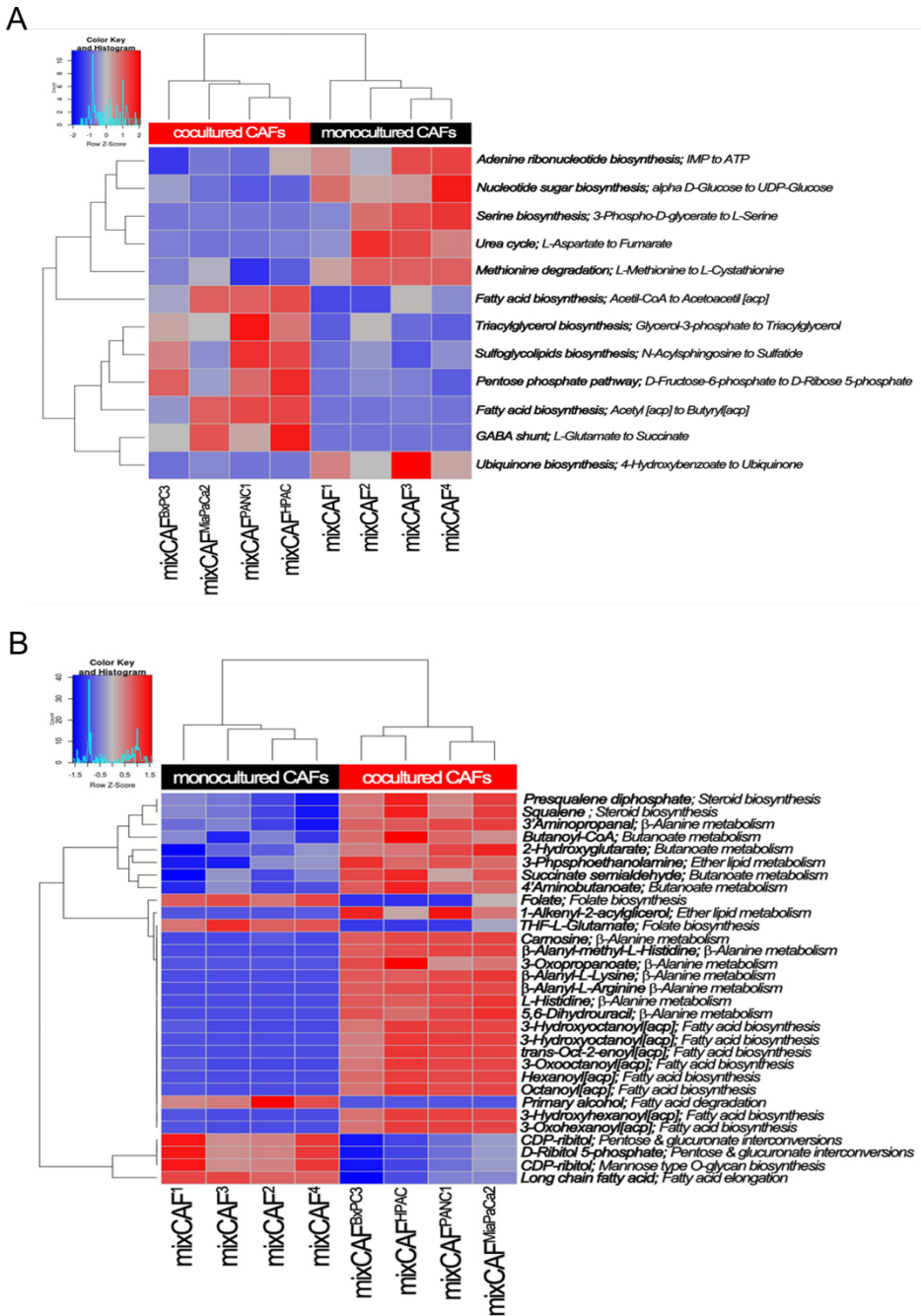


Figure 19. Data of the metabolic reconstruction analysis performed with Metabolizer and Metabolica. (A) Heatmap of significantly altered KEGG modules using Metabolizer tool. (B)

Results

Heatmap of *in silico* prediction of differentially altered metabolite production using Metabolica tool.

1.5 ssGSEA CLUSTERED PATIENTS TO PARTICULAR *IN VITRO* CAFs GENE SIGNATURES

A single sample GSEA (ssGSEA) grouped patients from a cohort according to a particular gene signature, and we got two different gene signatures depending on the culture conditions. So, we performed a ssGSEA to see how patients from two independent datasets were grouped depending on our signatures.

We took DEG (FDR < 0.05; FC > 2) that defined our signatures and performed a ssGSEA over the patients' datasets, the Moffitt and the TCGA – PAAD cohorts. The first analysis was done over the Moffitt series taking DEG that defined our 2 phenotypes (mono-culture *versus* co-culture). This analysis divided the patients into two clusters (Figure 20). Most patients with Moffitt normal stroma were grouped in the mono-cultured CAFs cluster (light blue), while most patients with Moffitt activated stroma (brown) were grouped in our co-cultured CAFs. Interestingly, patients segregated according to the tumor cell type (basal-like/QM, or classical; orange and dark blue, respectively) were randomly distributed.

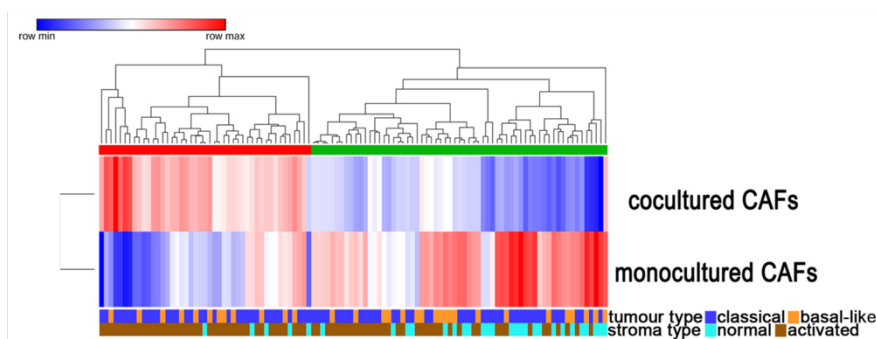


Figure 20. Heatmap of ssGSEA of CAFs signatures. ssGSEA heatmap of CAFs signatures in the Moffitt patients' dataset revealed two different clusters of patients according to the dendrogram. Green cluster: highly correlated with mono-cultured CAFs signature; red cluster: highly correlated with co-cultured CAFs signature. Similar results were obtained with the TCGA patients' dataset.

2. PROGNOSTIC VALUE OF CAF SIGNATURES

ssGSEA grouped patients to a particular gene signature (Figure 20). We analyzed the survival probability of these groups of patients (clusters) to assess the prognostic association of our CAFs profiles in two different patients' cohorts (Moffitt series and TCGA – PAAD series).

2.1 MONO-CULTURED CAFs CORRELATED WITH BETTER SURVIVAL PROBABILITY IN THE TWO-CLASSES SIGNATURES

The survival analysis of the two-classes transcriptomic signatures in the Moffitt patients' dataset (Figure 20) showed that patients with higher expression of the mono-cultured CAFs signature had a better prognosis than patients with high expression of the co-cultured CAFs signature (Figure 21). The Moffitt dataset included 108 patients and the median of survival probability was 21 months for the mono-culture versus 13 months for patients with higher expression of co-cultured CAFs signature.

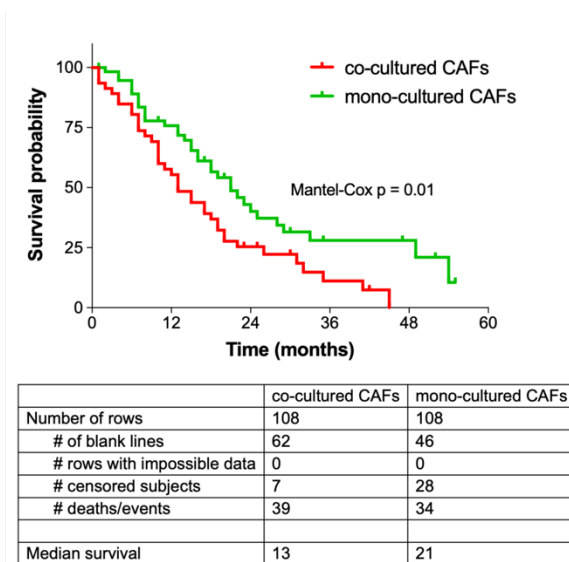


Figure 21. Prognostic association of two-classes transcriptomic signatures of CAFs in the Moffitt series. The survival analysis associated the expression of mono-cultured CAFs signature with a better prognosis. Mantel-Cox proportional-hazards regression model ($p = 0.01$).

2.1.1 Cholesterol and TNF were the hallmarks with prognostic value in the two-classes signatures

We aimed to explore which biological processes from our CAFs had an impact on the survival of patients. We used the information provided by the MSigDB Hallmarks dataset to generate different signatures. The signatures were created by using the *leading-edge* genes for each of the hallmark's gene sets statistically significant (FDR < 0.05). Genes in the leading-edge are those contributing the most for a particular phenotype. Then, we performed a ssGSEA over the Moffitt patients' dataset. Those processes that occur in CAFs with an impact on patients' survival were the illustrated in Figure 16A.

Next, with the ssGSEA clusters, we performed the survival analysis applying the TCGA dataset. Using the complete dataset none of the gene sets were associated to prognosis. However, the prognosis value changed when we segregated the tumors taking their fibroblast content into account. For that, tumors were separated according to the MCP-counter (Microenvironment Cell Population-counter) (Becht et al., 2016). In those patients whose tumors have a percentage of fibroblasts > 50%, an enrichment in the cholesterol homeostasis (Figure 22A) and in the inflammation mediated by $\text{NF}\kappa\beta$ (Figure 22B) had a deep impact on the prognosis.

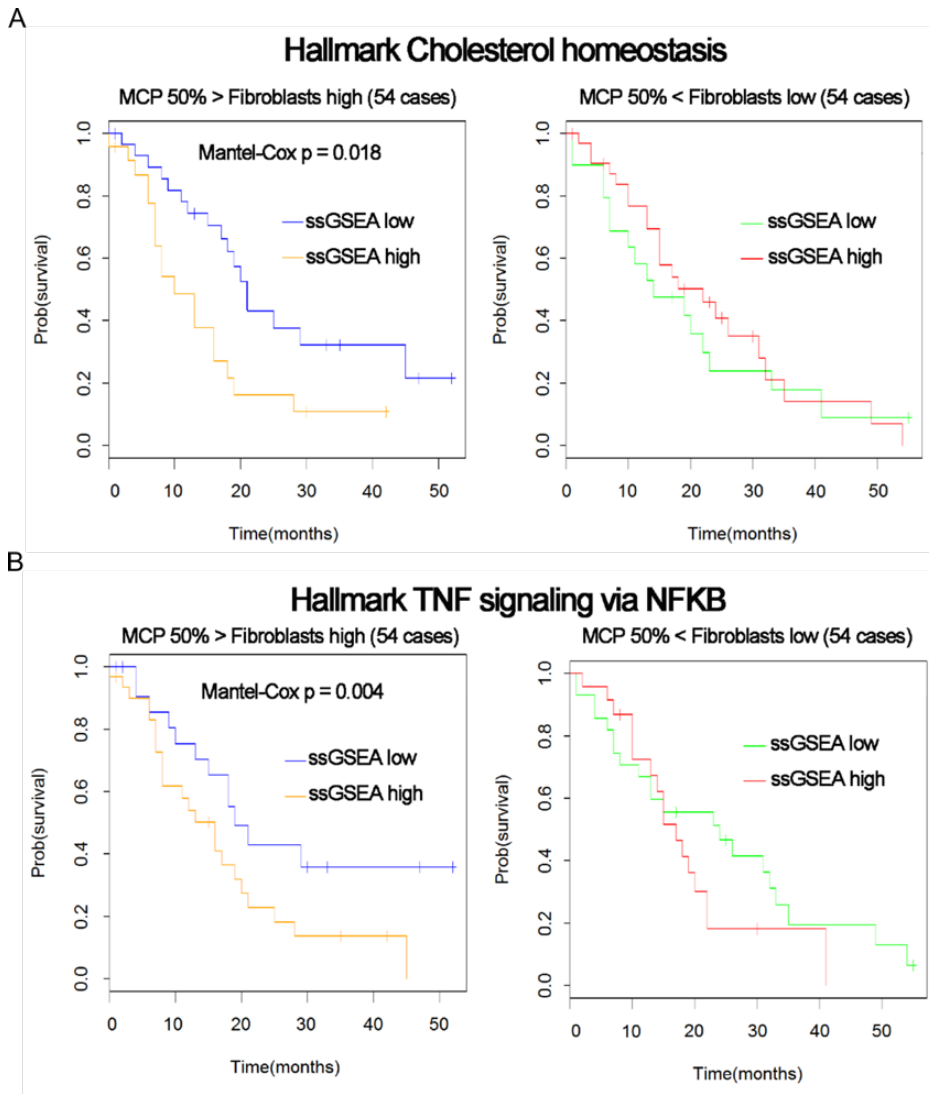


Figure 22. Prognostic association of cholesterol homeostasis (A) and TNF signaling via NFκβ (B) hallmarks. Patients from the Moffitt dataset were divided into fibroblast high (50% = 54 patients) or fibroblast low (50% = 54 patients) using MCP-counter for both hallmarks. (A) ssGSEA of cholesterol homeostasis hallmark had prognostic value for high fibroblast patients with a worse prognosis for the patients with an enrichment in the cholesterol homeostasis process; $p=0.018$ by Mantel-Cox analysis. (B) ssGSEA TNF signaling via NFκβ hallmark had prognostic value for high fibroblast patients with a better prognosis for the ssGSEA low patients; $p=0.004$ by Mantel-Cox analysis.

In the cholesterol homeostasis process, the analysis demonstrated that patients with high fibroblast content and included in the ssGSEA high cluster had a worse

Results

prognosis (Figure 22A – left). On the contrary, the survival analysis over patients included in the low stroma tumors clusters, the cholesterol homeostasis hallmark did not provided prognostic value (Figure 22A – right).

The same analysis was performed for the TNF signaling via $\text{NF}\kappa\beta$ (Figure 22B) and the obtained results showed a worse prognosis for patients with fibroblast enriched tumors and included in the ssGSEA high cluster (Figure 22B – left). The differences between both clusters in patients with low fibroblast content tumors did not reveal significative value (Figure 22B – right).

Therefore, when we considered patients with high stroma content tumors, the overexpression of the leading-edge genes from cholesterol and TNF pathways were associated with a worse prognosis. However, if the survival analysis was performed over low stroma content tumor patients, there were no significant differences. This fact means that the prognostic value of these leading-edge genes is probably determined by the stroma.

2.2 THREE-CLASSES TRANSCRIPTOMIC SIGNATURES SHOWED DIFFERENCES IN THE SURVIVAL PROBABILITY FOR TWO INDEPENDENT PATIENTS' DATASETS

As we remarked before, when we assessed the prognostic value of our CAFs signatures on the Moffitt dataset, we noticed a randomly distribution of patients according to their tumor cell type. Classical and basal-like/QM were equally distributed in the two clusters. This fact led us to explore differences in our CAFs, taking into account whether they had been co-cultured with classical or quasimesenchymal tumor cells.

For this purpose, we considered a Bayesian approach to explore differentially expressed genes across three groups instead of a dichotomic approach explained so far.

The analysis reported three different signatures (Figure 23), corresponding to a CAFs mono-cultured, CAFs co-cultured with basal-like/quasimesenchymal cells (MIA PaCa-2 and PANC-1) and CAFs co-cultured with classical cells (HPAC and BxPc3).

The Bayesian analysis reported three signatures defining a set of upregulated genes in CAFs depending on the tumor cells included in the co-culture. One signature for CAFs co-cultured with basal-like/QM cells (Figure 23 – yellow cluster), a set of genes acquired after the co-culture with classical tumor cells (Figure 23 – blue cluster) and, a group of genes upregulated in mono-cultured CAFs (Figure 23 – red cluster). The green cluster illustrate acquired genes in common, those that are upregulated in CAFs with both tumor cell types.

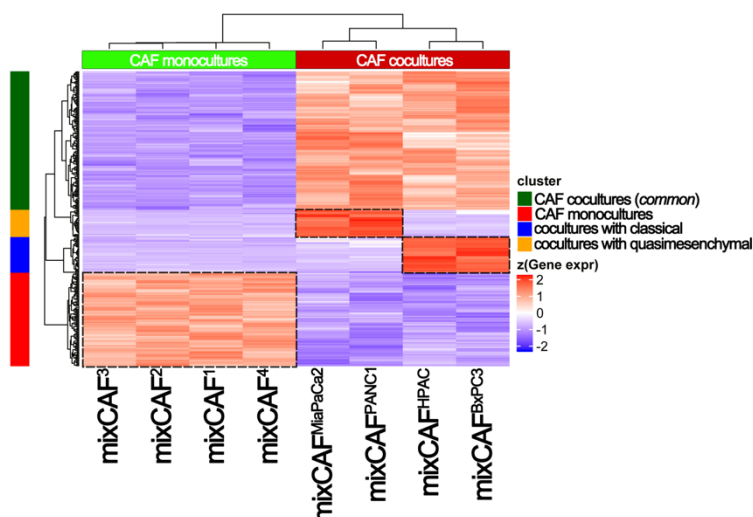
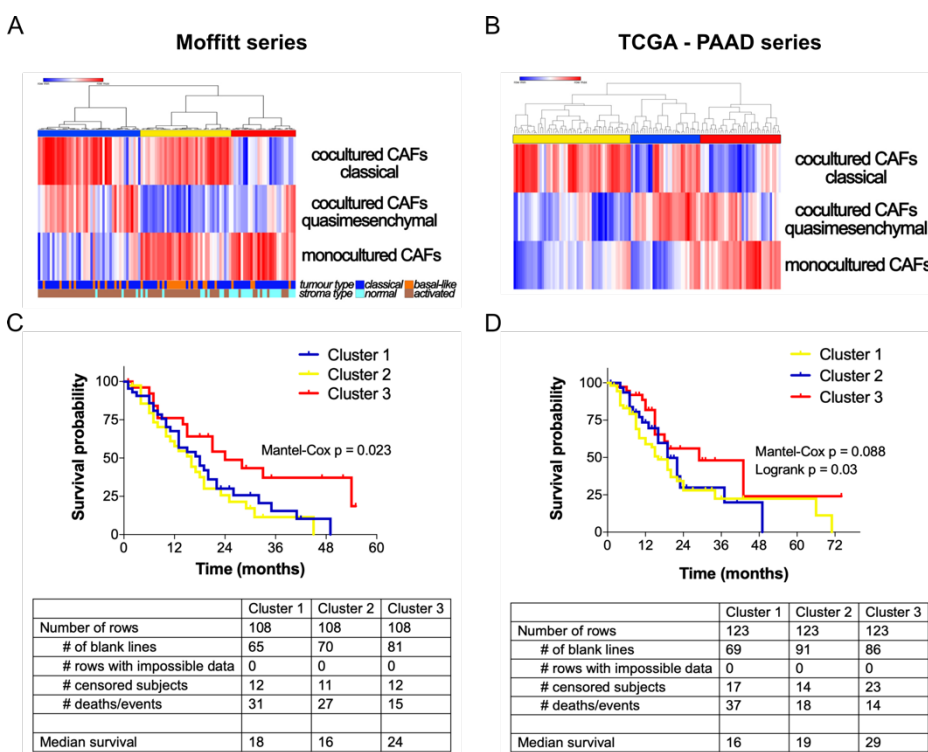


Figure 23. Heatmap of ssGSEA of CAFs' signatures. ssGSEA of CAFs signatures grouped the patients in three clusters (blue, yellow, and red) in the Moffitt patients' datasets when the tumor cell type (classical or quasimesenchymal) were considered to perform the analysis. The green cluster included patients with common upregulated genes in the co-culture with both tumor cell types.

Following the previous analyses, we performed the ssGSEA over both cohorts (Moffitt and TCGA – PAAD). The analysis was done with the previous Bayesian signatures, those obtained from CAFs considering the tumor cell type included in the co-culture. The three signatures reported three clusters in both patient's datasets (Figure 24A and B). The red cluster included patients with overexpression of mono-cultured CAFs signature; the yellow cluster contained patients with CAFs co-cultured with classical cells signature and, the blue cluster grouped patients with CAFs co-cultured with basal-like/QM cells signature. Moreover, we checked how patients are grouped considering the type of tumor cells and the type of stroma according to the Moffitt classification system. As Figure 21A shows,

Results

patients included in the red cluster, the one with overexpression of mono-cultured CAFs signature, also grouped most patients with Moffitt normal stroma. Most patients with overexpression of Moffitt activated stroma were grouped in between cluster blue and yellow. The distribution of patients considering the type of tumor cell included in the co-culture did not completely correlate with our signatures since, patients with classical tumor type signature were mostly included in our mono-culture and co-cultured with QM cells signatures, while most patients with basal-like tumor type signature were grouped in our co-cultured with classical cells signature. The main feature of co-cultured CAFs signatures was the loss of mono-cultured CAFs signature.



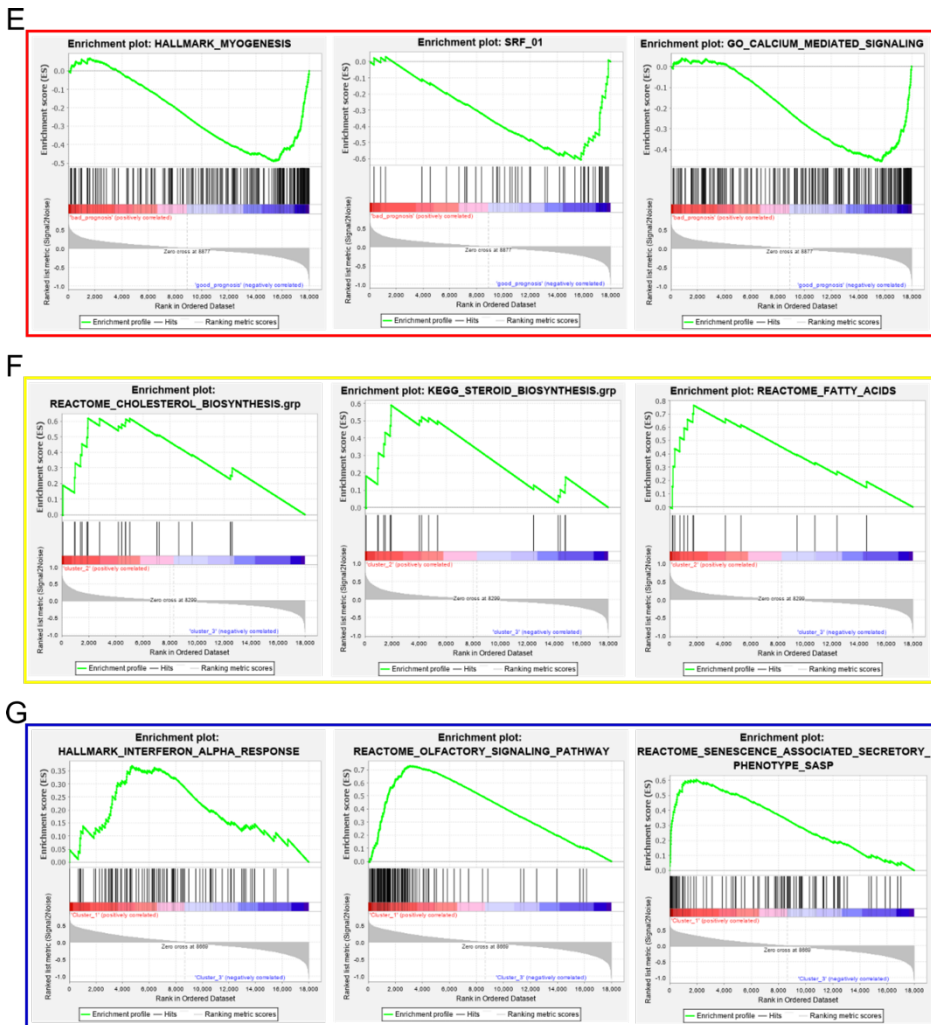


Figure 24. Three-classes transcriptomic signatures (A, B), survival probability (C, D), and enrichment plots of enriched GSEA processes in each cluster (E, F, G). Heatmaps of three-classes CAFs signatures in the Moffitt series (A) and the TCGA – PAAD series (B) classify patients of each dataset in three clusters: mono-cultured CAFs, CAFs co-cultured with classical tumor cells and, CAFs co-cultured with quasimesenchymal tumor cells. (C, D) The survival analysis showed that the presence of mono-cultured CAFs overexpressed genes (cluster 3) correlated with better survival probability while the presence of co-cultured CAFs overexpressed signatures (cluster 1 and cluster 2) associated with lower survival probability for both datasets (C: Moffitt, $p=0.023$ by Mantel-Cox; D: TCGA – PAAD, $p=0.088$ by Mantel-Cox). (E) Enrichment plot of overexpressed processes in the mono-culture (red cluster 3). (F) Enrichment plot of overexpressed processes in the co-culture with classical cells (yellow cluster 2 in the Moffitt dataset or yellow cluster 1 in

Results

the TCGA – PAAD cohort). (G) Enrichment plot of overexpressed processes in the co-culture with QM cells (blue cluster 1 in the Moffitt dataset or blue cluster 2 in the TCGA – PAAD cohort).

The survival analysis of the three-classes transcriptomic signatures showed that patients with higher expression of the mono-cultured CAFs signature (Figure 24C and D; cluster 3 – red line) were associated with better prognosis in two different PDAC patients' dataset (Moffitt and TCGA – PAAD). Opposite, patients with high expression of co-cultured CAFs signature (Figure 24C and D; clusters 1 and 2) were associated with a worse prognosis.

The Moffitt dataset included 108 patients (as the authors did in the already published manuscript in Nature Medicine, we excluded from the analyses those patients with a low percentage of stroma according to the NMF analysis reported). The median survival probability was 24, 16, and 18 patients for the overexpression of mono-culture, the co-culture with classical cells, and the co-culture with QM cells signatures, respectively. Survival differences between signatures had a significant value ($p = 0.023$).

The TCGA – PAAD dataset included 123 patients (we excluded the 25% of patients with low stroma percentage according to the MCP-counter values). The median survival probability was 29, 16, and 19 patients for the overexpression of mono-culture signature, the co-culture with Classical cells, and the co-culture with Basal-like/quasimesenchymal cells signatures, respectively.

We also performed GSEA of patients included in each cluster. Patients with better prognosis (cluster 3 – red) had enrichment in myogenesis, serum response factor, and calcium-mediated signaling processes. All of them linked to muscle production (Figure 24E) and matching with our previous results. Figure 24F shows the EP of the GSEA for the patients included in the cluster with overexpression of CAFs co-cultured with Classical cells signature and, all of them, were processes related to lipid biosynthesis. Finally, GSEA of patients with overexpression of CAFs co-cultured with Basal-like/Quasimesenchymal cells signature showed enrichment in inflammation-related processes (Figure 24G).

2.3 MYOFIBROBLAST-LIKE PHENOTYPE CORRELATED WITH A BETTER PROGNOSIS

Features that better define our phenotypes were myofibroblast markers for the mono-culture of CAFs and the cholesterol (Mevalonate) and inflammation pathways for the co-cultured CAFs. To correlate these signatures with the Moffitt cohort, we performed a GSEA in the Moffitt dataset where patients were classified into two groups according to the prognosis.

As in GSEA we could only compare two groups, the first comparison was performed between cluster 3 (good prognosis) and cluster 1 plus 2 (bad prognosis). The enrichment plot demonstrated that myofibroblast markers correlated with cluster 3 which grouped patients with overexpression of mono-cultured CAFs signature and associated with better prognosis. (Figure 25 – left EP).

In the GSEA for the cholesterol pathway, as we could only compare two groups of patients, we compared the cluster 3 (mono-culture) versus cluster 2 (co-culture with classical cells), so classical cells used the cholesterol pathways more efficiently than Basal-like/Quasimesenchymal cells (Nicolle et al., 2017). This comparison demonstrated that cluster 2 correlated better with the Mevalonate (cholesterol) pathway (Figure 25 – right EP).

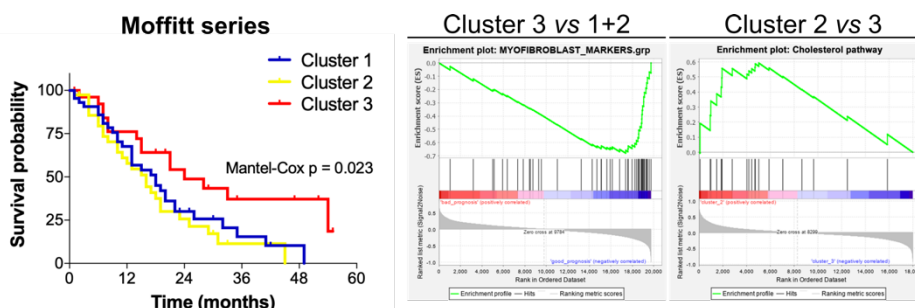


Figure 25. Survival probability of the three-classes signature (right panel) and enrichment plots (EP) of myofibroblast markers and cholesterol pathway (left panel) in the Moffitt patient's dataset. The survival analysis showed that the presence of mono-cultured CAFs overexpressed genes (cluster 3) correlated with better survival probability while the presence of co-cultured CAFs overexpressed genes (cluster 1 and cluster 2) associated with lower survival ($p=0.023$ by Mantel-Cox). GSEA of myofibroblast markers correlated better with mono-cultured CAFs

signature (cluster 3) and GSEA of cholesterol correlated better with co-cultured CAFs signature (cluster 2).

3. IDENTIFICATION OF SPECIFIC BIOMARKERS WITHIN THE DIFFERENT PHENOTYPES IN *IN VITRO* CULTURES

3.1 CAFs FROM PDAC SHOWED HETEROGENEITY AT TRANSCRIPTIONAL LEVEL

As already mentioned, RNA-seq data were obtained from a mixture of CAFs isolated from different patients. Considering previous studies that reveal the presence of CAFs heterogeneity (Elyada et al., 2019; Moffitt et al., 2015; Neuzillet et al., 2019; Öhlund et al., 2017), we wanted to characterize the isolated CAFs that we used in the initial *in vitro* approximation (Figure 11) at transcriptional and functional levels.

3.1.1 Identification of different phenotypes in CAFs isolated from primary human PDAC

We checked the expression levels of some classical CAFs' markers and some markers described in previous studies over our five PDAC CAFs at basal conditions (DMEM-GlutaMAX supplemented with 2% FBS).

The analysis revealed the presence of 3 main subtypes of CAFs, that we called myoCAF, lipoCAF, and ecmCAF considering their protein expression profiles. Among the five different CAFs used in the initial culture, 3 of them correlated better with these subtypes both, at protein (Figure 26A) and at RNA levels (Figure 26B).

CAF A had a myoCAF profile with high levels of MYH11, ACTA2, and PDPN at RNA and at protein levels. Besides, CAF A also showed a high expression of *SRF* at RNA. We also evaluated expression of some other proteins associated with myogenesis such as CALDESMON and CALPONIN-1 and, both of them were higher in CAF A together with loss of expression of PDGFR α .

CAF B, the ones that we called lipoCAF because of the high expression of PPAR γ , were also characterized by the expression of S100-A4 both, at a protein level and RNA levels. This CAFs showed discrete protein levels of extracellular matrix

proteins like PERIOSTIN and FIBRONECTIN and relatively high levels of FAP. They also displayed high levels of PDGFR α .

CAF C had the most inflammatory profile with high levels of interleukins (*IL-6* and *IL-1 β*) and chemokines ligands (*CCL2*) at a transcriptional level. Western blot analysis also showed high levels of FAP and extracellular matrix proteins such as FIBRONECTIN, PERIOSTIN. We named CAF C as ecmCAF.

However, we observed some discrepancies between RNA and protein for some markers. In any case, we have always given relevance to protein values.

Finally, we also checked VIMENTIN expression because it is considered a pan-marker of CAFs and, its expression showed almost no differences between CAF A, CAF B, and CAF C.

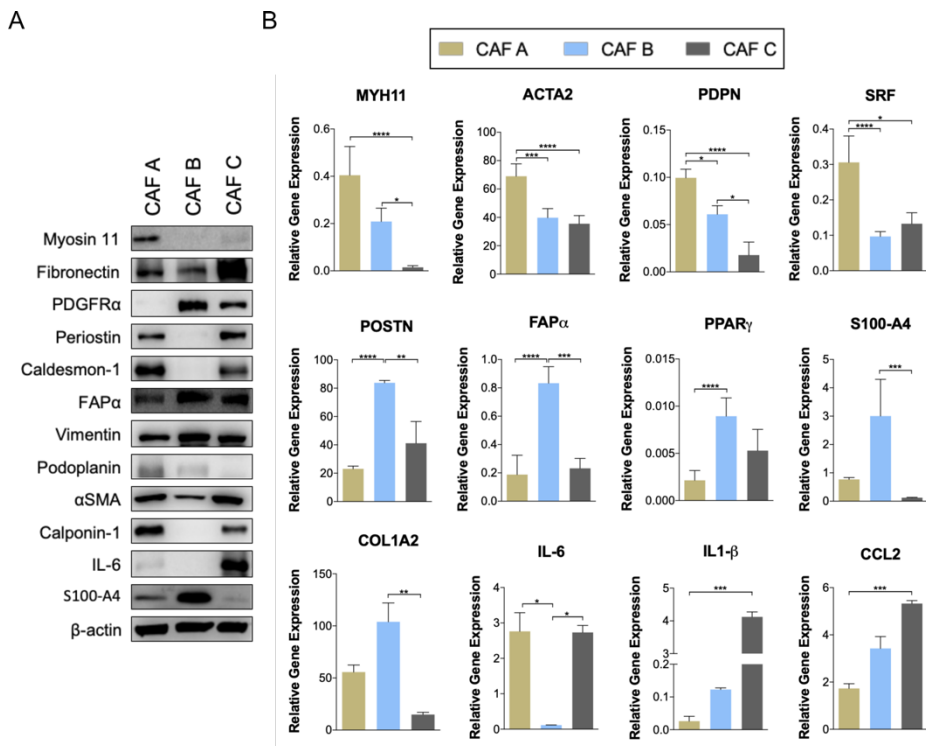


Figure 26. CAFs subtypes characterization by protein and gene expression. (A) Protein expression of different CAFs biomarkers in CAF A, CAF B, and CAF C, at basal conditions. (B) Relative gene expression (mean \pm SD) of different CAFs biomarkers in CAF A, CAF B, and CAF C, at basal conditions. HKG: QARS. Data represented as mean \pm SD of 3 independent experiment

Results

with at the minimum 3 technical replicates. Kruskal-Wallis test multiple comparisons with Dunn's correction (* $p < 0,05$; ** $p < 0,01$; *** $p < 0,0001$; **** $p \leq 0,00009$).

From this characterization, we worked with these 3 CAFs subtypes (CAF A, CAF B, and CAF C) to simplify the subsequent assays.

3.1.2 The correlation plot of “classical” CAFs markers in the Moffitt series classify patients in three clusters with a different prognostic association

Following, we tried to correlate the expression profile of our CAFs subtypes with a patients' cohort. For that, we chose a set of genes considered as classical CAFs' markers according to the bibliography to check how they are grouped in the Moffitt patients' dataset.

We selected 15 genes to explore first, the correlation between them using the expression values of Moffitt's (Figure 27) and TCGA – PAAD patients' cohorts (data not shown). Lately, we used ssGSEA and patients in both cohorts to explore the prognostic value of the generated clusters of CAFs

Patients included in the myoCAF cluster showed high expression of *ACTA2*, *MYH11*, *CNN1*, *DES*, and *SRF* (Figure 27A – green), and they were associated with the best prognosis (Figure 27B – green). Instead, the ecmCAF cluster included patients with high expression of *FAP*, *SPARC*, *POSTN*, different types of collagens, and lower levels of *ACTA2* (Figure 27A – blue). And, the lipoCAF cluster included patients with high expression of *S100-A4*, *PPAR γ* , *SCD*, *ABCG1*, and *NR1D1* (Figure 27A – red). The median survival of ecmCAF and lipoCAF clusters showed almost no differences between them (Figure 27B – red, blue).

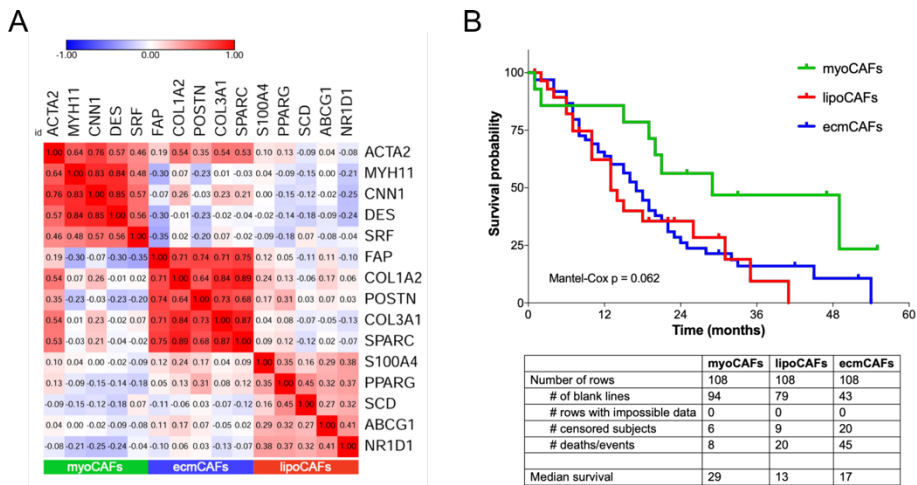


Figure 27. Correlation plot of CAFs' markers in the Moffitt series. (A) Corrplot of 15 CAFs' markers in the Moffitt series defined 3 subsets: myoCAFs, ecmCAFs, and lipoCAFs. (B) Survival analysis of the subsets demonstrated that myoCAFs subset had a better prognosis ($p=0.062$ by Mantel-Cox).

Next, among all genes included in each subset, we selected the most representative in each one to perform a survival analysis in the Moffitt cohort. The idea was to check the survival probability associated with the expression of a particular "classical" CAFs gene, not associated with a set of genes.

ACTA2 was the gene selected to represent the myoCAF subset because it is a classical marker of myofibroblasts. *FAP* was the gene selected to represent de ecmCAF subpopulation because it is the protein associated with fibroblast activation and consequently with the production of ECM. Finally, *S100-A4* or *FSP-1* was the one selected for the lipoCAFs.

The survival analysis (Figure 28B) of these genes showed that patients of the Moffitt dataset with higher expression of *ACTA2* gene were associated with better prognosis, almost reaching an statistical significance. Similar values were obtained using the TCGA – PAAD dataset.

CAFs' classical markers in the Moffitt series (no low stroma samples)

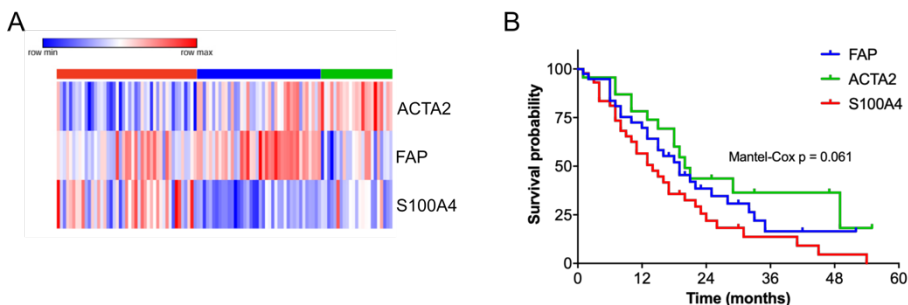


Figure 28. Heatmap of CAFs' classical markers (A) and survival probability (B). CAFs' classical markers had prognostic value in the Moffitt patients' dataset where patients with high expression of *ACTA2* showed better survival probability ($p=0.061$ by Mantel-Cox).

3.2 CAFs FROM PDAC SHOWED HETEROGENEITY AT FUNCTIONAL LEVEL

Since we observed differences at transcriptional levels with a prognostic value between our CAFs subtypes. We tried to characterize these CAFs at a functional level. In particular, we evaluated the proliferation rate and the intracellular lipid content of our 3 CAFs subtypes.

3.2.1 CAF C (ecmCAF) had the highest proliferation rate

We checked the proliferation rate of our CAFs for a week at basal conditions. As shown in Figure 29, CAF C proliferated faster compared with the other two CAFs subtypes with significant differences ($p<0.05$).

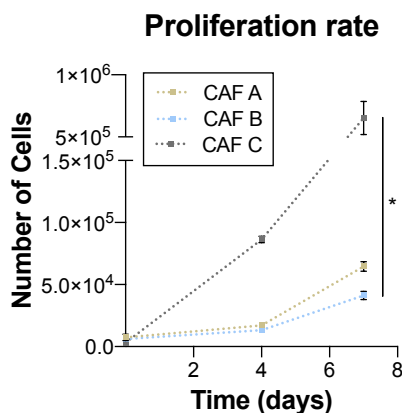


Figure 29. Proliferation rate of CAFs subtypes. Data represented as mean \pm SD of 3 independent experiment with at the minimum 3 technical replicates. Kruskal-Wallis test with Dunns' correction, $p=0.0219$.

3.2.2 CAF B (lipoCAF) had a higher content of intracellular lipids

As we defined CAF B as the lipoCAF because of the expression of *PPAR γ* , *S100-A4*, and *PDGFR α* and these genes are related to the production of lipids (McGowan, 2019).

We performed an ICF to stain lipids at basal conditions and, as expected, CAF B showed higher amounts of lipids (Figure 30). Nile red is a lipophilic dye with a double excitation-emission spectrum able to stain intracellular neutral lipids (green) and polar membrane lipids (red).

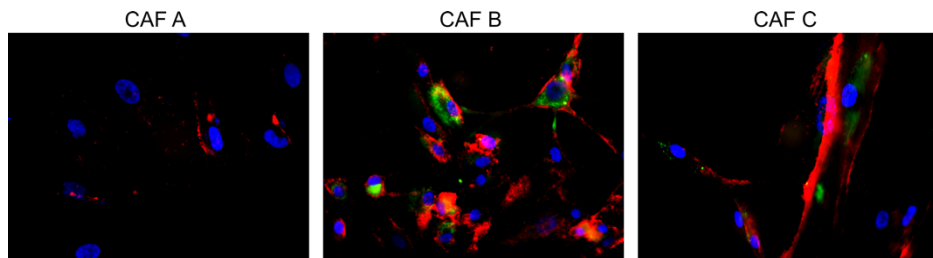


Figure 30. Nile red staining in the 3 CAFs subtypes. Green: intracellular neutral lipids (triglycerides); red: polar membrane lipids (phospholipids); blue: DAPI staining for nucleic acids.

3.3 CULTURE CONDITIONS MODIFY CAFs PHENOTYPE

Data from RNA-seq revealed that CAFs had higher expression of genes related to myogenesis when they were cultured as mono-culture and, the expression of these genes was associated with better prognosis. However, CAFs co-cultured with tumor cells lost the expression of genes associated with a myofibroblast phenotype.

To explore changes in the expression profile related to the culture conditions, we performed *in vitro* cultures of our CAF subtypes (CAF A, CAF B, or CAF C) with or without tumor cells (direct co-cultures or mono-cultures, respectively).

3.3.1 Transcriptional background of CAFs (CAF A, CAF B or CAF C) mediate their phenotype in the direct co-culture (DCC) with tumor cells

First, we tried to reproduce phenotypical changes observed in RNA-seq analysis in our CAFs subtypes (CAF A, CAF B, and CAF C). For that, we seeded CAFs in 3 different culture conditions: a mono-culture of CAF A, CAF B, or CAF C, a DCC of CAF A, CAF B or CAF C with HPAC cells and, a DCC of CAF A, CAF B, or CAF C with MIA PaCa-2 cells. DCC were incubated for 3 days, then, the cells were sorted and we performed qRT-PCR.

We checked the expression levels of classical CAF markers, some of them considered myofibroblast markers and were associated with a good prognosis both in Moffitt series and TCGA, and some other considered fibroblasts-activated markers and were associated with a bad prognosis (Figure 31A). Besides, we also checked the expression levels of genes from lipid biosynthesis (Figure 31B) due to their involvement in the co-culture signature and the prognostic association.

CAF A (green bars) loss myogenic markers (*MYH11*, *SRF*, and *ACTA2*) when they were co-cultured with tumor cells. Besides, we observed an increase in the expression of fibroblasts-activated and adipogenic differentiation genes (*FAP*, *S100-A4*, and *PPAR γ*). No increase in lipid biosynthesis genes was observed in DCC conditions (Figure 31B – green dotted and striped bars). *FASN* increased in the DCC with HPAC cells without significant differences.

CAF B (blue bars) had the more activated profile at basal conditions (Figure 31 – plain bars) but, under co-culture conditions, the expression of fibroblast-activated genes was reduced and they gained in the expression of myogenic genes. Genes of the mevalonate pathway (*HMGCR* and *SQLE*) increased in the co-culture conditions in this CAFs subtype.

CAF C (grey bars), despite having a more inflammatory profile at basal conditions, suffered a decrease in the expression of myofibroblast markers and gained in the expression of activation markers in the DCC (Figure 31A – grey bars).

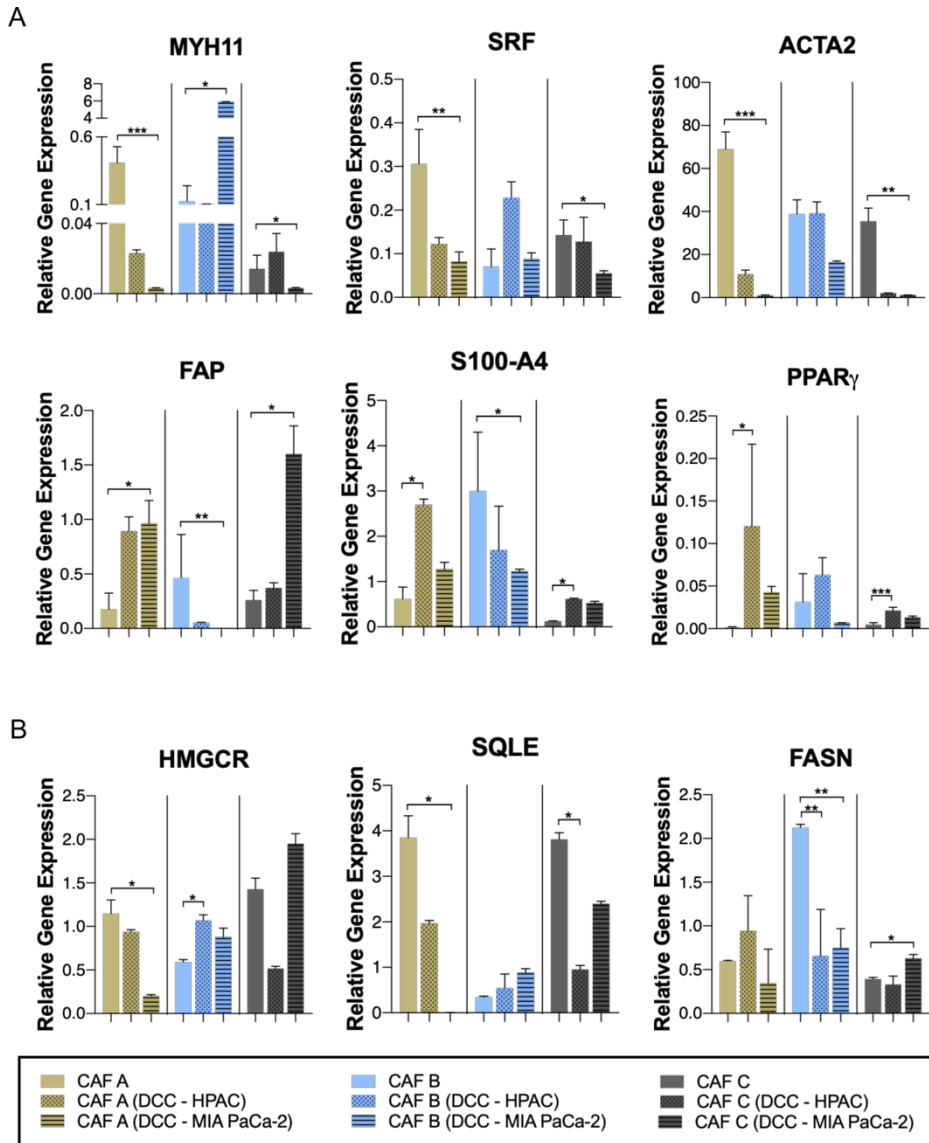


Figure 31. Gene expression profile of CAFs subtypes mono-cultured and co-cultured with tumor cells. (A) CAFs' classical markers gene expression. (B) Lipid metabolism genes expression profile. Comparisons performed: bar 1 vs 2 and 3 of each CAFs subtype (CAF A: green bars, CAF B: blue bars, CAF C: grey bars); bar 1, plain: mono-culture of CAFs, basal conditions; bar 2, dotted: CAFs co-cultured with HPAC tumor cells; bar 3, striped: CAFs co-cultured with MIA PaCa-2 tumor cells. Data represented as mean \pm SD of 3 independent experiment with at the minimum 3 technical replicates. Kruskal-Wallis test multiple comparison with Dunn's correction (* $p < 0,05$; ** $p < 0,01$; *** $p < 0,0001$; **** $p \leq 0,00009$).

CAF A and CAF C had similar expression profiles when co-cultured with tumoral cells despite having a different profile at basal conditions. Obtained results demonstrated that co-culture conditions did not change the expression profile of all CAFs subtypes in the same manner. We supposed that phenotypical changes observed in the RNA-seq analysis could be a result of a cooperation between the different CAFs subtypes included in the culture (mixCAFs). And, the genetic background of CAFs mediated their phenotype in the direct co-culture with tumor cells.

Gene expression analysis for the co-culture condition was performed for both types of tumor cells (HPAC, the classical and, MIA PaCa-2, the basal-like/QM), as the differences depending on the tumor type were minimal, we referred these conditions as co-culture. Most comparisons have not significant results may be because of the number of replicates performed. In these cases, we just can refer to them as a tendency.

3.3.2 The mixture of CAFs (mixCAFs) modify the expression pattern of the CAFs subtypes

The next step was focused on the evaluation of how the presence of different CAFs subtypes in the same culture plate modify their phenotype. That is, if the different CAFs subtypes phenotypes are modified towards a common phenotype or if they maintain distinct genetic features depending on their background when they were seeded together. For that, we seeded a mixture of CAF A, CAF B, and CAF C in a mono-culture and in a direct co-culture with tumor cells. Each CAFs was labeled with a Cell Trace of a different color to separate them by cell sorting (Figure 32) and, we analyzed the gene expression by qRT-PCR.

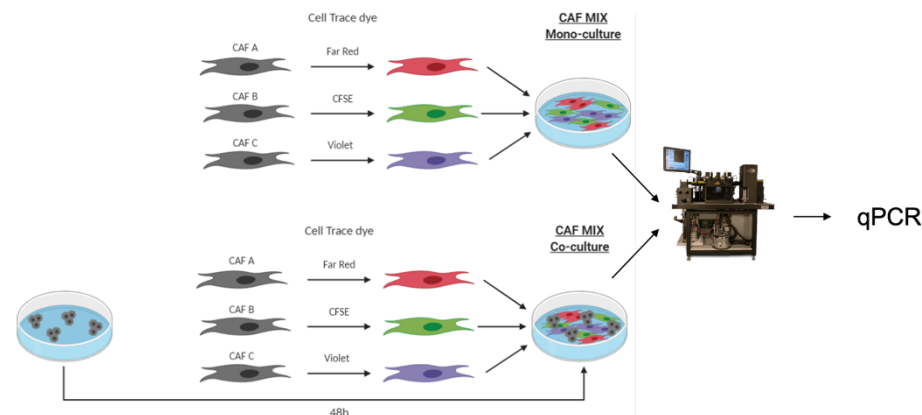


Figure 32. Schematic representation of the experimental design. (Top) Mono-culture of a mixture of 3 different CAF subtypes (CAF A + CAF B + CAF C) labeled with a Cell Trace of different color. (Down) Co-culture of a mixture of 3 different CAF subtypes (CAF A + CAF B + CAF C) labeled with a Cell Trace of a different color seeded with pancreatic tumor cells. Staining CAFs with different colors allowed us to separate them after being cultured together.

The first comparison was done between each CAFs subtype at basal conditions and the same CAFs subtype isolated from a mono-culture of mixCAFs (Figure 33 – bar 1 vs bar 2).

CAF A reduced *MYH11* and *ACTA2* expression and gain *SRF* expression; most of the activation markers were almost not modified, only *S100-A4* diminished.

CAF B showed a reduction in myofibroblast markers (*MYH11*, *SRF*, and *ACTA2*), in fibroblast-activation markers (*FAP* and *S100-A4*) and in adipogenic markers (*PPAR γ* and *CEPBA*).

In the case of CAF C, most of the markers were slightly modified, with *FAP* and *ACTA2* as the genes with the greatest decrease but any of them with significant differences.

The same comparison was done for lipid metabolism genes (Figure 33B); CAF A and CAF C showed a reduction in cholesterol biosynthesis genes (*HMGCR* and *SQLE*) and an insignificant increase in *FASN*, the rate-limiting enzyme of FA biosynthesis. However, *HMGCR*, *SQLE*, and *FASN* increased insignificantly in the CAF B isolated from the mixCAFs compared with CAF B at basal conditions.

The second comparison was done between CAFs subtypes isolated from a mono-culture of mixCAFs and the same CAFs subtypes isolated from a mixCAFs co-

Results

cultured with tumor cells, HPAC or MIA PaCa-2 (Figure 33 – bar 2 vs bar 3, and bar 2 vs bar 4).

CAF A decreased the expression of all myofibroblast markers, and more pronounced in the co-culture with MIA PaCa-2 cells. The expression of fibroblast-activation markers and adipogenic markers increased for both co-cultures, *PPAR γ* had significant value in the co-culture with HPAC cells.

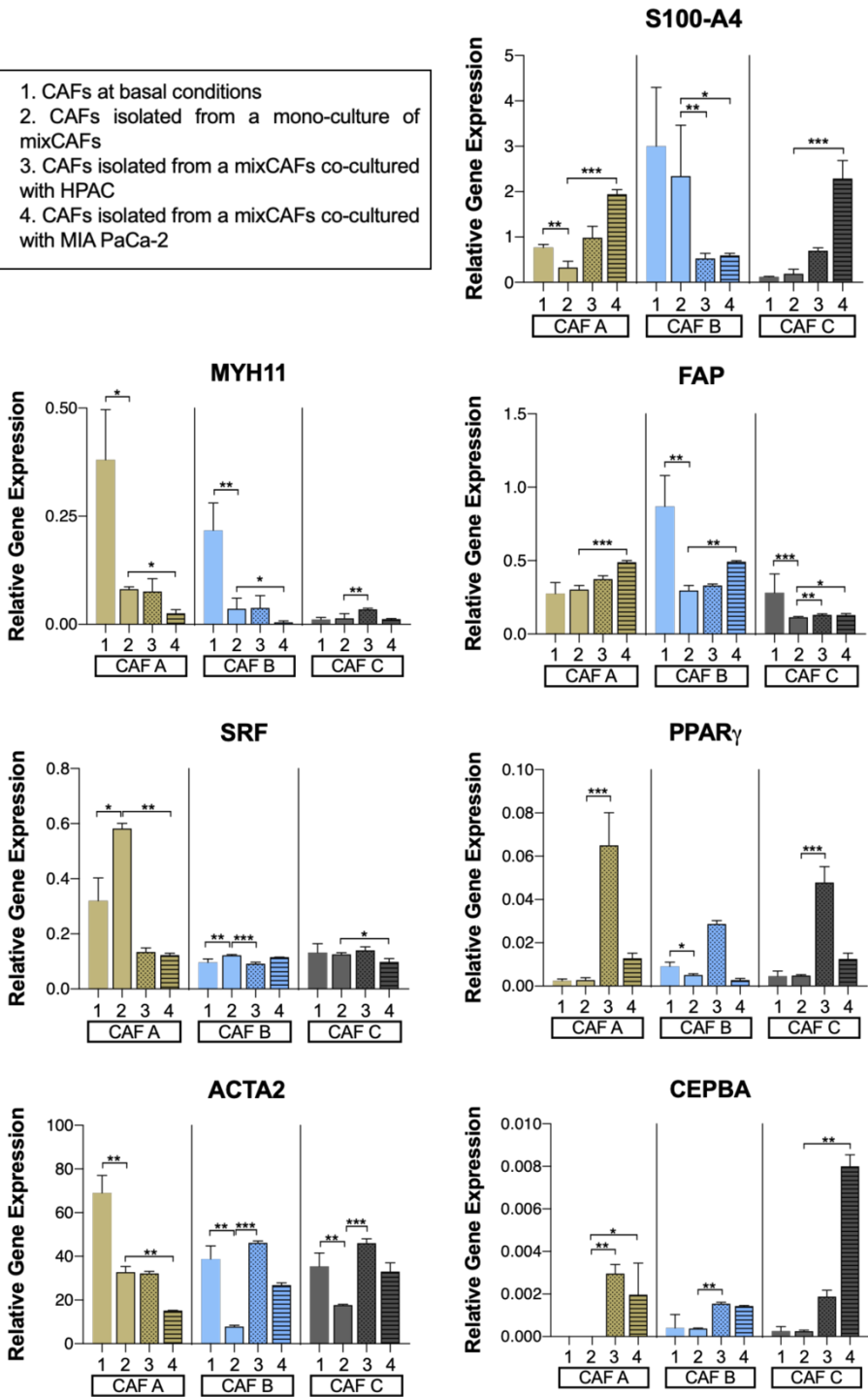
CAF B showed an increase in *ACTA2* expression with significant results in the co-culture with HPAC cells, and a reduction in the expression of *MYH11* and *SRF* for both tumor cell types. In case of fibroblast-activated markers, *S100-A4* expression decreased with significant results and *FAP* increased for both comparisons. *CEPBA* expression increased in both co-cultures and *PPAR γ* increased more in the co-culture with HPAC, but there were no significant results in any condition.

In the co-culture with HPAC cells, CAF C showed a slight increase in *SRF* and, *MYH11* and *ACTA2* increased significantly. In the co-culture with MIA PaCa-2 cells, *MYH11* and *SRF* slightly reduced and *ACTA2* increased without significant differences. In the case of fibroblast-activation markers, *FAP* and *S100-A4* increased. Adipogenic markers increased in both co-cultures, *PPAR γ* had a significant increment in the co-culture with HPAC cells (bar 2 vs bar 3) while *CEPBA* was significant in the co-culture with MIA PaCa-2 cells (bar 2 vs bar 4).

Finally, we also compared the gene expression levels of lipid metabolism genes between CAFs subtypes isolated from a mono-culture of mixCAF_s and the same CAFs subtypes isolated from a mixCAF_s co-cultured with tumor cells (Figure 33B) and we observed an increase in all genes (*HMGCR*, *SQLC*, and *FASN*) for all CAFs subtypes in both co-cultures. Significant differences were found in the co-culture with MIA PaCa-2 and just in the co-culture with HPAC for *FASN* expression in CAF C.

A

1. CAFs at basal conditions
2. CAFs isolated from a mono-culture of mixCAF
3. CAFs isolated from a mixCAF co-cultured with HPAC
4. CAFs isolated from a mixCAF co-cultured with MIA PaCa-2



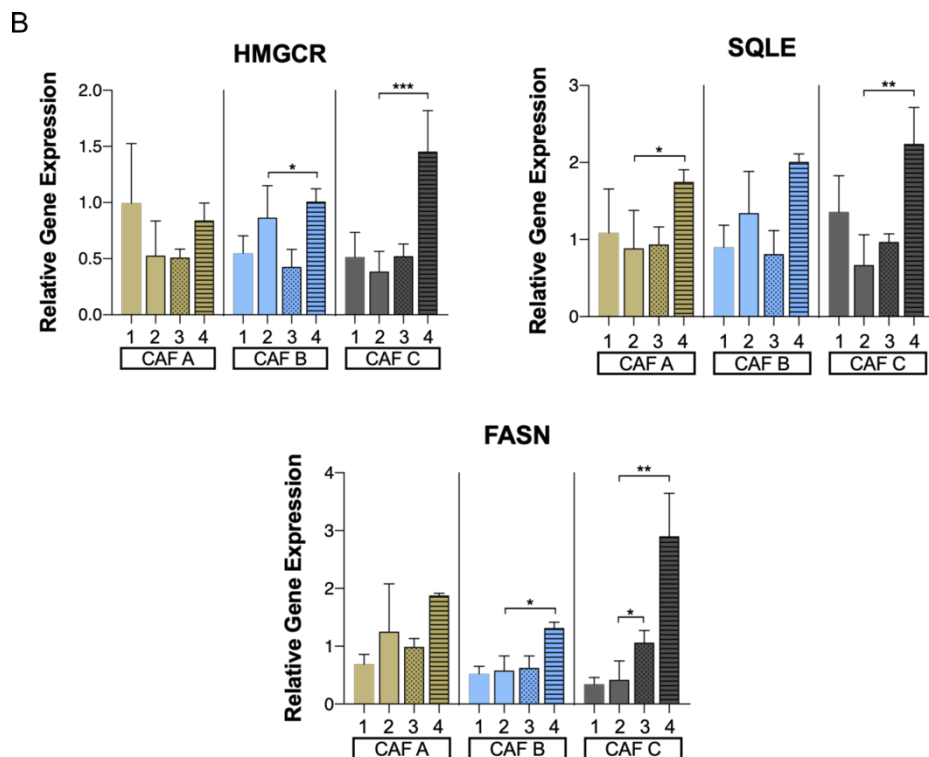


Figure 33. Gene expression profile of CAFs subtypes isolated from a mixCAFs mono-cultured and co-cultured with tumor cells. (A) CAFs' classical markers gene expression. (B) Lipid metabolism genes expression profile. Comparisons performed: bar 1 vs bar 2 for each CAFs subtype; bar 1 vs bar 3 and 4 for each CAFs subtype. Bar 1: mono-culture of CAFs subtypes at basal conditions; bar 2: CAFs isolated from a mixCAFs; bar 3: CAFs isolated from a mixCAFs co-cultured with HPAC tumor cells; bar 4: CAFs isolated from a mixCAFs co-cultured with MIA PaCa-2 tumor cells. CAF A: green bars; CAF B: blue bars; CAF C: grey bars. Data represented as mean \pm SD of 2 independent experiment with 3 technical replicates. Mann-Whitney test or Kruskal-Wallis multiple comparison test with Dunn's correction (* $p < 0,05$; ** $p < 0,01$; *** $p < 0,0001$; **** $p \leq 0,00009$).

3.3.3 Myofibroblast markers and fibroblast-activation markers expression in the mixture of 3 CAFs correlated with the mixture of 5 CAFs

We observed in previous results that CAFs acquired different expression patterns after co-culture depending on their transcriptomic background. In this experiment, we evaluated the expression patterns of mono-culture and co-culture of a mixCAFs to perform the same comparison than in RNA-seq. Therefore, we seeded a mixture of the 3 CAFs subtypes that we defined (mixCAFs: CAF A + CAF B + CAF C) as mono-

culture and the same mixCAFs cultured with tumor cells. We compared the expression of the mixCAFs as mono-culture versus the co-cultures (Figure 34).

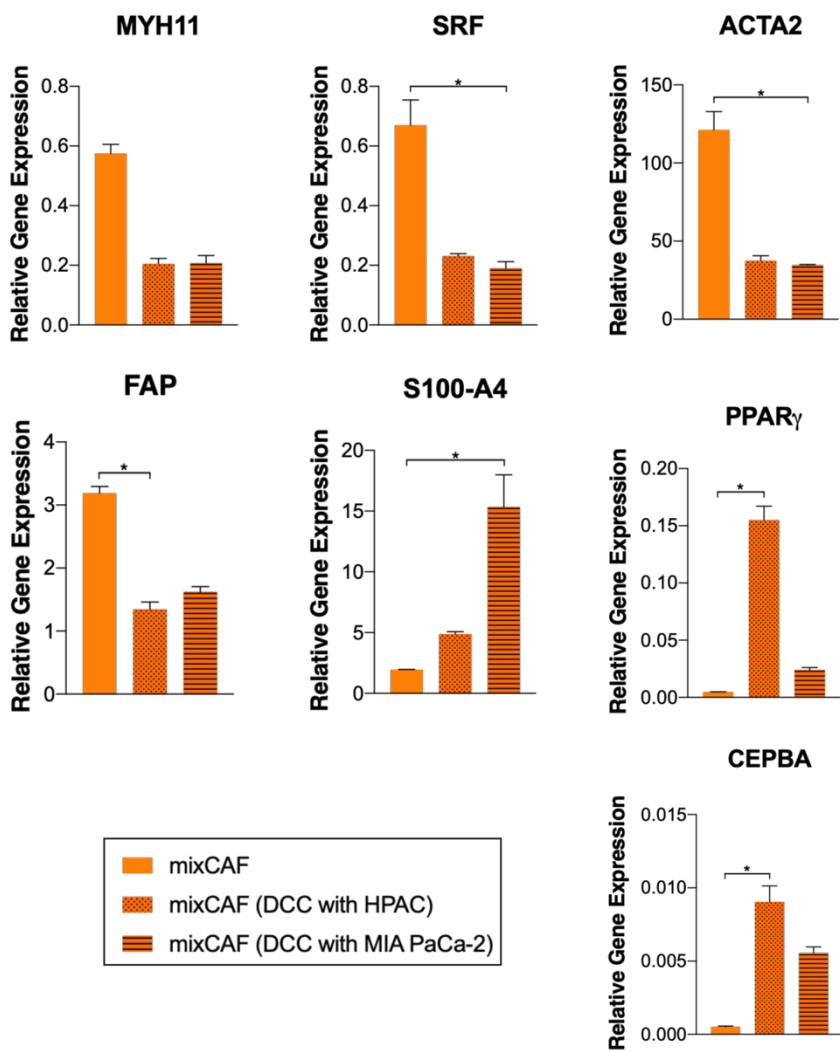
The expression of myofibroblast markers (*MYH11*, *SRF*, and *ACTA2*) was reduced in the mixCAFs co-cultured with tumor cells. The reduction had significant results for *SRF* and *ACTA2* expression in the co-culture with HPAC cells. This reduction was in accordance with the *in silico* data where the mono-culture signature showed upregulation in myogenic processes that were lost in the co-culture condition. Besides, the expression of these processes associated with a better prognosis.

The expression of *S100-A4* increased but *FAP* decreased in the co-culture with both tumor cells. Although in both co-cultures the tendency was the same, *FAP* reduction was significant for the co-culture with HPAC cells and *S100-A4* increment was significant for the co-culture with MIA PaCa-2 cells.

Adipogenic markers (*PPAR γ* and *CEPBA*) expression increased in the co-culture with both tumor cell type but significant differences were observed in the co-culture with HPAC cells.

In this setting, we also checked changes in the expression of lipid metabolism genes. In the co-culture with HPAC cells, *FASN* expression increased while *HMGCR* and *SQLE* were not modified. In the co-culture with MIA PaCa-2 cells, the expression of these 3 genes was reduced in comparison with the mono-culture of mixCAFs. However, there were no significant differences between the mono-culture of mixCAFs and the co-culture of mixCAFs for any gene and tumor cell type.

A



B

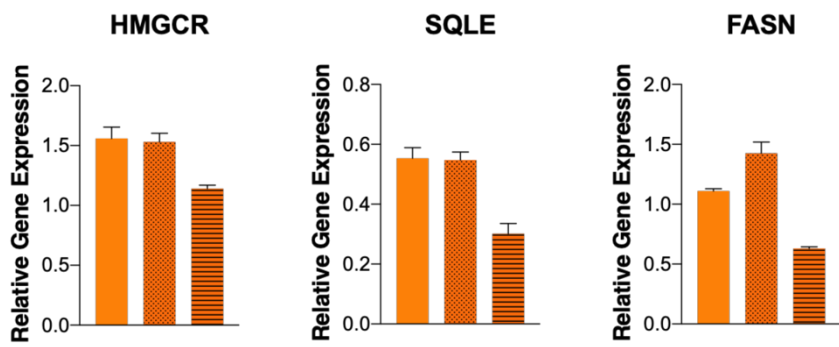


Figure 34. Gene expression profile of mono-culture of mixCAFs and co-culture of mixCAFs with tumor cells. (A) CAFs' classical markers gene expression. (B) Lipid metabolism genes expression profile. DCC: direct co-culture. Data represented as mean \pm SD of 2 independent experiment with at the minimum 3 technical replicates. Kruskal-Wallis multiple comparison with Dunn's correction (* $p < 0,05$; ** $p < 0,01$; *** $p < 0,0001$; **** $p \leq 0,00009$).

4. CAFs SUBTYPES IN HUMAN PDAC SAMPLES

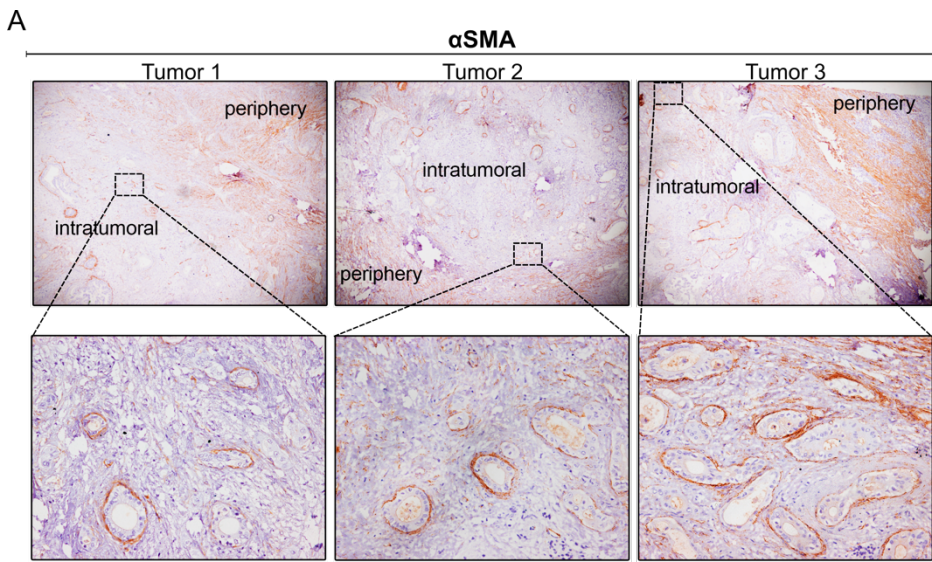
Lately, many authors have been described CAFs' heterogeneity. For instance, Öhlund *et al.* (Öhlund et al., 2017) defined the intratumoral heterogeneity and they described the presence of 2 main populations of CAFs (myoCAFs and iCAFs) considering the protein expression profile and the location within a tumor regarding tumor glands. In our previous experiments, we also described *in vitro* heterogeneity in our CAFs isolated from human PDAC.

With this premises and considering α SMA and FAP as distinguishing markers of CAFs populations, we checked the expression of these proteins in different human PDAC samples.

Firstly, we evaluated the histological distribution of α SMA expression and, as is showed in Figure 35A, α SMA was expressed in 2 different locations within a tumor regarding the tumor glands. In the first line CAFs surrounding the tumor glands, the intratumor α SMA expression. And, α SMA is also expressed in the periphery of the tumor bulk. This result confirmed the existence of the same CAFs subtype in different location within a tumor.

Secondly, we evaluated the expression of α SMA and FAP in serial sections of the PDAC samples (Figure 35B and C). CAFs with myofibroblast features (myoCAFs) that expressed α SMA were localized close to the tumor (Figure 35B – left). While, CAFs that expressed FAP were localized in a desmoplastic area in between tumor glands (Figure 35B – right). In Figure 35C, we checked the expression of both proteins (α SMA and FAP) by a double fluorescent staining. These results demonstrated the coexistence of different CAFs subpopulations in the same tumor sample and that these subpopulations were located in different areas of the tumor.

Results



Coexistence of different CAFs subpopulations in the same tumor sample

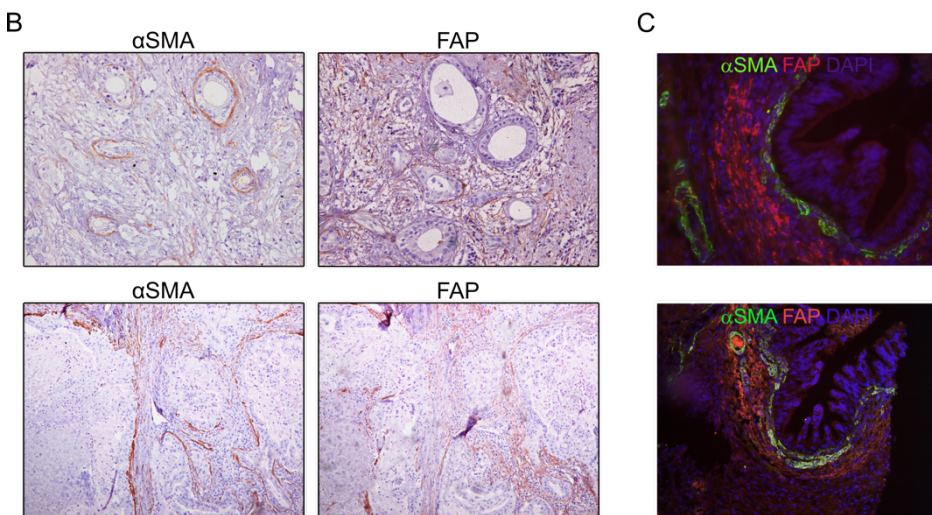


Figure 35. α SMA and FAP protein expression detected by immunohistochemistry (IHC) (A and B) and double immunohistofluorescence (D-IHF) (C) in human PDAC tissue samples. (A) IHC of α SMA in three different PDAC tissue sample; microscope objective: 5X and 20X (B) IHC of α SMA and FAP expression in 2 different human PDAC tissue samples; microscope objective: 20X. (C) D-IHF of α SMA (green) and FAP (red) in a human PDAC sample and DAPI staining (blue) for nucleic acids; microscope objective: 40X.

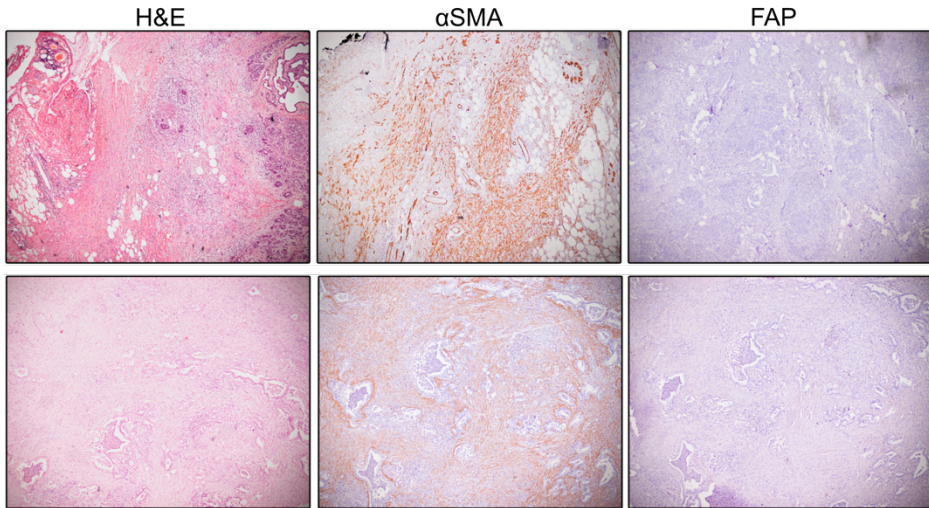
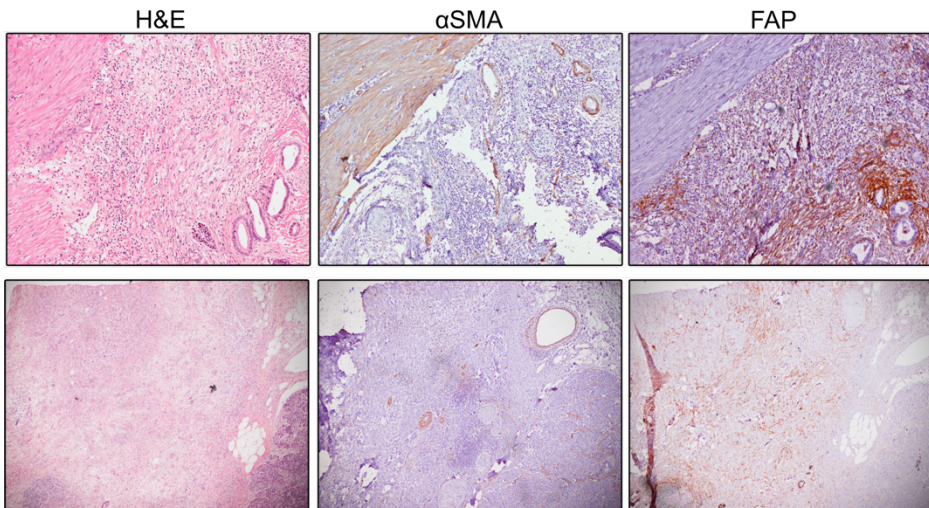
α SMA^{high}/FAP^{low}: myofibroblast high tumors **α SMA^{low}/FAP^{high}: myofibroblast low tumors**

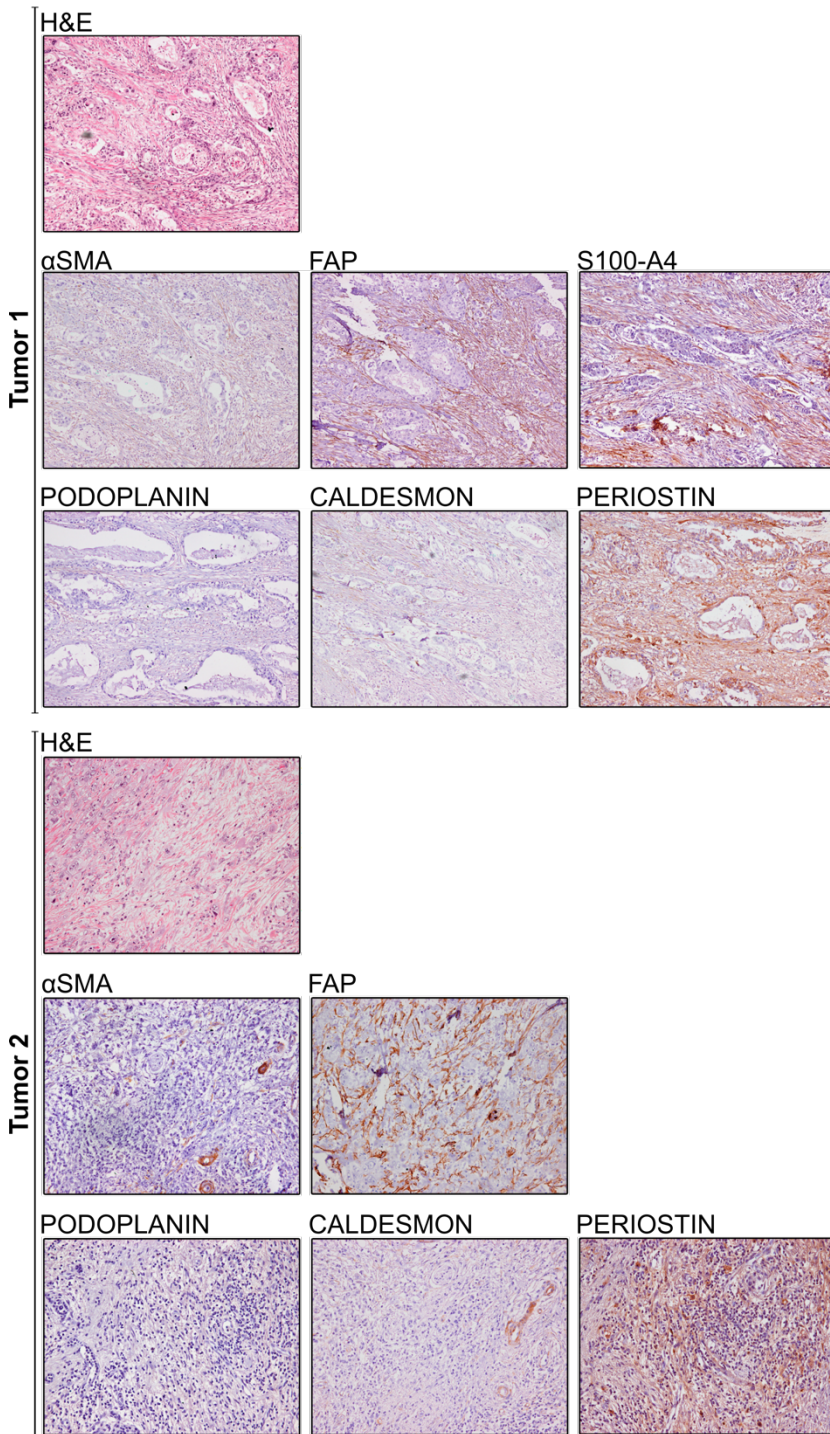
Figure 36. Histological study of 4 human PDAC tissue samples by H&E staining and α SMA and FAP protein expression detected by immunohistochemistry. (Top) 2 human PDAC samples with histological features of well differentiated tumors, high expression of α SMA, and low expression of FAP. (Down) 2 human PDAC samples with histological features of poor differentiated tumors, low expression of α SMA, and high expression of FAP. H&E: hematoxylin and eosin; microscope objective: 10X.

Results

Analyzing the distribution of these CAFs subpopulation in human PDAC samples, we noticed the existence of two types of PDAC tumors. Ones with high expression of α SMA and low expression of FAP (Figure 36 - top panel) and, others with low expression of α SMA and high expression of FAP (Figure 36 - down panel). That is, patients with high or low expression of myofibroblast markers, respectively. Histologically, myofibroblast high tumors (α SMA^{high}/FAP^{low}) used to be moderately to well differentiated tumors, i.e. tumor cells form glands embedded in a desmoplastic stroma. Opposite, myofibroblast low tumors (α SMA^{low}/FAP^{high}) were mainly, poor differentiated tumors with a reactive stroma without bundle organization. Given the prognostic value of the myofibroblast signature, we would expect a better survival probability for the set of patients with myofibroblast high tumors.

As we mentioned before, the transcriptomic characterization of our CAFs defined 3 phenotypes (myoCAF, lipoCAF and ecmCAF). Each phenotype was characterized by the *in vitro* expression of specific biomarkers. The study of two of these biomarkers (α SMA and FAP) in human tissue samples allowed us to visualize and localize their expression. And, it also allowed us to defined two types of human tumors (Figure 35 and Figure 36).

Afterwards, we evaluated the expression of other markers. The results of this detailed analysis gave robustness to the existence of two types of human tumors. Since, we observed that one tumor type is characterized by low expression of α SMA and negative expression of other myofibroblast markers such as, PODOPLANIN and CALDESMON. As well as, high expression of FAP, PERIOSTIN and S100-A4 (Figure 37 – Tumor 1). The second tumor analyzed was also characterized by low expression of α SMA, negative expression of other myofibroblast markers and, high expression of FAP and PERIOSTIN. However, it was negative for S100-A4 expression.



Results

Figure 37. H&E staining and IHC protein detection in 2 myofibroblast low human PDAC. (Top) Human PDAC sample with low expression of myofibroblast markers (α SMA, PODOPLANIN and CALDESMON) and high expression of activated fibroblast markers (FAP, PERIOSTIN and S100-A4). (Down) Human PDAC sample with low expression of myofibroblast markers (α SMA, PODOPLANIN and CALDESMON) and high expression of FAP and PERIOSTIN but no expression of S100-A4 (data not show). H&E: hematoxylin and eosin; microscope objective: 20X.

Finally, we tried to relate our *in vitro* CAFs phenotypes with the tumor location and the expression pattern. Considering our *in vitro* phenotype, these expression pattern observed in tumor 1 (Figure 37) could be correlated with our CAF B because of the expression of FAP and S100-A4. Besides, according to Öhlund et al. description, the population of CAFs localized close to the tumor glands that express α SMA, could associate with myCAF. Moreover, the population of CAFs localized far from tumor glands that express FAP, could associate with iCAF (Figure 35). It is important to highlight that, in our *in vitro* cultures, tumor cells do not organize as tumor glands therefore, the stroma organization resembles a reactive stroma characteristic of low differentiated PDAC tumors.

5. CELL-BASED FUNCTIONAL ASSAYS

Since we observed differences at transcriptomic, protein, and functional levels between our CAFs subtypes, we evaluated the possible effects of these differences over tumor cells.

We checked differences mediated by paracrine communication where there was no contact between cells (CAFs and tumor cells) and the communication was through soluble factors. Specifically, we evaluated differences in the migration capacity of MIA PaCa-2 cells, and colony formation and proliferation capacity of HPAC and MIA PaCa-2 cells.

5.1 MIA PaCa-2 CELLS MIGRATION CAPACITY IS MODULATED BY CAFs' CONDITIONED MEDIUM

We checked the effects over the migration capacity of MIA PaCa-2 cells by two different methods. The wound closing assay (Figure 38A) and the directional migration capacity (Figure 38B).

Wound healing assays were performed putting conditioned media (CM) of different CAFs subtypes on MIA PaCa-2 cells and comparing the percentage of wound closing.

In the directional migration experiment, we seeded MIA PaCa-2 cells in an 8 μ m porous membrane, and the attractant substrates (CAFs) were seeded on the well, migrant cells pass through the membrane. In this indirect co-culture (ICC) method, there was a constant supply of soluble factors by CAFs without contact between cells.

The conditioned medium of CAF A showed the lowest capacity to promote wound closing in comparison with CAF B and CAF C media. However, directional migration showed opposite results where the indirect co-culture with CAF A promoted MIA PaCa-2 cells migration through the membrane. This fact could be associated with a higher response of CAF A to tumor cells. Despite that, differences in directional migration were not significant.

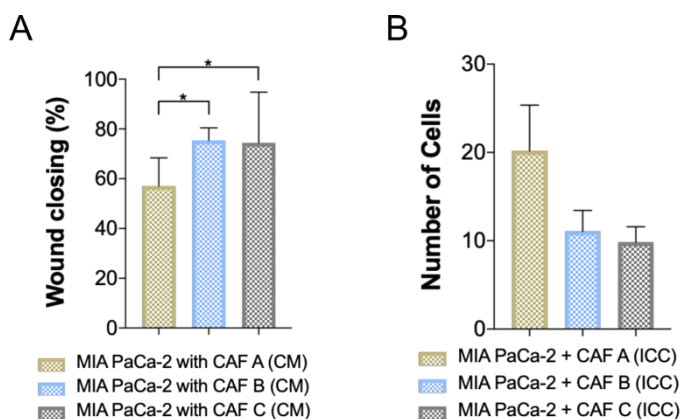


Figure 38. Migration capacity of MIA PaCa-2 cells. (A) Percentage of wound healing closing (media \pm SD) mediated by conditioned medium of CAF in 5 independent experiments. .Kruskal-Wallis multiple comparison with Dunn's correction (* p <0,05; ** p <0,01; *** p <0,0001; **** p <0,00009). (B) Directional migration capacity of MIA PaCa-2 cells (media \pm SEM) induced by an indirect co-culture with CAFs subtypes in 4 independent experiments. No statistical differences between groups.

Migration capacity was only checked in MIA PaCa-2 cells because they showed the highest migration capacity.

5.2 COLONY FORMATION AND PROLIFERATION CAPACITY OF TUMOR CELLS ARE MEDIATED BY CAFs' CONDITIONED MEDIUM

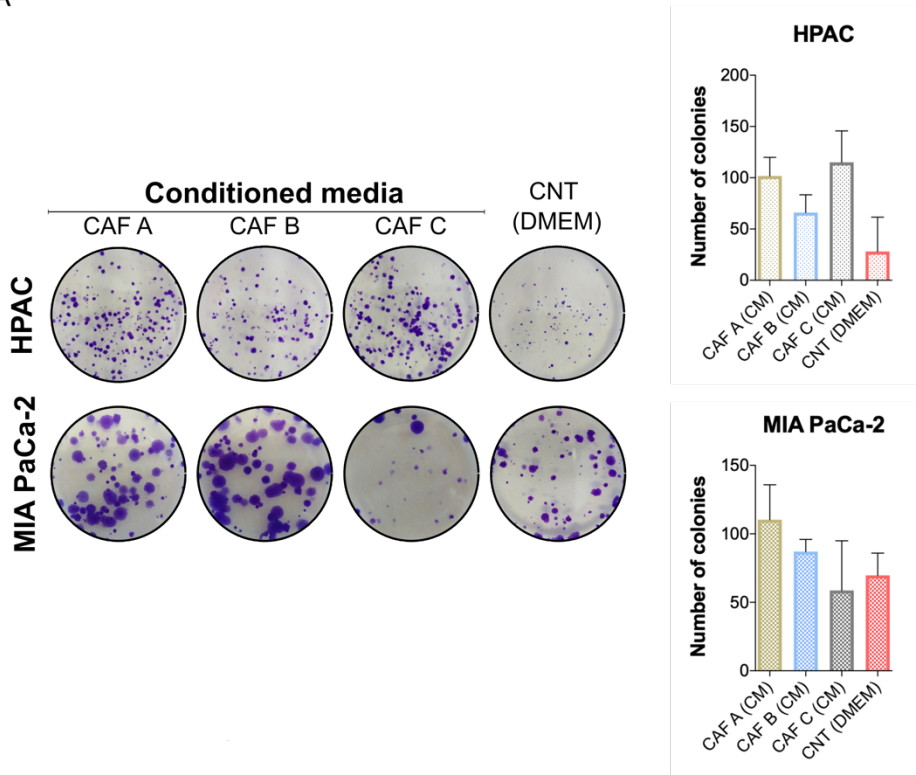
Conditioned medium (CM) of CAFs subtypes (CAF A, CAF B, and CAF C) increased colony formation and proliferation capacity of HPAC cells compared with control media (DMEM). In the case of MIA PaCa-2 cells, conditioned medium of CAF A and CAF B increased colony formation capacity in comparison with the CNT, opposite that happened with CAF C (CM), this last condition showed the highest SD between replicates. The results did not have significant differences in any case (Figure 39A).

Proliferation capacity (Figure 39B) of MIA PaCa-2 cells showed small differences between different media. However, CM of CAFs increased the proliferation capacity of HPAC cells with significant differences in the proliferation mediated by CAF C (CM) compared with the CNT.

All the experiments where we used conditioned media from CAFs were performed at 2% of FBS. The control condition was DMEM supplemented with 2% FBS.

Paracrine signaling between CAFs and tumor cells mediated by the soluble factors in the conditioned media of CAFs was not enough to promote significant changes in tumor cells. However, we demonstrated that the presence of both cell types (CAF and tumor cells) in the culture could modify the CAF phenotype. With these premises, we thought about the juxtacrine signaling, where the direct contact CAFs – tumor cells (direct co-culture, DCC) could mediate changes in CAFs with the corresponding response over tumor cells.

A



B

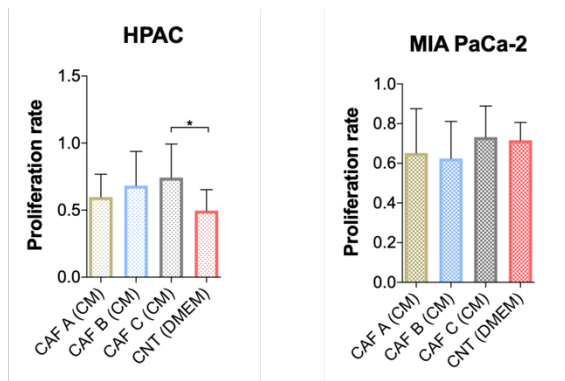


Figure 39. Clonogenic (A) and proliferation (B) capacity of tumor cells (HPAC and MIA PaCa-2) mediated by CAFs subtypes (CAF A, CAF B, CAF C) conditioned media (CM). (A - left panel) Representative image of one experiment from a total of 3 independent experiments. (A - right panel) Number of colonies (media \pm SD) of 3 independent experiments without statistical differences. (B) Proliferation rate (media \pm SD) of 5 independent experiments. Kruskal-Wallis multiple comparison with Dunn's correction (* $p < 0,05$; ** $p < 0,01$; *** $p < 0,0001$; **** $p \leq 0,00009$)

6. REV-ERB-INDUCED PHENOTYPE MOLDING

The objective 2 proposed in this thesis was design strategies to reprogram pancreatic CAFs towards a less tumor-supportive subpopulation. Previous results defined possible pathways or genes susceptible to be up- or downregulated in CAFs. We considered 3 different options to transform the CAFs in a less tumor-supportive subpopulation. One option could be transforming CAFs in a more myofibroblast population since the expression of myofibroblast signature is associated to a better prognosis. The second option could be the downregulation of the lipoCAF phenotype since the activation of lipid metabolic pathways is associated to a worse prognosis. Finally, the third option could be the modulation of CAFs toward a quiescent state in which they are less activated.

As we described previously, REV-ERB is a nuclear receptor (NR) that represses the expression of genes involved in the regulation of inflammation, myogenic differentiation, lipid and cholesterol homeostasis, and cancer. And, its gene, the *NR1D1*, was upregulated in our co-culture signature. Therefore, to check which effect we were able to achieve, we treated CAFs with SR9009 and SR8278, the agonist and the antagonist of REV-ERB, respectively.

The agonist SR9009 increases the effects of REV-REBs, that is, it promotes the repression of downstream target genes. Opposite, the antagonist SR8278 blocked REV-ERBs function, therefore, it causes an increase of downstream target genes.

REV-ERBs are NR also involved in the control of circadian rhythms, the reason why first of all, we established the best time point and doses to treat CAFs with SRs. We considered as optimum the moment in which *NR1D1* levels were the highest, specifically, 24h after FBS-induced synchronization. The dose of 10 μ M was established according to the bibliography and after the confirmation that REV-ERBs do not affect the proliferation and viability of the tumor cell.

6.1 REV-ERB TREATMENT MODIFY CAFs SUBTYPES (CAF A, CAF B, AND CAF C) PHENOTYPES. THE RESPONSE OF EACH CAFs SUBTYPES IS MEDIATED BY THE GENETIC BACKGROUND

The different CAFs subtypes (CAF A, CAF B, and CAF C) were treated with DMSO, being the control condition, SR9009 or SR8278. Then, we compared the expression

levels of the different CAFs markers and the lipid metabolism genes between the control and the corresponding treatments.

As shown in Figure 40A, CAFs subtypes treated with REV-ERB agonist (SR9009) revealed a reduction in all myofibroblast markers (*MYH11*, *SRF*, and *ACTA2*), except for *ACTA2* in CAF B that suffered a small increase without significant differences in comparison with the control condition.

Fibroblast-activation markers expression decreased in CAF B, with significant differences in comparison with the control. However, CAF A and CAF C showed an increase in the expression of both genes (*S100-A4* and *FAP*) but only in CAF C the differences had significant value.

PPAR γ expression increased for all CAFs subtypes and the expression levels between SR9009 treatment compared with the control had significant differences for CAF B and CAF C.

SR9009 treatment also reduced the expression of *HMGCR*, *SQLE*, and *FASN* in CAF B. *SQLE* expression also decreased in CAF A and CAF C. However, CAF A and CAF C did not respond to the treatment in an equal manner for the other metabolic genes. *HMGCR* slightly decreased in CAF A but increased in CAF C, while *FASN* decreased in CAF C but increased in CAF A. Any of these differences showed significant results (Figure 40B).

Considering the possibility to increase myofibroblast related genes expression to reprogram CAFs, we also treated CAFs subtypes with the REV-ERB antagonist (Figure 40A). Then, we checked if the expression levels of myogenic genes increase while the expression of activation-related genes decreased. In this case, *MYH11* increased in CAF A and CAF C but slightly decreased in CAF B. *SRF* expression just increase in CAF C, CAF B revealed a slight reduction in *SRF* expression, and in CAF A the expression was almost not modified. Finally, *ACTA2* expression increased in CAF A and CAF C while it was slightly reduced in CAF B.

The expression of fibroblast-activation genes (*S100-A4* and *FAP*) was not almost modified in any CAFs subtypes in comparison with the control.

PPAR γ expression increased in comparison with the control but no as much as in SR9009 treatment.

Results

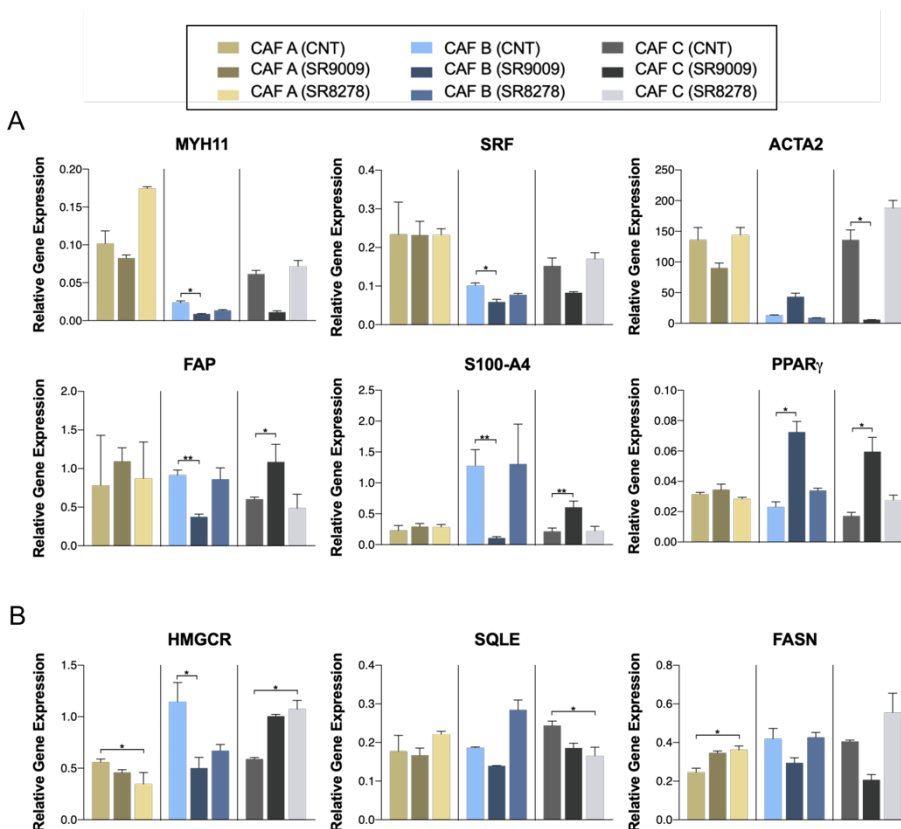


Figure 40. Relative gene expression (mean \pm SD) of CAFs subtypes (CAF A, CAF B, and CAF C) treated with REV-ERB agonist (SR9009) and antagonist (SR8278) compared with the control (DMSO). (A) CAFs' classical markers gene expression. (B) Lipid metabolism genes expression profile. Comparisons performed: bar 1 vs 2 and 3 of each CAFs subtype (CAF A: green bars, CAF B: blue bars, CAF C: grey bars). Data represented as mean \pm SD of 2 independent experiment with at the minimum 3 technical replicates. Kruskal-Wallis test multiple comparison with Dunn's correction (* $p < 0,05$; ** $p < 0,01$; * $p < 0,0001$; **** $p \leq 0,00009$).**

CAF's subtypes also showed a different response to SR8278 considering the expression of metabolic genes (Figure 40B). *FASN* expression increased in all CAF's subtypes. *HMGCR* expression increased in CAF C while, it decreased in CAF A and CAF B. And, *SQLE* expression was higher in CAF A and CAF B after SR8278 treatment but its expression was reduced in CAF C.

Despite in general SR9009 decrease the expression and SR8278 increase the expression of REV-ERB target genes, the effects were not generalized for all genes and CAF's subtypes. So, once more we concluded that the transcriptomic background of CAF's subtypes mediates their response to REV-ERB treatments.

The fact that SR9009 caused a general decreased in the expression of REV-ERB downstream target genes (myogenesis, fibroblast-activation genes, and lipid metabolism genes) lead us to think in the induction of a quiescent state in CAFs. Quiescence acquisition is supported by the increase in *PPAR* γ expression levels after SR9009 since *PPAR* γ is a NR involved in cellular differentiation.

Individual phenotypes of CAFs subtypes were substantially modified when we cultured them as a mixture of CAFs. Thus, the next step was focused on the evaluation of a dedifferentiated state in the mixCAF_s, those responsible for the prognostic value got from *in silico* data.

6.2 mixCAF_s ACQUIRED A DEDIFFERENTIATED STATE AFTER SR9009 TREATMENT

It is well described that quiescent cells can store lipids as cytoplasmic lipid droplets (LD), a capacity that they lose when they become activated (Auciello et al., 2019; Sherman et al., 2014; Sunami et al., 2018). Activated cells remodel the intracellular lipidome and they transfer proteins and lipids to neighboring cancer cells (Auciello et al., 2019; Balaban et al., 2017; Santi et al., 2015). Moreover, quiescent pancreatic stellate cells (qPSC) reduce the expression of some fibroblast markers (Han et al., 2018; Sherman et al., 2014).

We analyzed the expression of these biomarkers and the lipid content in the mixture of CAFs after pharmacological REV-ERB modulation.

6.2.1 The treatment with REV-ERB agonist SR9009 increased lipid droplets (LD) content in the mixCAF_s

We compared the number of intracellular lipids in the mixCAF_s at basal conditions, mixCAF_s treated with DMSO as control condition and mixCAF_s treated with SR9009 and SR8278. As expected, the mixCAF_s treated with the REV-ERB agonist SR9009, stored more intracellular lipids (green staining) than the control condition (Figure 41).

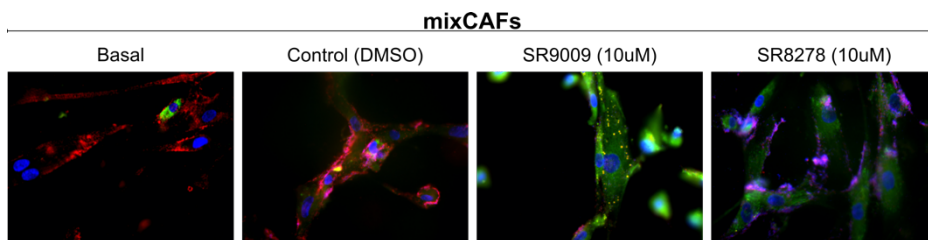


Figure 41. Nile red staining in a mono-culture of mixCAFs treated with REV-ERB agonist (SR9009), REV-ERB antagonist (SR8278), and DMSO (control). Green: intracellular neutral lipids (triglycerides); red: polar membrane lipids (phospholipids); blue: DAPI staining for nucleic acids.

6.2.2 Treatment with SR9009 decreased the expression of REV-ERB downstream target genes in mixCAFs

Following the idea of the modulation towards a dedifferentiated population, we checked the expression of some fibroblast markers to confirm the acquisition of a quiescent state. We checked and compared changes in a mono-culture of mixCAFs treated with the REV-ERB drugs.

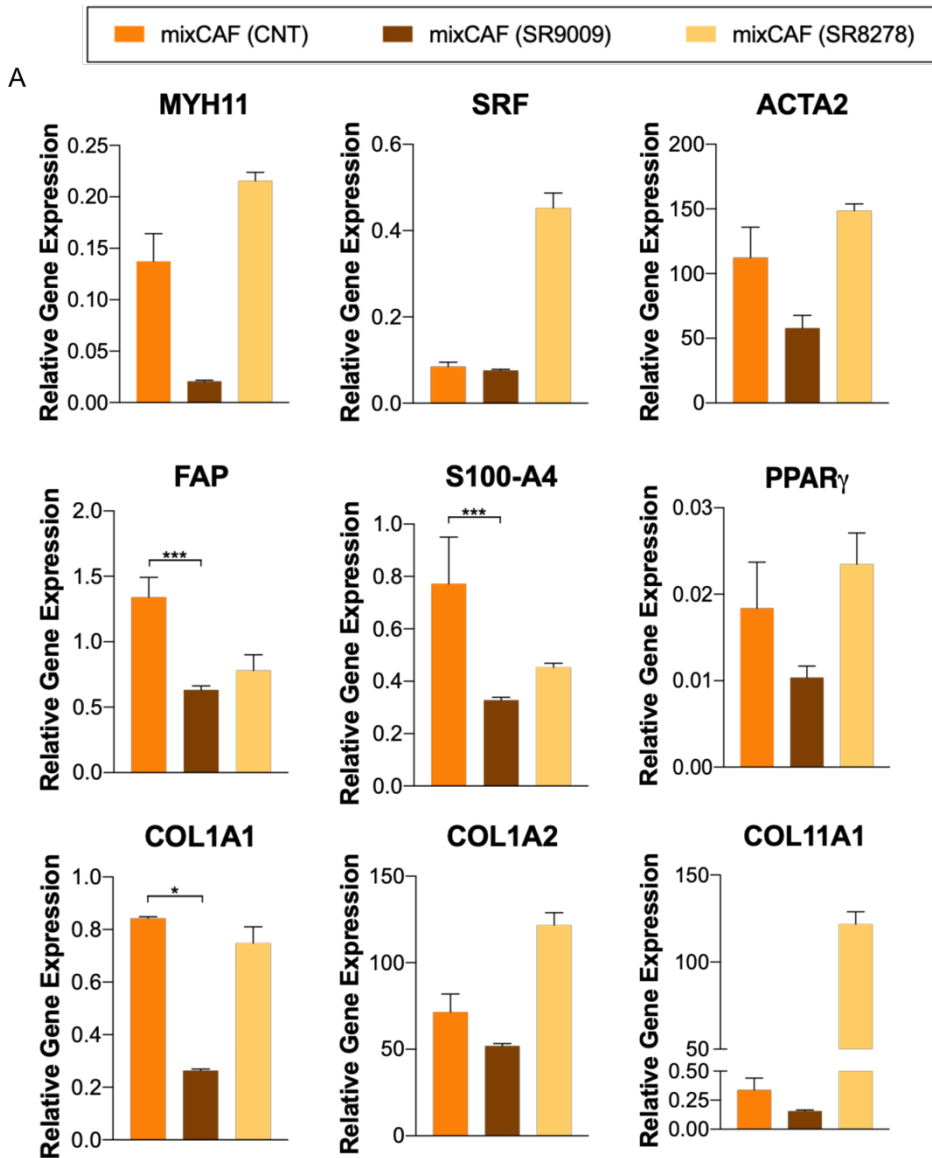
The transcriptomic comparison of mixCAFs control and mixCAF treated with SR9009 (Figure 42A) revealed a reduction in myofibroblast markers (*MYH11*, *SRF*, and *ACTA2*) and, a statistical reduction in fibroblast-activation markers (*FAP* and *S100-A4*). However, opposite to the results obtained in the CAFs subtypes treated with SR9009 (Figure 40A), in the mixCAFs treated with SR9009, we also observed a reduction in *PPAR γ* without significant differences.

Despite the reduction in *PPAR γ* expression after SR9009 treatment, we checked the expression of some ECM components since cells in a quiescent state have low capacity to synthesize ECM. The decreased expression levels of *COL1A1*, *COL1A2*, and *COL11A1* demonstrated a reduction in the ECM production in the mixCAFs after SR9009 (Figure 42A).

The expression levels of lipid metabolism genes (Figure 42B), downstream pathways of REV-ERB, also decreased in the mixCAFs after SR9009 treatment.

The transcriptomic analysis of mixCAFs treated with the REV-ERB antagonist SR8278 (Figure 42), demonstrated an increase in all studied genes except for *FAP* and *S100-A4*, in comparison with the control. If we compared SR8278 with SR9009

treatment, there was an increment in the expression for all genes in the SR8278 condition.



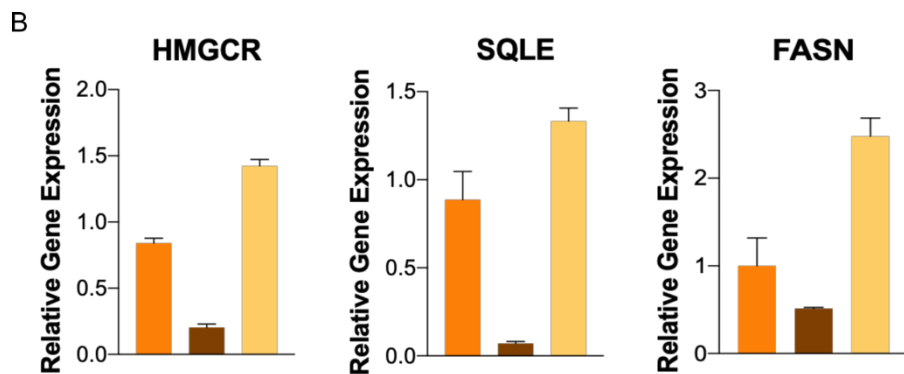


Figure 42. Gene expression levels (mean \pm SD) of a mixture of our CAFs subtypes (mixCAF: CAF A + CAF B + CAF C) in mono-culture treated with REV-ERB agonist (SR9009) and antagonist (SR8278) and compared with the control. (A) qRT-PCR analysis of different CAFs markers. (B) qRT-PCR analysis of lipid metabolism genes. HKG: QARS. REV-ERBs treatments were performed after CAFs circadian rhythm synchronization at 10 μ M for 24h. Control conditions were treated with DMSO at the same dosage regimen. Data represented as mean \pm SD of 2 independent experiment with at the minimum 3 technical replicates. Kruskal-Wallis test multiple comparison with Dunn's correction (* $p < 0,05$; ** $p < 0,01$; * $p < 0,0001$; **** $p \leq 0,00009$).**

6.2.3 Pre-treatment of mixCAF with SR9009 diminished the expression of activated-fibroblast markers and maintain the expression of PSC under co-culture conditions

Previous results demonstrated that co-culture with tumor cells changed the expression pattern of CAFs, and the treatment with SR9009 modify CAFs phenotype. In the following experiments, we considered both conditions, S9009 treatment plus co-culture with HPAC cells.

We checked changes in the expression patterns by qRT-PCR (Figure 43) and by ICF (Figure 44) of a mixCAF pre-treated with SR9009, the REV-ERB agonist, and then, co-cultured with HPAC tumor cells. For qRT-PCR analysis, CAFs were separated from tumor cells by FACS, and later on, we performed the RNA extraction.

The results of the transcriptomic comparison between the control (DMSO) and SR9009 treatment (Figure 43) showed a reduction in *MYH11*, *SRF*, *FAP*, and *S100-A4* with significant results. While the reduction in *ACTA2* was not significant. These results agreed with the acquisition of a quiescent state. However, *PPAR γ* expression increased in the pre-treatment with SR9009, result that is opposite to that observed in the treatment of mixCAF mono-culture (Figure 42A).

The same comparison was performed for lipid metabolism genes, and the analysis noticed a reduction in the expression of these three genes with significant differences for *HMGCR* and *SQLE*.

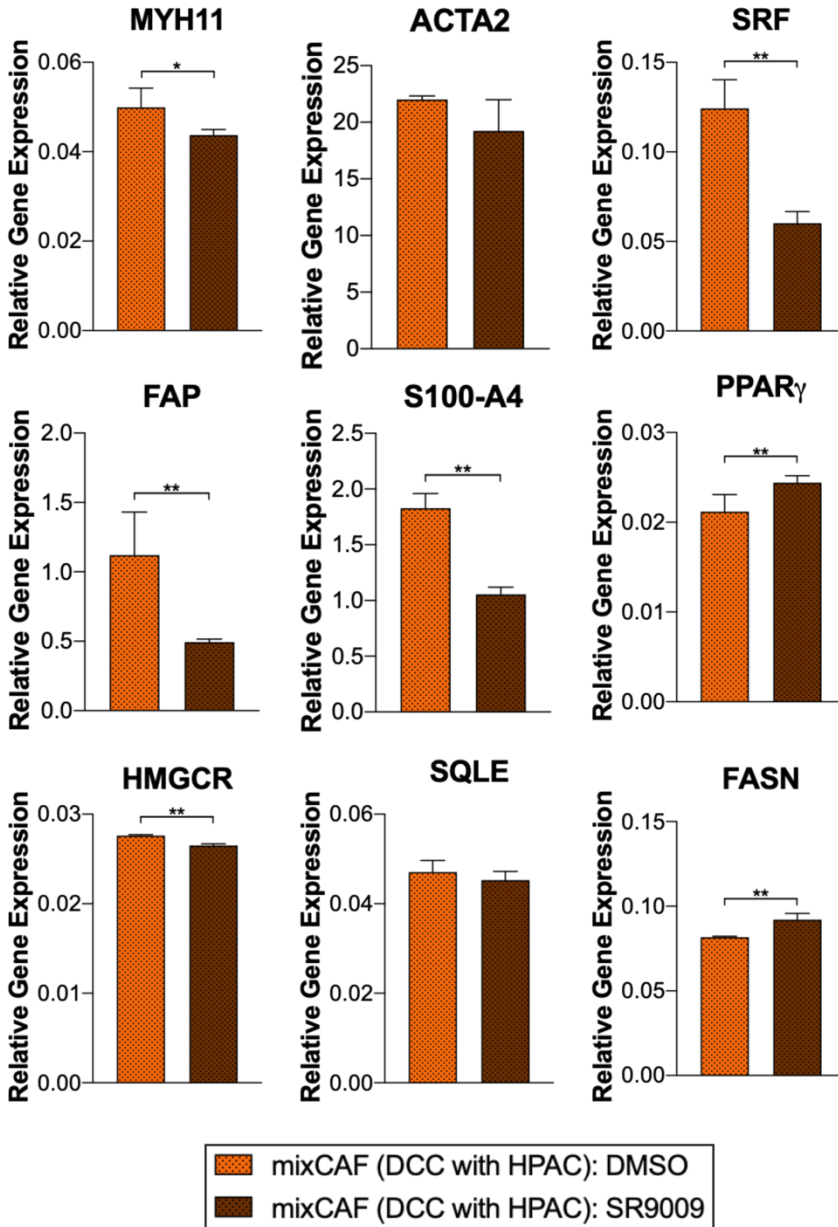


Figure 43. Gene expression levels (mean \pm SD) of a mixture of our CAFs subtypes (mixCAFs: CAF A + CAF B + CAF C) treated with REV-ERB agonist (SR9009) and co-cultured with HPAC cells.

Results

(A) qRT-PCR analysis of different CAFs markers and lipid metabolism genes. HKG: QARS. REV-ERBs treatments were performed after CAFs circadian rhythm synchronization at 10 μ M for 24h. Control conditions were treated with DMSO at the same dosage regimen. Data represented as mean \pm SD of 2 independent experiment with at the minimum 3 technical replicates. Mann-Whitney U test (* p<0,05; ** p<0,01; *** p<0,0001; **** p \leq 0,00009).

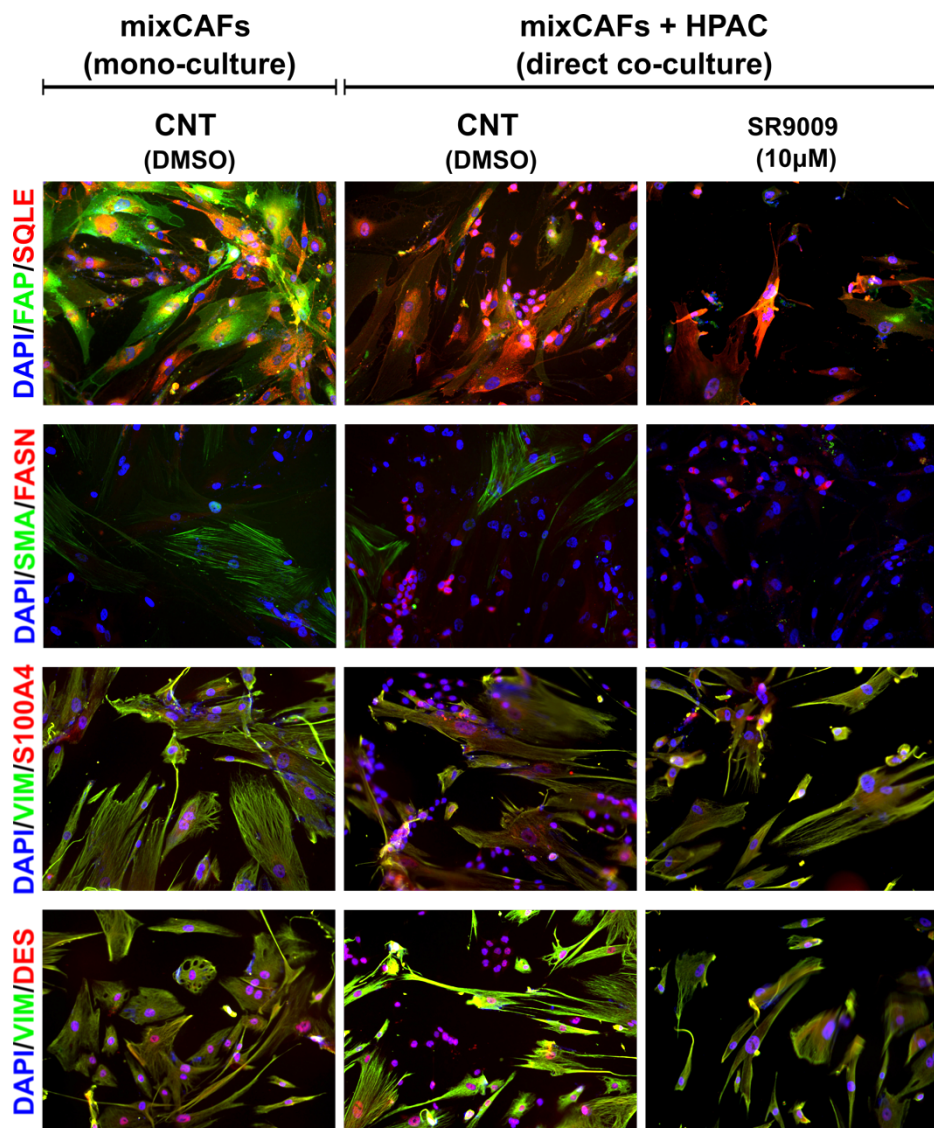


Figure 44. Protein expression detected by immunofluorescence (ICF) of a mixture of our CAF subtypes (mixCAFs: CAF A + CAF B + CAF C) treated with REV-ERB drugs (SR9009 and SR8278). From left to right column: mono-culture of a mixCAFs, control condition; direct co-culture of mixCAFs and HPAC cells, control condition; direct co-culture of mixCAFs and HPAC cells, mixCAFs

pre-treated with SR9009. DAPI: blue staining for nucleic acids. Protein names are described as gene, the corresponding extended names are in ANNEX 1.

We also checked the protein expression pattern after SR9009 treatment by immunocytofluorescence. Figure 44 demonstrates a modulation towards a dedifferentiated state where fibroblast did not become more myofibroblast neither CAFs expressed activation biomarkers. They just acquired a less-activated phenotype with loss of α SMA (myofibroblast marker) and a reduction in the expression of FAP (fibroblast-activation marker).

Pancreatic stellate cells (PSC) have been described as a precursor of activated fibroblast. Therefore, we finally checked the expression of quiescent PSC biomarkers such as VIMENTIN and DESMIN. Results demonstrated that CAFs pre-treated with SR9009 did not lose the expression of quiescent PSC proteins.

DISCUSSION

1. CAFs' HETEROGENEITY IN PDAC

For a long time, studies based on cancer have focused on tumor cells. Since a few years ago, the tumor microenvironment (TME) has taken importance because tumor cells need to establish crosstalk with ECM, endothelial, immune cells, and CAFs, for tumor formation (Erkan et al., 2012).

CAFs could arise from mesenchymal stem cells (MSC), endothelial cells, hepatic stellate cells (HSC), pancreatic stellate cells (PSC), adipocytes, or from resting tissue fibroblasts (Kalluri, 2016). Once CAFs are present in the tumor stroma, they develop different functions that can be tumor suppressive at initial stages of tumorigenesis (Kalluri, 2016) but switch towards pro-tumorigenic as the disease progress (Sahai et al., 2020).

In the tumor stroma, CAFs acquired the expression of activated-fibroblast markers (S100-A4, α SMA, FAP, PDGFR α and β , and DESMIN) (Kalluri, 2016). But none of these are specific markers for fibroblasts, and CAFs may not express all of these markers at the same time, introducing the idea of CAFs' heterogeneity (Berdiel-Acer et al., 2014; Elyada et al., 2019; Moffitt et al., 2015; Neuzillet et al., 2019; Öhlund et al., 2017). Moreover, the presence of different CAFs' markers, signatures, or phenotypes can associate with prognosis (Moffitt et al., 2015; www.portal.gdc.cancer.gov/projects/TCGA-PAAD).

Have the CAFs signatures defined by *in vitro* cultures a prognostic value?

The transcriptomic differences from our RNA-seq data revealed the existence two phenotypes. Up-regulated processes in our mono-cultured CAFs corresponded with Moffitt normal stroma, and up-regulated processes in our co-cultured CAFs with Moffitt activated stroma. These two phenotypes also correlated with a lung cancer dataset (Rudisch et al., 2015). Therefore, we demonstrated that the *in vitro* culture of CAFs with PDAC tumor cells modify the CAFs' expression profile, a phenomenon that also occurs in other cancer types (Moffitt et al., 2015; Rudisch et al., 2015). The survival analysis of our signatures performed on two different patients' datasets reasserted the validity of our *in vitro* data. It confirmed that patients with an overexpression of the mono-cultured CAFs signature had a better prognosis. (Moffitt et al., 2015; www.portal.gdc.cancer.gov/projects/TCGA-PAAD).

Discussion

Cancer cells are metabolically active and tumor growth is associated with high lipid and cholesterol production. Studies of the prognostic value of metabolism carried out in the tumor showed that tumor glucose consumption correlates with poor prognosis (Pavlova and Thompson, 2016), and high levels of FASN in patient tumor tissues is also associated with poor prognosis (Buckley et al., 2017; Jones and Infante, 2015). Moreover, a lipogenic phenotype and glycolytic metabolism in tumor cells constitute a malignant phenotype (Menendez and Lupu, 2007).

Unlike previous works, we studied the prognostic value of up- or downregulation of metabolites, enzymes, and metabolic pathways in the TME, specifically in CAFs. In the metabolic ambit, CAFs have a dual role. They suppress tumor growth by generating a nutrient-poor environment. And, CAFs can promote tumor growth by secreting factors that assist PDAC cells (Auciello et al., 2019). We demonstrated that patients with high fibroblast content and included in the cluster with high expression of cholesterol homeostasis pathway had a worse prognosis.

In addition to metabolic input, CAFs can also assist tumor growth by providing soluble growth factors, chemokines, proteolytic enzymes, and cytokines to cancer cells (Erkan et al., 2012). The tumor necrosis factor (TNF) is a transmembrane protein with multiple biological functions and dysregulation of TNF production is involved in many human diseases. For instance, TNF plays an important role in the regulation of the inflammatory process in tumor development. Specifically, an inflammatory microenvironment is associated with tumor migration, invasion, and metastasis (Tang et al., 2017). In PDAC, we demonstrated that the overexpression of inflammation mediated by $\text{NF}\kappa\beta$ pathways in patients with fibroblast enriched tumors had a worse prognosis.

Therefore, in PDAC patients with high stroma content tumors, the overexpression of cholesterol and TNF pathways were associated with a worse prognosis.

Are there different phenotypes in CAFs isolated from human PDAC samples?

The study of the expression profiles of CAFs isolated from human PDAC samples confirmed the existence of heterogeneity in this cell population. This heterogeneity could be determined by the origin of the fibroblast precursor cell, for instance, lipofibroblasts could be a source of myofibroblasts (El Agha et al., 2017; Kalluri, 2016; Xie et al., 2018); by the time-point of isolation since fibroblasts

suffer dynamic changes during their transformation process (Friedman et al., 2020); as well as by the tumor area from which they were isolated (Neuzillet et al., 2019; Öhlund et al., 2017).

We defined 3 CAFs subtypes isolated from human PDAC samples. The expression pattern of CAF A had a myofibroblast expression pattern (Öhlund et al., 2017) associated with better prognosis taking the myoCAF signature or just the *ACTA2* expression into account (Moffitt et al., 2015). According to the expression pattern and the properties of subtypes B and C described by Neuzillet *et al.*, our CAF A seem to be a combination of both subtypes, because of the expression of *MYH11*, α SMA, and PDPN and the better prognosis (Neuzillet et al., 2019). CAF B were defined as lipoCAF because of the expression of *S100-A4* (Bochet et al., 2013; Zhang et al., 2018), adipogenic-related genes (*PPAR γ*) and the highest intracellular lipid content (Auciello et al., 2019; El Agha et al., 2017; Elyada et al., 2019). POSTN and collagens are ECM components secreted by CAFs and, the ECM production is related with proliferation (Kalluri, 2016; Whittle and Hingorani, 2019). CAF C had an inflammatory profile (iCAF) with the highest levels of cytokines and cytokine ligands (Öhlund et al., 2017), but they also had remarkable expression of ECM proteins. CAFs subtype C was classified as ecmCAF and they showed the highest proliferation rate. However, the fact that all CAFs express VIMENTIN confirmed that they are different subtypes of CAFs since it is considered a pan-marker of fibroblasts.

ACTA2, *MYH11*, *SRF*, *CALD1*, *TAGLN*, *CNN1*, and *DES* are classic markers of myofibroblasts, among others (El Agha et al., 2017; Goikuria et al., 2018; Lambrechts et al., 2018b; Moffitt et al., 2015). The survival analysis of the group of patients with higher expression of myoCAF profile just as the subset of patients with *ACTA2* overexpression, correlated with a better prognosis (Lambrechts et al., 2018b; Moffitt et al., 2015).

S100-A4 or *FSP-1* is considered a gene which expression is related to an adipogenic profile (Bochet et al., 2013) as occur with *NR1D1*, *ABCG1*, and *PPAR γ* (El Agha et al., 2017; Xie et al., 2018). However, *FAP* and *SPARC* are usually included in an activated-fibroblast subset (Moffitt et al., 2015; Puleo et al., 2018). Thus, the correlation plot with the Moffitt dataset distributed patients with *FAP* and *S100-A4* expression in different subsets, the ecmCAF and the lipoCAF, respectively. However, in our CAFs subtypes, the CAF B (lipoCAFs) have the higher expression of

both genes, which could be related to the fact that they are activated fibroblasts arising from adipocytes (Jotzu et al., 2011; Kalluri, 2016; Sahai et al., 2020). Moreover, patients with *FAP* expression associated with a worse prognosis (Hussain et al., 2020; Mezheyeuski et al., 2020; Moffitt et al., 2015), and the same occur with *S100-A4* expression (Ikenaga et al., 2009; Lee et al., 2004; Moffitt et al., 2015; Rudland et al., 2000). Hence, taking the expression profile of CAF B into account, they should be the more pro-tumoral ones within our subtypes.

Does heterogeneity of CAFs cause differences in paracrine communication with tumor cells?

CAFs present in the tumor stroma communicated with tumor cells and other cells within the TME. This crosstalk could be mediated by secreted soluble factors or by direct cell-to-cell contact.

In the paracrine communication, CAFs secrete soluble factors that diffuse and act on a neighboring tumor cell. This signaling process could modulate angiogenesis, wound healing, cell motility, and metastasis (Gascard and Tlsty, 2016; Nurmik et al., 2020; Sahai et al., 2020). Our evaluation of the paracrine communication effect in the migration capacity of tumor cells suggests that CAF A at basal conditions have a lower capacity to promote migration. However, in an indirect co-culture system, where tumor cells could send signals to CAFs, CAF A may respond to these signals by secreting soluble factors that promote tumor cell migration (Auciello et al., 2019; Iovanna and Closa, 2017; Sunami et al., 2018).

Besides, the results obtained in proliferation and clonogenic capacity of tumor cells suggest a double-way effect since conditioned media of CAFs subtypes act distinctly on different tumor cells. It could be because of CAFs subtypes have different secretion profile and, tumor cells (the classical or the basal-like/QM) are also different in terms of proliferation, transcriptomic profile, metabolism, so on (Bailey et al., 2016; Collisson et al., 2011; Daemen et al., 2015; Karasinska et al., 2020; Moffitt et al., 2015; Yu et al., 2019). We defined CAFs subtypes taking their transcriptomic profile into account. These profiles were associated with a prognostic value. However, we were not able to relate the prognosis with the effect caused on the tumor cells in terms of paracrine communication.

Our experiments based on paracrine communication compare the effects caused by CM of different CAFs subtypes over the tumor cells. We have observed a

tendency to promote higher proliferation and clonogenic capacity of tumor cells exposed to CM of CAFs in comparison with the control medium. However, we have not been able to relate an expression profile of CAFs with a specific function in tumor cells. Previous works in which they defined specific functions of CM of CAFs are based in the comparison of CM from CAFs versus CM from normal fibroblasts and PSC (Díaz-Maroto et al., 2019; Gong et al., 2020; Habisch et al., 2010). Opposite, in our setting we compared the effects of CM from different CAFs, i.e. all of them are tumor-associated fibroblasts with a more or less activated profile than normal fibroblasts.

Does the direct co-culture with tumor cells cause changes in the transcriptome of CAFs?

Transcriptomic profiles obtained from the direct co-culture of our CAFs subtypes with tumor cells demonstrated that co-culture conditions do not modify the expression pattern of all CAFs subtypes in the same manner. And, the transcriptomic background of each CAFs subtype mediated their phenotype after the direct co-culture with tumor cells.

Results of our RNA-seq analysis concluded that CAFs co-cultured with tumor cells acquired a more activated phenotype which is associated with a worse prognosis. However, they showed decreased expression of *ACTA2* (Figure 21). This result can be controversial since, in the context of idiopathic pulmonary fibrosis (IPF), the fibroblasts become activated when they gain in the expression of α SMA, and its expression is associated with a worse prognosis (El Agha et al., 2017; Xie et al., 2018). Nonetheless, in the context of cancer, despite the decrease in the expression of *ACTA2*, CAFs remain activated fibroblast because they are located in a tumoral environment (Kalluri, 2016; Öhlund et al., 2017; Sahai et al., 2020), and the decrease in the expression of *ACTA2* is associated with a worse prognosis (Moffitt et al., 2015; www.portal.gdc.cancer.gov/projects/TCGA-PAAD). The *ACTA2* reduction plus the increase in the expression of fibroblast-activation markers (*FAP* and *S100-A4*) are responsible for the worst prognosis in the co-culture.

The transcriptomic profile that defined each CAFs subtype at basal conditions is also maintained when CAFs subtypes are cultured as a mixture with the other CAFs subtypes, despite expression levels diminishes. This fact could be related to the

Discussion

plasticity phenomenon described by Friedman *et al.* but, in our scenario, the dynamic behavior of CAFs would be determined by the co-culture instead of by the tumor evolve (Friedman *et al.*, 2020).

The increase in lipid metabolism genes observed in the CAFs co-cultured with tumor cells supports the idea of metabolic crosstalk (Pavlova and Thompson, 2016; Sunami *et al.*, 2018). In addition, this increase is higher when CAFs are cultured with MIA PaCa-2, which are classified as glycolytic (Daemen *et al.*, 2015). Glycolytic cells are supposed to be less efficient in the production of lipids, therefore, they induce higher expression of lipid biosynthesis genes in the CAFs (Daemen *et al.*, 2015; Karasinska *et al.*, 2020; Pavlova and Thompson, 2016; Pereira *et al.*, 2019). Co-culture conditions also increased *PPAR γ* and *CEPBA* (Xiong, 2015).

Whereas, the expression levels of lipid metabolism genes in the mixCAF_s co-cultured with tumor cells do not increase. Results that are opposite to those obtained from de RNA-seq data. Despite that, the expression of *S100-A4* and other adipogenic-related markers (*PPAR γ* and *CEPBA*) increased in the co-culture with both tumor cell type (Bochet *et al.*, 2013; Xiong, 2015) hence, the overexpression of *S100-A4* plus low expression levels of *ACTA2* and *FAP* agree with the acquisition of adipocyte-derived fibroblasts phenotype (Bochet *et al.*, 2013).

Can our CAFs subpopulations be found in human PDAC samples?

In the field of characterization, we defined different CAFs' subpopulations depending on their expression profile. Previous results described that this profile changes with the environment where the CAFs are located (Friedman *et al.*, 2020; Hussain *et al.*, 2020; Lambrechts *et al.*, 2018b; Neuzillet *et al.*, 2019; Öhlund *et al.*, 2017). In human PDAC samples, our results revealed that these different CAFs subpopulations could coexist in the same tumor sample. Moreover, there are a group of tumors with low expression of α SMA and high expression of FAP (α SMA^{low}/FAP^{high}), i.e. patients with low expression of myofibroblast markers (Hussain *et al.*, 2020; Öhlund *et al.*, 2017). While, there are other tumor samples with high expression of α SMA and low expression of FAP (α SMA^{high}/FAP^{low}), i.e. patients with high expression of myofibroblast markers. Given the prognostic value of the myofibroblast signature, we would expect a worse survival probability for these sets of patients. If we consider the prognostic value of the markers selected as representative markers to each signature (*ACTA2*, *FAP*, and *S100-A4*; Moffitt

correlation plot), patients with high expression of *FAP* showed a worse survival probability compared with those with upregulated *ACTA2*, the gene that codifies for α SMA.

2. REPROGRAMMING CAFs TOWARDS A LESS SUPPORTIVE SUBPOPULATION

Faced with the possibility to modulate CAFs towards a less tumor-supportive population and considering the results obtained in previous experiments, we thought about different options, all of them supported by different studies. First, promoting the expression of the myofibroblast phenotype (El Agha et al., 2017; Lambrechts et al., 2018b; Öhlund et al., 2017; Xie et al., 2018). Second, by reducing the expression of adipogenic-related genes (El Agha et al., 2017; Lambrechts et al., 2018b; Öhlund et al., 2017; Xie et al., 2018). And third, by inducing a quiescent state (Chronopoulos et al., 2016; Miao et al., 2017; Neuzillet et al., 2019; Sherman et al., 2014).

Reduction of lipids biosynthesis and cholesterol homeostasis could be a good strategy because these pathways appeared overexpressed in our co-cultured mixCAFs and, the overexpression of the cholesterol biosynthesis pathway was associated with a worse prognosis in the PDAC patients' dataset (Moffitt et al., 2015). In turn, promoting an increase in the myogenic pathways and related genes could also be a good strategy because they were overexpressed in our mono-cultured mixCAFs and, therefore, they were associated with better prognosis in the PDAC patients' dataset (Moffitt et al., 2015).

Selecting between nuclear receptor agonism or antagonism. What is the best treatment to perform the CAFs phenotype molding?

A way to modulate these processes is through the use of nuclear receptors (NR) (Chan et al., 2018; Chatterjee et al., 2019; Cheng et al., 2019; Chronopoulos et al., 2016; Everett and Lazar, 2014; Kojetin and Burris, 2014; Marciano et al., 2014). In particular, REV-ERBs acts over different tissues by repressing the expression of genes involved in the regulation of circadian rhythms, the lipid and cholesterol homeostasis, and the adipose tissue and myoblast differentiation (Everett and Lazar, 2014).

Discussion

In the field of PDAC and TME, the supposed successful treatment looks for the activation of myogenesis (Moffitt et al., 2015). Although, in other pathologies, promoting myogenesis causes poorer results (Chatterjee et al., 2019; Wang et al., 2020; Welch et al., 2017; Woldt et al., 2013). Hence, fibrosis and myogenesis have a different outcome depending on the tissue type and the pathology. To promote the increase in the expression of genes related with myogenesis and, keeping in mind results of mentioned studies based on skeletal muscle disorders (Cunningham et al., 2020; El Agha et al., 2017; Welch et al., 2017), CAFs subtypes were treated with SR8278. SR8278 is a REV-ERB α antagonist, whose *in vitro* treatments caused an increase in the expression of REV-ERB α target genes (Kojetin et al., 2011).

SR8278 was not able to increase myogenesis-related genes in all CAFs types. In fact, in those CAFs subtype with lower expression of *MYH11*, *ACTA2*, and *SRF* at basal conditions (CAF B), SR8278 caused the opposite effect and further reduce the expression levels of those genes. This effect may be because SR8278 is not a dual REV-ERB antagonist. It antagonizes the α subunit while the β subunit can replace the blocked one and develop its functions (Bugge et al., 2012). In addition, it has been described that in cancer cells, the expression of subunit β is higher than α in many different tissue types (De Mei et al., 2015; Wang et al., 2015).

REV-ERB α antagonist increased the expression of fibroblast-activation genes as metabolic genes. Therefore, treatment with SR8278 seems not to be successful in terms of PDAC treatment because of the upregulation of genes associated with a worse prognosis.

At the same time, as an attempt to block the transcription of genes related to bad prognosis such as *FAP*, *S100-A4* or, the lipid metabolism-related genes (Moffitt et al., 2015), CAFs subtypes were treated with SR9009, a dual REV-ERB agonist (α and β) that exhibits a specific, direct and reversible binding (Kojetin and Burris, 2014). SR9009 treatment caused a reduction of REV-ERBs target genes with some exceptions. Despite it also decreased the expression of myogenic genes and, the expression of myogenesis related genes is associated with a better prognosis (Moffitt et al., 2015; www.portal.gdc.cancer.gov/projects/TCGA-PAAD), we considered SR9009 as the proper treatment to modulate CAFs because it decreases the expression of the studied genes associated with a worse prognosis.

Conversely, SR9009 increases *PPAR* γ expression levels. *PPAR* γ is another nuclear receptor that acts as a transcription factor regulating the expression of target genes involved in the regulation of metabolic processes, inflammation and, also cell differentiation (Ahmadian et al., 2013). Specifically, the involvement of *PPAR* γ in cell differentiation processes leads us to think in a transformation of CAFs toward other cell differentiation state (Cheng et al., 2019; El Agha et al., 2017; Hazra et al., 2004). The complexity in the understanding of CAFs dedifferentiation is due to the different cellular phenotypes that CAFs are able to express together with the fact that CAFs may arise from many different cell types (Jotzu et al., 2010; Kalluri, 2016).

The obtained results from REV-ERBs treatments are indicative of which drug (SR8278 or SR9009) is the best option to treat CAFs and to modulate their transcriptomic profile. However, CAFs subtypes respond differently to REV-ERBs treatments. Previously, we reported different gene expression profiles in the CAFs subtypes after the co-culture with tumor cells. The same event was observed in the CAFs subtypes treated with both REV-ERBs modulators. Also, we have demonstrated that these different CAFs subtypes coexist in the same tumor sample, evidence supported by other works (Hussain et al., 2020; Neuzillet et al., 2019; Öhlund et al., 2017). By all of that, we evaluated the effect of REV-ERBs drugs in a mixture of CAFs made by our CAFs subtypes.

In the mixCAF_s, SR9009 caused a generalized reduction in the expression of REV-ERB downstream target genes (myogenesis, fibroblast-activation genes, and lipid metabolism genes). In this setting, the REV-ERBs stimulation induced the reprogramming or modulation toward a less-activated phenotype (Welch et al., 2017). This less-activated state could be considered an acquisition of quiescence (Habisch et al., 2010; Hazra et al., 2004; Kim et al., 2010).

Looking for a dedifferentiated state. What are the characteristic biomarkers?

The quiescence is a cellular state in which cells are non-dividing, they are retained, in a reversible manner, in the G₀ phase of the cell cycle (Inchul J Cho et al., 2019). Quiescent cells show a suppressed metabolic rate with a higher capacity to store intracellular lipids (Auciello et al., 2019; Sherman et al., 2014). They lose the expression of periostin and collagens which means a lower capacity to produce

Discussion

ECM, and they also lose the expression of α SMA. However, quiescent cells still maintain the expression of vimentin and desmin (Inchul J Cho et al., 2019; Habisch et al., 2010; Sherman et al., 2014).

However, depending on the origin of the quiescent cell, the expression of specific quiescent markers differs. For example, quiescent hepatic stellate cells (qHSCs) mainly overexpress adipogenic markers such as *PPAR γ* and *CEPBA* and downregulate *ACTA2* and *LOX* (lysyl oxidase). qHSCs contain abundant cytoplasmic LD and show a low proliferation rate (El Taghdouini et al., 2015; Tsukamoto, 2005). Nevertheless, Taghdouini *et al.* described an intermediate phenotype between activated and quiescent HSCs characterized by the expression of several inflammation-related genes previously identified in inactivated HSC (El Taghdouini et al., 2015).

In turn, quiescent PSCs display a reduction in the lipid metabolism genes with a higher capacity to store lipids (Schnittert et al., 2018; Sherman et al., 2014). Besides, the quiescent biomarkers FABP4 (Sherman et al., 2014) and DESMIN (Chronopoulos et al., 2016; Habisch et al., 2010) are overexpressed while α SMA and VIMENTIN are downregulated (Chronopoulos et al., 2016). By contrast, other authors define the increase in VIMENTIN expression as indicative of PSC quiescence (Habisch et al., 2010).

Some studies are suggesting that quiescent fibroblasts express higher levels of pro-inflammatory genes, and possess an active metabolic profile and further migration capacity than proliferative fibroblasts (Chen et al., 2012). *Ppar γ 2* is induced during the adipocyte differentiation process in which murine embryonic fibroblasts become activated and functional adipocytes (Kumar et al., 2010).

According to previous statements, we demonstrated that REV-ERB agonist (SR9009) treatment promoted the acquisition of a dedifferentiated state in the mixCAFs. SR9009 reduced the expression of the rate-limiting enzymes of cholesterol and lipid biosynthesis, *HMGCR* and *FASN*, as *SQLE*, which means a reduction of metabolic processes (Inchul J Cho et al., 2019). The treatment also diminished collagens' production (Cunningham et al., 2020; Han et al., 2018). The mixCAFs showed a reduction of fibroblast activation markers (*ACTA2*, *FAP*, *S100-A4*) (Cunningham et al., 2020; Hazra et al., 2004; Kim et al., 2010; Sherman et al., 2014) and, increased their capacity to store cytoplasmic lipids as lipid droplets (Auciello et al., 2019; Sherman et al., 2014).

As described previously, dedifferentiated status is defined by up- or downregulation of different markers, pathways, and functions depending on the cell type that becomes quiescent. Besides, it is also described the heterogeneity in CAFs' origin. Therefore, the discrepancies observed in the expression of some biomarkers in the supposed quiescence acquisition by CAFs may be a consequence of the distinct origin of the CAFs subtypes included in the mixture (Kalluri, 2016) or because of the plasticity of CAFs during the quiescence acquisition process (Friedman et al., 2020). These statements also support the differences observed in the REV-ERBs treatment of CAFs subtypes.

Independently to discrepancies in the gene expression, we demonstrated the acquisition of quiescence in a mono-culture of mixCAFs as well as acquisition and maintenance in a co-culture of mixCAFs with tumor cells.

Pre-treatment of CAFs with SR9009 and subsequent co-culture with tumor cells have allowed demonstrating that CAFs do not lose the dedifferentiation state after the crosstalk with tumor cells. The *in vitro* experiments prove that SR9009 treatment modifies CAFs toward a quiescent state, a fact confirmed by an increase in *PPAR γ* (El Taghdouini et al., 2015; Tsukamoto, 2005) and a reduction in *ACTA2* (Inchul J. Cho et al., 2019; Chronopoulos et al., 2016; El Taghdouini et al., 2015; Habisch et al., 2010; Sherman et al., 2014; Tsukamoto, 2005) and in fibroblast-activation genes (*FAP* and *S100-A4*) (Cunningham et al., 2020; Hazra et al., 2004; Kim et al., 2010; Sherman et al., 2014). However, the reduction in metabolic genes (Auciello et al., 2019; Inchul J. Cho et al., 2019; Sherman et al., 2014) is almost imperceptible with a slight increase in *FASN* at RNA levels. An increase that was not observed at a protein level.

Our previous experiments have confirmed the heterogeneity of CAFs as well as the culture conditions (mono-culture or co-culture) modify the CAFs' signatures and their prognosis. After SR9009 treatment, CAFs turn into a less-activated state known as quiescence. This state is maintained even after the co-culture of these CAFs with tumor cells. So, we demonstrated that the quiescent state is stable and CAFs do not lose it by the crosstalk with tumor cells.

Moving forward: effect of the dedifferentiation of CAFs on tumor development

Discussion

We obtained encouraging results in the field of CAFs reprogramming. However, further studies are needed to evaluate how this REV-ERB-induced phenotype molding performed in CAFs affects the tumor cells since previous studies based on stromal reprogramming by nuclear receptors revealed several final results.

For example, loss of AR in CAFs aggravates the metastatic capacity of prostate cancer cells (Cheng et al., 2019; Valkenburg et al., 2018). ER modulation in CAFs showed unlike effects depending on the tumor type (Cheng et al., 2019; Valkenburg et al., 2018). The work developed by Chan *et al.* demonstrated that conditioned medium from CAFs pretreated with some NR antagonists abolished the cisplatin resistance in squamous cell carcinoma. They also demonstrated that the disruption of NR expression in CAFs, decreased the expression of chemoresistance-related genes in squamous tumor cells (Chan et al., 2017).

Other studies found successful results with the activation of NR. For instance, the activation of stromal VDR increased the efficacy of gemcitabine chemotherapy in a mouse model of PDAC (Sherman et al., 2014). Coactivation of PPAR γ and RXR in CAFs modify their activation and supportive properties in breast cancer and melanoma (Cheng et al., 2019). In breast cancer, tumor cells that are exposed to conditioned medium from CAFs treated with FXR agonists showed less capacity to proliferate and invade (Cheng et al., 2019).

CONCLUSIONS

1. The analysis of transcriptomic differences of RNA-seq data obtained from the *in vitro* culture of CAFs with or without PDAC tumor cells revealed the existence two phenotypes, the mono-culture of mixCAF and the co-culture of mixCAF.
2. Survival analysis of our signatures on the Moffitt patients' dataset confirmed that patients with an overexpression of the mono-cultured CAF signature showed a better prognosis with statistically significant differences.
3. Survival analysis of cholesterol pathway and TNF signaling via NF κ B pathway confirmed that their overexpression was associated with a worse prognosis in 75% of PDAC patients.
4. The expression profiles of CAFs isolated from human PDAC samples confirmed the existence of heterogeneity.
5. A high expression of myoCAF profile or even a high expression of a single marker representative of that population such as ACTA2, were correlated with a better prognosis.
6. The *in vitro* culture of CAFs with PDAC tumor cells modify the CAFs' expression profile. Specifically, CAFs co-cultured with tumor cells acquired a more activated phenotype which is associated with a worse prognosis.
7. Protein expression in human PDAC tissue samples revealed that different CAF subpopulations coexist in the same tumor sample.
8. Protein expression in human PDAC tissue samples also revealed the existence of patients with low expression of myofibroblast markers (α SMA^{low}/FAP^{high}) or, patients with high expression of myofibroblast markers (α SMA^{high}/FAP^{low}).
9. CAF heterogeneity is also observed in the response to REV-ERB treatments since CAF subtypes respond differently to REV-ERBs drugs.
10. The REV-ERB agonist SR9009 decreases the expression of the studied genes associated with a worse prognosis.
11. SR9009 promoted the acquisition of a dedifferentiated state in the mixCAF.

Conclusions

12. Dedifferentiated CAFs are maintained in this cellular state even after the co-culture with tumor cells. The crosstalk CAFs-tumor cells do not revert the dedifferentiation of CAFs.

REFERENCES

A

- Adamska, A., Domenichini, A., Falasca, M., 2017. Pancreatic Ductal Adenocarcinoma: Current and Evolving Therapies. *Int. J. Mol. Sci.* 18, 1338.
- Adham, M., Perinel, J., 2019. Palliative therapy in pancreatic cancer—palliative surgery. *Transl. Gastroenterol. Hepatol.* 4, 1–8.
- Ahmadian, M., Suh, J.M., Hah, N., Liddle, C., Atkins, A.R., Downes, M., Evans, R.M., 2013. PPAR γ signaling and metabolism: the good, the bad and the future. *Nat. Med.* 19, 557–566.
- Altman, B.J., Hsieh, A.L., Sengupta, A., Krishnanaiah, S.Y., Stine, Z.E., Walton, Z.E., Gouw, A.M., Venkataraman, A., Li, B., Goraksha-Hicks, P., Diskin, S.J., Bellovin, D.I., Simon, M.C., Rathmell, J.C., Lazar, M.A., Maris, J.M., Felsher, D.W., Hogenesch, J.B., Weljie, A.M., Dang, C. V., 2015. MYC Disrupts the Circadian Clock and Metabolism in Cancer Cells. *Cell Metab.* 22, 1009–1019.
- Auciello, F.R., Bulusu, V., Oon, C., Tait-Mulder, J., Berry, M., Bhattacharyya, S., Tumanov, S., Allen-Petersen, B.L., Link, J., Kendsersky, N.D., Vringer, E., Schug, M., Novo, D., Hwang, R.F., Evans, R.M., Nixon, C., Dorrell, C., Morton, J.P., Norman, J.C., Sears, R.C., Kamphorst, J.J., Sherman, M.H., 2019. A stromal lysolipid–autotaxin signaling axis promotes pancreatic tumor progression. *Cancer Discov.* 9, 617–627.
- Avagliano, A., Granato, G., Ruocco, M.R., Romano, V., Belviso, I., Carfora, A., Montagnani, S., Arcucci, A., 2018. Metabolic Reprogramming of Cancer Associated Fibroblasts: The Slavery of Stromal Fibroblasts. *Biomed Res. Int.* 2018, 1–12.

B

- Bailey, P., Chang, D.K., Nones, K., Johns, A.L., Patch, A.-M., Gingras, M.-C., Miller, D.K., Christ, A.N., Bruxner, T.J.C., Quinn, M.C., Nourse, C., Murtaugh, L.C., Harliwong, I., Idrisoglu, S., Manning, S., Nourbakhsh, E., Wani, S., Fink, L., Holmes, O., Chin, V., Anderson, M.J., Kazakoff, S., Leonard, C., Newell, F., Waddell, Nick, Wood, S., Xu, Q., Wilson, P.J., Cloonan, N., Kassahn, K.S., Taylor, D., Quek, K., Robertson, A., Pantano, L., Mincarelli, L., Sanchez, L.N., Evers, L., Wu, J., Pinese, M., Cowley, M.J., Jones, M.D., Colvin, E.K., Nagrial, A.M., Humphrey, E.S., Chantrill, L.A., Mawson, A., Humphris, J., Chou, A., Pajic, M., Scarlett, C.J., Pinho, A. V., Giry-Laterriere, M., Rooman, I., Samra, J.S., Kench, J.G., Lovell, J.A., Merrett, N.D., Toon, C.W., Epari, K., Nguyen, N.Q., Barbour, A., Zeps, N., Moran-Jones, K., Jamieson, N.B., Graham, J.S., Duthie, F., Oien, K., Hair, J., Grützmann, R., Maitra, A., Iacobuzio-Donahue, C.A., Wolfgang, C.L., Morgan, R.A., Lawlor, R.T., Corbo, V., Bassi, C., Rusev, B., Capelli, P., Salvia, R., Tortora, G., Mukhopadhyay, D., Petersen, G.M., Munzy, D.M., Fisher, W.E., Karim, S.A., Eshleman, J.R., Hruban,

References

- R.H., Pilarsky, C., Morton, J.P., Sansom, O.J., Scarpa, A., Musgrove, E.A., Bailey, U.-M.H., Hofmann, O., Sutherland, R.L., Wheeler, D.A., Gill, A.J., Gibbs, R.A., Pearson, J. V., Waddell, Nicola, Biankin, A. V., Grimmond, S.M., 2016. Genomic analyses identify molecular subtypes of pancreatic cancer. *Nature* 531, 47–52.
- Balaban, S., Shearer, R.F., Lee, L.S., van Geldermalsen, M., Schreuder, M., Shtein, H.C., Cairns, R., Thomas, K.C., Fazakerley, D.J., Grewal, T., Holst, J., Saunders, D.N., Hoy, A.J., 2017. Adipocyte lipolysis links obesity to breast cancer growth: adipocyte-derived fatty acids drive breast cancer cell proliferation and migration. *Cancer Metab.* 5, 1.
- Barbie, D.A., Tamayo, P., Boehm, J.S., Kim, S.Y., Moody, S.E., Dunn, I.F., Schinzel, A.C., Sandy, P., Meylan, E., Scholl, C., Fröhling, S., Chan, E.M., Sos, M.L., Michel, K., Mermel, C., Silver, S.J., Weir, B.A., Reiling, J.H., Sheng, Q., Gupta, P.B., Wadlow, R.C., Le, H., Hoersch, S., Wittner, B.S., Ramaswamy, S., Livingston, D.M., Sabatini, D.M., Meyerson, M., Thomas, R.K., Lander, E.S., Mesirov, J.P., Root, D.E., Gilliland, D.G., Jacks, T., Hahn, W.C., 2009. Systematic RNA interference reveals that oncogenic KRAS-driven cancers require TBK1. *Nature* 462, 108–112.
- Becht, E., Giraldo, N.A., Lacroix, L., Buttard, B., Elarouci, N., Petitprez, F., Selves, J., Laurent-Puig, P., Sautès-Fridman, C., Fridman, W.H., de Reyniès, A., 2016. Estimating the population abundance of tissue-infiltrating immune and stromal cell populations using gene expression. *Genome Biol.* 17, 218.
- Beloribi-Djefaflija, S., Vasseur, S., Guillaumond, F., 2016. Lipid metabolic reprogramming in cancer cells. *Oncogenesis* 5, e189–e189.
- Berdiel-Acer, M., Sanz-Pamplona, R., Calon, A., Cuadras, D., Berenguer, A., Sanjuan, X., Paules, M.J., Salazar, R., Moreno, V., Batlle, E., Villanueva, A., Molleví, D.G., 2014. Differences between CAFs and their paired NCF from adjacent colonic mucosa reveal functional heterogeneity of CAFs, providing prognostic information. *Mol. Oncol.* 8, 1290–1305.
- Blaus, B., 2014. Medical gallery of Blausen Medical 2014. *WikiJournal Med.* 1, 10.
- Bochet, L., Lehuédé, C., Dauvillier, S., Wang, Y.Y., Dirat, B., Laurent, V., Dray, C., Guiet, R., Maridonneau-Parini, I., Gonidec, S. Le, Couderc, B., Escourrou, G., Valet, P., Muller, C., 2013. Adipocyte-derived fibroblasts promote tumor progression and contribute to the desmoplastic reaction in breast cancer. *Cancer Res.* 73, 5657–5668.
- Buckanovich, R.J., Facciabene, A., Kim, S., Benencia, F., Sasaroli, D., Balint, K., Katsaros, D., O'Brien-Jenkins, A., Gimotty, P.A., Coukos, G., 2008. Endothelin B receptor mediates the endothelial barrier to T cell homing to tumors and disables immune therapy. *Nat. Med.* 14, 28–36.
- Buckley, D., Duke, G., Heuer, T.S., O'Farrell, M., Wagman, A.S., McCulloch, W., Kemble, G., 2017. Fatty acid synthase – Modern tumor cell biology insights into a classical oncology target. *Pharmacol. Ther.* 177, 23–31.

Bugge, A., Feng, D., Everett, L.J., Briggs, E.R., Mullican, S.E., Wang, F., Jager, J., Lazar, M.A., 2012. Rev-erb α and Rev-erb β coordinately protect the circadian clock and normal metabolic function. *Genes Dev.* 26, 657–667.

C

Carroll, R.G., Zastona, Z., Galván-Peña, S., Koppe, E.L., Sévin, D.C., Angiari, S., Triantafilou, M., Triantafilou, K., Modis, L.K., O’Neill, L.A., 2018. An unexpected link between fatty acid synthase and cholesterol synthesis in proinflammatory macrophage activation. *J. Biol. Chem.* 293, 5509–5521.

Catenacci, D.V.T., Junttila, M.R., Karrison, T., Bahary, N., Horiba, M.N., Nattam, S.R., Marsh, R., Wallace, J., Kozloff, M., Rajdev, L., Cohen, D., Wade, J., Sleckman, B., Lenz, H.-J., Stiff, P., Kumar, P., Xu, P., Henderson, L., Takebe, N., Salgia, R., Wang, X., Stadler, W.M., de Sauvage, F.J., Kindler, H.L., 2015. Randomized Phase Ib/II Study of Gemcitabine Plus Placebo or Vismodegib, a Hedgehog Pathway Inhibitor, in Patients With Metastatic Pancreatic Cancer. *J. Clin. Oncol. Off. J. Am. Soc. Clin. Oncol.* 33, 4284–4292.

Chan, J., Sng, M., Teo, Z., Chong, H., Twang, J., Tan, N., 2017. Targeting nuclear receptors in cancer-associated fibroblasts as concurrent therapy to inhibit development of chemoresistant tumors. *Nat. Publ. Gr.* 37, 160–173.

Chan, J.S.K., Sng, M.K., Teo, Z.Q., Chong, H.C., Twang, J.S., Tan, N.S., 2018. Targeting nuclear receptors in cancer-associated fibroblasts as concurrent therapy to inhibit development of chemoresistant tumors. *Oncogene* 37, 160–173.

Chandana, S.R., Babiker, H.M., Mahadevan, D., 2019. Therapeutic trends in pancreatic ductal adenocarcinoma (PDAC). *Expert Opin. Investig. Drugs.*

Chatterjee, S., Yin, H., Li, W., Lee, J., Yechoor, V.K., Ma, K., 2019. The Nuclear Receptor and Clock Repressor Rev-erb α Suppresses Myogenesis. *Sci. Rep.* 9.

Chen, B.-R., Cheng, H.-H., Lin, W.-C., Wang, K.-H., Liou, J.-Y., Chen, P.-F., Wu, K.K., 2012. Quiescent Fibroblasts Are More Active in Mounting Robust Inflammatory Responses Than Proliferative Fibroblasts. *PLoS One* 7, e49232.

Chen, R., 2012. Targeting Tumor Stroma: A Novel Therapeutic Approach to Pancreatic Cancer Treatment. *Pancreat. Disord. Ther.* 02, 2–3.

Cheng, H.S., Lee, J.X.T., Wahli, W., Tan, N.S., 2019. Exploiting vulnerabilities of cancer by targeting nuclear receptors of stromal cells in tumor microenvironment. *Mol. Cancer* 18, 1–19.

Cho, Inchul J, Lui, P.P., Obajdin, J., Riccio, F., Stroukov, W., Willis, T.L., Spagnoli, F., Watt, F.M., 2019. Mechanisms, Hallmarks, and Implications of Stem Cell Quiescence. *Stem cell reports* 12, 1190–1200.

Cho, Inchul J., Lui, P.P.W., Obajdin, J., Riccio, F., Stroukov, W., Willis, T.L., Spagnoli, F.,

References

- Watt, F.M., 2019. Mechanisms, Hallmarks, and Implications of Stem Cell Quiescence. *Stem Cell Reports* 12, 1190–1200.
- Chronopoulos, A., Robinson, B., Sarper, M., Cortes, E., Auernheimer, V., Lachowski, D., Attwood, S., García, R., Ghassemi, S., Fabry, B., del Río Hernández, A., 2016. ATRA mechanically reprograms pancreatic stellate cells to suppress matrix remodelling and inhibit cancer cell invasion. *Nat. Commun.* 7, 12630.
- Collisson, E.A., Sadanandam, A., Olson, P., Gibb, W.J., Truitt, M., Gu, S., Cooc, J., Weinkle, J., Kim, G.E., Jakkula, L., Feiler, H.S., Ko, A.H., Olshen, A.B., Danenberg, K.L., Tempero, M.A., Spellman, P.T., Hanahan, D., Gray, J.W., 2011. Subtypes of Pancreatic Ductal Adenocarcinoma and Their Differing Responses to Therapy. *Nat Med* 17, 500–503.
- Çubuk, C., Hidalgo, M.R., Amadoz, A., Rian, K., Salavert, F., Pujana, M.A., Mateo, F., Herranz, C., Carbonell-Caballero, J., Dopazo, J., 2019. Differential metabolic activity and discovery of therapeutic targets using summarized metabolic pathway models. *NPJ Syst. Biol. Appl.* 5, 7.
- Cunningham, P.S., Meijer, P., Nazgiewicz, A., Anderson, S.G., Borthwick, L.A., Bagnall, J., Kitchen, G.B., Lodyga, M., Begley, N., Venkateswaran, R. V., Shah, R., Mercer, P.F., Durrington, H.J., Henderson, N.C., Piper-Hanley, K., Fisher, A.J., Chambers, R.C., Bechtold, D.A., Gibbs, J.E., Loudon, A.S., Rutter, M.K., Hinz, B., Ray, D.W., Blaikley, J.F., 2020. The circadian clock protein REVERB α inhibits pulmonary fibrosis development. *Proc. Natl. Acad. Sci. U. S. A.* 117, 1139–1147.

D

- Daemen, A., Peterson, D., Sahu, N., McCord, R., Du, X., Liu, B., Kowanetz, K., Hong, R., Moffat, J., Gao, M., Boudreau, A., Mroue, R., Corson, L., O'Brien, T., Qing, J., Sampath, D., Merchant, M., Yauch, R., Manning, G., Settleman, J., Hatzivassiliou, G., Evangelista, M., DePinho, R.A., 2015. Metabolite profiling stratifies pancreatic ductal adenocarcinomas into subtypes with distinct sensitivities to metabolic inhibitors. *Proc. Natl. Acad. Sci. U. S. A.* 112, E4410–E4417.
- De Jesus-Acosta, A., O'Dwyer, P.J., Ramanathan, R.K., Von Hoff, D.D., Maitra, A., Rasheed, Z., Zheng, L., Rajeshkumar, N. V., Le, D.T., Hoering, A., Bolejack, V., Yabuuchi, S., Laheru, D.A., 2014. A phase II study of vismodegib, a hedgehog (Hh) pathway inhibitor, combined with gemcitabine and nab-paclitaxel (nab-P) in patients (pts) with untreated metastatic pancreatic ductal adenocarcinoma (PDA). *J. Clin. Oncol.* 32, 257.
- De Mei, C., Ercolani, L., Parodi, C., Veronesi, M., Vecchio, C. Lo, Bottegoni, G., Torrente, E., Scarpelli, R., Marotta, R., Ruffili, R., Mattioli, M., Reggiani, A., Wade, M., Grimaldi, B., 2015. Dual inhibition of REV-ERB β and autophagy as a novel pharmacological approach to induce cytotoxicity in cancer cells. *Oncogene* 34, 2597–2608.

- De Sostoa, J., Fajardo, C.A., Moreno, R., Ramos, M.D., Farrera-Sal, M., Alemany, R., 2019. Targeting the tumor stroma with an oncolytic adenovirus secreting a fibroblast activation protein-targeted bispecific T-cell engager. *J. Immunother. Cancer* 7, 1–15.
- Deer, E.L., González-Hernández, J., Coursen, J.D., Shea, J.E., Ngatia, J., Scaife, C.L., Firpo, M.A., Mulvihill, S.J., 2010. Phenotype and genotype of pancreatic cancer cell lines. *Pancreas* 39, 425–35.
- Díaz-Maroto, N.G., Sanz-Pamplona, R., Berdiel-Acer, M., Cimas, F.J., García, E., Gonçalves-Ribeiro, S., Albert, N., Garcia-Vicien, G., Capella, G., Moreno, V., Salazar, R., Villanueva, A., Molleví, D.G., 2019. Noncanonical TGF β pathway relieves the blockade of IL1B/TGF β -mediated crosstalk between tumor and stroma: TGFBR1 and TAK1 inhibition in colorectal cancer. *Clin. Cancer Res.* 25, 4466–4479.
- Distler, M., Aust, D., Weitz, J., Pilarsky, C., Grützmann, R., 2014. Precursor Lesions for Sporadic Pancreatic Cancer: PanIN, IPMN, and MCN. *Biomed Res. Int.* 2014, 1–11.

E

- El Agha, E., Moiseenko, A., Kheirollahi, V., De Langhe, S., Crnkovic, S., Kwapiszewska, G., Kosanovic, D., Schwind, F., Schermuly, R.T., Henneke, I., MacKenzie, B.A., Quantius, J., Herold, S., Ntokou, A., Ahlbrecht, K., Morty, R.E., Günther, A., Seeger, W., Bellusci, S., 2017. Two-Way Conversion between Lipogenic and Myogenic Fibroblastic Phenotypes Marks the Progression and Resolution of Lung Fibrosis. *Cell Stem Cell* 20, 261-273.e3.
- El Taghdouini, A., Najimi, M., Sancho-Bru, P., Sokal, E., van Grunsven, L.A., 2015. In vitro reversion of activated primary human hepatic stellate cells. *Fibrogenes. Tissue Repair* 8, 1–15.
- Elahi-Gedwillo, K.Y., Carlson, M., Zettervall, J., Provenzano, P.P., 2019. Antifibrotic therapy disrupts stromal barriers and modulates the immune landscape in pancreatic ductal adenocarcinoma. *Cancer Res.* 79, 372–386.
- Ellyard, J.I., Simson, L., Parish, C.R., 2007. Th2-mediated anti-tumour immunity: friend or foe? *Tissue Antigens* 70, 1–11.
- Elyada, E., Bolisetty, M., Laise, P., Flynn, W.F., Courtois, E.T., Burkhart, R.A., Teinor, J.A., Belleau, P., Biffi, G., Lucito, M.S., Sivajothi, S., Armstrong, T.D., Engle, D.D., Yu, K.H., Hao, Y., Wolfgang, C.L., Park, Y., Preall, J., Jaffee, E.M., Califano, A., Robson, P., Tuveson, D.A., 2019. Cross-species single-cell analysis of pancreatic ductal adenocarcinoma reveals antigen-presenting cancer-associated fibroblasts. *Cancer Discov.* 9, 1102–1123.
- Erkan, M., Hausmann, S., Michalski, C.W., Fingerle, A.A., Dobritz, M., Kleeff, J., Friess,

References

H., 2012. The role of stroma in pancreatic cancer: Diagnostic and therapeutic implications. *Nat. Rev. Gastroenterol. Hepatol.* 9, 454–467.

Everett, L.J., Lazar, M.A., 2014. Nuclear receptor Rev-erb α : up, down, and all around. *Trends Endocrinol. Metab.* 25, 586–592.

F

Feig, C., Jones, J.O., Kraman, M., Wells, R.J.B., Deonarine, A., Chan, D.S., Connell, C.M., Roberts, E.W., Zhao, Q., Caballero, O.L., Teichmann, S. a, Janowitz, T., 2013. Targeting CXCL12 from FAP-expressing carcinoma-associated fibroblasts synergizes with anti-PD-L1 immunotherapy in pancreatic cancer. *Proc Natl Acad Sci U S A* 110, 20212–20217.

Feng, D., Liu, T., Sun, Z., Bugge, A., Mullican, S.E., Alenghat, T., Liu, X.S., Lazar, M.A., 2011. A Circadian Rhythm Orchestrated by Histone Deacetylase 3 Controls Hepatic Lipid Metabolism. *Science (80-.)*. 331, 1315–1319.

Friedman, G., Levi-Galibov, O., David, E., Bornstein, C., Giladi, A., Dadiani, M., Mayo, A., Halperin, C., Pevsner-Fischer, M., Lavon, H., Nevo, R., Stein, Y., Ali, H.R., Caldas, C., Nili-Gal-Yam, E., Alon, U., Amit, I., Scherz-Shouval, R., 2020. Cancer-associated fibroblast compositions change with breast-cancer progression linking S100A4 and PDPN ratios with clinical outcome. *bioRxiv* 2020.01.12.903039.

G

Gascard, P., Tlsty, T.D., 2016. Carcinoma-associated fibroblasts: Orchestrating the composition of malignancy. *Genes Dev.* 30, 1002–1019.

Goikuria, H., Freijo, M., Vega Manrique, R., Sastre, M., Elizagaray, E., Lorenzo, A., Vandenbroeck, K., Alloza, I., 2018. Characterization of Carotid Smooth Muscle Cells during Phenotypic Transition. *Cells* 7, 23.

Gong, J., Lin, Y., Zhang, H., Liu, C., Cheng, Z., Yang, X., Zhang, J., Xiao, Y., Sang, N., Qian, X., Wang, L., Cen, X., Du, X., Zhao, Y., 2020. Reprogramming of lipid metabolism in cancer-associated fibroblasts potentiates migration of colorectal cancer cells. *Cell Death Dis.* 11, 267.

Goossens, P., Rodriguez-Vita, J., Etzerodt, A., Masse, M., Rastoin, O., Gouirand, V., Ulas, T., Papantonopoulou, O., Van Eck, M., Auphan-Anezin, N., Bebien, M., Verthuy, C., Vu Manh, T.P., Turner, M., Dalod, M., Schultze, J.L., Lawrence, T., 2019. Membrane Cholesterol Efflux Drives Tumor-Associated Macrophage Reprogramming and Tumor Progression. *Cell Metab.* 29, 1376-1389.e4.

Gradiz, R., Silva, H.C., Carvalho, L., Botelho, M.F., Mota-Pinto, A., 2016. MIA PaCa-2 and PANC-1 - pancreas ductal adenocarcinoma cell lines with neuroendocrine differentiation and somatostatin receptors. *Sci. Rep.* 6, 21648.

- Guillaumond, F., Bidaut, G., Ouaiissi, M., Servais, S., Gouirand, V., Olivares, O., Lac, S., Borge, L., Roques, J., Gayet, O., Pinault, M., Guimaraes, C., Nigri, J., Loncle, C., Lavaut, M.N., Garcia, S., Tailleuxi, A., Staels, B., Calvom, E., Tomasini, R., Iovanna, J.L., Vasseur, S., 2015. Cholesterol uptake disruption, in association with chemotherapy, is a promising combined metabolic therapy for pancreatic adenocarcinoma. *Proc. Natl. Acad. Sci. U. S. A.* 112, 2473–2478.
- Guillén-Ponce, C., Blázquez, J., González, I., De-Madaria, E., Montáns, J., Carrato, A., 2017. Diagnosis and staging of pancreatic ductal adenocarcinoma. *Clin. Transl. Oncol.* 19, 1205–1216.

H

- H. Bekkali, N., Oppong, K., 2017. Pancreatic ductal adenocarcinoma epidemiology and risk assessment: Could we prevent? Possibility for an early diagnosis. *Endosc. Ultrasound* 6, 58.
- Habisch, H., Zhou, S., Siech, M., Bachem, M.G., 2010. Interaction of stellate cells with pancreatic carcinoma cells. *Cancers (Basel)*. 2, 1661–1682.
- Han, X., Li, Y., Xu, Y., Zhao, X., Zhang, Y., Yang, X., Wang, Y., Zhao, R., Anderson, G.J., Zhao, Y., Nie, G., 2018. Reversal of pancreatic desmoplasia by re-educating stellate cells with a tumour microenvironment-activated nanosystem. *Nat. Commun.* 9, 3390.
- Hata, T., Kawamoto, K., Eguchi, H., Kamada, Y., Takamatsu, S., Maekawa, T., Nagaoka, S., Yamada, D., Iwagami, Y., Asaoka, T., Noda, T., Wada, H., Gotoh, K., Masamune, A., Miyoshi, E., Mori, M., Doki, Y., 2017. Fatty Acid–Mediated Stromal Reprogramming of Pancreatic Stellate Cells Induces Inflammation and Fibrosis That Fuels Pancreatic Cancer. *Pancreas* 46, 1259–1266.
- Hazra, S., Xiong, S., Wang, J., Rippe, R.A., Chatterjee, V.K.K., Tsukamoto, H., 2004. Peroxisome Proliferator-activated Receptor γ Induces a Phenotypic Switch from Activated to Quiescent Hepatic Stellate Cells. *J. Biol. Chem.* 279, 11392–11401.
- Hezel, A.F., Kimmelman, A.C., Stanger, B.Z., Bardeesy, N., DePinho, R.A., 2006. Genetics and biology of pancreatic ductal adenocarcinoma. *Genes Dev.* 20, 1218–1249.
- Hida, K., Maishi, N., Annan, D.A., Hida, Y., 2018. Contribution of Tumor Endothelial Cells in Cancer Progression. *Int. J. Mol. Sci.* 19, 1272.
- Hidalgo, M.R., Cubuk, C., Amadoz, A., Salavert, F., Carbonell-Caballero, J., Dopazo, J., 2017. High throughput estimation of functional cell activities reveals disease mechanisms and predicts relevant clinical outcomes. *Oncotarget* 8, 5160–5178.
- Hingorani, S.R., Zheng, L., Bullock, A.J., Seery, T.E., Harris, W.P., Sigal, D.S., Braiteh, F., Ritch, P.S., Zalupski, M.M., Bahary, N., Oberstein, P.E., Wang-Gillam, A., Wu, W., Chondros, D., Jiang, P., Khelifa, S., Pu, J., Aldrich, C., Hendifar, A.E., 2018. HALO 202: Randomized Phase II Study of PEGPH20 Plus Nab-Paclitaxel/Gemcitabine

References

Versus Nab-Paclitaxel/Gemcitabine in Patients With Untreated, Metastatic Pancreatic Ductal Adenocarcinoma. *J. Clin. Oncol. Off. J. Am. Soc. Clin. Oncol.* 36, 359–366.

Hruban, R.H., Fukushima, N., 2007. Pancreatic adenocarcinoma: Update on the surgical pathology of carcinomas of ductal origin and panins. *Mod. Pathol.* 20, 61–70.

Hussain, A., Voisin, V., Poon, S., Karamboulas, C., Bui, N.H.B., Meens, J., Dmytryshyn, J., Ho, V.W., Tang, K.H., Paterson, J., Clarke, B.A., Bernardini, M.Q., Bader, G.D., Neel, B.G., Ailles, L.E., 2020. Distinct fibroblast functional states drive clinical outcomes in ovarian cancer and are regulated by TCF21. *J. Exp. Med.* 217.

I

Ikenaga, N., Ohuchida, K., Mizumoto, K., Yu, J., Fujita, H., Nakata, K., Ueda, J., Sato, N., Nagai, E., Tanaka, M., 2009. S100A4 mRNA is a diagnostic and prognostic marker in pancreatic carcinoma. *J. Gastrointest. Surg.* 13, 1852–1858.

Iovanna, J.L., Closa, D., 2017. Factors released by the tumor far microenvironment are decisive for pancreatic adenocarcinoma development and progression. *Oncoimmunology* 6, e1358840.

J

Jacobetz, M.A., Chan, D.S., Neesse, A., Bapiro, T.E., Cook, N., Frese, K.K., Feig, C., Nakagawa, T., Caldwell, M.E., Zecchini, H.I., Lolkema, M.P., Jiang, P., Kultti, A., Thompson, C.B., Maneval, D.C., Jodrell, D.I., Frost, G.I., Shepard, H.M., Skepper, J.N., Tuveson, D.A., 2013. Hyaluronan impairs vascular function and drug delivery in a mouse model of pancreatic cancer. *Gut* 62, 112–120.

Jiang, H., Hegde, S., Knolhoff, B.L., Zhu, Y., Herndon, J.M., Meyer, M.A., Nywening, T.M., Hawkins, W.G., Shapiro, I.M., Weaver, D.T., Pachter, J.A., Wang-Gillam, A., DeNardo, D.G., 2016. Targeting focal adhesion kinase renders pancreatic cancers responsive to checkpoint immunotherapy. *Nat. Med.* 22, 851–860.

Jones, S.F., Infante, J.R., 2015. Molecular Pathways: Fatty Acid Synthase. *Clin Cancer Res* 21, 5434–8.

Jotzu, C., Alt, E., Welte, G., Li, J., Hennessy, B.T., Devarajan, E., Krishnappa, S., Pinilla, S., Droll, L., Song, Y.-H., 2010. Adipose tissue-derived stem cells differentiate into carcinoma-associated fibroblast-like cells under the influence of tumor-derived factors. *Anal. Cell. Pathol.* 33, 61–79.

Jotzu, C., Alt, E., Welte, G., Li, J., Hennessy, B.T., Devarajan, E., Krishnappa, S., Pinilla, S., Droll, L., Song, Y.-H., 2011. Adipose tissue derived stem cells differentiate into carcinoma-associated fibroblast-like cells under the influence of tumor derived factors. *Cell. Oncol.* 34, 55–67.

K

- Kalluri, R., 2016. The biology and function of fibroblasts in cancer. *Nat. Rev. Cancer* 16, 582–598.
- Karakas, Y., Lacin, S., Yalcin, S., 2018. Recent advances in the management of pancreatic adenocarcinoma. *Expert Rev. Anticancer Ther.* 18, 51–62.
- Karasinska, J.M., Topham, J.T., Kalloger, S.E., Jang, G.H., Denroche, R.E., Culibrk, L., Williamson, L.M., Wong, H.L., Lee, M.K.C., O’Kane, G.M., Moore, R.A., Mungall, A.J., Moore, M.J., Warren, C., Metcalfe, A., Notta, F., Knox, J.J., Gallinger, S., Laskin, J., Marra, M.A., Jones, S.J.M., Renouf, D.J., Schaeffer, D.F., 2020. Altered gene expression along the glycolysis–cholesterol synthesis axis is associated with outcome in pancreatic cancer. *Clin. Cancer Res.* 26, 135–146.
- Kim, N., Choi, S., Lim, C., Lee, H., Oh, J., 2010. Albumin mediates PPAR- γ or C/EBP- α -induced phenotypic changes in pancreatic stellate cells. *Biochem. Biophys. Res. Commun.* 391, 640–644.
- Knutson, K.L., Disis, M.L., 2005. Tumor antigen-specific T helper cells in cancer immunity and immunotherapy. *Cancer Immunol. Immunother.* 54, 721–728.
- Ko, A.H., LoConte, N., Tempero, M.A., Walker, E.J., Kate Kelley, R., Lewis, S., Chang, W.-C., Kantoff, E., Vannier, M.W., Catenacci, D. V, Venook, A.P., Kindler, H.L., 2016. A Phase I Study of FOLFIRINOX Plus IPI-926, a Hedgehog Pathway Inhibitor, for Advanced Pancreatic Adenocarcinoma. *Pancreas* 45, 370–375.
- Kojetin, D., Wang, Y., Kamenecka, T.M., Burris, T.P., 2011. Identification of SR8278, a synthetic antagonist of the nuclear heme receptor REV-ERB. *ACS Chem. Biol.* 6, 131–134.
- Kojetin, D.J., Burris, T.P., 2014. REV-ERB and ROR nuclear receptors as drug targets. *Nat. Rev. Drug Discov.* 13, 197–216.
- Kumar, N., Solt, L.A., Wang, Y., Rogers, P.M., Bhattacharyya, G., Kamenecka, T.M., Stayrook, K.R., Crumbley, C., Floyd, Z.E., Gimble, J.M., Griffin, P.R., Burris, T.P., 2010. Regulation of adipogenesis by natural and synthetic REV-ERB ligands. *Endocrinology* 151, 3015–3025.
- Kuzu, O.F., Noory, M.A., Robertson, G.P., 2016. The role of cholesterol in cancer. *Cancer Res.* 76, 2063–2070.

L

- Lambrechts, D., Wauters, E., Boeckx, B., Aibar, S., Nittner, D., Burton, O., Bassez, A., Decaluwé, H., Pircher, A., Van den Eynde, K., Weynand, B., Verbeken, E., De Leyn, P., Liston, A., Vansteenkiste, J., Carmeliet, P., Aerts, S., Thienpont, B., 2018a. Phenotype molding of stromal cells in the lung tumor microenvironment.

References

- Nat. Med. 24, 1277–1289.
- Lambrechts, D., Wauters, E., Boeckx, B., Aibar, S., Nittner, D., Burton, O., Bassez, A., Decaluwé, H., Pircher, A., Van den Eynde, K., Weynand, B., Verbeken, E., De Leyn, P., Liston, A., Vansteenkiste, J., Carmeliet, P., Aerts, S., Thienpont, B., 2018b. Phenotype molding of stromal cells in the lung tumor microenvironment. *Nat. Med.* 24, 1277–1289.
- Le Martelot, G., Claudel, T., Gatfield, D., Schaad, O., Kornmann, B., Lo Sasso, G., Moschetta, A., Schibler, U., 2009. REV-ERB α participates in circadian SREBP signaling and bile acid homeostasis. *PLoS Biol.* 7, 1–12.
- Lee, J.J., Perera, R.M., Wang, H., Wu, D.-C., Liu, X.S., Han, S., Fitamant, J., Jones, P.D., Ghanta, K.S., Kawano, S., Nagle, J.M., Deshpande, V., Boucher, Y., Kato, T., Chen, J.K., Willmann, J.K., Bardeesy, N., Beachy, P.A., 2014. Stromal response to Hedgehog signaling restrains pancreatic cancer progression. *Proc. Natl. Acad. Sci.* 111, E3091–E3100.
- Lee, W.Y., Su, W.C., Lin, P.W., Guo, H.R., Chang, T.W., Chen, H.H.W., 2004. Expression of S100A4 and Met: Potential Predictors for Metastasis and Survival in Early-Stage Breast Cancer. *Oncology* 66, 429–438.
- Li, H., Fan, X., Houghton, J.M., 2007. Tumor microenvironment: The role of the tumor stroma in cancer. *J. Cell. Biochem.* 101, 805–815.
- Li, J.-T., Wang, Y.-P., Yin, M., Lei, Q.-Y., 2019. Metabolism remodeling in pancreatic ductal adenocarcinoma. *Cell Stress* 3, 361–368.
- Lo, A., Wang, L.-C.S., Scholler, J., Monslow, J., Avery, D., Newick, K., O’Brien, S., Evans, R.A., Bajor, D.J., Clendenin, C., Durham, A.C., Buza, E.L., Vonderheide, R.H., June, C.H., Albelda, S.M., Pure, E., 2015. Tumor-Promoting Desmoplasia Is Disrupted by Depleting FAP-Expressing Stromal Cells. *Cancer Res.* 75, 2800–2810.
- Longnecker, D., 2014. Anatomy and Histology of the Pancreas. *Pancreapedia Exocrine Pancreas Knowl. Base* 1–26.
- Lu, P., Weaver, V.M., Werb, Z., 2012. The extracellular matrix: A dynamic niche in cancer progression. *J. Cell Biol.* 196, 395–406.

M

- Maeda, S., Unno, M., Yu, J., 2019. Adjuvant and neoadjuvant therapy for pancreatic cancer. *J. Pancreatol.* 2, 100–106.
- Malanchi, I., Santamaria-Martínez, A., Susanto, E., Peng, H., Lehr, H.-A., Delaloye, J.-F., Huelsken, J., 2011. Interactions between cancer stem cells and their niche govern metastatic colonization. *Nature* 481, 85–89.
- Marciano, D.P., Chang, M.R., Corzo, C.A., Goswami, D., Lam, V.Q., Pascal, B.D., Griffin, P.R., 2014. The therapeutic potential of nuclear receptor modulators for

- treatment of metabolic disorders: PPAR γ , RORs, and Rev-erbs. *Cell Metab.*
- McGowan, S.E., 2019. The lipofibroblast: More than a lipid-storage depot. *Am. J. Physiol. - Lung Cell. Mol. Physiol.* 316, L869–L871.
- Menendez, J.A., Lupu, R., 2007. Fatty acid synthase and the lipogenic phenotype in cancer pathogenesis. *Nat. Rev. Cancer* 7, 763–777.
- Meyer, K.A., Neeley, C.K., Baker, N.A., Washabaugh, A.R., Flesher, C.G., Nelson, B.S., Frankel, T.L., Lumeng, C.N., Lyssiotis, C.A., Wynn, M.L., Rhim, A.D., O'Rourke, R.W., 2016. Adipocytes promote pancreatic cancer cell proliferation via glutamine transfer. *Biochem. Biophys. Reports* 7, 144–149.
- Mezheyeuski, A., Segersten, U., Leiss, L.W., Malmström, P.U., Hatina, J., Östman, A., Strell, C., 2020. Fibroblasts in urothelial bladder cancer define stroma phenotypes that are associated with clinical outcome. *Sci. Rep.* 10, 1–12.
- Miao, L., Liu, Q., Lin, C.M., Luo, C., Wang, Y., Liu, L., Yin, W., Hu, S., Kim, W.Y., Huang, L., 2017. Targeting tumor-associated fibroblasts for therapeutic delivery in desmoplastic tumors. *Cancer Res.* 77, 719–731.
- Moffitt, R.A., Marayati, R., Flate, E.L., Volmar, K.E., Loeza, S.G.H., Hoadley, K.A., Rashid, N.U., Williams, L.A., Eaton, S.C., Chung, A.H., Smyla, J.K., Anderson, J.M., Kim, H.J., Bentrem, D.J., Talamonti, M.S., Iacobuzio-Donahue, C.A., Hollingsworth, M.A., Yeh, J.J., 2015. Virtual microdissection identifies distinct tumor- and stroma-specific subtypes of pancreatic ductal adenocarcinoma. *Nat. Genet.* 47, 1168–1178.
- Mpekris, F., Papageorgis, P., Polydorou, C., Voutouri, C., Kalli, M., Pirentis, A.P., Stylianopoulos, T., 2017. Sonic-hedgehog pathway inhibition normalizes desmoplastic tumor microenvironment to improve chemo- and nanotherapy. *J. Control. Release* 261, 105–112.

N

- Nardi, F., Fitchev, P., Franco, O.E., Ivanisevic, J., Scheibler, A., Hayward, S.W., Brendler, C.B., Welte, M.A., Crawford, S.E., 2018. PEDF regulates plasticity of a novel lipid-MTOC axis in prostate cancer-associated fibroblasts. *J. Cell Sci.* 131, 1–16.
- Neuzillet, C., Tijeras-Raballand, A., Ragulan, C., Cros, J., Patil, Y., Martinet, M., Erkan, M., Kleeff, J., Wilson, J., Apte, M., Tosolini, M., Wilson, A.S., Delvecchio, F.R., Bousquet, C., Paradis, V., Hammel, P., Sadanandam, A., Kocher, H.M., 2019. Inter- and intra-tumoural heterogeneity in cancer-associated fibroblasts of human pancreatic ductal adenocarcinoma. *J. Pathol.* 248, 51–65.
- Nicolle, R., Blum, Y., Marisa, L., Loncle, C., Gayet, O., Moutardier, V., Turrini, O., Giovannini, M., Bian, B., Bigonnet, M., Rubis, M., Elarouci, N., Armenoult, L., Ayadi, M., Duconseil, P., Gasmı, M., Ouaiııı, M., Maignan, A., Lomberk, G., Boher, J.M., Ewald, J., Bories, E., Garnier, J., Goncalves, A., Poizat, F., Raoul, J.L., Secq,

References

- V., Garcia, S., Grandval, P., Barraud-Blanc, M., Norguet, E., Gilibert, M., Delpero, J.R., Roques, J., Calvo, E., Guillaumond, F., Vasseur, S., Urrutia, R., de Reyniès, A., Dusetti, N., Iovanna, J., 2017. Pancreatic Adenocarcinoma Therapeutic Targets Revealed by Tumor-Stroma Cross-Talk Analyses in Patient-Derived Xenografts. *Cell Rep.* 21, 2458–2470.
- Nurmik, M., Ullmann, P., Rodriguez, F., Haan, S., Letellier, E., 2020. In search of definitions: Cancer-associated fibroblasts and their markers. *Int. J. Cancer* 146, 895–905.
- ## O
- Öhlund, D., Handly-Santana, A., Biffi, G., Elyada, E., Almeida, A.S., Ponz-Sarvisé, M., Corbo, V., Oni, T.E., Hearn, S.A., Lee, E.J., Chio, I.I.C., Hwang, C.-I., Tiriác, H., Baker, L.A., Engle, D.D., Feig, C., Kultti, A., Egeblad, M., Fearon, D.T., Crawford, J.M., Clevers, H., Park, Y., Tuveson, D.A., 2017. Distinct populations of inflammatory fibroblasts and myofibroblasts in pancreatic cancer. *J. Exp. Med.* 214, 579–596.
- Olive, K.P., Jacobetz, M.A., Davidson, C.J., Gopinathan, A., McIntyre, D., Honess, D., Madhu, B., Goldgraben, M.A., Caldwell, M.E., Allard, D., Frese, K.K., DeNicola, G., Feig, C., Combs, C., Winter, S.P., Ireland-Zecchini, H., Reichelt, S., Howat, W.J., Chang, A., Dhara, M., Wang, L., Rückert, F., Grützmann, R., Pilarsky, C., Izeradjene, K., Hingorani, S.R., Huang, P., Davies, S.E., Plunkett, W., Egorin, M., Hruban, R.H., Whitebread, N., McGovern, K., Adams, J., Iacobuzio-Donahue, C., Griffiths, J., Tuveson, D.A., 2009. Inhibition of Hedgehog signaling enhances delivery of chemotherapy in a mouse model of pancreatic cancer. *Science* (80-). 324, 1457–1461.
- Orozco, C.A., Martinez-Bosch, N., Guerrero, P.E., Vinaixa, J., Dalotto-Moreno, T., Iglesias, M., Moreno, M., Djurec, M., Poirier, F., Gabius, H.J., Fernandez-Zapico, M.E., Hwang, R.F., Guerra, C., Rabinovich, G.A., Navarro, P., 2018. Targeting galectin-1 inhibits pancreatic cancer progression by modulating tumor–stroma crosstalk. *Proc. Natl. Acad. Sci. U. S. A.* 115, E3769–E3778.
- Ottenhof, N.A., Milne, A.N.A., Morsink, F.H.M., Drillenburger, P., Ten Kate, F.J.W., Maitra, A., Offerhaus, G.J., 2009. Pancreatic intraepithelial neoplasia and pancreatic tumorigenesis: Of mice and men. *Arch. Pathol. Lab. Med.* 133, 375–381.
- Özdemir, B.C., Pentcheva-Hoang, T., Carstens, J.L., Zheng, X., Wu, C.C., Simpson, T.R., Laklai, H., Sugimoto, H., Kahlert, C., Novitskiy, S. V., DeJesus-Acosta, A., Sharma, P., Heidari, P., Mahmood, U., Chin, L., Moses, H.L., Weaver, V.M., Maitra, A., Allison, J.P., LeBleu, V.S., Kalluri, R., 2014. Depletion of carcinoma-associated fibroblasts and fibrosis induces immunosuppression and accelerates pancreas cancer with reduced survival. *Cancer Cell* 25, 719–734.

P

- Pavlova, N.N., Thompson, C.B., 2016. The Emerging Hallmarks of Cancer Metabolism. *Cell Metab.* 23, 27–47.
- Pereira, B.A., Vennin, C., Papanicolaou, M., Chambers, C.R., Herrmann, D., Morton, J.P., Cox, T.R., Timpson, P., 2019. CAF Subpopulations: A New Reservoir of Stromal Targets in Pancreatic Cancer. *Trends in Cancer*.
- Phipson, B., Lee, S., Majewski, I.J., Alexander, W.S., Smyth, G.K., 2016. ROBUST HYPERPARAMETER ESTIMATION PROTECTS AGAINST HYPERVARIABLE GENES AND IMPROVES POWER TO DETECT DIFFERENTIAL EXPRESSION. *Ann. Appl. Stat.* 10, 946–963.
- Provenzano, P.P., Cuevas, C., Chang, A.E., Goel, V.K., Von Hoff, D.D., Hingorani, S.R., 2012. Enzymatic Targeting of the Stroma Ablates Physical Barriers to Treatment of Pancreatic Ductal Adenocarcinoma. *Cancer Cell* 21, 418–429.
- Puleo, F., Nicolle, R., Blum, Y., Cros, J., Marisa, L., Demetter, P., Quertinmont, E., Svrcek, M., Elarouci, N., Iovanna, J., Franchimont, D., Verset, L., Galdon, M.G., Devière, J., de Reyniès, A., Laurent-Puig, P., Van Laethem, J.L., Bachet, J.B., Maréchal, R., 2018. Stratification of Pancreatic Ductal Adenocarcinomas Based on Tumor and Microenvironment Features. *Gastroenterology* 155, 1999–2013.e3.

Q

- Qin, C., Yang, G., Yang, J., Ren, B., Wang, H., Chen, G., Zhao, F., You, L., Wang, W., Zhao, Y., 2020. Metabolism of pancreatic cancer: paving the way to better anticancer strategies. *Mol. Cancer* 19, 50.

R

- Ramakrishnan, S.N., Lau, P., Crowther, L.M., Cleasby, M.E., Millard, S., Leong, G.M., Cooney, G.J., Muscat, G.E.O., 2009. Rev-erb beta regulates the Srebp-1c promoter and mRNA expression in skeletal muscle cells. *Biochem. Biophys. Res. Commun.* 388, 654–659.
- Ramakrishnan, S.N., Muscat, G.E.O., 2006. The Orphan Rev-Erb Nuclear Receptors: A Link between Metabolism, Circadian Rhythm and Inflammation? *Nucl. Recept. Signal.* 4, nrs.04009.
- Raufi, A.G., Manji, G.A., Chabot, J.A., Bates, S.E., 2019. Neoadjuvant Treatment for Pancreatic Cancer. *Semin. Oncol.* 46, 19–27.
- Rawla, P., Sunkara, T., Gaduputi, V., 2019. Epidemiology of Pancreatic Cancer: Global Trends, Etiology and Risk Factors. *World J. Oncol.* 10, 10–27.

References

- Rhim, A.D., Oberstein, P.E., Thomas, D.H., Mirek, E.T., Palermo, C.F., Sastra, S.A., Dekleva, E.N., Saunders, T., Becerra, C.P., Tattersall, I.W., Westphalen, C.B., Kitajewski, J., Fernandez-Barrena, M.G., Fernandez-Zapico, M.E., Iacobuzio-Donahue, C., Olive, K.P., Stanger, B.Z., 2014. Stromal Elements Act to Restrain, Rather Than Support, Pancreatic Ductal Adenocarcinoma. *Cancer Cell* 25, 735–747.
- Rudisch, A., Dewhurst, M.R., Horga, L.G., Kramer, N., Harrer, N., Dong, M., Van Der Kuip, H., Wernitznig, A., Bernthaler, A., Dolznig, H., Sommergruber, W., 2015. High EMT signature score of invasive Non-Small Cell Lung Cancer (NSCLC) cells correlates with NFκB driven colony-stimulating factor 2 (CSF2/GM-CSF) secretion by neighboring stromal fibroblasts. *PLoS One* 10, 1–31.
- Rudland, P.S., Platt-Higgins, A., Renshaw, C., West, C.R., Winstanley, J.H.R., Robertson, L., Barraclough, R., 2000. Prognostic significance of the metastasis-inducing protein S100A4 (p9Ka) in human breast cancer. *Cancer Res.* 60, 1595–1603.

S

- Sahai, E., Astsaturou, I., Cukierman, E., DeNardo, D.G., Egeblad, M., Evans, R.M., Fearon, D., Greten, F.R., Hingorani, S.R., Hunter, T., Hynes, R.O., Jain, R.K., Janowitz, T., Jorgensen, C., Kimmelman, A.C., Kolonin, M.G., Maki, R.G., Powers, R.S., Puré, E., Ramirez, D.C., Scherz-Shouval, R., Sherman, M.H., Stewart, S., Tlsty, T.D., Tuveson, D.A., Watt, F.M., Weaver, V., Weeraratna, A.T., Werb, Z., 2020. A framework for advancing our understanding of cancer-associated fibroblasts. *Nat. Rev. Cancer* 20, 174–186.
- Santi, A., Caselli, A., Ranaldi, F., Paoli, P., Mugnaioni, C., Michelucci, E., Cirri, P., 2015. Cancer associated fibroblasts transfer lipids and proteins to cancer cells through cargo vesicles supporting tumor growth. *Biochim. Biophys. Acta - Mol. Cell Res.* 1853, 3211–3223.
- Schnittert, J., Heinrich, M.A., Kuninty, P.R., Storm, G., Prakash, J., 2018. Reprogramming tumor stroma using an endogenous lipid lipoxin A4 to treat pancreatic cancer. *Cancer Lett.* 420, 247–258.
- Seufferlein, T., Ettrich, T.J., 2019. Treatment of pancreatic cancer—neoadjuvant treatment in resectable pancreatic cancer (PDAC). *Transl. Gastroenterol. Hepatol.* 4, 21–21.
- Sherman, M.H., Yu, R.T., Engle, D.D., Ding, N., Atkins, A.R., Tiriach, H., Collisson, E.A., Connor, F., Van Dyke, T., Kozlov, S., Martin, P., Tseng, T.W., Dawson, D.W., Donahue, T.R., Masamune, A., Shimosegawa, T., Apte, M. V., Wilson, J.S., Ng, B., Lau, S.L., Gunton, J.E., Wahl, G.M., Hunter, T., Drebin, J.A., O'Dwyer, P.J., Liddle, C., Tuveson, D.A., Downes, M., Evans, R.M., 2014. Vitamin D receptor-mediated stromal reprogramming suppresses pancreatitis and enhances pancreatic cancer therapy. *Cell* 159, 80–93.

- Sitaula, S., Zhang, J., Ruiz, F., Burris, T.P., 2017. Rev-erb regulation of cholesterologenesis. *Biochem. Pharmacol.* 131, 68–77.
- Solt, L.A., Kojetin, D.J., Burris, T.P., 2011. The REV-ERBs and RORs: molecular links between circadian rhythms and lipid homeostasis. *Future Med. Chem.* 3, 623–638.
- Subramanian, A., Tamayo, P., Mootha, V.K., Mukherjee, S., Ebert, B.L., Gillette, M.A., Paulovich, A., Pomeroy, S.L., Golub, T.R., Lander, E.S., Mesirov, J.P., 2005. Gene set enrichment analysis: A knowledge-based approach for interpreting genome-wide expression profiles. *Proc. Natl. Acad. Sci.* 102, 15545–15550.
- Sulli, G., Rommel, A., Wang, X., Kolar, M.J., Puca, F., Saghatelian, A., Plikus, M. V., Verma, I.M., Panda, S., 2018. Pharmacological activation of REV-ERBs is lethal in cancer and oncogene-induced senescence. *Nature* 553, 351–355.
- Sunami, Y., Rebelo, A., Kleeff, J., 2018. Lipid metabolism and lipid droplets in pancreatic cancer and stellate cells. *Cancers (Basel)*. 10, 3.
- Swierczynski, J., Hebanowska, A., Sledzinski, T., 2014. Role of abnormal lipid metabolism in development, progression, diagnosis and therapy of pancreatic cancer. *World J. Gastroenterol.* 20, 2279–303.
- Szymańska, K., 2018. Pancreatic Cancer: Diagnosis and Treatment. In: Reference Module in Biomedical Sciences. Elsevier, pp. 193–198.

I

- Tang, D., Tao, D., Fang, Y., Deng, C., Xu, Q., Zhou, J., 2017. TNF-Alpha Promotes Invasion and Metastasis via NF-Kappa B Pathway in Oral Squamous Cell Carcinoma. *Med. Sci. Monit. Basic Res.* 23, 141–149.
- Tempero, M.A., Van Cutsem, E., Sigal, D., Oh, D.-Y., Fazio, N., Macarulla, T., Hitre, E., Hammel, P., Hendifar, A.E., Bates, S.E., Li, C.-P., De La Fouchardiere, C., Heinemann, V., Maraveyas, A., Bahary, N., Layos, L., Sahai, V., Zheng, L., Lacy, J., Bullock, A.J., 2020. HALO 109-301: A randomized, double-blind, placebo-controlled, phase 3 study of pegvorhyaluronidase alfa (PEGPH20) + nab-paclitaxel/gemcitabine (AG) in patients (pts) with previously untreated hyaluronan (HA)-high metastatic pancreatic ductal adenocarcinoma. *J. Clin. Oncol.* 38, 638.
- Tesfaye, A.A., Philip, P.A., 2019. Adjuvant treatment of surgically resectable pancreatic ductal adenocarcinoma. *Clin. Adv. Hematol. Oncol.* 17, 54–63.
- The medical biochemistry page, n.d. The medical biochemistry page [WWW Document].
- Torres, C., Grippo, P.J., 2018. Pancreatic cancer subtypes: a roadmap for precision medicine. *Ann. Med.* 50, 277–287.

References

Tsukamoto, H., 2005. Adipogenic phenotype of hepatic stellate cells. *Alcohol. Clin. Exp. Res.* 29, 132–133.

V

Valkenburg, K.C., De Groot, A.E., Pienta, K.J., 2018. Targeting the tumour stroma to improve cancer therapy. *Nat. Rev. Clin. Oncol.* 15, 366–381.

Veenstra, V., Garcia-Garijo, A., van Laarhoven, H., Bijlsma, M., 2018. Extracellular Influences: Molecular Subclasses and the Microenvironment in Pancreatic Cancer. *Cancers (Basel)*. 10, 34.

W

Wagner, P.M., Monjes, N.M., Guido, M.E., 2019. Chemotherapeutic Effect of SR9009, a REV-ERB Agonist, on the Human Glioblastoma T98G Cells. *ASN Neuro* 11, 1–14.

Wang, S., Li, F., Lin, Y., Wu, B., 2020. Targeting REV-ERB α for therapeutic purposes: promises and challenges. *Theranostics* 10, 4168–4182.

Wang, Y., Kojetin, D., Burris, T.P., 2015. Anti-proliferative actions of a synthetic REV-ERB α/β agonist in breast cancer cells. *Biochem. Pharmacol.* 96, 315–322.

Welch, R.D., Billon, C., Valfort, A.-C., Burris, T.P., Flaveny, C.A., 2017. Pharmacological inhibition of REV-ERB stimulates differentiation, inhibits turnover and reduces fibrosis in dystrophic muscle. *Sci. Rep.* 7, 17142.

Werb, Z., Pengfei, L., 2015. The Role of Stroma in Tumor Development. *Cancer J* 21, 250–253.

Whittle, M.C., Hingorani, S.R., 2019. Fibroblasts in Pancreatic Ductal Adenocarcinoma: Biological Mechanisms and Therapeutic Targets. *Gastroenterology*.

Woldt, E., Sebti, Y., Solt, L.A., Duhem, C., Lancel, S., Eeckhoutte, J., Hesselink, M.K.C., Paquet, C., Delhay, S., Shin, Y., Kamenecka, T.M., Schaart, G., Lefebvre, P., Nevière, R., Burris, T.P., Schrauwen, P., Staels, B., Duez, H., 2013. Rev-erb- α modulates skeletal muscle oxidative capacity by regulating mitochondrial biogenesis and autophagy. *Nat. Med.* 19, 1039–1046.

X

Xie, T., Wang, Y., Deng, N., Huang, G., Taghavifar, F., Geng, Y., Liu, N., Kulur, V., Yao, C., Chen, P., Liu, Z., Stripp, B., Tang, J., Liang, J., Noble, P.W., Jiang, D., 2018. Single-Cell Deconvolution of Fibroblast Heterogeneity in Mouse Pulmonary Fibrosis. *Cell Rep.* 22, 3625–3640.

Xiong, Y., 2015. Hematopoietic stem cell-derived adipocytes and fibroblasts in the

tumor microenvironment. *World J. Stem Cells* 7, 253.

Y

- Yanase, M., Ikeda, H., Matsui, A., Noiri, E., Tomiya, T., Arai, M., Inoue, Y., Tejima, K., Nagashima, K., Nishikawa, T., Kimura, S., Fujiwara, K., Rojkind, M., Ogata, I., 2004. HMG-CoA reductase inhibitor modulates collagen GEL-contraction by hepatic myofibroblast-like stellate cell line: involvement of geranylgeranylated proteins. *Comp. Hepatol.* 3, S21.
- Yao, W., Maitra, A., Ying, H., 2020. Recent insights into the biology of pancreatic cancer. *EBioMedicine* 53, 102655.
- Ye, J., DeBose-Boyd, R.A., 2011. Regulation of Cholesterol and Fatty Acid Synthesis. *Cold Spring Harb. Perspect. Biol.* 3, a004754–a004754.
- Yin, L., Wu, N., Lazar, M.A., 2010. Nuclear receptor Rev-erb α : a heme receptor that coordinates circadian rhythm and metabolism. *Nucl. Recept. Signal.* 8, 1.
- Yu, K., Chen, B., Aran, D., Charalel, J., Yau, C., Wolf, D.M., van 't Veer, L.J., Butte, A.J., Goldstein, T., Sirota, M., 2019. Comprehensive transcriptomic analysis of cell lines as models of primary tumors across 22 tumor types. *Nat. Commun.* 10, 3574.

Z

- Zhang, D., Wang, Y., Shi, Z., Liu, J., Sun, P., Hou, X., Zhang, J., Zhao, S., Zhou, B.P., Mi, J., 2015. Metabolic Reprogramming of Cancer-Associated Fibroblasts by IDH3 α Downregulation. *Cell Rep.* 10, 1335–1348.
- Zhang, R., Gao, Y., Zhao, X., Gao, M., Wu, Y., Han, Y., Qiao, Y., Luo, Z., Yang, L., Chen, J., Ge, G., 2018. FSP1-positive fibroblasts are adipogenic niche and regulate adipose homeostasis. *PLOS Biol.* 16, e2001493.
- Zhao, J., Wang, H., Hsiao, C.H., Chow, D.S.L., Koay, E.J., Kang, Y., Wen, X., Huang, Q., Ma, Y., Bankson, J.A., Ullrich, S.E., Overwijk, W., Maitra, A., Piwnicka-Worms, D., Fleming, J.B., Li, C., 2018. Simultaneous inhibition of hedgehog signaling and tumor proliferation remodels stroma and enhances pancreatic cancer therapy. *Biomaterials* 159, 215–228.

WEB PAGES

www.aecc.es (AECC)

References

www.bccancer.bc.ca/drug-database-site

www.cancer.org (American Cancer Society)

www.ecis.jrc.ec.europa.eu (ECIS)

www.hopkinsmedicine.org (JONHS HOPKINS MEDICINE)

www.nih.gov (NIH)

www.openstax.org

www.pubchem.ncbi.nlm.nih.gov (PUBCHEM)

www.selleckchem.com

www.themedicalbiochemistrypage.org

www.who.int (WHO)

ANNEXES

ANNEX 1

Equivalence table of human gene – protein and the corresponding extended name.

GENE	PROTEIN SYMBOL	EXTENDED NAME
<i>ACTA2</i>	α SMA (ACTA)	Actin, aortic smooth muscle
<i>CALD1</i>	CALD1	Caldesmon-1
<i>CGN</i>	CING	Cingulin
<i>CNN1</i>	CNN1	Calponin 1
<i>FAP</i>	FAP α (SEPR)	Fibroblast Activation Protein α
<i>FN1</i>	FINC	Fibronectin
<i>IL-6</i>	IL6	Interleukin-6
<i>KCNN4</i>	KCNN4	Intermediate conductance calcium-activated potassium channel protein 4
<i>LLGL2</i>	L2GL2	LLGL scribble cell polarity complex component 2
<i>MYH11</i>	MYH11	Myosin-11
<i>PDGFRA</i>	PDGFRA	Platelet-derived growth factor receptor alpha
<i>PDPN</i>	PDPN	Podoplanin
<i>POSTN</i>	POSTN	Periostin
<i>RARB</i>	RARB	Retinoic acid receptor beta
<i>S100A4</i>	FSP-1 (S10A4)	Fibroblast-Specific Protein-1
<i>SQLE</i>	ERG1	Squalene monooxygenase
<i>VIM</i>	VIME	Vimentin
<i>ACTB</i>	ACTB	Beta-Actin
<i>DES</i>	DESM	Desmin

GENE	PROTEIN SYMBOL	EXTENDED NAME
<i>FASN</i>	FAS	Fatty Acid Synthase

ANNEX 2

Complete table of the metabolic reconstruction by hiPathia.

CATEGORY 1	CATEGORY 2	GO FUNCTION	T	FC	P.VALUE	FDR P.VALUE	CO-CULTURED CAFS
Lipids	cholesterol	positive regulation of cholesterol efflux	8.234	0.020	0.0001	0.018	UP
Lipids	lipid	lipid metabolic process	8.004	0.035	0.0001	0.018	UP
Lipids	lipid	long-chain fatty acid metabolic process	7.972	0.026	0.0001	0.018	UP
Lipids	lipid	membrane raft localization	7.599	0.020	0.0002	0.018	UP
Invasion and metastasis	mobility	regulation of exocytosis	7,599	0,020	0,0002	0,018	UP
Invasion and metastasis	mobility	cytokinesis	7,053	0,010	0,0003	0,018	UP
Invasion and metastasis	mobility	positive regulation of filopodium assembly	7,053	0,010	0,0003	0,018	UP
Apoptosis	apoptosis	positive regulation of fibroblast apoptotic process	6,782	0,038	0,0003	0,020	UP
Apoptosis	apoptosis	intrinsic apoptotic signaling pathway in response to DNA damage	6,782	0,038	0,0003	0,020	UP

CATEGORY 1	CATEGORY 2	GO FUNCTION	T	FC	P.VALUE	FDR P.VALUE	CO-CULTURED CAFs
Invasion and metastasis	mobility	positive regulation of protein homooligomerization	5,601	0,038	0,0010	0,032	UP
Energetics	glucose	acetyl-CoA biosynthetic process from pyruvate	5,505	0,038	0,0011	0,032	UP
Energetics	glucose	tricarboxylic acid cycle	5,505	0,038	0,0011	0,032	UP
Energetics	glucose	pyruvate metabolic process	5,505	0,038	0,0011	0,032	UP
Invasion and metastasis	adhesion	membrane to membrane docking	5,300	0,032	0,0013	0,033	UP
Invasion and metastasis	mobility	leukocyte migration	5,300	0,032	0,0013	0,033	UP
Invasion and metastasis	mobility	microtubule cytoskeleton organization	5,243	0,044	0,0014	0,033	UP
Invasion and metastasis	mobility	positive regulation of microtubule polymerization	5,243	0,044	0,0014	0,033	UP
Invasion and metastasis	mobility	positive regulation of axon extension	5,243	0,044	0,0014	0,033	UP
Immune response	immune	positive regulation of I-kappaB kinase/NF-kappaB signaling	5,204	0,026	0,0015	0,034	UP
Immune response	immune	leukocyte tethering or rolling	5,157	0,024	0,0016	0,035	UP
Apoptosis	apoptosis	negative regulation of extrinsic apoptotic signaling pathway via death domain receptors	5,121	0,040	0,0016	0,036	UP

Annexes

CATEGORY 1	CATEGORY 2	GO FUNCTION	T	FC	P.VALUE	FDR P.VALUE	CO-CULTURED CAFs
Lipids	lipid	phosphatidylcholine acyl-chain remodeling	5,008	0,045	0,0018	0,039	UP
Invasion and metastasis	signaling	protein palmitoylation	5,008	0,045	0,0018	0,039	UP
Invasion and metastasis	mobility	protein localization to synapse	4,841	0,094	0,0022	0,044	UP
Invasion and metastasis	adhesion	adhesion of symbiont to host	4,836	0,069	0,0022	0,044	UP
Invasion and metastasis	adhesion	receptor-mediated virion attachment to host cell	4,836	0,069	0,0022	0,044	UP
Invasion and metastasis	signaling	establishment of protein localization	4,834	0,047	0,0022	0,044	UP
Proliferative signaling	proliferation	cellular response to cGMP	4,726	0,026	0,0025	0,047	UP
Instability and mutation	HeatShock	response to temperature stimulus	-4,769	-0,084	0,0024	0,045	DOWN
Immune response	immune	positive regulation of interferon-alpha production	-4,783	-0,035	0,0023	0,045	DOWN
Energetics	glucose	response to glucose	-4,860	-0,020	0,0021	0,044	DOWN
Immune response	immune	negative regulation of antigen processing and presentation of peptide or polysaccharide antigen via MHC class II	-5,355	-0,017	0,0013	0,032	DOWN
Immune response	immune	negative regulation of dendritic cell	-5,355	-0,017	0,0013	0,032	DOWN

CATEGORY 1	CATEGORY 2	GO FUNCTION	T	FC	P.VALUE	FDR P.VALUE	CO-CULTURED CAFs
		antigen processing and presentation					
Lipids	lipid	negative regulation of plasma membrane long-chain fatty acid transport	-5,355	-0,017	0,0013	0,032	DOWN
Energetics	signaling	negative regulation of cGMP-mediated signaling	-5,355	-0,017	0,0013	0,032	DOWN
Proliferative signaling	proliferation	negative regulation of fibroblast growth factor receptor signaling pathway	-5,355	-0,017	0,0013	0,032	DOWN
Energetics	ion transport	response to magnesium ion	-5,355	-0,017	0,0013	0,032	DOWN
Apoptosis	apoptosis	engulfment of apoptotic cell	-5,355	-0,017	0,0013	0,032	DOWN
Invasion and metastasis	mobility	positive regulation of fibroblast migration	-5,355	-0,017	0,0013	0,032	DOWN
Immune response	immune	negative regulation of interleukin-12 production	-5,355	-0,017	0,0013	0,032	DOWN
Immune response	immune	positive regulation of macrophage activation	-5,355	-0,017	0,0013	0,032	DOWN
Invasion and metastasis	mobility	positive regulation of chemotaxis	-5,355	-0,017	0,0013	0,032	DOWN
Immune response	immune	positive regulation of tumor necrosis factor biosynthetic process	-5,355	-0,017	0,0013	0,032	DOWN
Invasion and metastasis	mobility	negative regulation of endothelial cell migration	-5,355	-0,017	0,0013	0,032	DOWN
Energetics		peptide cross-linking	-5,355	-0,017	0,0013	0,032	DOWN

Annexes

CATEGORY 1	CATEGORY 2	GO FUNCTION	T	FC	P.VALUE	FDR P.VALUE	CO-CULTURED CAFs
Proliferative signaling	proliferation	negative regulation of endothelial cell proliferation	-5,355	-0,017	0,0013	0,032	DOWN
Invasion and metastasis	mobility	negative regulation of blood vessel endothelial cell migration	-5,620	-0,029	0,0010	0,032	DOWN
Instability and mutation	OS	positive regulation of reactive oxygen species metabolic process	-5,660	-0,022	0,0009	0,032	DOWN
Invasion and metastasis	glutamate	ionotropic glutamate receptor signaling pathway	-6,029	-0,028	0,0006	0,028	DOWN
Proliferative signaling	signaling	positive regulation of protein import into nucleus, translocation	-6,102	-0,022	0,0006	0,027	DOWN
Immune response	immune	positive regulation of IP-10 production	-6,172	-0,043	0,0006	0,026	DOWN
Immune response	immune	positive regulation of chemokine (C-C motif) ligand 5 production	-6,172	-0,043	0,0006	0,026	DOWN
Immune response	immune	positive regulation of type I interferon-mediated signaling pathway	-6,172	-0,043	0,0006	0,026	DOWN
Immune response	immune	positive regulation of tumor necrosis factor production	-6,172	-0,043	0,0006	0,026	DOWN
Immune response	immune	interferon-beta production	-6,172	-0,043	0,0006	0,026	DOWN
Immune response	immune	innate immune response	-6,172	-0,043	0,0006	0,026	DOWN

CATEGORY 1	CATEGORY 2	GO FUNCTION	T	FC	P.VALUE	FDR P.VALUE	CO-CULTURED CAFs
Immune response	immune	positive regulation of defense response to virus by host	-6,637	-0,017	0,0004	0,021	DOWN
Energetics	glucose	cellular response to glucose stimulus	-7,014	-0,027	0,0003	0,018	DOWN
Invasion and metastasis	mobility	positive regulation of fast-twitch skeletal muscle fiber contraction	-7,024	-0,068	0,0003	0,018	DOWN
Invasion and metastasis	mobility	relaxation of skeletal muscle	-7,024	-0,068	0,0003	0,018	DOWN
Proliferative signaling		regulation of osteoblast differentiation	-7,028	-0,030	0,0003	0,018	DOWN
Invasion and metastasis	adhesion	regulation of bicellular tight junction assembly	-7,028	-0,030	0,0003	0,018	DOWN
Invasion and metastasis	mobility	negative regulation of ATPase activity	-7,220	-0,026	0,0002	0,018	DOWN
Proliferative signaling	proliferation	cleavage furrow formation	-7,841	-0,041	0,0001	0,018	DOWN
Lipids	lipid	positive regulation of lipase activity	-7,841	-0,041	0,0001	0,018	DOWN
Energetics	calcium	negative regulation of calcium ion transmembrane transporter activity	-9.480	-0.048	0.0000	0.011	DOWN
Energetics	calcium	negative regulation of calcium ion binding	-9.480	-0.048	0.0000	0.011	DOWN
Energetics	calcium	regulation of calcium-transporting ATPase activity	-9.480	-0.048	0.0000	0.011	DOWN

Annexes

CATEGORY 1	CATEGORY 2	GO FUNCTION	T	FC	P.VALUE	FDR P.VALUE	CO-CULTURED CAF5
Energetics	calcium	negative regulation of calcium-transporting ATPase activity	-9.480	-0.048	0.0000	0.011	DOWN
Energetics	calcium	negative regulation of calcium ion transport	-9.480	-0.048	0.0000	0.011	DOWN